frontiers | Research Topics

Applications of medicine in treating pulmonary fibrosis

Edited by
Wenjun Li, Isaac Kirubakaran Sundar, Changjun Lv, Shi Xin, Song Qin and HaiBo Hu

Published in
Frontiers in Pharmacology

ISSN 1664-8714
ISBN 978-2-8325-3024-5
DOI 10.3389/978-2-8325-3024-5

About Frontiers

Frontiers is more than just an open access publisher of scholarly articles: it is a pioneering approach to the world of academia, radically improving the way scholarly research is managed. The grand vision of Frontiers is a world where all people have an equal opportunity to seek, share and generate knowledge. Frontiers provides immediate and permanent online open access to all its publications, but this alone is not enough to realize our grand goals.

Frontiers journal series

The Frontiers journal series is a multi-tier and interdisciplinary set of open-access, online journals, promising a paradigm shift from the current review, selection and dissemination processes in academic publishing. All Frontiers journals are driven by researchers for researchers; therefore, they constitute a service to the scholarly community. At the same time, the *Frontiers journal series* operates on a revolutionary invention, the tiered publishing system, initially addressing specific communities of scholars, and gradually climbing up to broader public understanding, thus serving the interests of the lay society, too.

Dedication to quality

Each Frontiers article is a landmark of the highest quality, thanks to genuinely collaborative interactions between authors and review editors, who include some of the world's best academicians. Research must be certified by peers before entering a stream of knowledge that may eventually reach the public - and shape society; therefore, Frontiers only applies the most rigorous and unbiased reviews. Frontiers revolutionizes research publishing by freely delivering the most outstanding research, evaluated with no bias from both the academic and social point of view. By applying the most advanced information technologies, Frontiers is catapulting scholarly publishing into a new generation.

What are Frontiers Research Topics?

Frontiers Research Topics are very popular trademarks of the *Frontiers journals series*: they are collections of at least ten articles, all centered on a particular subject. With their unique mix of varied contributions from Original Research to Review Articles, Frontiers Research Topics unify the most influential researchers, the latest key findings and historical advances in a hot research area.

Find out more on how to host your own Frontiers Research Topic or contribute to one as an author by contacting the Frontiers editorial office: frontiersin.org/about/contact

Applications of medicine in treating pulmonary fibrosis

Topic editors

Wenjun Li — Yantai Institute of Coastal Zone Research, Chinese Academy of Sciences (CAS), China

Isaac Kirubakaran Sundar — University of Kansas Medical Center, United States

Changjun Lv — Binzhou Medical University Hospital, China

Shi Xin — Manchester Metropolitan University, United Kingdom

Song Qin — Yantai Institute of Coastal Zone Research, Chinese Academy of Sciences (CAS), China

HaiBo Hu — QingDao Hiser Hospital, China

Citation

Li, W., Sundar, I. K., Lv, C., Xin, S., Qin, S., Hu, H., eds. (2023). *Applications of medicine in treating pulmonary fibrosis*. Lausanne: Frontiers Media SA.

doi: 10.3389/978-2-8325-3024-5

Table of contents

04 Editorial: Applications of medicine in treating pulmonary fibrosis
Wenjun Li, Xin Shi, Changjun Lv, Haibo Hu, Isaac Kirubakaran Sundar and Song Qin

07 Yiqi Huayu decoction alleviates bleomycin-induced pulmonary fibrosis in rats by inhibiting senescence
Biao Zuo, Ling Zuo, Xu-Qin Du, Su Yuan, Chen Xuan, Yu-Di Zhang, Zhi-Wei Chen and Wen-Fu Cao

23 Optimizing antidotal treatment with the oral HSP90 inhibitor TAS-116 against hydrochloric acid-induced pulmonary fibrosis in mice
Pavel A. Solopov, Ruben Manuel Luciano Colunga Biancatelli, Christiana Dimitropolou, Tierney Day and John D. Catravas

37 Senescent AECII and the implication for idiopathic pulmonary fibrosis treatment
Tingwei Zhang, Jinjin Zhang, Changjun Lv, Hongbo Li and Xiaodong Song

51 Deficiency of endothelial FGFR1 alleviates hyperoxia-induced bronchopulmonary dysplasia in neonatal mice
Yanrong Long, Hongbin Chen, Junchao Deng, Junjie Ning, Pengbo Yang, Lina Qiao and Zhongwei Cao

68 Analysis of the safety and efficacy of different plasma concentrations of pirfenidone in patients with idiopathic pulmonary fibrosis
Hui Li, Jing Yang, Shanshan Chen, Peile Wang, Xueqing Yu, Qingwei Zhou, Xiaojian Zhang and Guojun Zhang

79 Enhanced secretion of hepatocyte growth factor in human umbilical cord mesenchymal stem cells ameliorates pulmonary fibrosis induced by bleomycin in rats
Huanjie Chen, Yulong Luo, Yiping Zhu, Yongshun Ye, Difei Chen, Xinyu Song, Zhulin Xiao, Ming Liu and Shiyue Li

91 Bu-Fei-Huo-Xue capsule alleviates bleomycin-induced pulmonary fibrosis in mice through modulating gut microbiota
Haibo Hu, Fengchan Wang, Ping Han, Peng Li, Kun Wang, Huan Song, Guojing Zhao, Yue Li, Xuechao Lu, Weihong Tao and Huantian Cui

103 Perspectives of PDE inhibitor on treating idiopathic pulmonary fibrosis
Xudan Yang, Zhihao Xu, Songhua Hu and Juan Shen

115 Arctiin-encapsulated DSPE-PEG bubble-like nanoparticles inhibit alveolar epithelial type 2 cell senescence to alleviate pulmonary fibrosis *via* the p38/p53/p21 pathway
Dian Xiong, Fei Gao, Jingbo Shao, Yueyun Pan, Song Wang, Dong Wei, Shugao Ye, Yuan Chen, Rui Chen, Bingqing Yue, Juan Li and Jingyu Chen

frontiers | Frontiers in Pharmacology

TYPE Editorial
PUBLISHED 04 July 2023
DOI 10.3389/fphar.2023.1212681

OPEN ACCESS

EDITED BY
Javier Echeverria,
University of Santiago, Chile

REVIEWED BY
Chenghai Liu,
Shanghai University of Traditional Chinese Medicine, China

*CORRESPONDENCE
Wenjun Li,
wjli@yic.ac.cn
Xin Shi,
jasonshi510@hotmail.com
Changjun Lv,
lucky_lcj@sina.com
Haibo Hu,
iamhhb1982@163.com
Isaac Kirubakaran Sundar,
isundar@kumc.edu
Song Qin,
sqin@yic.ac.cn

RECEIVED 26 April 2023
ACCEPTED 28 June 2023
PUBLISHED 04 July 2023

CITATION
Li W, Shi X, Lv C, Hu H, Sundar IK and Qin S (2023), Editorial: Applications of medicine in treating pulmonary fibrosis.
Front. Pharmacol. 14:1212681.
doi: 10.3389/fphar.2023.1212681

Editorial: Applications of medicine in treating pulmonary fibrosis

Wenjun Li[1]*, Xin Shi[2]*, Changjun Lv[3]*, Haibo Hu[4]*, Isaac Kirubakaran Sundar[5]* and Song Qin[1]*

[1]Yantai Institute of Coastal Zone Research, Chinese Academy of Sciences, Yantai, China, [2]Shandong Technology and Business University, Yantai, China, [3]Binzhou Medical University Hospital, Binzhou Medical University, Binzhou, China, [4]Qingdao Hospital of Traditional Chinese Medicine (Qingdao Hiser Hospital), Qingdao, China, [5]Department of Internal Medicine, Division of Pulmonary Critical Care and Sleep Medicine, University of Kansas Medical Center, Kansas City, KS, United States

KEYWORDS

pulmonary fibrosis, traditional medicine, synthetic drugs, biological drugs, clinical trials

Editorial on the Research Topic
Applications of medicine in treating pulmonary fibrosis

Pulmonary fibrosis (PF) is a pathology characterized by an inflammatory response and abnormal deposition of extracellular matrix, which manifests as progressive and irreversible damage to lung tissue structures, ultimately leading to organ dysfunction, respiratory failure, and death (Meyker, 2017). The inflammatory response, oxidative stress, and epithelial-to-mesenchymal transition are important factors that predispose to the development and progression of pulmonary fibrosis (Moss et al., 2022). Therefore, drugs that target these pathological alterations will facilitate the development of PF therapy. Glucocorticoids and antioxidants are used in the early treatment of pulmonary fibrosis, which could reduce the inflammatory response and oxidative stress in the lungs and can prevent the pathological changes of tissue fibrosis (Spagnolo et al., 2021). However, these drugs only slow down the decline in lung function and do not reverse the histopathological changes in the lung. Currently, lung transplantation is considered to be the only effective treatment, but the complex etiology and limited availability of donor organs make it difficult to achieve effective treatment. There is lack of new therapies for the treatment of pulmonary fibrosis and to elucidate the underlying mechanisms and potential targets for the pathogenesis of pulmonary fibrosis.

Pirfenidone is an approved drug with efficacy in PF, which reduces organ fibrosis by inhibiting collagen synthesis, decreasing inflammatory mediators, and reducing oxidative stress, and is widely used in clinical practice (Raghu, 2017). However, the adverse effects associated with pirfenidone vary considerably between individuals, and the dose is not fixed. A study by Li et al. evaluated the efficacy and safety of different plasma concentrations of pirfenidone in patients with pulmonary fibrosis, and found that high doses of pirfenidone (1800 mg/d) reduced the risk of exacerbation in patients with PF, while provoking side effects in the gastrointestinal system and the skin. However, the presence of these side effects did not discontinue treatment in patients with PF, as the high concentration of pirfenidone is beneficial for the retardation of the patient's condition (Li et al.).

Traditional Chinese medicine (TCM) is an important part of clinical practice and can be used in combination with each other to achieve a reduction in toxicity and an increase in effectiveness. The exploration and application of TCM in the treatment of PF are gradually increasing. Numerous researchers have found that the progression of PF is closely related to gut microbiota changes, which also suggests that regulating the gut microbiota could provide a new strategy for the treatment of PF. For example, in this Research Topic, Hu et al. evaluated Bu-Fei-Huo-Xue capsules significantly

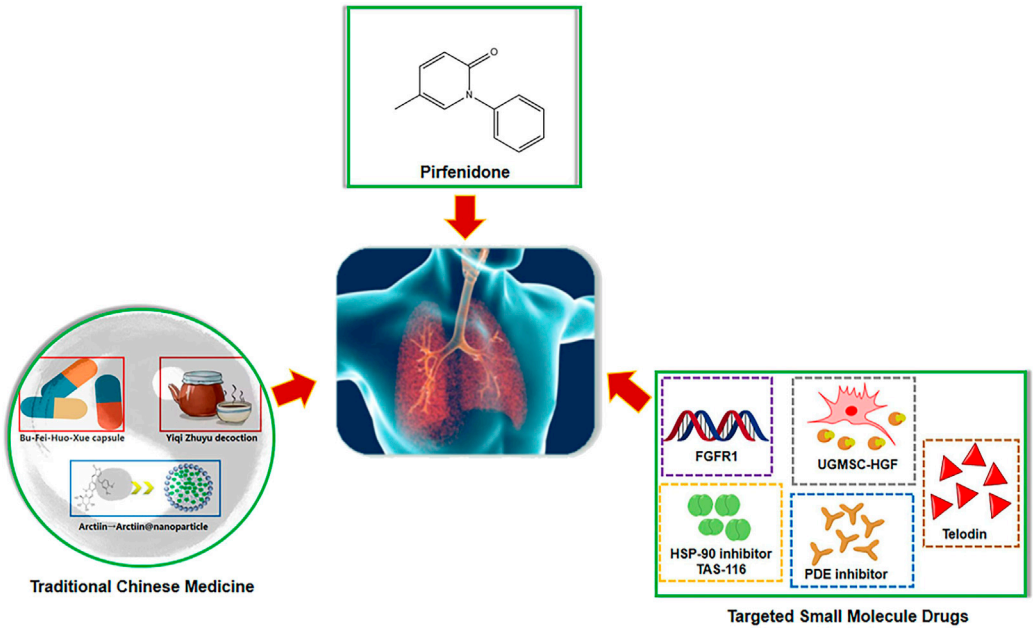

FIGURE 1
The drugs used to treat pulmonary fibrosis in this Research Topic include pirfenidone, traditional Chinese medicine and other novel small molecule drugs that target pro-fibrotic phenotypes.

improved collagen deposition, reduced levels of inflammatory factors in the lungs, and inhibited oxidative stress in mice with PF. It is interesting that Bu-Fei-Huo-Xue capsules also affected the diversity and relative abundance of the intestinal microbiota (Hu et al.), suggesting that the mechanism of Bu-Fei-Huo-Xue capsules on PF may be related to the regulation of gut microbiota. Based on a combination of net pharmacology and animal models, Zuo et al. revealed that Yiqi Huayu decoction was effective in reducing lung tissue damage, improving lung function, reducing inflammatory responses, and decreasing aging-related secretory phenotypes, including interleukin (IL)-1L and transforming growth factor-β1 (TGF-β1) in rats with PF. Similarly, Xiong et al. determined arctiin as an active component from *Arctium lappa* L. to exert therapeutic activity against PF by network pharmacology and prepared arctigenin nanoparticles. The result showed that arctiin nanoparticles exhibited good anti-aging properties *in vivo* and could attenuate AEC II senescence and PF via inhibiting the p38/p53/p21 pathway (Xiong et al.). The use of new technologies combined with conventional animal models to systematically and comprehensively elucidate the relationship between PF and disease targets, and between targets and drugs, will hopefully overcome the challenge of therapeutic strategies lagging behind medical advances and clinical needs.

The pursuit of an effective therapeutic target is the most important approach in anti-fibrotic drug discovery. Researchers have described several targets in this Research Topic. Long et al. reported that specific deletion of FGFR1 was able to protect lung tissue from hyperoxia injury, which may be attributed to the regulation of FGFR1 on both common and aerosol capillary endothelial cells, improving vascular and alveolar generation as well as respiratory indexes. In addition, the target-based discovery of small molecule drugs is an important research direction for the treatment of PF. Solopov et al. demonstrated that TAS-116, an HSP-90 inhibitor, could serve as an effective antidote against lung injury induced by hydrochloric acid, and it was able to reduce the overexpression of NLRP3 inflammasome and inhibit the activation of profibrotic pathways during the peak period of lung injury, thereby exerting lung protective activity. The cAMP and cGMP are intracellular second messengers that play important roles in multiple physiological functions. Yang et al. concluded that phosphodiesterase is involved in the metabolism of nucleotides, and its inhibitors can increase the concentration of intracellular cyclic nucleotides, thereby regulating cAMP and cGMP for their anti-fibrotic effects in the lungs. Moreover, Chen et al. reported that umbilical cord MSCs-hepatocyte growth factor would be a promising therapeutic option for PF, as over-expression of hepatocyte growth factor could enhance the anti-fibrotic effects of umbilical cord MSCs by interacting with IL-17-producing cells in lung tissue. A number of studies have revealed that senescent phenotypes such as aberrant telomere shortening seen in alveolar type II epithelial cells promote the development of PF (Duckworth et al., 2021). Zhang et al. show that Telodin, a newly discovered small molecule peptide inhibitor of telomere dysfunction, could reduce telomere shortening, expand the mouse AEC II stem cell population, and prevent chronic stress-induced premature lung senescence and fibrosis, which will promisingly be a new strategy to terminate pulmonary fibrosis.

We collectively identified a range of attractive therapeutic agents for PF, including pirfenidone, traditional Chinese medicine, and targeted novel small molecule inhibitors (Figure 1). Many studies have also presented complex gene-target-chemical components and molecular mechanisms underlying the development of PF. All these findings will provide lead structures for the development of anti-fibrotic drugs and further define their efficacy and pharmacokinetics *in vivo*. Further research on which specific anti-fibrotic drugs benefit

patients with PF will help medical personnel to develop a more rational individualized protocol for the diagnosis and treatment.

Author contributions

WL, XS, CL, HH, IS and SQ drafted and reviewed the manuscript.

Acknowledgments

We thank all the contributing authors and reviewers for their valuable contributions to this Research Topic.

Conflict of interest

The authors declare that the research was conducted in the absence of any commercial or financial relationships that could be construed as a potential conflict of interest.

Publisher's note

References

Duckworth, A., Gibbons, M. A., Allen, R. J., Almond, H., Beaumont, R. N., Wood, A. R., et al. (2021). Telomere length and risk of idiopathic pulmonary fibrosis and chronic obstructive pulmonary disease: A mendelian randomisation study. *Lancet. Respir. Med.* 9 (3), 285–294. doi:10.1016/S2213-2600(20)30364-7

Meyer, K. C. (2017). Pulmonary fibrosis, part I: Epidemiology, pathogenesis, and diagnosis. *Expert Rev. Respir. Med.* 11 (5), 343–359. doi:10.1080/17476348.2017.1312346

Moss, B. J., Ryter, S. W., and Rosas, I. O. (2022). Pathogenic mechanisms underlying idiopathic pulmonary fibrosis. *Annu. Rev. pathology* 17, 515–546. doi:10.1146/annurev-pathol-042320-030240

Raghu, G. (2017). Pharmacotherapy for idiopathic pulmonary fibrosis: Current landscape and future potential. *Eur. Respir. Rev. official J. Eur. Respir. Soc.* 26 (145), 170071. doi:10.1183/16000617.0071-2017

Spagnolo, P., Kropski, J. A., Jones, M. G., Lee, J. S., Rossi, G., Karampitsakos, T., et al. (2021). Idiopathic pulmonary fibrosis: Disease mechanisms and drug development. *Pharmacol. Ther.* 222, 107798. doi:10.1016/j.pharmthera.2020.107798

frontiers | Frontiers in Pharmacology

TYPE Original Research
PUBLISHED 28 October 2022
DOI 10.3389/fphar.2022.1033919

OPEN ACCESS

EDITED BY
HaiBo Hu,
QingDao Hiser Hospital, China

REVIEWED BY
Pavel Solopov,
Old Dominion University, United States
Li Peng,
Shanxi Agricultural University, China

*CORRESPONDENCE
Wen-Fu Cao,
caowenfu20220401@163.com

†These authors have contributed equally to this work

SPECIALTY SECTION
This article was submitted to Ethnopharmacology, a section of the journal Frontiers in Pharmacology

RECEIVED 01 September 2022
ACCEPTED 17 October 2022
PUBLISHED 28 October 2022

CITATION
Zuo B, Zuo L, Du X-Q, Yuan S, Xuan C, Zhang Y-D, Chen Z-W and Cao W-F (2022), Yiqi Huayu decoction alleviates bleomycin-induced pulmonary fibrosis in rats by inhibiting senescence. *Front. Pharmacol.* 13:1033919. doi: 10.3389/fphar.2022.1033919

Yiqi Huayu decoction alleviates bleomycin-induced pulmonary fibrosis in rats by inhibiting senescence

Biao Zuo[1,2†], Ling Zuo[1,2†], Xu-Qin Du[1,2], Su Yuan[1,2], Chen Xuan[1,2], Yu-Di Zhang[1,2], Zhi-Wei Chen[1,2] and Wen-Fu Cao[1,2*]

[1]College of Traditional Chinese Medicine, Chongqing Medical University, Chongqing, China, [2]Chongqing Key Laboratory of Traditional Chinese Medicine for Prevention and Cure of Metabolic Diseases, Chongqing, China

Overview: In treating pulmonary fibrosis (PF), traditional Chinese medicine (TCM) has received much attention, but its mechanism is unclear. The pharmacological mechanisms of TCM can be explored through network pharmacology. However, due to its virtual screening properties, it still needs to be verified by *in vitro* or *in vivo* experiments. Therefore, we investigated the anti-PF mechanism of Yiqi Huayu Decoction (YHD) by combining network pharmacology with *in vivo* experiments.

Methods: Firstly, we used classical bleomycin (BLM)-induced rat model of PF and administrated fibrotic rats with YHD (low-, medium-, and high-dose). We comprehensively assessed the treatment effect of YHD according to body weight, lung coefficient, lung function, and histopathologic examination. Second, we predict the potential targets by ultra-high-performance liquid chromatography-tandem mass spectrometry (UHPLC-MS/MS) combined with network pharmacology. In brief, we obtained the chemical ingredients of YHD based on the UHPLC-MS/MS and TCMSP database. We collected drug targets from TCMSP, HERB, and Swiss target prediction databases based on active ingredients. Disease targets were acquired from drug libraries, Genecards, HERB, and TTD databases. The intersecting targets of drugs and disease were screened out. The STRING database can obtain protein-protein interaction (PPI) networks and hub target proteins. Molecular Complex Detection (MCODE) clustering analysis combined with enrichment analysis can explore the possible biological mechanisms of YHD. Enrichment analyses were conducted through the R package and the David database, including the Kyoto Encyclopedia of Genes

Abbreviations: α-SMA, α-smooth muscle actin; AM, *Astragalus* membranaceus (Fisch.) Bunge; BLM, bleomycin; ELISAs, enzyme-linked immunosorbent assays.; FRC, functional residual capacity; GO, gene ontology; H&E, Hematoxylin-Eosin stain; HYP, hydroxyproline; IL-6, interleukin 6; KEGG, Kyoto encyclopedia of genes and genomes; MCODE, molecular complex detection analysis; PF, pulmonary fibrosis; PPI, protein-protein interaction; ROS, reactive oxygen species; Rt-qPCR, real-time quantitative polymerase chain reaction; SASPs, senescence-associated secretory phenotypes; sGaw, specific airway conductance; SM, Salvia miltiorrhiza Bunge; sRaw, specific airway resistance; TCM, traditional Chinese medicine; TGF-β1, transforming growth factor-β1; TNF-α, tumor necrosis factor-alpha; UHPLC-MS/MS, ultra-high-performance liquid chromatography tandem mass spectrometry; WB, western blot; YHD, yiqi huayu decoction.

and Genomes (KEGG), Gene Ontology (GO), and Reactome. Then, we further validated the target genes and target proteins predicted by network pharmacology. Protein and gene expression detection by immunohistochemistry, Western blot (WB), and real-time quantitative PCR (rt-qPCR).

Results: The results showed that high-dose YHD effectively attenuated BLM-induced lung injury and fibrosis in rats, as evidenced by improved lung function, relief of inflammatory response, and reduced collagen deposition. We screened nine core targets and cellular senescence pathways by UHPLC-MS/MS analysis and network pharmacology. We subsequently validated key targets of cellular senescence signaling pathways. WB and rt-qPCR indicated that high-dose YHD decreased protein and gene expression of senescence-related markers, including p53 (TP53), p21 (CDKN1A), and p16 (CDKN2A). Increased reactive oxygen species (ROS) are upstream triggers of the senescence program. The senescence-associated secretory phenotypes (SASPs), containing interleukin 6 (IL-6), tumor necrosis factor-alpha (TNF-α), and transforming growth factor-β1 (TGF-β1), can further exacerbate the progression of senescence. High-dose YHD inhibited ROS production in lung tissue and consistently reduced the SASPs expression in serum.

Conclusion: Our study suggests that YHD improves lung pathological injury and lung function in PF rats. This protective effect may be related to the ability of YHD to inhibit cellular senescence.

KEYWORDS

Yiqi Huayu decoction, pulmonary fibrosis, network pharmacology, cellular senescence, senescence-associated secretory phenotypes

1 Introduction

Pulmonary fibrosis (PF) is a chronic, progressive, and irreversible fibrotic lung disease, and its prominent feature is matrix stiffening (Moss et al., 2022). Symptoms of PF are mainly characterized by worsening dyspnea and ventilatory and ventilatory dysfunction (Martinez et al., 2017). Patients with PF have an inferior prognosis, with hypoxemia and respiratory failure leading to death (Moss et al., 2022). With a median survival of only 2.5–3.5 years, PF's terrible prognosis rivals some of the worst malignancies. With a high mortality rate and incurable properties, PF has received more attention, especially after the peak of the Coronavirus disease outbreak in 2019 (COVID-19) (Gentile et al., 2020; Spagnolo et al., 2020; Aul et al., 2021; Tanni et al., 2021). However, there are currently no radical drugs in clinical practice to cope with this devastating lung disease (Spagnolo et al., 2021). Therefore, the development of effective treatment for PF is urged.

PF is an aging-related disease, and cellular senescence is crucial in the aging phenotype (Schafer et al., 2017). The accelerated senescence of alveolar epithelial cells is increasingly recognized as a primary cause of epithelial dysfunction and PF pathogenesis (Yao et al., 2021). Senescent alveolar epithelial cells not only lose their ability to regenerate and repair, but also exert deleterious effects on neighboring cells by secreting various pro-inflammatory cytokines, profibrotic factors, and growth factors (Kadota et al., 2018). Those secretions are defined as senescence-associated secretory phenotypes (SASPs). Recently, senotherapeutics and senolytics have become emerging hotspots (Justice et al., 2019; Merkt et al., 2020; Wissler Gerdes et al., 2021).

Because TCM can improve patient quality of life and survival rate, it has enormous potential in treating PF(Li and Kan, 2017). Yiqi Huayu decoction (YHD), a modified traditional Chinese prescription, has been applied to the clinical treatment of PF(Zhang et al., 2018). YHD consists of two botanical drugs: *Astragalus* mongholicus Bunge and Salvia miltiorrhiza Bunge. This prescription can improve PF by tonifying the lung, benefiting Qi, activating blood circulation, and removing blood stasis. Increasing evidence suggests that YHD can potentially prevent or treat various fibrotic diseases by suppressing inflammatory responses, inhibiting myofibroblast activation, and promoting collagen degradation (Qin et al., 2018; Han et al., 2021). The clinical application of YHD in PF has been validated, but its mechanism is unclear because its components and targets are complex. Therefore, it is valuable to further investigate the mechanism of YHD in treating PF.

In our study, we used a classical bleomycin-induced rat model of PF and administered different doses of YHD. The therapeutic effect of YHD was evaluated comprehensively by body weight, lung coefficient, survival rate, lung function, and pathological sections of rats. Network pharmacology is an effective tool for predicting complex pharmacological mechanisms and has been widely used by TCM researchers.

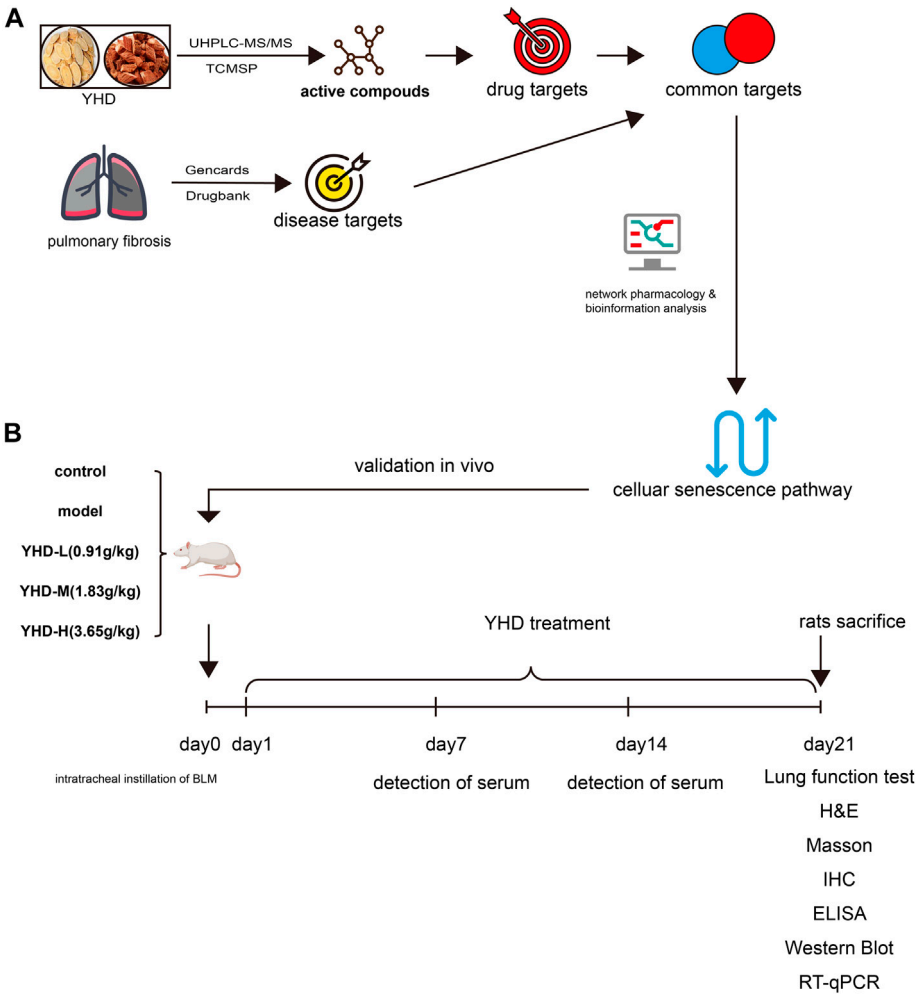

FIGURE 1
Experimental flow diagram. **(A)**Network pharmacology **(B)** Animal experiment. Pulmonary fibrosis was induced in rats by tracheal drops of bleomycin at day 0. From day 1 to day 21, rats were given YHD by gavage once a day, and orbital blood was collected from rats once a week. Each group of rats ended up with at least 6 biological replicates.

Through component identification (UHPLC-MS/MS analysis) and network pharmacology, we screened out key targets and signaling pathways to reveal the mechanism of YHD in treating PF. We then further validated key markers on cellular senescence signaling pathways with different approaches. An overview of our study is shown in Figure 1.

2 Materials and methods

2.1 Drugs and reagents

YHD granules are provided by Yifang Pharmaceutical (Guangdong, China) to ensure accurate dosage. Each herb underwent a series of processes, including decocting, extracting, concentrating, drying, and finally preparing into granules. These granules were identified by professor Wen-fu Cao of Chongqing Medical University. The granules sample are saved in Chongqing Key Laboratory of Traditional Chinese Medicine for Prevention and Cure of Metabolic Diseases. Detection kits for hydroxyproline are available from Nanjing Jiancheng Bioengineering Institute (Nanjing, China). Detection kits for reactive oxygen species (ROS) are available from Nanjing Fengfeng Biomedical Technology Co. (Nanjing, China). The TGF-β1, IL-6, and TNF-α detection kits were provided by Jiubang Biotechnology (Fujian, China). All reagents for rt-qPCR were from Takara Bio (Kusatsu, Japan). All primers for qPCR were synthesized by Tsingke Biology Technology (Beijing, China). Acetonitrile, methanol, and formic acid (LC-MS grade) were purchased from CNW Technologies (Dusseldorf,

TABLE 1 Compositions of YHD.

Scientific name	Botanical dosage (g)	Corresponding dosage of granules (g)	Occupied percent (%)
Astragalus mongholicus Bunge [Fabaceae; Astragali radix]	60	12	68.97
Salvia miltiorrhiza Bunge [Lamiaceae; Salviae miltiorrhizae radix et rhizoma]	30	5.4	31.03

Germany). Antibodies against GAPDH (ab181602), p16 (ab51243), and P21 (ab109199) were offered by Abcam (Cambridge, United Kingdom). Antibodies against P53 (sc-99) were purchased from Santa Cruz. Antibodies against Collagen I (GB11022-3), Collagen Ⅲ(GB111629), and α-SMA (GB111364) were acquired from Servicebio (Wuhan, China).

2.2 Preparation of Yiqi Huayu decoction

YHD consists of two botanical drugs: *Astragalus* mongholicus Bunge (AM) and Salvia miltiorrhiza Bunge (SM). Table 1 shows detailed YHD information and composition ratios. All original medicinal materials are made into granules according to the procedures of the Chinese Pharmacopoeia. Specifically, the original herbs were soaked in 7 times the volume of purified water for 30 min, brought to a boil over high heat, and continued to decoct for 60 min. After filtering off the liquid, water was added again, brought to a boil over high heat, and the decoction was continued for 40 min. Finally, the liquid obtained from the two decoctions was mixed, dried, concentrated, and packaged into granules. 60 g of raw astragalus was concentrated into 12 g of granules, and 30 g of salvia was concentrated into 5.4 g of granules. The YHD oral liquids were made by mixing granules of single botanical drugs with double-distilled water and dissolving them. The daily dose of YHD granules in adults is 0.29 g/kg. Rats' daily dose was calculated as 1.827 g/kg using the conversion ratio of surface area between rats and humans (6.3). This dose was used as the medium dose. The low dose of YHD was 0.9135 g/kg, whereas the high dose was 3.654 g/kg.

2.3 Ultra-high-performance liquid chromatography tandem mass spectrometry

100 mg YHD sample dissolved in 500ul extraction solution (Methanol: water = 4:1, the internal standard concentration is 10 ug/mL). Vortex for 30 s, sonicate at 45 Hz for 4 min, and sonicate in an ice-water bath for 1 h; After standing at - 40°C for 1 h, the sample was centrifuged at 4°C, 12,000 rpm (centrifugal force 13,800 (×g), radius 8.6 cm) for 15 min; The supernatant was filtered through a 0.22 um microporous membrane. 5ul filtered supernatant was detected for UHPLC-MS/MS analysis.

2.4 Animals

Thirty adult male Sprague-Dawley rats (weighing 200–220 g) were used as research subjects. All animals were supplied by the Laboratory Animal Center of Chongqing Medical University and kept in a specific pathogen-free room at the center. The laboratory was maintained at 22.9 (°C) with a relative humidity of 46.4% and a 12-h dark photoperiod. All rats were fed standard chow and water for 7 days in the laboratory before the experiment.

2.5 Model preparation and administration

After 7 days of adoption, all rats were randomly divided into five groups (n = 6 in each group) as follows: control group, model group, YHD at low-, medium-, and high-dose group (0.9135,1.827, 3.654 g/kg/day). On day 0, rats in the control group were treated with an equal volume of saline, and the other groups' rats were intratracheally injected with BLM dissolved in saline. Briefly, rats were anesthetized (2% sodium pentobarbital) and instilled with BLM solution (5 mg/kg) by the intratracheal route. From day 1 to day 21, rats in the control and model groups were treated with saline, while rats in the low-, medium-, and high-dose YHD groups were treated with the corresponding doses of YHD. All rats were sacrificed on day 21st. The lower 1/3 of the left lung was fixed with 4% paraformaldehyde and sectioned for H&E, MASSON, and immunohistochemical staining. The remaining lung tissues were stored at -80°C for future analyses.

2.6 Lung function test

On day 21st, rat lung function was measured using the FinePointe non-invasive testing system (FinePointe™ NAM, Data Sciences International). Specifically, the rat is secured in a closed box with an airflow monitoring apparatus attached to one end of the box. Different respiratory parameters such as breathing frequency (F), minute volume (MV), tidal ventilation volume (TV), specific airway conductance (sGaw), functional residual capacity (FRC), and specific airway resistance (sRaw) were derived from the airflow. The average values calculated by the system are counted as raw data.

2.7 Hydroxyproline and reactive oxygen species

Hydroxyproline (HYP) contents in lung tissues were measured using the Hydroxyproline Assay Kit (Nanjing Jiancheng Corp. Nanjing, China) according to the manufacturer's instructions. In brief, 50 mg of lung tissue was mixed with 1 ml of hydrolase and placed in a boiling water bath for 20 min. The supernatant was centrifuged at 3,500 rpm/min for 10 min, and the absorbance was measured at 550 nm. The detection of reactive oxygen species (ROS) in lung tissue is according to the kit instructions. Specifically, 50 mg of lung tissue was homogenized in 1 ml of homogenizing Buffer, and the supernatant was harvested by centrifugation. We sequentially added 200 ul of supernatant and 2 μl of liquid containing the fluorescent probe to the 96-well plate. Fluorescence intensity was measured at excitation wavelength 510 nm and emission wavelength 610 nm. After measuring the protein concentration of the supernatant, the fluorescence intensity/protein concentration indicates the intensity of tissue reactive oxygen species.

2.8 Histological analysis and immunohistochemistry

The left lung tissues were fixed in 4% paraformaldehyde for 24 h, embedded in paraffin. According to the manufacturer's instructions, histological sections were used for hematoxylin-eosin (H&E), Masson, and immunohistochemical (IHC) experiments. Alveolitis was assessed with H&E-stained sections, and fibrosis was assessed with Masson's trichrome-stained sections. The inflammation and fibrosis scores were assessed quantitatively based on previous literature (Szapiel et al., 1979). All the sections were analyzed by microscopy (BX53, Olympus Corporation, Japan).

2.8.1 Hematoxylin-eosin Staining

Paraffin sections were deparaffinized, stained with hematoxylin staining solution for 5 min, rinsed with distilled water, dehydrated with graded alcohol, and then stained with eosin staining solution for 5 min, and dehydrated and sealed. Sections were rinsed with 1% glacial acetic acid for differentiation, dehydrated with absolute ethanol, and fixed.

2.8.2 Masson staining

Sections were immersed in Masson A solution overnight and washed with water. And the sections were filled into a dye solution mixed with Masson B solution and Masson C solution in equal proportions, soaked for 1 min, washed with water, differentiated with 1% hydrochloric acid alcohol, and washed with water. Next, the sections were plunged into Masson D solution for 6 min, rinsed with water, and plunged into Masson E solution for 1 min. After a slight drain, the sections were directly stained with Masson F solution for 2–30 s. Sections were rinsed with 1% glacial acetic acid for differentiation, dehydrated with absolute ethanol, and fixed.

TABLE 2 Primer sequences used for rt-qPCR.

Gene name		Sequences
P53	Forward	ACAGTTAGGGGGTACCTGGC
	Reverse	GACTCAGAGGGAGCTCGATG
P21	Forward	CCTGGTGATGTCCGACCTG
	Reverse	CCATGAGCGCATCGCAATC
P16	Forward	GAGGGCTTCCTAGACACTCTGGTAG
	Reverse	AGATACCGCAAATACCGCACGAC
GAPDH	Forward	GACATGCCGCCTGGAGAAAC
	Reverse	AGCCCAGGATGCCCTTTAGT

2.8.3 Immunohistochemistry

We incubated the sections at 95°C for 20 min with citrate antigen retrieval solution. These sections were incubated with primary antibodies Collagen-I (GB11022-3), Collagen-III(GB111629), and α-SMA (GB111364) overnight, and then secondary antibodies were incubated with these sections for 50 min. Image-Pro Plus software (Media Cybernetics, United States) calculated cumulative optical densities.

2.9 Real-time quantitative PCR analysis

The mRNA expression levels of p53, p21, p16, and GAPDH in lung tissue were detected by rt-qPCR. Trizol reagent (Takara) extracted total RNA from lung tissue following the manufacturer's protocol. Reverse transcription was carried out using the PrimeScript RT Reagent Kit (Takara). qRT-PCR was performed with the SYBR PrimeScript PCR kit II (Takara). A housekeeping gene, GAPDH, was used to standardize Ct values. Fold changes in mRNA expression were calculated by relative quantification ($2^{-\Delta\Delta Ct}$). Primer sequences used for PCR are shown in Table 2.

2.10 Western blotting analysis

Hub target proteins were subsequently validated by western blotting using specific antibodies. Briefly, we extracted proteins from rat lung tissue using lysates and protease inhibitors. Protein content was quantified with the BCA reagent kit. Proteins were separated by electrophoresis on SDS-PAGE gels and then transferred to the PVDF membranes. The membrane and primary antibodies were incubated overnight at 4°C after blocking with 5% skimmed milk. Following 5 washes with TBST, the membrane was incubated for 1 h with HRP-conjugated secondary antibodies. Finally, a chemiluminescence

reagent was added to the membrane surface, and the imaging system visualized the target protein.

2.11 Enzyme-linked immunosorbent Assay

A quantitative ELISA was used to determine the levels of TNF-α, TGF-β1, and IL-6 in serum. The ELISA kits were all purchased from Jiubang Biotechnology (Fujian, China). All operations were performed strictly following the kit instructions. Briefly, serum samples (10 μl) and diluent solutions (40 ul) were separately added to the wells on a 96-well plate. Next, each well was added to HRP-labelled secondary antibodies and then incubated at 37°C for 60 min. Finally, we measured the optical density of each hole at 450 nm after adding 50 ml termination solution within 15 min.

2.12 Network pharmacology

2.12.1 Obtaining the Yiqi Huayu decoction targets and PF-related gene sets

First, we screened the active ingredients of YHD from UHPLC-MS/MS analysis and Traditional Chinese Medicine Systems Pharmacology Database and Analysis Platform (TCMSP) (Ru et al., 2014). The screening criteria are that the oral bioavailability (OB) ≥ 30% and the drug-like (DL) index ≥0.18 (Li and Kan, 2021; Xia et al., 2020). Based on the active compound, we searched compound-related target genes in different databases (TCMSP, HERB, Swiss Target Prediction) (Gfeller et al., 2014; Ru et al., 2014; Fang et al., 2021). With the help of Uniprot, an AMSM target gene set is acquired after gene symbol annotation (Apweiler et al., 2004). Then, we searched PF-related genes in four databases: the Drugbank database, Genecards database, HERB database, and TTD database (Rebhan et al., 1997; Chen et al., 2002; Wishart et al., 2008; Fang et al., 2021). By combining the search results, we established a set of PF-related genes. PF-related genes and AMSM target genes were intersected to determine the common targets between drugs and diseases.

TCMSP database (https://www.tcmsp-e.com/).

Swiss Target Prediction web server (http://www.swisstargetprediction.ch).

HERB database (http://herb.ac.cn/).

Uniprot database (http://beta.uniprot.org/).

Drugbank database (https://go.drugbank.com).

Genecards database (https://www.genecards.org).

TTD database (http://db.idrblab.net/ttd/).

2.12.2 Protein-protein interaction network and critical subnetwork

STRING database was used to construct the PPI network based on the common gene set (Damian et al., 2011). After setting the parameter as high confidence (0.9), the PPI network from STRING was imported into Cytoscape for further analysis. We applied two methods (CytoNca and CytoHubba) to screen the core subnetwork. Firstly, we used CytoNca(a plugin in Cytoscape) to analyze the PPI network (Tang et al., 2015). In detail, based on the primary score file calculated by CytoNca, we constructed a primary subnetwork consisting of the top 10 genes. Second, we used CytoHubba (another plugin in Cytoscape) to analyze the PPI network again (Chin et al., 2014). This approach analyzed the top 10 genes in the PPI network and constructed the critical subnetwork without checking the first-stage nodes.

STRING (https://www.string-db.org).

Cytoscape (version 3.8.2).

2.12.3 Enrichment analysis and cluster analysis

A series of enrichment analyses were performed to determine the underlying mechanism, including gene ontology (GO), Kyoto Encyclopedia of Genes and Genomes (KEGG), and Reactome pathway analysis (Kanehisa and Goto, 2000; Harris et al., 2004; Joshi-Tope et al., 2005). KEGG and GO enrichment analysis was conducted using R's "ClusterProfile" package (version 3.4.0) (Yu et al., 2012). The enrichment analysis of the Reactome pathway is completed using the DAVID database (Dennis et al., 2003). MCODE, a plugin for Cytoscape, carried out the clustering analysis. MCODE is mainly based on PPI network density and K-score for clustering analysis (The following parameters were set: degree cutoff = 2, node score cutoff = 0.2, K-score = 2, max. depth = 100) (Bader and Hogue, 2003).

2.13 Statistical analysis

The statistical analyses were conducted using GraphPad Prism version 8.0 (GraphPad Software, United States). All raw data are shown as mean ± SEM. A one-way ANOVA was performed after satisfying a normal distribution, followed by a Tukey multiple comparison test. *p*-values less than 0.05 were considered statistically significant.

3 Results

3.1 Components analysis of Yiqi HuaYu decoction

In order to identify the chemical components in Yiqi Huayu decoctions (YHD), UHPLC-MS/MS was used to analyze the samples. The total ion chromatograms (positive and negative) of YHD were obtained by UHPLC-MS/MS(Figures 2A–B). A total of 563 compounds were identified from the YHD samples. These compounds included 143 terpenoids, 86 flavonoids, 48 phenylpropanoids, 47 alkaloids, 45 miscellaneous, 34 phenols, 19 fatty acyls, 17 organic acids and their derivatives, 16 amino acid derivatives, 12 coumarins, *etc.* See

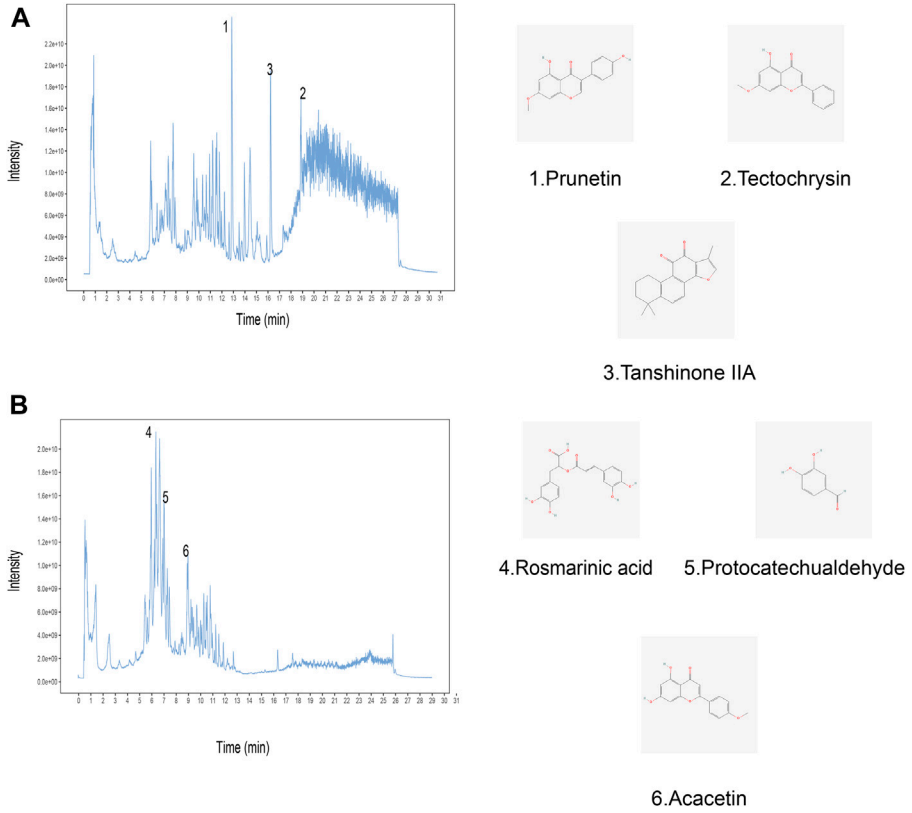

FIGURE 2
Identification of chemical components of YHD by ultra-high performance liquid chromatography-tandem mass spectrometry (UHPLC–MS/MS). Total ion chromatography in **(A)** positive and **(B)** negative ion modes for YHD samples is shown. The numbers correspond to the compounds on the left. The molecular structures of the compounds are on the right.

the Supplementary Table S1 for detailed ingredient information. Figure 2 demonstrates six key compounds: 1) Prunetin, 2) Tectochrysin, 3) Tanshinone IIa, 4) Rosmarinic acid, 5) Protocatechualdehyde, and 6) Acacetin.

3.2 Yiqi HuaYu decoction alleviated bleomycin-induced pulmonary fibrosis in the rat

Rat survival rates, body weights, and lung coefficients were recorded to verify the therapeutic effects of YHD on PF. Following intratracheal instillation of BLM at day 0, total two rats in the model group died (on day 2 and day 6, respectively), and one in the low-dose YHD group died (on day 2). Conversely, no rats died in the remaining three groups (Figure 3A). The lung coefficient can reflect the degree of inflammation and edema in the lung tissue (Shen et al., 2020). Rats in the model and YHD-L groups had a higher lung coefficient than those in the control group ($p < 0.001$). The medium- and high-dose YHD reduced the lung coefficients of fibrotic rats (Figure 3B). The body weight reflects the health status of fibrotic rats. Compared to the normal control group, the rats in the model group showed significant early weight loss (on day 7) and later slowed weight growth (on day 21). Different doses of YHD had a tendency to improve rat body weight, although there was no statistical difference (Figure 3C).

Pathological staining can more intuitively observe alveolar structure and degree of fibrosis. H&E staining showed obvious morphologic changes in the lung in the model group, including thickening of the alveolar septum, alveolar structure destruction, and heavy inflammatory cell infiltration in the alveolar space and lung interstitium (Figure 3D). In addition, the lung tissues of rats in the model group also displayed increased collagen deposition, as indicated by the increased blue fiber bundles in Masson-stained lung sections. The results of the inflammation and fibrosis scores showed that YHD treatment reduced the infiltration of inflammatory cells and decreased the deposition of collagen fibers. A significant dose effect was seen between the low-dose and high-dose groups (Figures 3E,F).

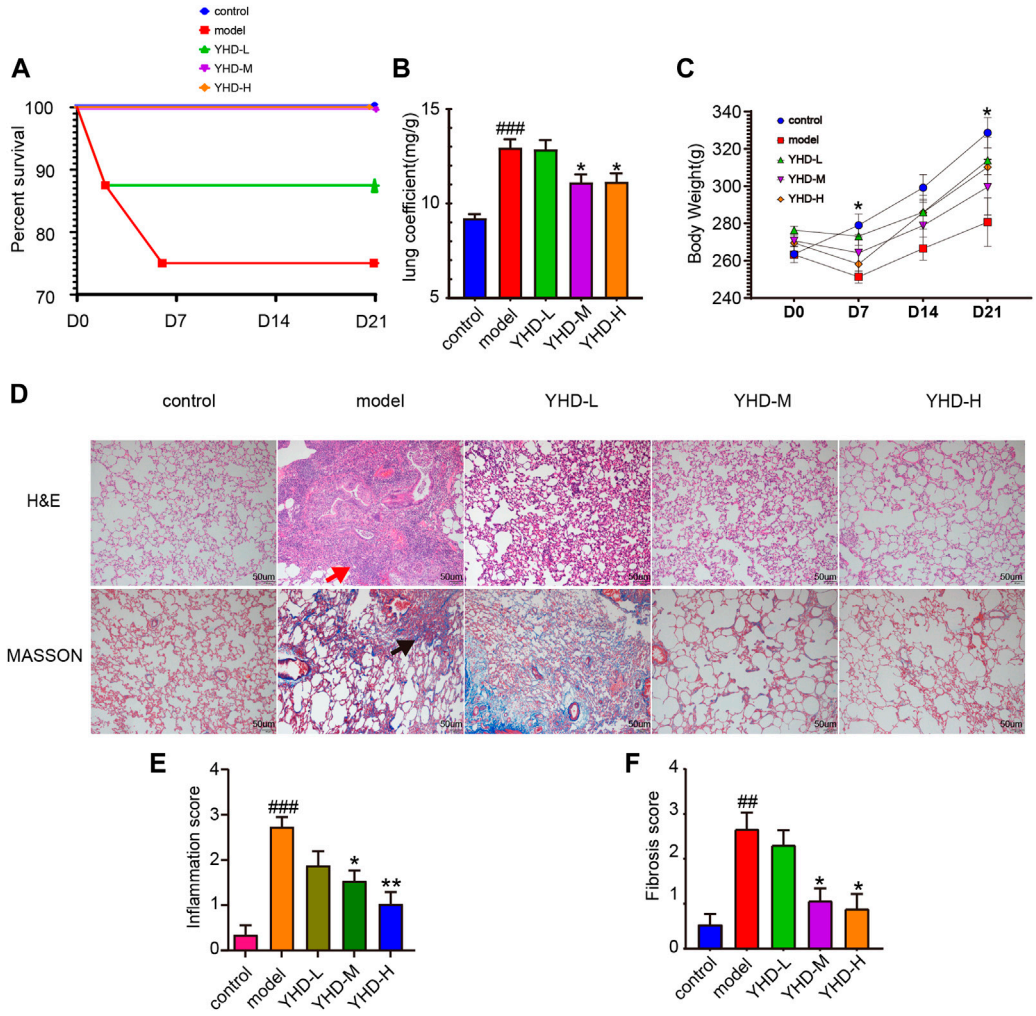

FIGURE 3
YHD alleviated BLM-induced PF in the rats. **(A)** Percent survival. Total two rats in the model group died (on day 2 and day 6, respectively), and one in the low-dose YHD group died (on day 2). No rats died in the remaining three groups. Each group of rats ended up with at least 6 biological replicates. **(B)**Lung coefficient. **(C)**Body weight. On day 7 and day 21, there was a statistical difference between the control and model group (n = 6). **(D)** Hematoxylin-Eosin and Masson staining (scale bar = 50 um). Thickening of the alveolar septum, destruction of alveolar structure, massive inflammatory cell infiltration in the alveolar space and interstitium (red arrows), and blue collagen fibers (black arrows). **(E–F)** Inflammation and fibrosis score. Inflammation and fibrosis scores were assessed based on HE-stained and MASSON-stained sections, respectively. Data were presented as the means ± SEM. ###$p < 0.001$, compared with the control group; *$p < 0.05$, **$p < 0.01$, compared with the model group, respectively.

3.3 High-dose Yiqi HuaYu decoction improved lung function of fibrotic rats and inhibited collagen deposition in lung interstitium

It is well known that PF can compromise lung function. Since high-dose YHD exhibited better therapeutic effects, we evaluated the improvement effect of high-dose YHD on lung function. High airway resistance is indicated by increased specific airway resistance (sRaw) and decreased specific airway conductance (sGaw). Decreased functional residual capacity (FRC) suggests alveolar contraction or collapse. Lung function results showed that sRaw and minute volume (MV) were elevated, while sGaw and FRC were decreased in model rats compared to control rats. After using high-dose YHD, sGaw and FRC increased, and sRaw decreased compared with the model rat (Figures 4A–D). These data indicated that high-dose YHD alleviated BLM-induced alveolar collapse and decreased airway resistance. High expression of α-SMA and excessive collagen deposition (mainly type I and type III) are characteristics of PF. By immunohistochemical staining of lung sections, we observed that a large amount of collagen (type I and type III) and α-SMA proteins were deposited in the lung interstitium of rats in the model group. However, high-dose YHD significantly reduced the expression of collagen protein (type I and III) and α-SMA (Figures 4F–I). In addition, hydroxyproline (HYP), an

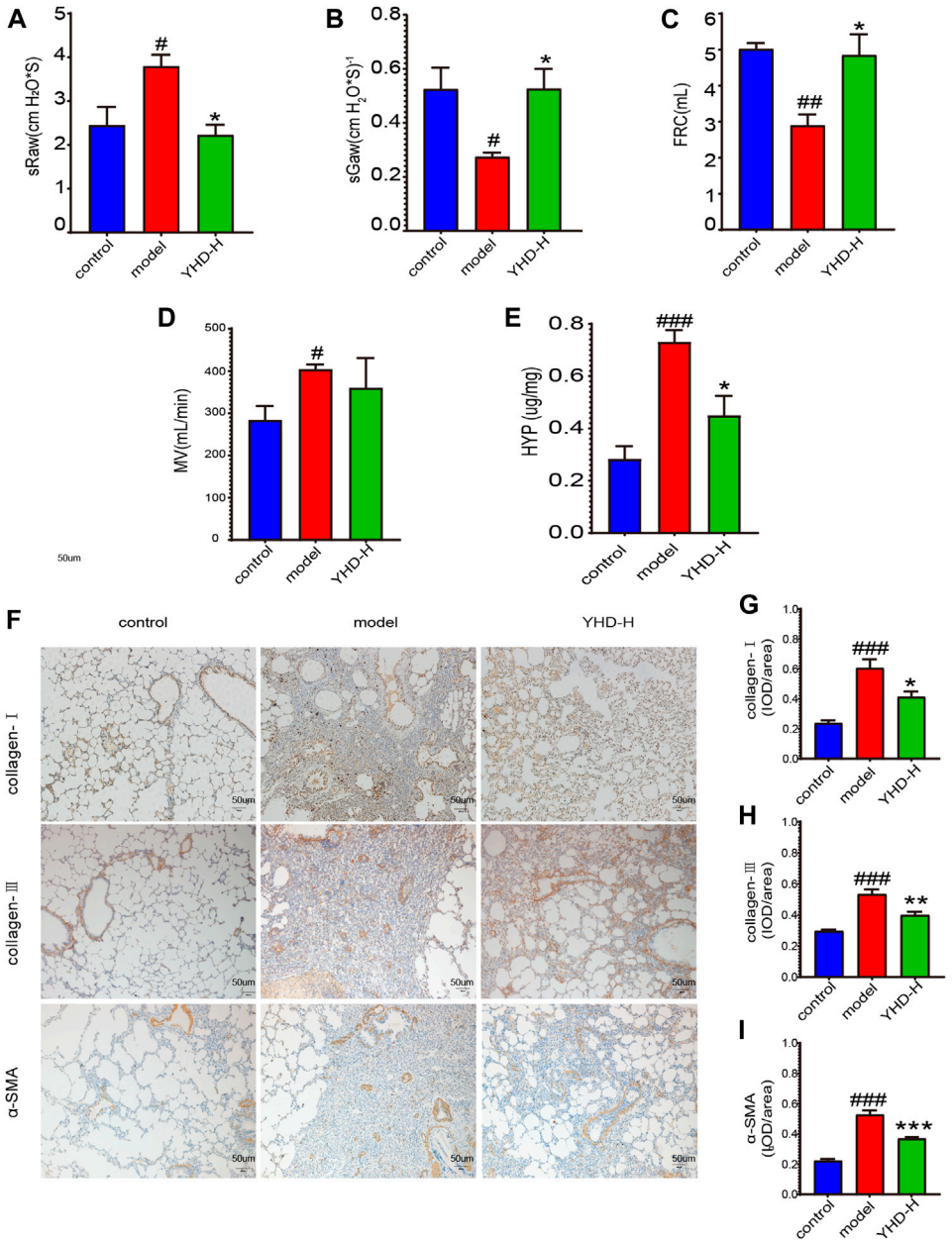

FIGURE 4
High-dose YHD improved lung function of fibrotic rats and inhibited collagen deposition in lung interstitium. **(A–D)** Lung function indicators: specific airway resistance (sRaw), specific airway conductance (sGaw), functional residual capacity (FRC), and minute volume (MV). **(E)** Hydroxyproline content. **(F)** Effects of high-dose YHD on pulmonary fibrosis by immunohistochemistry (scale bar = 50 um). **(G–I)** Image-Pro Plus software was used to statistically analyze the immunohistochemical staining results of collagen-Ⅰ, collagen-Ⅲ, and α-SMA. Data were presented as the means ± SEM ($n = 6$). #$p < 0.05$, ##$p < 0.01$, ###$p < 0.001$, compared with the control group; *$p < 0.05$, **$p < 0.01$, ***$p < 0.01$, compared with the model group, respectively.

essential component of collagen synthesis, was also measured (Medugorac, 1980). The lung tissue of rats in the model group contained more HYP compared with the control group ($p < 0.001$). Conversely, high-dose YHD decreased lung hydroxyproline levels in fibrotic rats (Figure 4E). These results indicate that YHD can reduce collagen deposition and activation of myofibroblasts.

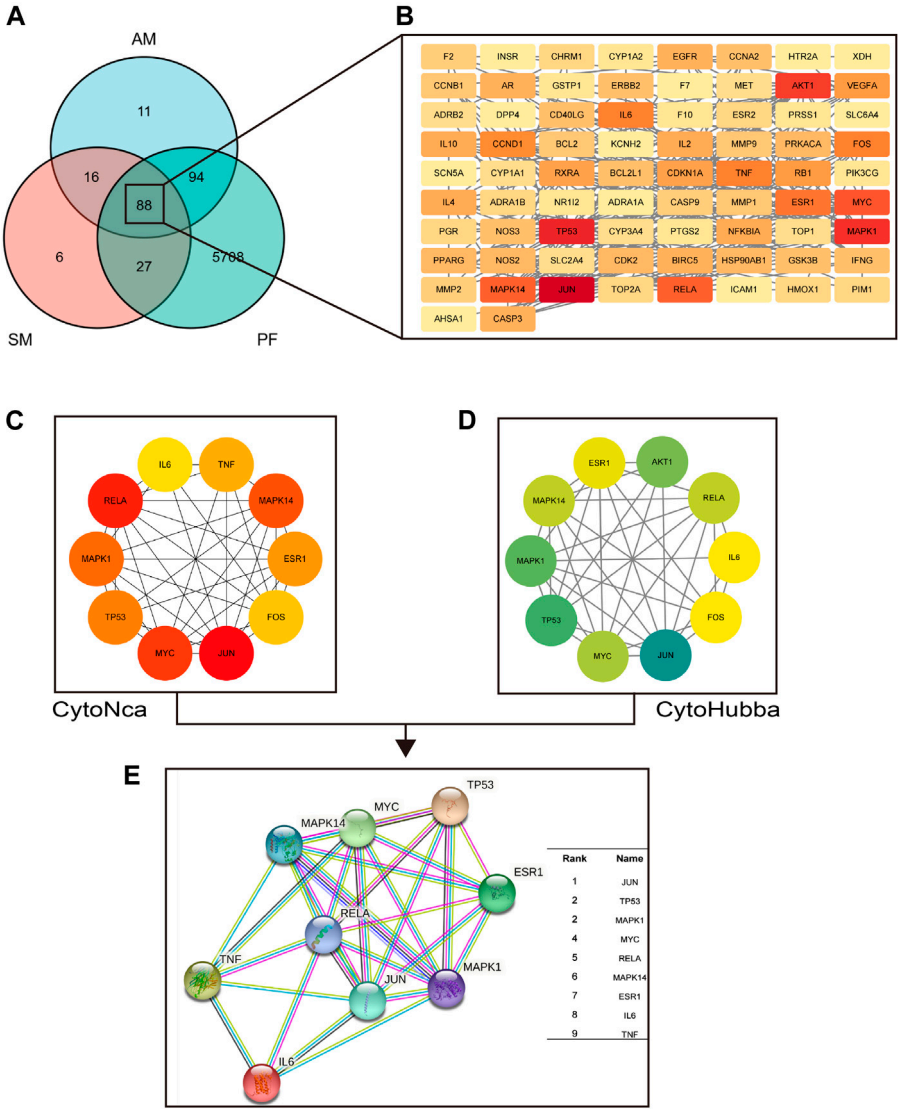

FIGURE 5
The hub target proteins of YHD in treating PF screened by network pharmacology. **(A–B)** the common target proteins between YHD and PF. Red nodes represent critical target proteins. **(C)** the top 10 target proteins screened by CytoNca algorithms. **(D)** the top 10 target proteins screened by CytoHubba algorithms. **(E)** the nine most critical target proteins obtained from the intersection. Two different algorithms screened target proteins, and the intersection was taken to obtain the most critical target proteins.

3.4 Network pharmacology

3.4.1 Identification of the theoretical active compounds and proteins targets of Yiqi HuaYu decoction

YHD effective compounds were collected from UHPLC-MS/MS analysis and the TCMSP database. Compounds that meet the requirements of oral bioavailability (OB) ≥ 30% and drug-like (DL) index≥0.18 can be considered potential drug candidate active ingredients (Xia et al., 2020). We screened 20 active compounds of *Astragalus* menbrunucrus (AM) and 65 active compounds of Salvia miltiorrhiza (SM). Supplementary Table S2 contains detailed information on these active compounds. Then, using the screened active compounds, we identified 209 a.m. target genes and 137 S M target genes from databases (TCMSP, HERB, and Swiss Target Prediction). In addition, we identified 5,917 pulmonary fibrosis (PF) target genes from databases (Drugbank, Genecards, HERB, and TTD). Finally, by taking the intersection, we get 88 overlapping common protein targets among AM, SM, and PF (Figure 5A). These common targets were used for further analysis. Supplementary Table S3 includes all target detail information.

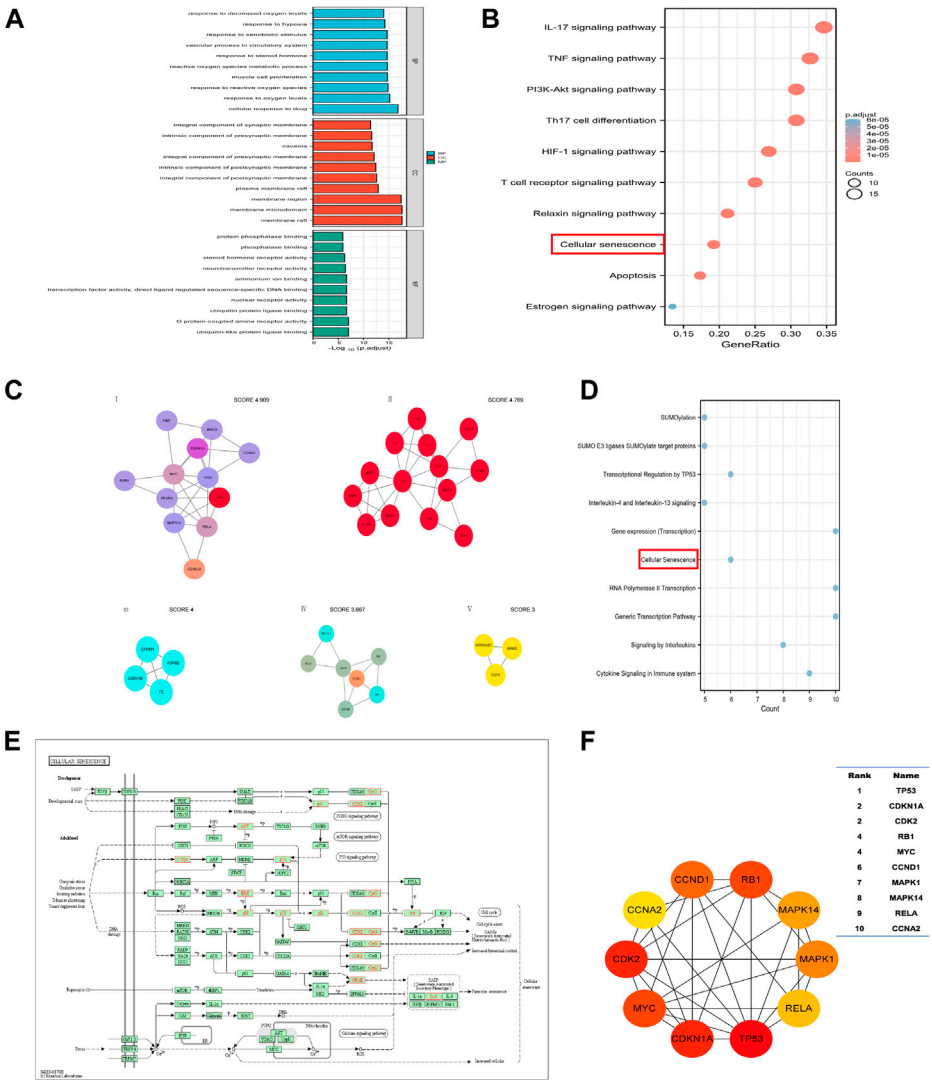

FIGURE 6
The critical pathways screened by network pharmacology. **(A)** GO enrichment analysis. **(B)** KEGG enrichment analysis. Cellular senescence signaling pathways were enriched for the first time. **(C)** The five clusters screed by MCODE analysis. **(D)** Reactome pathway enrichment analysis of the cluster I. The cellular senescence signaling pathway was again enriched. **(E–F)** The cellular senescence pathway and key markers (TP53/P53, CDKN1A/P21) on the pathway.

3.4.2 Hub target proteins and critical signal pathway

We could identify hub target proteins through the protein-protein interaction (PPI) network. Figure 5B shows the PPI network obtain from the STRING database. The nodes in red represent key hub proteins. In addition, we used two algorithms (CytoHubba and CytoNCA) to find the critical top ten proteins in 88 common targets (Figures 5C,D). Finally, by taking the intersection, we found nine key proteins (Figure 5E): JUN, TP53, MAPK1, MYC, RELA, MAPK14, ESR1, IL-6, and TNF.

Enrichment analysis can identify key signaling pathways and biological functions. The categories covered by GO enrichment analysis were molecular function (MF), cellular component (CC), and biological process (BP). Based on the 88 common targets, we obtained 174 KEGG pathways and 2513 GO terms, including 2266 BP, 81 CC, and 166 MF. As shown in Figure 6A, the top 10 terms in BP, CC, and MF are listed. The most enriched BP terms were associated with oxygen metabolism, including response to oxygen levels, response to reactive oxygen species, reactive oxygen species metabolic process, response to hypoxia, and response to decreased oxygen levels. We screened out the top 10 signaling pathways related to PF (Figure 6B). These pathways are mainly related to the inflammatory response (IL-17 signaling pathway and TNF signaling pathway), immune response (Th17 cell

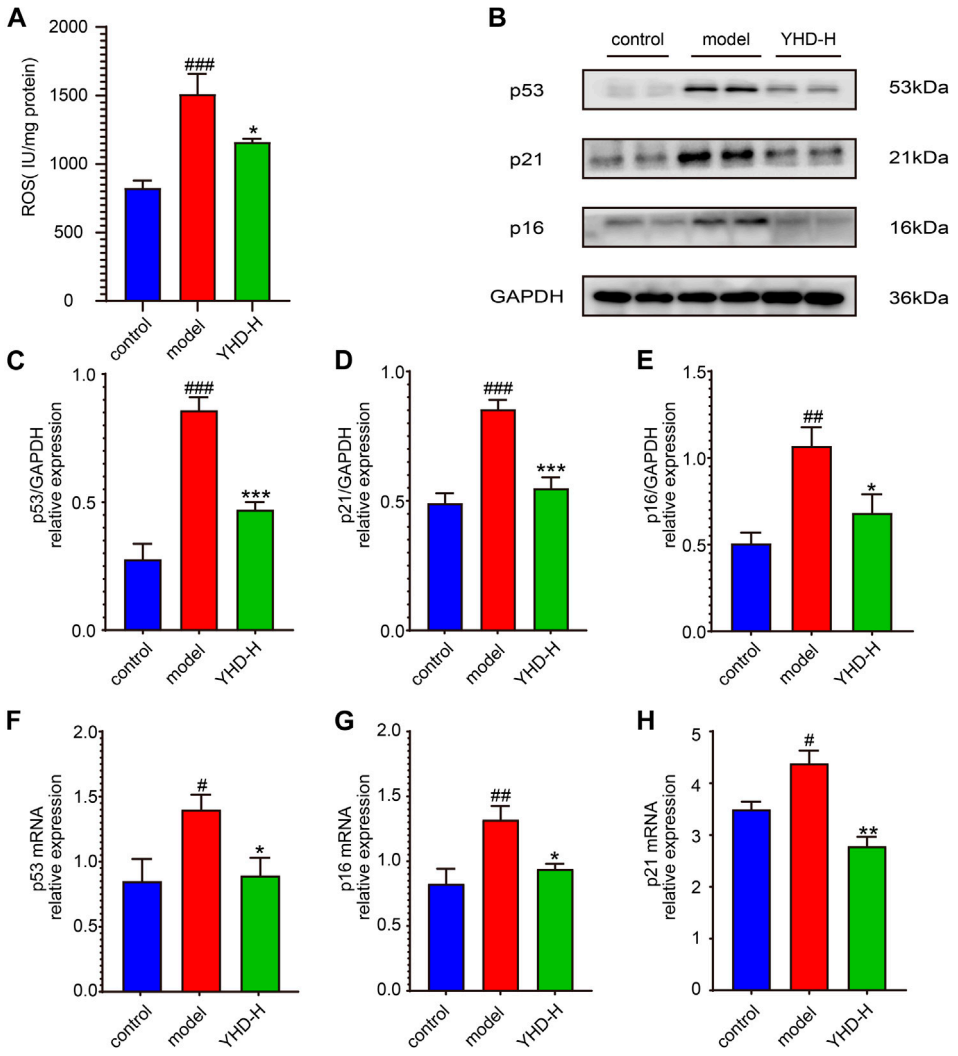

FIGURE 7
High-dose YHD inhibited cellular senescence. **(A)** the relative content of ROS in the lung tissue. **(B)** Western blotting of p53, p21, and p16 in the lung of fibrotic rats. **(C–E)** The relative protein expression of p53, p21, and p16 in the lung. **(F–H)** The relative gene expression of p53, p21, and p16 in the lung by rt-qPCR. Data were presented as the means ± SEM (n = 6 each group). #p < 0.05, ##p < 0.01, ###p < 0.001, compared with the control group; *p < 0.05, **p < 0.01, ***p < 0.001, compared with the model group.

differentiation and T cell receptor signaling pathway), and cell cycle regulation (apoptosis and cellular senescence).

Molecular Complex Detection (MCODE) analysis can screen out key functional modules of molecular networks. Through MCODE, we obtained 5 key cluster subnetworks (Figure 6C). Each clustering subnetwork is scored, with higher scores representing more critical. We performed Reactome pathway analysis on the first cluster subnetwork and found that cellular senescence signaling pathways were enriched again (Figure 6D). Figure 6E shows a cellular senescence signaling pathway diagram, with red labels representing 13 target proteins enriched in this pathway. Figure 6F shows the top ten proteins among the 13 senescence-related proteins, and the upper right table shows their degree rankings.

3.5 High-dose Yiqi HuaYu decoction inhibited cellular senescence

Because the cellular senescence pathway is enriched multiple times, we examined the key markers TP53 (p53) and CDKN1A (p21) on this pathway. In addition, CDKN2A (p16), another key marker of cellular senescence, was detected despite not being captured by network pharmacology. On both the protein and gene levels, the lung tissues of the model rats showed significantly higher expression of p53, p21, and p16 than the control group. Nevertheless, high-dose YHD significantly decreased the expression of these senescence markers (Figures 7B–H).

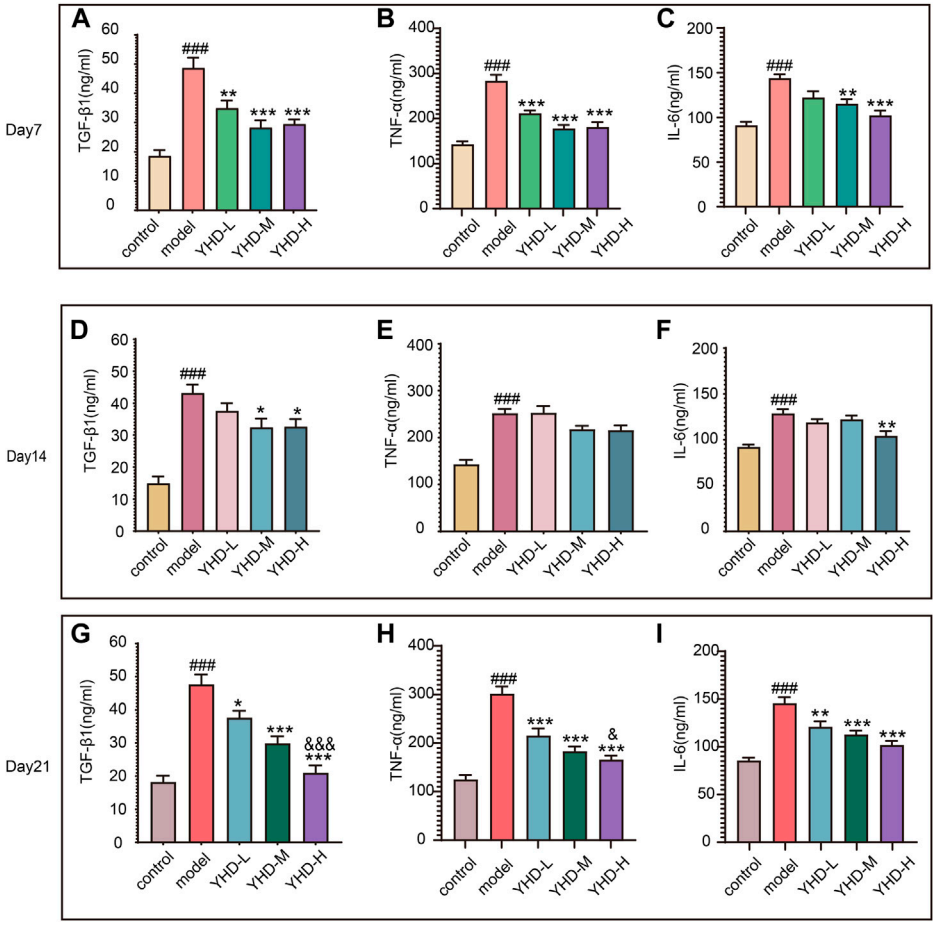

FIGURE 8
High-dose YHD inhibited SASPs. Senescent cells can secrete a combination of factors collectively known as the SASPs, including TGF-β1, TNF-α, and IL-6. The content of TGF-β1, TNF-α, and IL-6 in rat orbital blood by ELISAs once a week (on day 7, day 14, and day 21). Data were presented as the means ± SEM (n = 6 each group). #p < 0.05, ##p < 0.01, ###p < 0.001, compared with the control group; *p < 0.05, **p < 0.01, ***p < 0.001, compared with the model group; &p < 0.05, &&p < 0.01, &&&p < 0.001, compared with the low-dose YHD group.

Increased reactive oxygen species (ROS) can induce cellular senescence, so we examined ROS expression in lung tissue (Figure 7A). As expected, the model rats had significantly higher levels of ROS in their lung tissue than the control rats (p < 0.001), while high-dose YHD could reduce its expression (p < 0.05).

Senescent cells can secrete various cytokines collectively known as the SASPs, including TGF-β1, TNF-α, and IL-6. SASPs can reinforce the senescence program and influence the tissue microenvironment. Therefore, we detected the contents of SASPs (TGF-β1, TNF-α, and IL-6) in rat orbital blood by ELISA once a week. ELISA results showed that the levels of TGF-β1, TNF-α, and IL-6 in the serum of model rats were significantly increased on day 7, 14, and 21 compared with the control group (p < 0.001). Conversely, different doses of YHD could decrease the content of these SASPs and show a significant gradient effect (Figures 8A–I).

Taken together, these results suggest that YHD can inhibit senescence and SASPs.

4 Discussion

There is currently no cure for PF, which frequently leads to organ failure and death (Moss et al., 2022). TCM is an excellent resource for drug innovation discovery, and we try to find shortcuts to treating PF from this treasure trove. Practitioners of TCM believe that the pathogenesis of PF is mainly Qi deficiency and blood stasis, so the therapy strategy is to tonify qi, activate blood, and remove stasis (Li and Kan, 2017). YHD consists of two botanical drugs: *Astragalus* mongholicus Bunge (AM) and Salvia miltiorrhiza Bunge (SM). Data mining analysis of TCM clinical prescriptions showed that AM and SM were the most frequently used herbs for tonifying Qi and activating Blood,

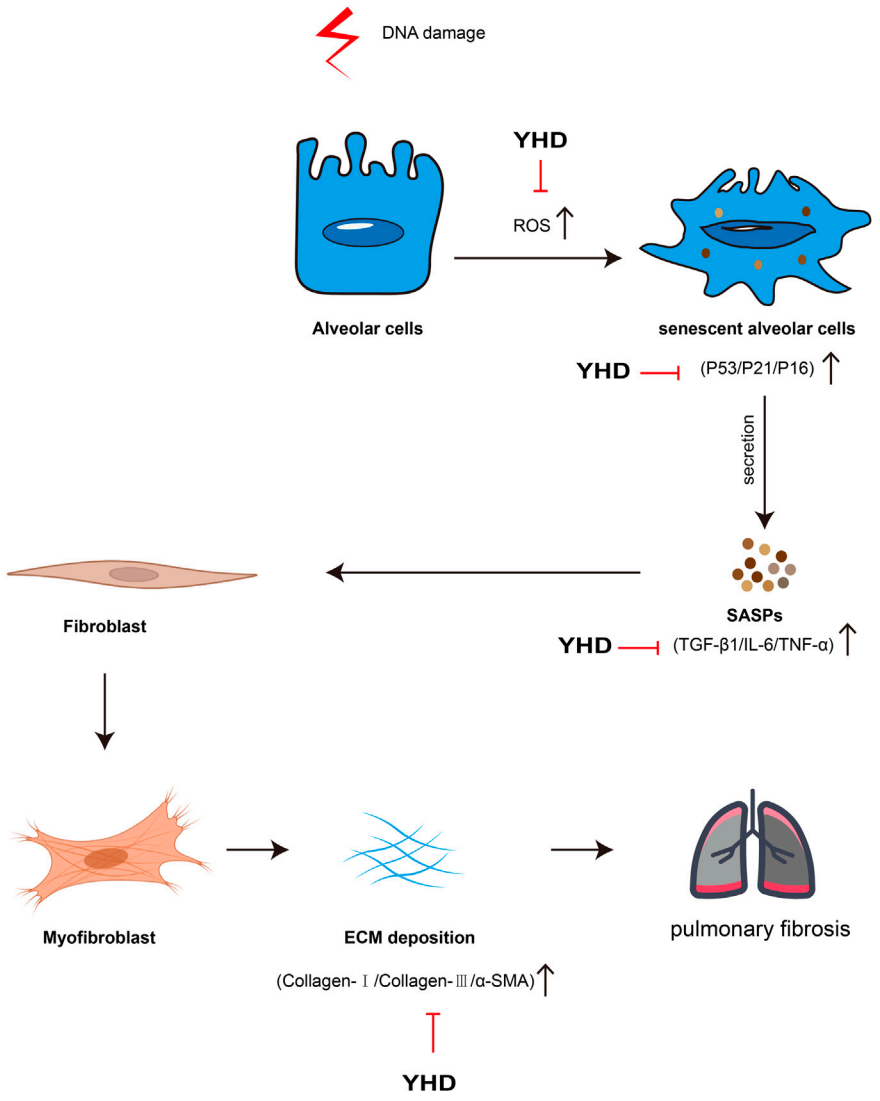

FIGURE 9
Schematic of Mechanism of YHD in treating PF. The red arrows indicate inhibitory effects.

respectively (Zhang et al., 2018). In our study, we confirmed the efficacy of YHD in an animal model and preliminarily explored the underlying mechanisms of this drug. The mechanism of YHD for PF is shown in Figure 9. Our study lays the foundation for developing novel drugs for PF while providing evidence support for the clinical promotion of YHD.

The diagnosis of PF and assessment of drug efficacy are difficult in clinical practice (Richeldi et al., 2017). Therefore, we assessed the efficacy of YHD by a comprehensive evaluation of body weight, lung coefficients, lung function, and pathological lung structures. We used BLM for the PF model, which is currently the most widely used animal model (Martinez et al., 2017). Our study demonstrated that YHD treatment significantly improved BLM-induced weight loss and pathological lung changes in rats. Excessive collagen deposition and myofibroblast activation are features of PF, and the high expression of α-SMA is a marker of myofibroblast activation (Moss et al., 2022). Previous studies have shown that YHD can inhibit collagen deposition (He et al., 2012). Consistent with their results, we found that YHD notably decreased the content of collagen (type Ⅰ and type Ⅲ) and α-SMA in fibrotic lung tissues. To better meet clinical criteria, we examined fibrotic rats' lung function. YHD could significantly improve high airway resistance in fibrotic rats. To summarize, these results demonstrated that YHD mitigated BLM-induced PF.

Cellular senescence is thought to be a major driver of the malignant progression of PF (Schafer et al., 2017). The process of cellular senescence is caused by multiple physiological and

pathological stresses that result in a permanent cell cycle arrest (Muñoz-Espín and Serrano, 2014). Cellular senescence consists of replicative and stress-related senescence (Hernandez-Segura et al., 2018). Replicative senescence is mainly due to the activation of p53 after DNA damage. Stress-related senescence is mainly due to oxidative stress damage, which activates the cyclin-dependent kinase inhibitor p16. Both pathways can activate the downstream cyclin-dependent kinase inhibitor p21 (Barnes et al., 2019). Activating p21 causes cells to exit the cell cycle, resulting in a permanent cell cycle arrest (Lv et al., 2021). In a recent study, researchers found that p53 and p21 were significantly highly expressed in the lung tissue of PF patients. Moreover, pifithrin-α, a specific p53 inhibitor, can reduce the senescence of type II alveolar cells, thereby alleviating experimental pulmonary fibrosis (Yao et al., 2021). We found that YHD inhibited cellular senescence markers, as evidenced by decreased gene and protein expression of p53, p21, and p16.

Despite being in a state of cell cycle arrest, senescent lung epithelial cells are still metabolically active (Yao et al., 2021). These senescent cells can secrete various growth factors, cytokines, and proteases, known as SASPs. Unfortunately, the SASPs cause low-grade chronic inflammation, which further triggers senescence and massive accumulation of extracellular matrix (Hernandez-Segura et al., 2018). Our experiment dynamically detected the levels of SASPs (TGF-β1, TNF-α, and IL-6) in rat serum. ELISA results showed that the progression of PF was accompanied by continuous stimulation of these SASPs. High-dose YHD consistently suppressed the expression of these SASPs in serum during the progress of PF. These results suggest that YHD can inhibit cellular senescence and SASPs, which may be beneficial in explaining the anti-fibrotic mechanism of YHD.

However, our study has some limitations. Because YHD intervention is difficult to perform on cell experiments, next, we will continue to screen active compounds of YHD and further explore their anti-fibrotic mechanisms.

5 Conclusion

In conclusion, our study suggests that YHD improves lung pathological injury and lung function in PF rats. This protective effect may be related to the ability of YHD to inhibit cellular senescence.

Data availability statement

The datasets presented in this study can be found in online repositories. The names of the repository/repositories and accession number(s) can be found in the article/Supplementary Material.

Ethics statement

The animal study was reviewed and approved by the Ethics Committee of Chongqing Medical University.

Author contributions

Conception and design: BZ, LZ, and W-FC. Acquisition of data: LZ, SY, and CX. Analysis of data: BZ, LZ, Y-DZ, X-QD, and Z-WC. Interpretation of data: Y-DZ, X-QD, Z-WC, and W-FC. Drafting the manuscript: BZ, LZ, and W-FC. Revising the manuscript: All authors. All authors have approved the final version to be published and agree to be responsible for all aspects of the work.

Funding

The research was supported by the National Natural Science Foundation of China (No. 81573860). The authors thank the National Natural Science Foundation of China for its financial support.

Acknowledgments

We thank the authors for the development of the database and software used in this paper.

Conflict of interest

The authors declare that the research was conducted in the absence of any commercial or financial relationships that could be construed as a potential conflict of interest.

Publisher's note

Supplementary material

The Supplementary Material for this article can be found online at: https://www.frontiersin.org/articles/10.3389/fphar.2022.1033919/full#supplementary-material

References

Apweiler, R., Bairoch, A., Wu, C. H., Barker, W. C., Boeckmann, B., Ferro, S., et al. (2004). UniProt: The universal protein knowledgebase. *Nucleic Acids Res.* 32, D115–D119. doi:10.1093/nar/gkh131

Aul, D. R., Gates, D. J., Draper, D. A., Dunleavy, D. A., Ruickbie, D. S., Meredith, D. H., et al. (2021). Complications after discharge with COVID-19 infection and risk factors associated with development of post-COVID pulmonary fibrosis. *Respir. Med.* 188, 106602. doi:10.1016/j.rmed.2021.106602

Bader, G. D., and Hogue, C. W. V. (2003). *An automated method for finding molecular complexes in large protein interaction networks*, 2.

Barnes, P. J., Baker, J., and Donnelly, L. E. (2019). Cellular senescence as a mechanism and target in chronic lung diseases. *Am. J. Respir. Crit. Care Med.* 200 (5), 556–564. doi:10.1164/rccm.201810-1975TR

Chen, X., Ji, Z. L., and Chen, Y. Z. (2002). TTD: Therapeutic target database. *Nucleic Acids Res.* 30 (1), 412–415. doi:10.1093/nar/30.1.412

Chin, C., Chen, S., Wu, H., Ho, C., Ko, M., and Lin, C. (2014). cytoHubba: identifying hub objects and sub-networks from complex interactome. *BMC Syst. Biol.* 8 (4), S11. doi:10.1186/1752-0509-8-S4-S11

Damian, S., Andrea, F., Michael, K., Milan, S., Alexander, R., Pablo, M., et al. (2011). The STRING database in 2011: Functional interaction networks of proteins, globally integrated and scored. *Nucleic Acids Res.* 39, 561–568. doi:10.1093/nar/gkq973

Dennis, G. J., Sherman, B. T., Hosack, D. A., Yang, J., Gao, W., Lane, H. C., et al. (2003). DAVID: Database for annotation, visualization, and integrated discovery. *Genome Biol.* 4 (5), P3. doi:10.1186/gb-2003-4-5-p3

Fang, S., Dong, L., Liu, L., Guo, J., Zhao, L., Zhang, J., et al. (2021). HERB: A high-throughput experiment- and reference-guided database of traditional Chinese medicine. *Nucleic Acids Res.* 49 (D1), D1197–D1206. doi:10.1093/nar/gkaa1063

Gentile, F., Aimo, A., Forfori, F., Catapano, G., Clemente, A., Cademartiri, F., et al. (2020). COVID-19 and risk of pulmonary fibrosis: The importance of planning ahead. *Eur. J. Prev. Cardiol.* 27 (13), 1442–1446. doi:10.1177/2047487320932695

Gfeller, D., Grosdidier, A., Wirth, M., Daina, A., Michielin, O., and Zoete, V. (2014). SwissTargetPrediction: A web server for target prediction of bioactive small molecules. *Nucleic Acids Res.* 42, W32–W38. doi:10.1093/nar/gku293

Han, C., Jiang, Y., Li, W., and Liu, Y. (2021). Astragalus membranaceus and Salvia miltiorrhiza ameliorates cyclosporin A-induced chronic nephrotoxicity through the "gut-kidney axis. *J. Ethnopharmacol.* 269, 113768. doi:10.1016/j.jep.2020.113768

Harris, M. A., Clark, J., Ireland, A., Lomax, J., Ashburner, M., Foulger, R., et al. (2004). The Gene Ontology (GO) database and informatics resource. *Nucleic Acids Res.* 32, D258–D261. doi:10.1093/nar/gkh036

He, S., Yang, Y., Liu, X., Huang, W., Zhang, X., Yang, S., et al. (2012). Compound Astragalus and Salvia miltiorrhiza extract inhibits cell proliferation, invasion and collagen synthesis in keloid fibroblasts by mediating transforming growth factor-β/Smad pathway. *Br. J. Dermatol.* 166 (3), 564–574. doi:10.1111/j.1365-2133.2011.10674.x

Hernandez-Segura, A., Nehme, J., and Demaria, M. (2018). Hallmarks of cellular senescence. *Trends Cell Biol.* 28 (6), 436–453. doi:10.1016/j.tcb.2018.02.001

Joshi-Tope, G., Gillespie, M., Vastrik, I., D'Eustachio, P., Schmidt, E., de Bono, B., et al. (2005). Reactome: A knowledgebase of biological pathways. *Nucleic Acids Res.* 33, D428–D432. doi:10.1093/nar/gki072

Justice, J. N., Nambiar, A. M., Tchkonia, T., Lebrasseur, N. K., Pascual, R., Hashmi, S. K., et al. (2019). Senolytics in idiopathic pulmonary fibrosis: Results from a first-in-human, open-label, pilot study. *EBioMedicine* 40, 554–563. doi:10.1016/j.ebiom.2018.12.052

Kadota, T., Fujita, Y., Yoshioka, Y., Araya, J., Kuwano, K., and Ochiya, T. (2018). Emerging role of extracellular vesicles as a senescence-associated secretory phenotype: Insights into the pathophysiology of lung diseases. *Mol. Asp. Med.* 60, 92–103. doi:10.1016/j.mam.2017.11.005

Kanehisa, M., and Goto, S. (2000). KEGG: Kyoto encyclopedia of genes and genomes. *Nucleic Acids Res.* 28 (1), 27–30. doi:10.1093/nar/28.1.27

Li, L., and Kan, L. (2017). Traditional Chinese medicine for pulmonary fibrosis therapy: Progress and future prospects. *J. Ethnopharmacol.* 198, 45–63. doi:10.1016/j.jep.2016.12.042

Lv, X., Liu, C., Liu, S., Li, Y., Wang, W., Li, K., et al. (2021). The cell cycle inhibitor P21 promotes the development of pulmonary fibrosis by suppressing lung alveolar regeneration. *Acta Pharm. Sin. B* 12, 735–746. doi:10.1016/j.apsb.2021.07.015

Martinez, F. J., Collard, H. R., Pardo, A., Raghu, G., Richeldi, L., Selman, M., et al. (2017). Idiopathic pulmonary fibrosis. *Nat. Rev. Dis. Prim.* 3 (1), 17074. doi:10.1038/nrdp.2017.74

Medugorac, I. (1980). Collagen content in different areas of normal and hypertrophied rat myocardium. *Cardiovasc. Res.* 14 (9), 551–554. doi:10.1093/cvr/14.9.551

Merkt, W., Bueno, M., Mora, A. L., and Lagares, D. (2020). Senotherapeutics: Targeting senescence in idiopathic pulmonary fibrosis. *Semin. Cell Dev. Biol.* 101, 104–110. doi:10.1016/j.semcdb.2019.12.008

Moss, B. J., Ryter, S. W., and Rosas, I. O. (2022). Pathogenic mechanisms underlying idiopathic pulmonary fibrosis. *Annu. Rev. Pathol.* 17 (1), 515–546. doi:10.1146/annurev-pathol-042320-030240

Muñoz-Espín, D., and Serrano, M. (2014). Cellular senescence: From physiology to pathology. *Nat. Rev. Mol. Cell Biol.* 15 (7), 482–496. doi:10.1038/nrm3823

Qin, L., Tan, H., Wang, Y., Xu, C., Feng, J., Li, M., et al. (2018). Astragalus membranaceus and salvia miltiorrhiza ameliorate lipopolysaccharide-induced acute lung injury in rats by regulating the toll-like receptor 4/nuclear factor-kappa B signaling pathway. *Evid. Based. Complement. Altern. Med.* 2018, 3017571. doi:10.1155/2018/3017571

Rebhan, M., Chalifa-Caspi, V., Prilusky, J., and Lancet, D. (1997). GeneCards: Integrating information about genes, proteins and diseases. *Trends Genet.* 13 (4), 163. doi:10.1016/s0168-9525(97)01103-7

Richeldi, L., Collard, H. R., and Jones, M. G. (2017). Idiopathic pulmonary fibrosis. *Lancet* 389 (10082), 1941–1952. doi:10.1016/S0140-6736(17)30866-8

Ru, J., Li, P., Wang, J., Zhou, W., Li, B., Huang, C., et al. (2014). TCMSP: A database of systems pharmacology for drug discovery from herbal medicines. *J. Cheminform.* 6, 13. doi:10.1186/1758-2946-6-13

Schafer, M. J., White, T. A., Iijima, K., Haak, A. J., Ligresti, G., Atkinson, E. J., et al. (2017). Cellular senescence mediates fibrotic pulmonary disease. *Nat. Commun.* 8, 14532. doi:10.1038/ncomms14532

Shen, M., Nan, Y., Zhang, L., Di, L., He, S., Li, Y., et al. (2020). Maimendong decoction improves pulmonary function in rats with idiopathic pulmonary fibrosis by inhibiting endoplasmic reticulum stress in AECIIs. *Front. Pharmacol.* 11, 1262. doi:10.3389/fphar.2020.01262

Spagnolo, P., Balestro, E., Aliberti, S., Cocconcelli, E., Biondini, D., Casa, G. D., et al. (2020). Pulmonary fibrosis secondary to COVID-19: A call to arms? The lancet. *Lancet. Respir. Med.* 8 (8), 750–752. doi:10.1016/S2213-2600(20)30222-8

Spagnolo, P., Kropski, J. A., Jones, M. G., Lee, J. S., Rossi, G., Karampitsakos, T., et al. (2021). Idiopathic pulmonary fibrosis: Disease mechanisms and drug development. *Pharmacol. Ther.* 222, 107798. doi:10.1016/j.pharmthera.2020.107798

Szapiel, S. V., Elson, N. A., Fulmer, J. D., Hunninghake, G. W., and Crystal, R. G. (1979). Bleomycin-induced interstitial pulmonary disease in the nude, athymic mouse. *Am. Rev. Respir. Dis.* 120 (4), 893–899. doi:10.1164/arrd.1979.120.4.893

Tang, Y., Li, M., Wang, J., Pan, Y., and Wu, F. (2015). CytoNCA: A cytoscape plugin for centrality analysis and evaluation of protein interaction networks. *Biosystems.* 127, 67–72. doi:10.1016/j.biosystems.2014.11.005

Tanni, S. E., Fabro, A. T., de Albuquerque, A., Ferreira, E. V. M., Verrastro, C. G. Y., Sawamura, M. V. Y., et al. (2021). Pulmonary fibrosis secondary to COVID-19: A narrative review. *Expert Rev. Respir. Med.* 15 (6), 791–803. doi:10.1080/17476348.2021.1916472

Wishart, D. S., Knox, C., Guo, A. C., Cheng, D., Shrivastava, S., Tzur, D., et al. (2008). DrugBank: A knowledgebase for drugs, drug actions and drug targets. *Nucleic Acids Res.* 36, D901–D906. doi:10.1093/nar/gkm958

Wissler Gerdes, E. O., Misra, A., Netto, J. M. E., Tchkonia, T., and Kirkland, J. L. (2021). Strategies for late phase preclinical and early clinical trials of senolytics. *Mech. Ageing Dev.* 200, 111591. doi:10.1016/j.mad.2021.111591

Xia, Q., Xun, Y., Lu, J., Lu, Y., Yang, Y., Zhou, P., et al. (2020). Network pharmacology and molecular docking analyses on Lianhua Qingwen capsule indicate Akt1 is a potential target to treat and prevent COVID-19. *Cell Proliferat.* 53 (12), e12949. doi:10.1111/cpr.12949

Yao, C., Guan, X., Carraro, G., Parimon, T., Liu, X., Huang, G., et al. (2021). Senescence of alveolar type 2 cells drives progressive pulmonary fibrosis. *Am. J. Respir. Crit. Care Med.* 203 (6), 707–717. doi:10.1164/rccm.202004-1274OC

Yu, G., Wang, L., Han, Y., and He, Q. (2012). clusterProfiler: an R package for comparing biological themes among gene clusters. *Omics a J. Integr. Biol.* 16 (5), 284–287. doi:10.1089/omi.2011.0118

Zhang, S., Wu, H., Liu, J., Gu, H., Li, X., and Zhang, T. (2018). Medication regularity of pulmonary fibrosis treatment by contemporary traditional Chinese medicine experts based on data mining. *J. Thorac. Dis.* 10 (3), 1775–1787. doi:10.21037/jtd.2018.03.11

frontiers | Frontiers in Pharmacology

TYPE Original Research
PUBLISHED 07 November 2022
DOI 10.3389/fphar.2022.1034464

OPEN ACCESS

EDITED BY
Isaac Kirubakaran Sundar,
University of Kansas Medical Center,
United States

REVIEWED BY
Guido Veit,
McGill University, Canada
Agnieszka Siejka,
Medical University of Lodz, Poland

*CORRESPONDENCE
Pavel A. Solopov,
psolopov@odu.edu

SPECIALTY SECTION
This article was submitted to Respiratory Pharmacology,
a section of the journal
Frontiers in Pharmacology

RECEIVED 01 September 2022
ACCEPTED 19 October 2022
PUBLISHED 07 November 2022

CITATION
Solopov PA, Colunga Biancatelli RML, Dimitropolou C, Day T and Catravas JD (2022), Optimizing antidotal treatment with the oral HSP90 inhibitor TAS-116 against hydrochloric acid-induced pulmonary fibrosis in mice.
Front. Pharmacol. 13:1034464.
doi: 10.3389/fphar.2022.1034464

Optimizing antidotal treatment with the oral HSP90 inhibitor TAS-116 against hydrochloric acid-induced pulmonary fibrosis in mice

Pavel A. Solopov[1]*, Ruben Manuel Luciano Colunga Biancatelli[1], Christiana Dimitropolou[1], Tierney Day[1] and John D. Catravas[1,2]

[1]Frank Reidy Research Center for Bioelectrics, Old Dominion University, Norfolk, VA, United States, [2]School of Medical Diagnostic & Translational Sciences, College of Health Sciences, Old Dominion University, Norfolk, VA, United States

Exposure to high concentrations of hydrochloric acid (HCl) can lead to severe acute and chronic lung injury. In the aftermath of accidental spills, victims may be treated for the acute symptoms, but the chronic injury is often overlooked. We have developed a mouse model of acute and chronic lung injury, in which the peak of acute lung injury occurs on the day 4 after HCl exposure. We have also demonstrated that HSP90 inhibitors are effective antidotes when administered starting 24 h after HCl. In this study we examined the hypothesis that the novel oral HSP90 inhibitor TAS-116 can effectively ameliorate HCl-induced lung injury even when treatment starts at the peak of the acute injury, as late as 96 h after HCl. C57Bl/6J mice were intratracheally instilled with 0.1N HCl. After 24 or 96 h, TAS-116 treatment began (3.5, 7 or 14 mg/kg, 5 times per week, p. o.) for either 2,3 or 4 or weeks. TAS-116 moderated the HCl-induced alveolar inflammation, as reflected in the reduction of white blood cells and total protein content in bronchoalveolar lavage fluid (BALF), overexpression of NLRP3 inflammasome, and inhibited the activation of pro-fibrotic pathways. Furthermore, TAS-116 normalized lung mechanics and decreased the deposition of extracellular matrix proteins in the lungs of mice exposed to HCl. Delayed and shortened treatment with TAS-116, successfully blocked the adverse chronic effects associated with acute exposure to HCl.

KEYWORDS

idiopathic pulmonarry fibrosis, Hsp90 inhibitior, TAS-116, mice, hydrochloric acid

1 Introduction

HCl is one of the most used industrial chemical compounds in the world with numerous applications in oil and gas production, as a cleaning agent, and in the steel and leather industries. Accidental spills of HCl occur every year in industrial settings or during transportation. Acute exposure to high concentrations can cause severe acute and chronic, potentially fatal, lung injury (Occupational exposures to mists and, 1992). The National Research Council concluded that exposure to HCl results in pain, coughing, inflammation, edema and desquamation in the upper respiratory tract. High concentrations might also produce constriction of the larynx and bronchi and closure of the glottis (National Research Council (US) Committee on Acute Exposure Guideline Levels, 2010). A clinical study involving 170 fire fighters identified hydrogen chloride as an important contributor to respiratory symptoms and one fatal case with hemorrhage, edema, and inflammation of the lungs was reported (Dyer and Esch, 1976). Since in some cases symptoms appeared 2-to 3 days after the incident (Boyce and Simpson, 1996), the victims often do not seek medical attention immediately after exposure.

Heat shock protein 90 (HSP90) is an ATP-dependent molecular chaperone that is present in procaryotic and eucaryotic cells and facilitates the maturation of clients (kinases, transcription factors, signaling proteins, steroid hormone receptors, and numerous other proteins) that are involved in various cellular pathways (Schopf et al., 2017). Inhibition of HSP90 transforms the HSP90-client protein complex, leading to reduced activity, misfolding, ubiquitination and proteasomal degradation of client proteins (Butler et al., 2015). Association with a multiplicity of signaling pathways has positioned HSP90 as a promising target for cancer treatment. Recent studies suggest that HSP90 inhibitors may have antifibrotic properties (Sontake et al., 2017; Sanchez et al., 2020). A wealth of epidemiological studies demonstrates a strong correlation between organ fibrosis and cancer (Landolt et al., 2020). Experimental and clinical investigations suggest that these diseases have overlapping properties, such as activation of fibroblasts and growth factors, progressive extracellular matrix (ECM) deposition and similar pathogenic pathways (Piersma et al., 2020).

In previous studies we reported that 4-week treatment with HSP90 inhibitors (AUY-922, i. p. or AT13387, s. c.) administered starting 24 h after exposure to 0.1N HCl, successfully prevented chronic lung injury and pulmonary fibrosis in mice (Marinova et al., 2020; Colunga Biancatelli et al., 2022a). 4-(1H-pyrazolo[3,4-b] pyridine-1-yl) benzamide, or TAS-116, also known as Pimitespib, is a highly selective inhibitor of heat shock protein 90α and β, -with null activity on GRP94 or TRAP-1- that demonstrates potent antitumor activity and minimal toxicity compared to earlier generations of HSP90 inhibitors (Ohkubo et al., 2015). TAS-116 is structurally distinct from other HSP90 inhibitors and exhibits less hepatotoxicity and lacks the ability to penetrate the blood brain barrier (Doi et al., 2019). Moreover, oral bioavailability of this inhibitor allows for a more flexible dosing schedule compared with parenteral administration. In this study, we investigated the optimal dosing and windows of administration of TAS-116 against HCl-induced pulmonary fibrosis and chronic lung injury in mice.

2 Materials and methods

2.1 Materials

TAS-116 (Pimitespib) was purchased from MedChemExpress, HCl (37%), ACS grade, methacholine chloride USP grade, radioimmunoprecipitation assay (RIPA) buffer, and protease inhibitor cocktail were supplied from Sigma-Aldrich Corporation (St. Louis, MO, United States). Socumb (pentobarbital sodium) USP grade, AnaSed (xylazine) USP grade, and Ketaset (ketamine) USP grade were obtained by Henry Schein Animal Health (Pittsburg, PA, United States). Formaldehyde ACS reagent, 37 wt%, was purchased from ThermoFisher Scientific (Waltham, MA, United States), the BCA Protein assay kit from Pierce Co. (Rockford, IL, United States), EDTA and Amersham Protran 0.45 μm nitrocellulose blotting membranes from GE Healthcare (Chicago, IL, United States), TRIzol and SuperScript VILO reverse transcriptase kit from Invitrogen (Carlsbad, CA, United States), RNeasy Mini Kit from Qiagen (Hilden, Germany), and SYBR Green Master Mix from Applied Biosystems (Carlsbad, CA, United States). All primers used for real-time quantitative PCR were purchased from Integrated DNA Technologies, Inc. (Coralville, IA, United States). SDS-PAGE, ProtoGel (30% acrylamide mix), and TEMED were from National Diagnostics (Atlanta, GA, United States), Tris-HCl buffer from Teknova (Hollister, CA, United States), 10% sodium dodecyl sulfate (SDS) and ammonium persulfate (APS) from ThermoFisher Scientific, and Protein Dual Color Standards and Tricine Sample Buffer from Bio-Rad Laboratories (Hercules, CA, United States). For antibodies used in Western blotting, rabbit total and phosphorylated MAPK ERK 44-42 (Thr202/Tyr204), rabbit total and phosphorylated SMAD2 (Ser423/425), NLRP3 inflammasome antibodies were obtained from Cell Signaling Technology, Inc. (Danvers, MA, United States), mouse HSP90, rabbit Phospho-HSP90 (Ser226), Collagen Type I A2 and Mouse/Human TGF-β1 ELISA Kit were purchased from ThermoFisher Scientific. Mouse monoclonal β-actin antibody from Sigma-Aldrich Corporation (dilution 1: 1000), and IRDye 800CW Goat anti-rabbit and IRDye 680RD Goat anti-mouse antibodies (dilution 1:5000) from LI-COR Biosciences (Lincoln, NE, United States).

2.2 Ethical statement

Animal studies were approved by the Institutional Animal Care and Use Committee (IACUC) of Old Dominion University (Protocol #19-014), abide by the principles of animal experimentation as published by the American Physiological Society, and were carried out in Animal Biosafety Level 2 (ABSL-2) facility at the Frank Reidy Research Center for Bioelectrics, ODU, Norfolk, VA.

2.3 Animals and treatment groups

Male C57Bl/6J mice, obtained from Jackson Laboratories (Bar Harbor, ME, United States), 8–10 weeks old, 23–26 g body weight, were housed in pathogen-free facility. Animals were intratracheally instilled with vehicle (normal saline) or HCl (0.1 N) and treated after 24 h with either vehicle (10% DMSO in corn oil) or with the HSP90 inhibitor TAS-116 (3.5, 7 or 14 mg/kg). Mice were randomly divided into six treatment groups: 1) mice that were exposed to normal saline (VEH); 2) mice that were exposed to 0.1N HCl and treated with vehicle (10% DMSO in corn oil) 5 times/week p. o. *via* gavage needle (HCl); (Wong et al., 2018) mice that were exposed to 0.1N HCl and treated orally with TAS-116 7 mg/kg 5 x/week starting 24 h post-instillation for 4 weeks (TAS 24 h 4w); 4) mice that were exposed to 0.1N HCl and treated orally with TAS-116, 7 mg/kg, 5 times/week starting 96 h post-instillation for 4 weeks (TAS 96 h 4w); 5) mice that were exposed to 0.1N HCl and treated orally with TAS-116 7 mg/kg 5 x/week starting 96 h post-instillation for 3 weeks (TAS 96 h 3w); 6) mice that were exposed to 0.1N HCl and treated orally with TAS-116 7 mg/kg 5 times/week starting 96 h post-instillation for 2 weeks (TAS 96 h 2w). On day 0, mice were anesthetized with intraperitoneal (i.p.) injections of xylazine (6 mg/kg) and ketamine (60 mg/kg). An i. p. bolus of sterile saline (10 μl/g) was given as pre-emptive fluid resuscitation. The surgical field was cleaned and disinfected with Betadine and 70% alcohol, a 1 cm neck skin incision and blunt dissection of salivary glands were made to visualize the trachea. Mice were suspended in upright position from their incisors and a fine, (20G) plastic i. v. catheter was inserted into the trachea (~1.5 cm) in such a way that it could be seen through the rings of the trachea. Freshly prepared 0.1 N hydrochloric acid (groups 2–6) or sterile saline (group 1) was instilled (2 μL/g body weight) and flushed with 100 μl air. The catheter was withdrawn, the neck incision closed by the surgical adhesive, and the animals were placed in the ventral position in a small chamber with oxygen and observed constantly for the next 4 h for signs of respiratory distress. Mice were returned to their cages and monitored first day hourly and then daily for abnormal physical appearances. All analyses were performed at 30 days post instillation of HCl.

2.4 Bronchoalveolar lavage fluid white blood cell number and total protein concentration

BALF was obtained by instilling and withdrawing sterile 1 x PBS (1 ml) *via* a tracheal cannula, as we previously described (Solopov et al., 2020). The total number of leukocytes was counted using a hemocytometer. After the BALF was centrifuged at 2500 $\times g$ for 10 min, the supernatant was collected for total protein analysis. The protein concentration was estimated using a bicinchoninic acid (BCA) Protein Assay Kit according to manufacturer's protocol. BALF supernatant TGF-β1 was analyzed in triplicate *via* a mouse/human TGF-β1 coated ELISA kit.

2.5 Histopathology, immunohistochemistry and lung fibrosis scoring

Mice were euthanized, the chest was opened and the lungs were fixed with formalin and embedded in paraffin, as we previously described (Solopov et al., 2020). Sections 5 μm thick were prepared from the blocks and stained with Masson's trichrome and for Inflammasome NLR Family Pyrin Domain-Containing Protein 3 (NLRP3) at a dilution of 1:1280. Twenty randomly selected fields from each slide were examined under ×20 and ×40 magnifications. All the trichrome-stained slides were scored by the Ashcroft scoring scale to estimate the severity of pulmonary fibrosis (Ashcroft et al., 1988) by an investigator blinded to the identity of the animal groups.

2.6 Lung tissue collection

Immediately after euthanasia, the lungs were dissected from the thorax, snap-frozen, and prepared for subsequent analysis as we previously described (Solopov et al., 2020).

2.7 Western blot analysis

Proteins in lung tissue homogenates were extracted from snap-frozen lungs by sonication in ice-cold RIPA buffer with added protease inhibitor cocktail (100:1). The protein lysates were mixed under slow agitation for 3 h at 4°C, and then centrifuged twice at 14000× *g* for 10 min. The supernatants were gently aspirated, and total protein concentration was measured using the micro-BCA assay. The samples were first mixed with Tricine Sample Buffer, then heated up to 95°C for 10 min, then separated on a 10% polyacrylamide SDS gel by electrophoresis. Proteins were then transferred from the gel to a nitrocellulose membrane and incubated overnight with the

appropriate primary antibody (1:1000), followed by 1 h incubation with the secondary antibody (1:5000) and detection by digital fluorescence imaging (LI-COR Odyssey CLx, Dallas, TX, United States). β-actin was used as the housekeeping gene. Densitometry of the bands was performed with ImageJ v.1.8.0 (http://imagej.nih.gov/ij (last access on 15 March 2022); National Institutes of Health, Bethesda, MD, United States). For ERK1/2 and phospho-ERK1/2, both 44 and 42 kDa bands were quantified and then summed.

2.8 RNA isolation and quantitative real-time PCR

Lung tissue, stored in an RNA later solution, was homogenized in TRIzol followed by a cleaning step using the RNeasy Mini Kit. The purified RNA was transcribed into cDNA using the SuperScriptTM IV VILO Reverse transcriptase kit (Invitrogen, Carlsbad, CA, United States) and was analyzed by real-time qPCR with SYBR Green Master Mix on a StepOne Plus Real-Time PCR System (Applied Biosystems v.2.3). The results were evaluated using the standard curve method and were expressed as the fold of the control values, normalized to β-actin. Specifically designed primer pairs and qPCR conditions were applied to selectively determine the expression of mouse *β-actin*, *Fibronectin*, *Collagen 1α2*, and *Elastin*, as previously described (Colunga Biancatelli et al., 2021a; Solopov et al., 2021).

2.9 Lung mechanics measurements

The mice were anesthetized with Socumb (pentobarbital sodium 50 mg/kg, i. p.), tracheostomized with a metal 1.2 mm (internal diameter) cannula, and connected to a FlexiVent ventilator (SCIREQ Inc., Montreal, QC, Canada), as previously published (Colunga Biancatelli et al., 2021a). Ventilation was performed at a tidal volume of 10 ml/kg and a respiratory rate of 150/min. Firstly, following a deep inflation, pressure volume (PV) loops were estimated by stepwise increasing airway pressure to 30 cm H_2O and then reversing the process. PV loops reflect the intrinsic elasticity of the lungs and shifted to the right in fibrosis. Secondly, Snapshot-150 and Quick Prime-3 maneuvers were performed. Increasing concentrations of methacholine (to 50 mg/ml) were loaded into the nebulizer and administered to mice. Respiratory system resistance (Rrs) and elastance (Ers), reflecting the behavior of the entire respiratory system (peripheral and conducting airways, chest wall, and parenchyma); Tissue damping (G), reflecting resistance of the large, conducting airways, parenchymal stiffness, and changes in inspiratory gas dynamics, was calculated, and are presented as the mean of 12 recordings for each animal.

2.10 Statistical analysis

The results are presented as means ± standard error of the mean. Statistical significance of differences between groups was determined by the one- or two-way ANOVA analysis, followed by the Tukey's or Bonferroni's post-hoc test, utilized GraphPad Prism v. 9.0 (GraphPad, San Diego, CA, United States). The difference among groups was considered significant at $p < 0.05$.

3 Results

3.1 Estimation of the optimal therapeutic dose of the HSP90 inhibitor, TAS-116, against pulmonary fibrosis

First, we determined the effective therapeutic dose of TAS-116 as a protective agent against chronic lung injury and pulmonary fibrosis. Three different doses (3.5 mg/kg, 7 mg/kg and 14 mg/kg) were administrated *per os* 5 times/week to 0.1N HCl-challenged mice, starting 24 h after HCl; analyses were performed 30 days post HCl. Mice, instilled with HCl and treated with the inhibitor in the dose 3.5 mg/kg did not show significant improvement in any of the parameters measured (BALF cellularity, lung elastin and fibronectin mRNA levels, histology, Ashcroft score) compared to untreated mice (Figure 1). Both higher doses demonstrated significant decrease of leucocyte levels in BALF, deposition of fibronectin and improvement of parenchymal architecture in lung tissue (Figures 1A,C–E). However, only mice, treated with the dose 7 mg/kg showed decrease of Elastin (Figure 1B). The data obtained served as the basis for using the dose 7 mg/kg as the most effective for subsequent studies.

3.2 Delayed treatment with the HSP90 inhibitor, TAS-116

3.2.1 Delayed treatment with TAS-116 reduces HCl-Induced chronic alveolar inflammation

To determine the antidotal effectiveness of delayed treatment with TAS-116, we studied groups of HCl-instilled mice that started receiving the inhibitor 24 h or 96 h post HCl instillation. Leucocyte content and total protein concentration in BALF increased at 30 days post HCl; treatment with TAS-116, 7 mg/kg, starting 24 h after HCl, successfully blocked these increases (Figures 2A,B). The expression of TGF-β in BALF (Figure 2C) and NLRP3 inflammasome (Figure 2D) were also restored to control levels. Furthermore, mice who started receiving treatment 96 h after HCl instillation demonstrated equally effective antidotal activities.

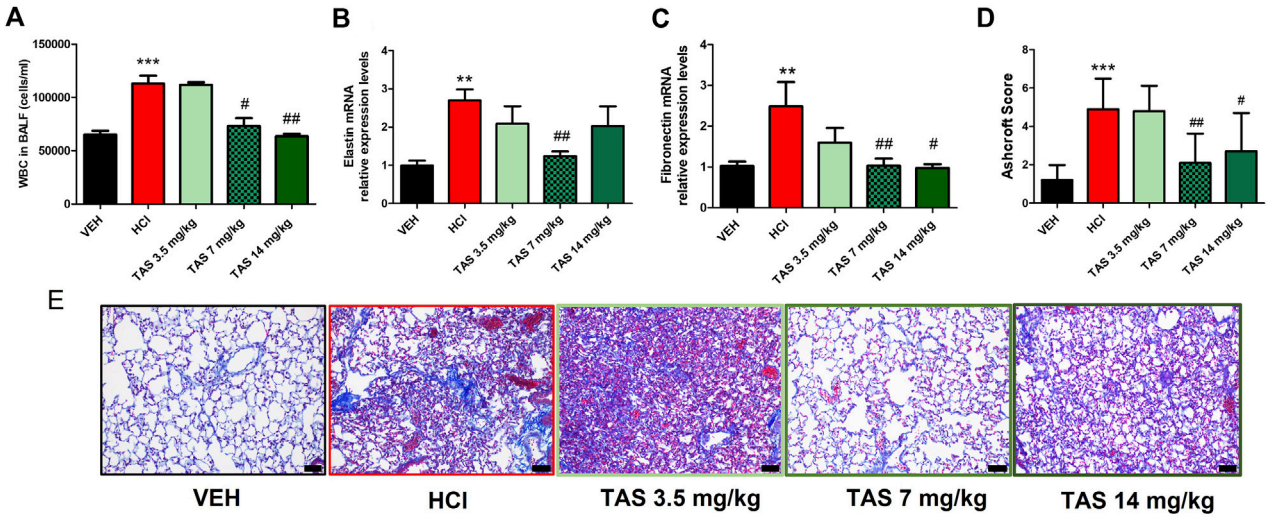

FIGURE 1
Analysis of lung injury after intratracheal instillaton of 0.1N HCl or saline followed by treatment, starting 24 h later, with the HSP90 inhibitor TAS-116 (3.5, 7 or 14 mg/kg 5×/week p. o.) for 30 days. Content of white blood cells in bronchoalveolar lavage fluid (BALF) $n = 6$ **(A)**; relative expression levels of Elastin **(B)** and Fibronectin **(C)** mRNA were analyzed by RT-PCR, $n = 4–5$; Ashcroft Score **(D)** and Masson's Trichrome staining **(E)** of lung sections, $n = 3$. Original magnification ×20; black scale bars correspond to 50 µm; *: $p < 0.05$; **: $p < 0.01$, ***: $p < 0.01$, from VEH; $^{\#}$: $p < 0.05$, $^{\#\#}$: $p < 0.01$ from HCl, with 1-way ANOVA and Tukey's post-hoc test.

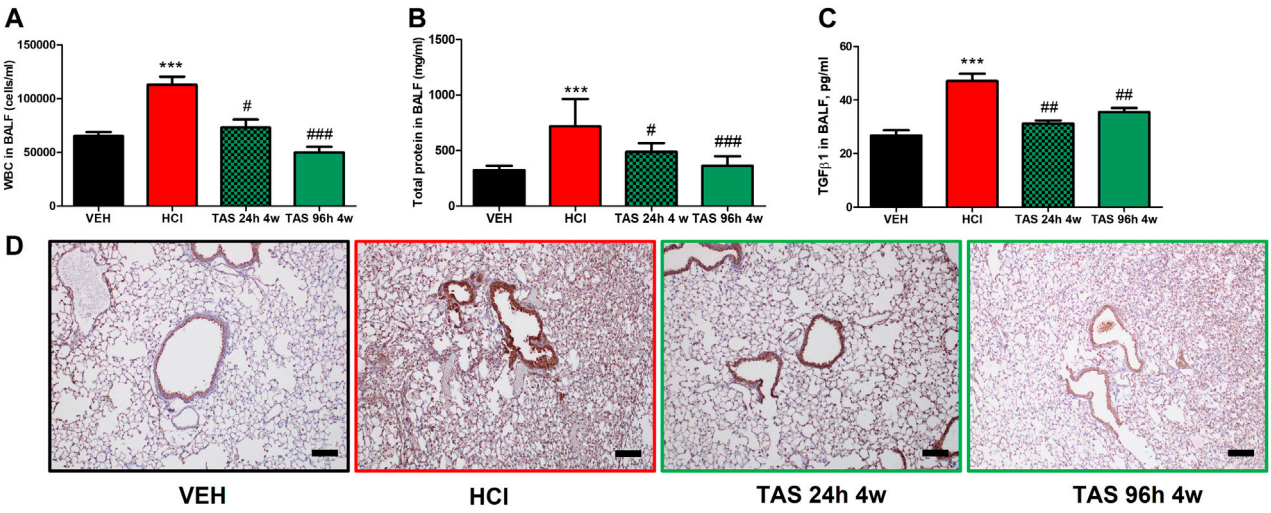

FIGURE 2
Oral treatment with TAS-116—starting either 24 or 96˚h after HCl-ameliorates alveolar inflammation. **(A)** White blood cells, **(B)** Total protein concentration and **(C)** TGF-β content in bronchoalveolar lavage fluid (BALF) at 30˚days post HCl instillation and treatment with TAS-116 at 7 mg/kg 5×/week starting 24 or 96 h post-HCl; **(D)** Immunohistochemical staining for the inflammasome NLRP3. Original magnification ×10; black scale bars correspond to 100 µm; $n = 6$ mice per group; ***: $p < 0.01$, from VEH; $^{\#}$: $p < 0.05$, $^{\#\#}$: $p < 0.01$, $^{\#\#\#}$: $p < 0.001$ from HCl, with 1-way ANOVA and Tukey's post-hoc test.

3.2.2 Delayed treatment with TAS-116 reduces hydrochloric acid-Induced pulmonary fibrosis

Formalin-fixed lung sections were stained with Masson's trichrome to visualize lung parenchymal changes and collagen deposition (Figure 3A). At 30 days after HCl instillation, a fibrotic process characterized by alveolar thickness and fibrous obliteration was observed. Mice receiving TAS-116, 7 mg/kg, 5 days/week, p. o., and starting either 24 h or 96 h after HCl, exhibited significantly decreased histopathologic changes and

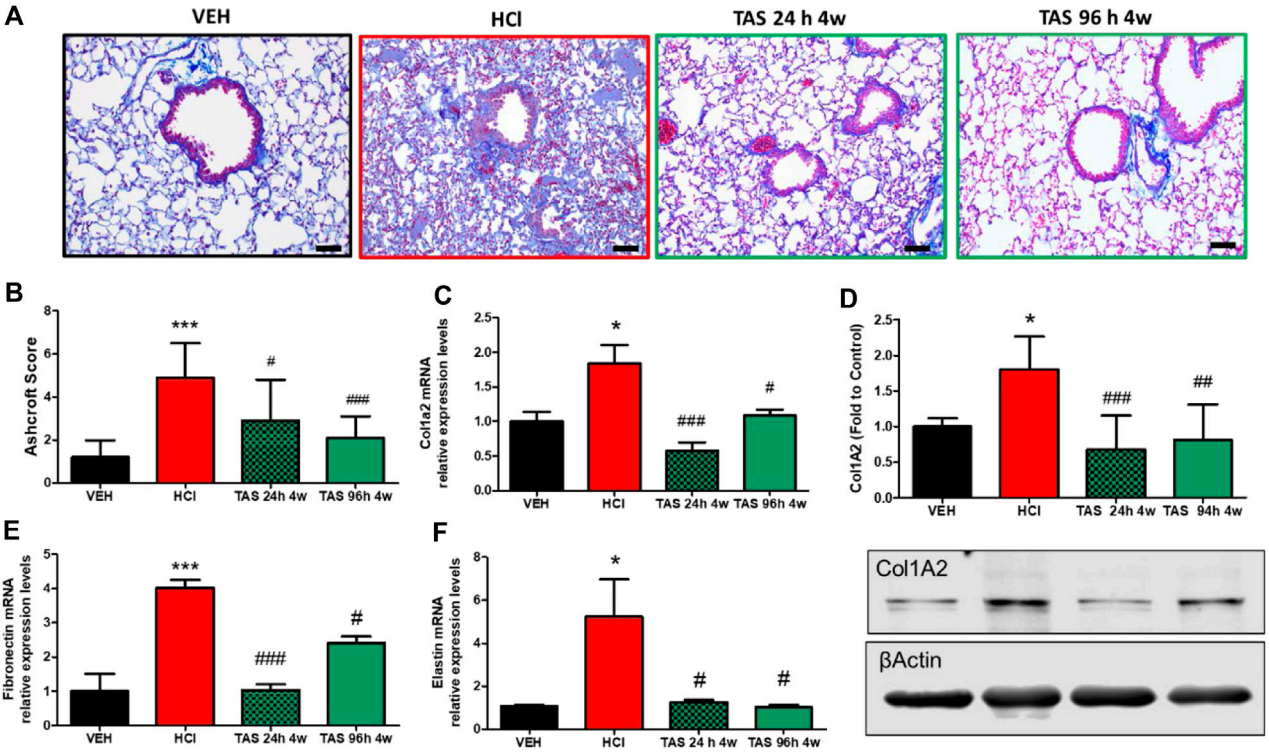

FIGURE 3
Oral treatment with TAS-116—starting either 24 or 96˚h after HCl-ameliorates HCl-induced pulmonary fibrosis. Mice were intratracheally instilled with 0.1N HCl or saline followed by treatment, starting 24 or 96 h later, with the HSP90 inhibitor TAS-116 (7 mg/kg 5x/week p. o.) for 4˚weeks. Masson's Trichrome staining of lung sections demonstrates massive fibrous obliteration and loss of parenchymal architecture in HCl-instilled mice **(A)**. The Ashcroft score depicts severe fibrosis in HCl-instilled mice and recovered lungs in TAS-116-treated groups of mice **(B)**. The level of collagen type I was indicated *via* qPCR **(C)** and Western Blotting **(D)**. mRNA expression of extracellular matrix Fibronectin **(E)** and Elastin **(F)** were measured *via* qPCR. Original magnification ×20; black scale bars correspond to 50 μm (Means ± SEM; $n = 4–6$; *: $p < 0.05$, ***: $p < 0.01$, from VEH; #: $p < 0.05$, ##: $p < 0.01$, ###: $p < 0.001$ from HCl, with one-way ANOVA and Tukey's.

Ashcroft score values (Figure 3B). Overexpression of collagen Type I (Figures 3C,D), fibronectin (Figure 3E), and fibronectin (Figure 3F), analyzed by western blotting and real-time qPCR were also decreased in both treatment groups compared to the group instilled with HCl alone.

3.2.3 TAS-116 Inhibits the activation of pro-fibrotic pathways

We analyzed the ability of TAS-116 to inhibit the expression of canonical and noncanonical pro-fibrotic signaling biomarkers: the activated forms of SMAD2 (mothers against decapentaplegic homolog 2), extracellular signal-regulated kinase (MAPK/ERK) and HSP90 (Figure 4). As we previously reported, instillation of hydrochloric acid increases the phosphorylation of SMAD2 and ERK1/2, and activates HSP90, at 30 days post-exposure. TAS-116, 7 mg/kg, 5x/week, starting 24 h after HCl did not significantly reduce pSMAD2 expression, however, treatment starting 96 h post HCl significantly reduced pSMAD2 expression when compared to HCl-instilled mice. At 30˚days post-exposure, both TAS-116 treatment plans successfully blocked ERK and HSP90 activation, when compared to HCl-instilled mice.

3.2.4 TAS-116 inhibits lung Dysfunction and airway hyper-responsiveness to methacholine

Changes in lung mechanics were tested 30 days after acid instillation. Animals challenged with HCl demonstrated a downward shift in pressure-volume (PV) loops compared to VEH mice (Figure 5A). Both groups treated with 7 mg/kg TAS-116 displayed significant improvement, but treatment that started 24 h after HCl exposure brought the loop to the physiological norm. Total respiratory system resistance (Rrs), elastance (Ers), and tissue damping (G), increased in response to rising concentrations of methacholine in HCl-instilled mice (Figures 5B-D). Both TAS-116 treatments were equally able to prevent increases in those parameters.

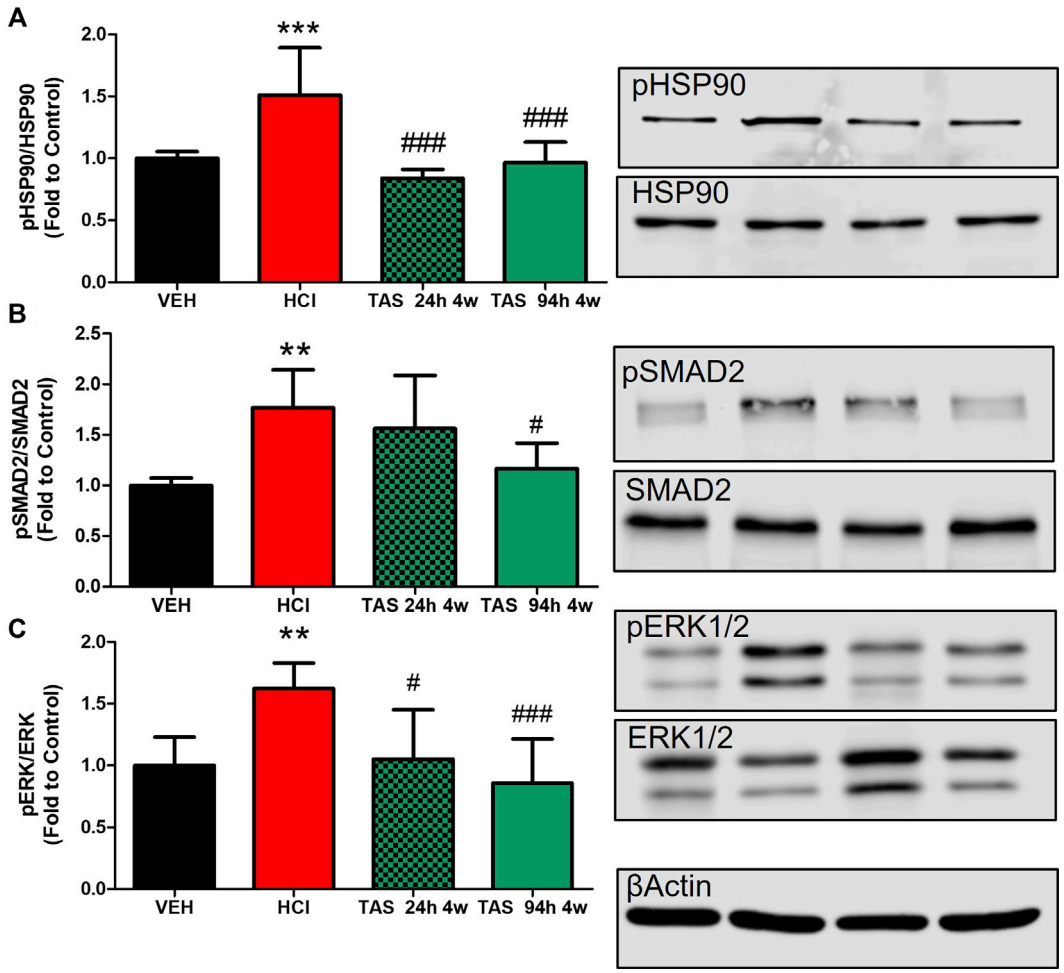

FIGURE 4
Oral treatment with TAS-116—starting either 24 or 96 h after HCl-ameliorates HCl-induced activation of pro-fibrotic pathways. **(A)** HSP90 activation (pHSP90) increased in HCl-instilled mice and was reduced in mice treated with TAS-116 24 h or 96 h post HCl. **(B)** Phosphorylated SMAD2 was significantly increased in mice instilled with HCl and reduced in group of mice, receiving treatment 96 h post instillation. **(C)** ERK1/2 (MAPK) activation (pERK) increased in HCl-instilled mice and reduced in both TAS-116-trated groups. Means ± SEM; ***: $p < 0.001$, **: $p < 0.01$, *: $p < 0.05$ from VEH; #: $p < 0.05$, ###: $p < 0.001$ from HCl, with one-way ANOVA and Tukey's, $n = 6–7$. VEH: Vehicle.

3.3 Shortened treatment time with the HSP90 inhibitor TAS-116

3.3.1 3 but not 2 weeks treatment with TAS-116 reduces HCl-induced chronic alveolar inflammation

Having ascertained that 96 h delayed treatment with the HSP90 inhibitor TAS-116 can successfully reduce lung injury, we then reduced treatment time from 4 to 3 or to 2 weeks, to define the shortest and most effective treatment plan. Bronchoalveolar lavage fluid samples were analyzed for alveolar WBC recruitment, total protein concentration and overexpression of the key pro-fibrotic cytokine TGFβ. Mice treated for 14 days, starting 96 h post HCl instillation, demonstrated reduction of only total protein concentration in BALF, while 3 weeks treatment significantly ameliorated WBC, protein and TGFβ content (Figure 6).

3.3.2 3 weeks treatment with TAS-116 reduces HCl-induced pulmonary fibrosis

Mice exposed to 0.1N HCl exhibited interstitial, peribronchial and perivascular accumulation of collagen and overexpression of ECM (Figure 7). Treatment with TAS-116 reduced by 2 weeks showed the improvement in collagen and elastin (Figures 7C,D,F), while 3 weeks-administration of inhibitor significantly improved histological signs of fibrosis (Figures 7A,B). The expression of fibronectin was not reduced by either treatment group (Figure 7E).

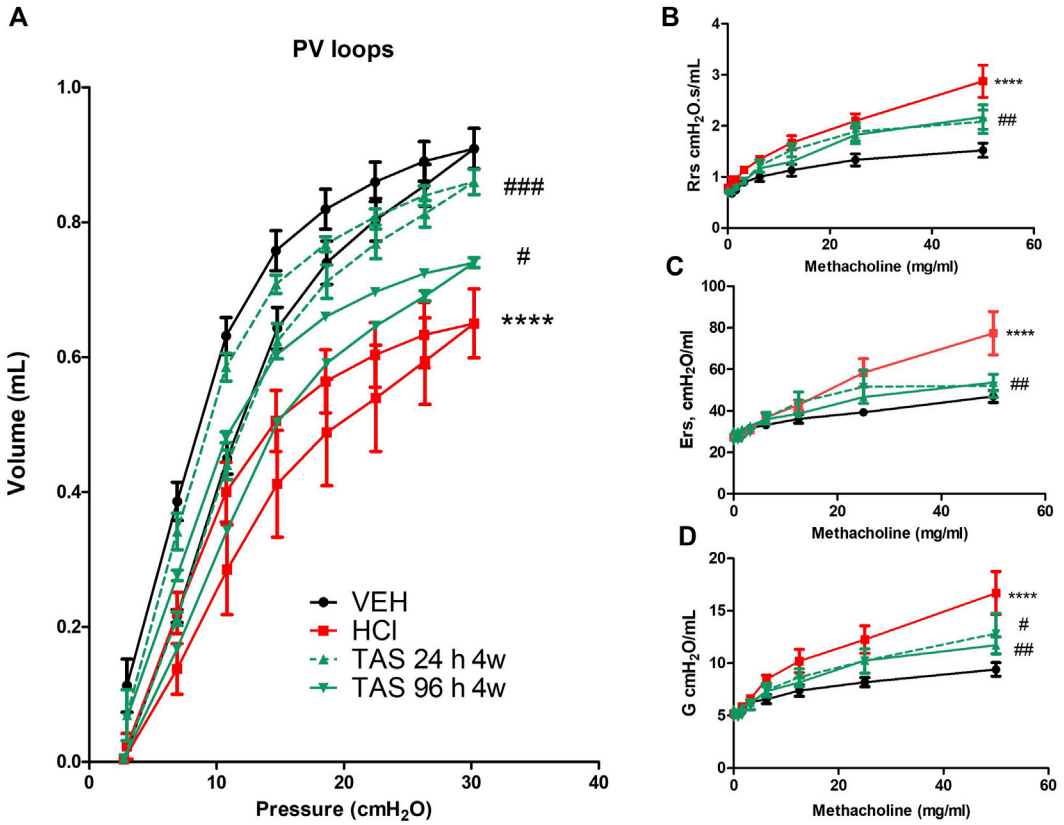

FIGURE 5
Oral treatment with TAS-116—starting either 24 or 96 h after HCl-ameliorates HCl-induced lung dysfunction. Both 24 h and 96 h treatment groups had a significant impact on preventing a downward shift of pressure volume (PV) loops after HCl instillation **(A)**. Respiratory system resistance (Rrs), elastance (Ers), and damping (G) increased, compared to control mice in all groups instilled with HCl **(B–D)**. This increase was significantly dampened in TAS-116 treated mice. Means ± SEM; $n = 6$ mice per group; ****: $p < 0.0001$ from VEH; #: $p < 0.05$, ##: $p < 0.01$, ###: $p < 0.001$ from HCl, with one- or two-way ANOVA and Tukey's post-hoc test.

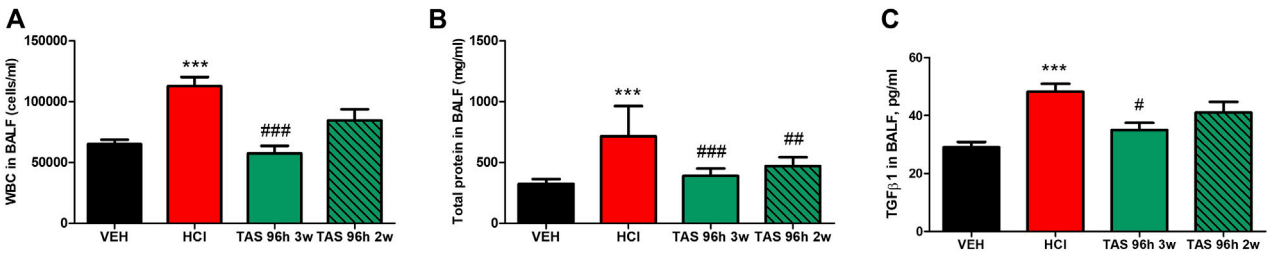

FIGURE 6
3 weeks treatment with TAS-116 ameliorates HCl-induced alveolar inflammation. **(A)** White blood cells, **(B)** total protein and **(C)** TGF-β concentrations in bronchoalveolar lavage fluid (BALF) at 30 days post HCl instillation and treatment with TAS-116, 7 mg/kg 5x/week, po, starting 96 h post-HCl; $n = 6$ mice per group; ***: $p < 0.001$ from VEH; #: $p < 0.05$, ##: $p < 0.01$, ###: $p < 0.001$ from HCl; with 1-way ANOVA and Tukey's post-test.

3.3.3 3 weeks treatment with TAS-116 inhibits the activation of pro-fibrotic pathways

Pro-fibrotic pathways were activated by HCl (Figure 8). Activation of HSP90 was significantly blocked in both 3- and 2-week TAS-116 treated groups. However, significant decrease in phosphorylation of SMAD2 and ERK1/2 was observed only in lung homogenates taken from mice after 3 weeks treatment with the HSP90 inhibitor.

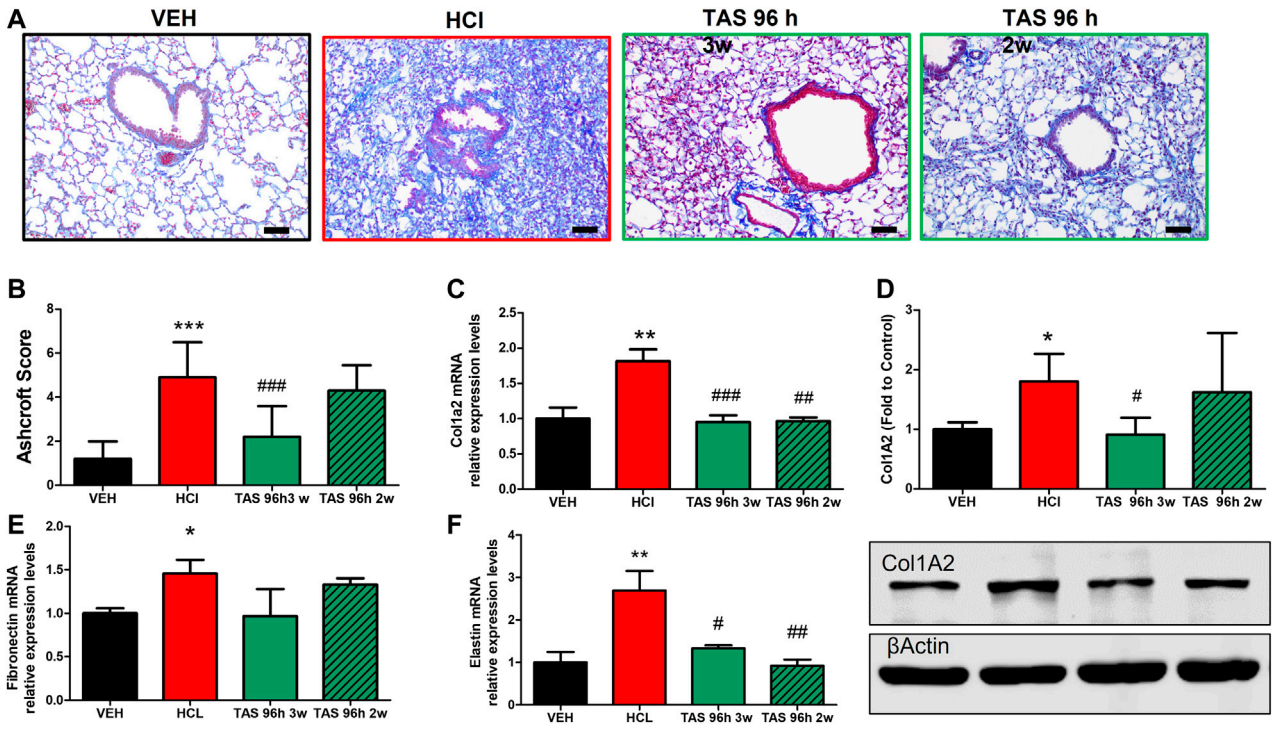

FIGURE 7
3 weeks treatment with TAS-116 ameliorates HCl-induced pulmonary fibrosis. Mice received intratracheal 0.1N HCl or saline followed by treatment, starting 96 h later, with TAS-116 (7 mg/kg 5×/week p. o.) for 2 or 3 weeks. Masson's Trichrome staining of lung sections demonstrates accumulation interstitial, peribronchial and perivascular collagen in HCl-instilled mice. Animals treated with TAS-116 for 3 weeks exhibited improved lung architecture **(A)** and lower Ashcroft score **(B)**. The level of collagen type I was indicated *via* qPCR **(C)** and Western Blotting **(D)**. mRNA expression of extracellular matrix Fibronectin **(E)** and Elastin **(F)** were measured *via* qPCR. Original magnification ×20; black scale bars correspond to 50 μm (Means ± SEM; $n = 4–6$; ***: $p < 0.001$; **: $p < 0.01$, *: $p < 0.05$ from VEH; $^{\#}$: $p < 0.05$, $^{\#\#}$: $p < 0.01$, $^{\#\#\#}$: $p < 0.001$ from HCl, with one-way ANOVA and Tukey's post-hoc test.

3.3.4 3 weeks treatment with TAS-116 improves HCl-induced lung dysfunction and airway hyper-responsiveness to methacholine

HCl-challenged animals showed a decrease in pressure-volume (PV) loops (Figure 9A). Mice, treated with 7 mg/kg TAS-116 for 3 weeks displayed complete recovery, in contrast to mice treated for 2 weeks that showed no improvement. Total respiratory system resistance (Rrs), elastance (Ers), and tissue damping (G), were increased in response to methacholine in HCl-treated mice; this was completely prevented by 3-week, but not 2-week treatment with TAS-116 (Figures 9B–D).

4 Discussion

In this study we used TAS-116, a novel class of selective inhibitors of heat shock protein 90, as a potential antidote against chronic lung injury and pulmonary fibrosis, caused by intratracheal exposure to hydrochloric acid. We selected this inhibitor based on the following features. Unlike past generation-inhibitors, TAS-116 targets cytosolic HSP90α and HSP90β, without affecting HSP90 in the mitochondria and endoplasmic reticulum (Ohkubo et al., 2015). HSP90, a causative factor in pulmonary fibrosis, was localized in both the cytosol and nucleus of fibroblasts (Sontake et al., 2017). Additionally, TAS-116 has oral bioavailability, which allows administration on an outpatient basis. Further, this drug has already shown its safety in a randomized, double-blind, Phase III clinical trial comparing TAS-116 to placebo in patients with gastrointestinal stromal tumor refractory to standard treatments (Honma et al., 2021).

Our first aim was to find an effective and safe dose of TAS-116 for mice against HCl-induced pulmonary fibrosis. In various clinical trials against cancer, this compound was used in doses of 80–160 mg on a 5 days on/2 days off regimen (Kurokawa et al., 2017; Kawazoe et al., 2021). In animal studies, the dose 14 mg/kg was considered as safe and effective for mice against tumors with the same administration schedule (Saito et al., 2020). In this study, we used three different doses in search of the minimal effective dose against

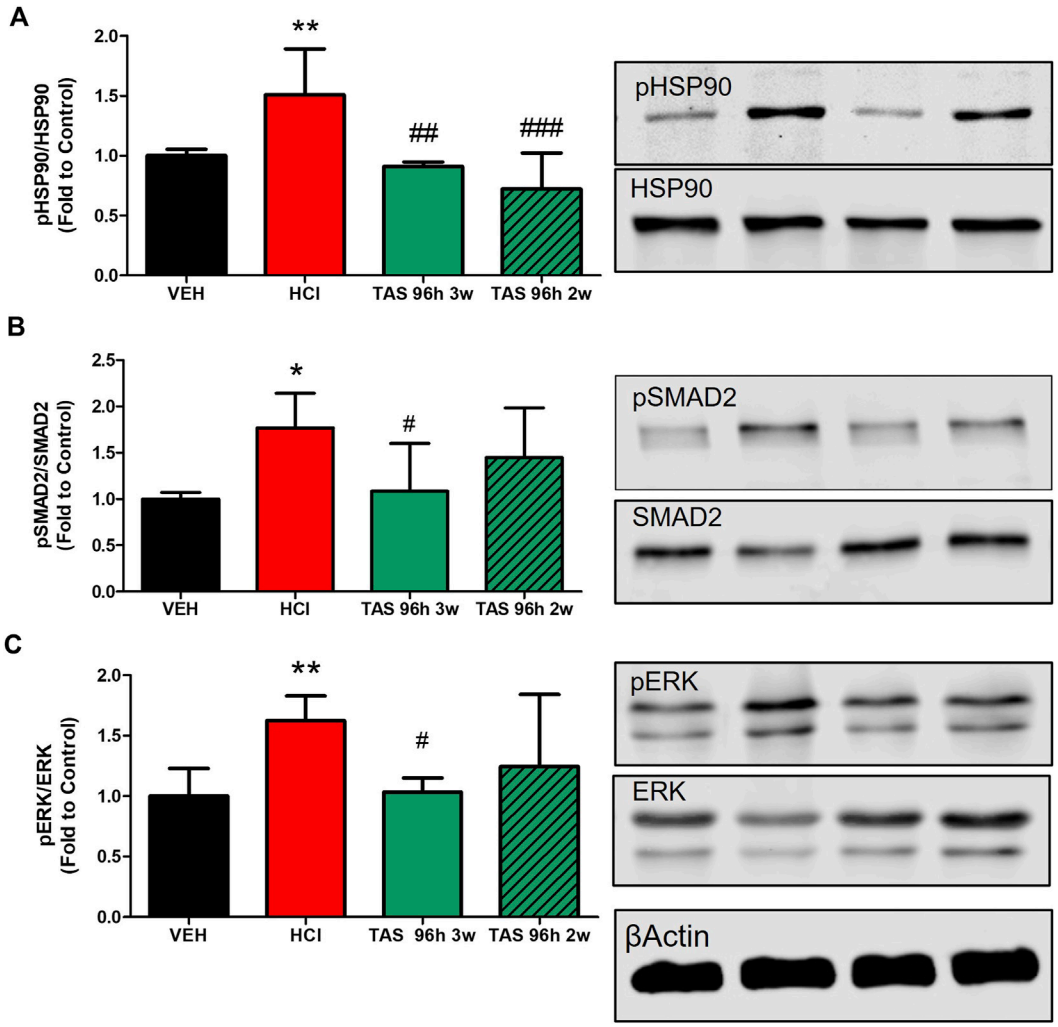

FIGURE 8
3 weeks treatment with TAS-116 ameliorates HCl-induced activation of pro-fibrotic pathways. **(A)** Heat Shock Protein 90 activation (pHSP90) increased in HCl-instilled mice and was reduced in mice, treated for 2 or 3 weeks with TAS-116, starting 96 h post HCl. **(B)** Active (phosphorylated) SMAD2 and **(C)** ERK1/2 were significantly increased in mice instilled with HCl and reduced in mice, treated for 3, but not 2 weeks with TAS-116. Means ± SEM; **: $p < 0.01$, *: $p < 0.05$ from VEH; $^{\#}$: $p < 0.05$, $^{\#\#}$: $p < 0.01$, $^{\#\#\#}$: $p < 0.001$ from HCl, with one-way ANOVA and Tukey's post-hoc test, n = 5–7.

PF. Mice, receiving 3.5 mg/kg starting 24 h after HCl instillation did not show significant improvements compare to untreated HCl-challenged mice, while mice receiving either 7 or 14 mg/kg of inhibitor demonstrated antidotal effects. Based on that, we considered that TAS-116, at 7 mg/kg, as the optimal therapeutic dose for mice.

Despite studies suggesting that the pathophysiology of pulmonary fibrosis is a product of fibroblast dysfunction, inflammation remains one of the critical factors in the disease. Patients with IPF have periods of exacerbations or acute decline. During exacerbations, the recruitment of inflammatory cells is seen in BALF with numerous proinflammatory mediators, cytokines, and growth factors (Parambil et al., 2005; Kim et al., 2006; Bringardner et al., 2008). We previously demonstrated that the peak of acute lung injury in mice occurs on the fourth day after HCl instillation but that low-to-moderate inflammation persists through day 30 (Marinova et al., 2019). The involvement of pro-inflammatory pathways in the development of PF has also been demonstrated in various mouse models (Izbicki et al., 2002; Marinova et al., 2019; Solopov et al., 2020). Several publications further suggest that the NLRP3 inflammasome plays an important role in fibrogenesis (Ma et al., 2020; Ranta-aho et al., 2021; Colunga Biancatelli et al., 2022b). Here, we analyzed the leucocyte and total protein contents in bronchoalveolar

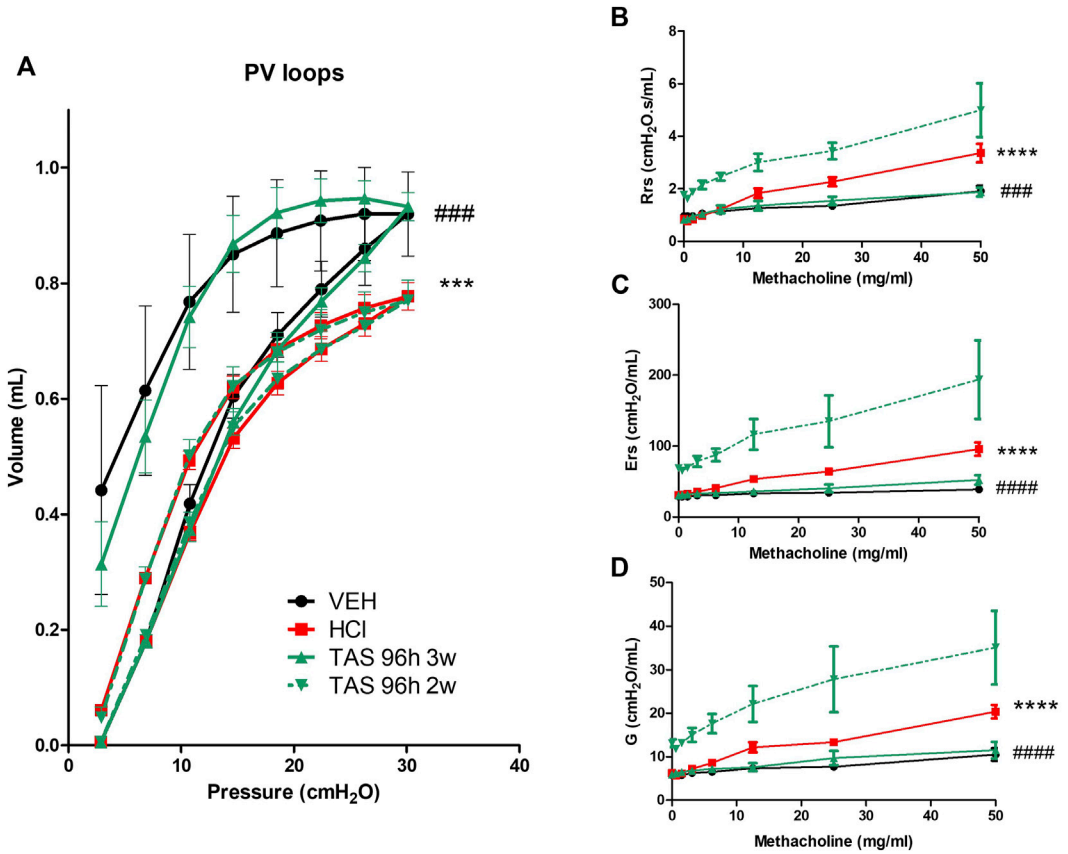

FIGURE 9
3 weeks treatment with TAS-116 ameliorates HCl-induced lung dysfunction and airway hyper-reactivity. **(A)** Pressure–Volume relationships **(B)** Total Respiratory System Resistance (Rrs), **(C)** total Respiratory System Elastance (Ers), and **(D)** tissue damping (G), All studies were performed at 30 days after HCl instillation. $n = 4–6$ mice per group; ***: $p < 0.001$, ****: $p < 0.0001$ from VEH; ###: $p < 0.001$, ####: $p < 0.0001$ from HCl, with 2-way ANOVA and Bonferroni's post-hoc test.

lavage, the expression of the pro-inflammatory and pro-fibrotic cytokine, TGF-β, and of NLRP3 inflammasome, which designate inflammation of alveoli, migration of immune cell, and alveolar-capillary hyper-permeability. All were significantly exacerbated by HCl, in agreement with previous studies by us and others. We previously reported the ability of HSP90 inhibitors (AT13387 and AUY-922) to modulate human pulmonary microvascular endothelial activation and barrier dysfunction, which is responsible for vascular permeability and exudation of inflammation products into the alveolar space (Colunga Biancatelli et al., 2021b; Colunga Biancatelli et al., 2022c). Treatment with HSP90 inhibitor TAS-116 in dose 7 mg/kg starting either 24 or 96 h post-HCl successfully ameliorated all signs of inflammation even with a shortened, 3 weeks treatment course.

Fibrosis is traditionally associated with pathological changes in the extracellular matrix. We have repeatedly reported that a single exposure to 0.1N hydrochloric acid leads to pulmonary fibrosis in mice, which is reflected in upregulation of ECM, and have considered HSP90 as a potential therapeutic target (Marinova et al., 2019; Solopov et al., 2020; Colunga Biancatelli et al., 2021a; Solopov et al., 2021). The expression of ECM proteins (fibronectin, elastin) varied in magnitude among studies (e.g., experiments shown in Figure 3 vs. Figure 7) but was always elevated at 30 days after HCl. The effectiveness of HSP90 inhibitors in modulating ECM secretion has been shown in several studies. HSP90 chaperones cannot directly engage nascent molecules of the matrix, however, there are indirect mechanism though which HSP90 inhibitors block overexpression of ECM. The HSP90α inhibitor 17-allylaminogeldanamycin (17-AAG) tightly decreases collagen-I expression in human primary cells (Wong et al., 2018). The exogenous beta isoform of Hsp90 activates the formation of extracellular fibronectin in breast cancer cells, while knockdown or inhibition of Hsp90β leads to reduced deposition and can be partially rescued by the addition of

exogenous Hsp90 (Hunter et al., 2014). As we previously reported, HSP90 inhibitors AUY-922 (Marinova et al., 2020) and AT-13383 (Colunga Biancatelli et al., 2022a) significantly downregulate the overexpression of collagen, fibronectin and elastin expression in mice with HCl-induced pulmonary fibrosis. In the present study, we observed the formation of interstitial, peribronchial and perivascular collagen masses that significantly changed lung architecture. Both 24 h- and delayed treatment with TAS-116 decreased collagen deposition and overexpression of fibronectin and elastin.

The cytoplasmic proteins SMAD2/3 mediate signals from activated TGF-β1 receptors. Phosphorylation of SMAD2/3 allows their binding to SMAD4, promoting translocation to the nucleus where numerous TGF-β1-responsive genes are activated. Hsp90 plays an important role in inflammatory processes by stabilizing and activating more than 300 'client' proteins, including key proinflammatory signaling molecules, such as nuclear transcription factors (e.g., NF-κB, STATs, p53) and kinases (e.g., Raf/MEK/ERK, PI3K/AKT, p38/MAPK) (Trepel et al., 2010). Activation of Hsp90 reflected in HSP90 deacetylation and tyrosine phosphorylation (Dimitropoulou et al., 2013). Heat shock protein 90 actively participates in the TGF-β signaling pathway and HSP90 inhibition reduces fibrogenesis and lung fibrosis progression in mice (Bonniaud et al., 2017). Sontake et al. found elevated HSP90 immunostaining in lung biopsy samples of patients with IPF. Moreover, the suppression of HSP90 by another inhibitor 17-AAG moderated migration of myofibroblasts and, as a result, ECM production. (Sontake et al., 2017). One of the client proteins of HSP90 is mitogen-activated protein kinase (MAPK). MAPK kinase (MEK)/extracellular signal–regulated kinase (ERK) is also involved in fibrogenesis *via* growth and proliferation. Activation of the ERK1/2 has been detected in human fibrotic lungs (Yoshida et al., 2002; Antoniou et al., 2010). Overexpression of TGF-α in lung epithelium of transgenic CCSP/TGF-α mice causes progressive lung fibrosis and inhibition of ERK prevents the progression (Le Cras et al., 2010). In gastrointestinal stromal tumors, TAS-116 inhibits ERK1/2 (Saito et al., 2020). We previously reported that HSP90 inhibitors AUY-922 and AT13387 reduce both SMAD2 and ERK phosphorylation *via* blocking the activation of HSP90 in mice treated with HCl. (Marinova et al., 2020; Colunga Biancatelli et al., 2022a). Here we show that oral treatment with TAS-116 exerts similar therapeutic effects.

Development of pulmonary fibrosis affects not just alveoli but also conducting airways and the lung vasculature. Patients with IPF show alterations in lung dynamics (Plantier et al., 2018). The instillation of HCl in mice provoked strong changes in lung mechanics such as elevated total Respiratory System Elastance, Respiratory System Resistance, and tissue damping. Furthermore, HCl shifted down pressure–volume loops. Mice exposed to HCl and treated with TAS-116 successfully restored systemic resistance, elastance, damping, and corrected the downward shift of PV loops.

In conclusion, we demonstrated that TAS-116 prevents the development of HCl-induced chronic lung injury and pulmonary fibrosis by blocking the overexpression of pro-fibrotic markers, reducing collagen deposition and maintaining lung dynamics within physiological ranges. Moreover, this HSP90 inhibitor is effective even when treatment begins at the peak of acute lung injury, 96 h post HCl exposure, and lasts for 3 weeks. These benefits of TAS-116, coupled with oral bioavailability, suggest that it may be a promising countermeasure against HCl-induced pulmonary fibrosis.

Data availability statement

The raw data supporting the conclusions of this article will be made available by the authors, without undue reservation.

Ethics statement

The animal study was reviewed and approved by IACUC Old Dominion Univesrsity.

Author contributions

Conceptualization, JC, PS, and RC; methodology, PS, RC, CD, and JC; validation, PS, RC, CD, and JC; formal analysis, PS, RC, TD, and CD; investigation, PS, RC, TD, and CD; resources, JC; data curation, PS, RC, and JC; writing–"original draft preparation, PS; writing–"review and editing, PS, RC, and JC; supervision, JC; project administration, JC; funding acquisition, JC All authors have read and agreed to the published version of the manuscript.

Funding

National Institute of Environmental Health Sciences U01ES030674.

Conflict of interest

The authors declare that the research was conducted in the absence of any commercial or financial relationships that could be construed as a potential conflict of interest.

Publisher's note

References

Antoniou, K. M., Margaritopoulos, G. A., Soufla, G., Symvoulakis, E., Vassalou, E., Lymbouridou, R., et al. (2010). Expression analysis of Akt and MAPK signaling pathways in lung tissue of patients with idiopathic pulmonary fibrosis (IPF). *J. Recept. Signal Transduct. Res.* 30 (4), 262–269. doi:10.3109/10799893.2010.489227

Ashcroft, T., Simpson, J. M., and Timbrell, V. (1988). Simple method of estimating severity of pulmonary fibrosis on a numerical scale. *J. Clin. Pathol.* 41 (4), 467–470. doi:10.1136/jcp.41.4.467

Bonniaud, P., Bellaye, P.-S., Burgy, O., and Kolb, M. (2017). Heat shock protein: A hot topic in idiopathic pulmonary fibrosis. *Eur. Respir. J.* 49 (2), 1602152. doi:10.1183/13993003.02152-2016

Boyce, S. H., and Simpson, K. A. (1996). Hydrochloric acid inhalation: Who needs admission? *J. Accid. Emerg. Med.* 13 (6), 422–424. doi:10.1136/emj.13.6.422

Bringardner, B. D., Baran, C. P., Eubank, T. D., and Marsh, C. B. (2008). The role of inflammation in the pathogenesis of idiopathic pulmonary fibrosis. *Antioxid. Redox Signal.* 10 (2), 287–301. doi:10.1089/ars.2007.1897

Butler, L. M., Ferraldeschi, R., Armstrong, H. K., Centenera, M. M., and Workman, P. (2015). Maximizing the therapeutic potential of HSP90 inhibitors. *Mol. Cancer Res.* 13 (11), 1445–1451. doi:10.1158/1541-7786.MCR-15-0234

Colunga Biancatelli, R. M. L., Solopov, P. A., Gregory, B., Khodour, Y., and Catravas, J. D. (2022). HSP90 inhibitors modulate SARS-CoV-2 spike protein subunit 1-induced human pulmonary microvascular endothelial activation and barrier dysfunction. *Front. Physiol.* 13, 812199. doi:10.3389/fphys.2022.812199

Colunga Biancatelli, R. M. L., Solopov, P., and Catravas, J. D. (2022). The inflammasome NLR family Pyrin domain-containing protein 3 (NLRP3) as a novel therapeutic target for idiopathic pulmonary fibrosis. *Am. J. Pathol.* 192, 837–846. doi:10.1016/j.ajpath.2022.03.003

Colunga Biancatelli, R. M. L., Solopov, P., Dimitropoulou, C., and Catravas, J. D. (2021). Age-dependent chronic lung injury and pulmonary fibrosis following single exposure to hydrochloric acid. *Int. J. Mol. Sci.* 22 (16), 8833. doi:10.3390/ijms22168833

Colunga Biancatelli, R. M. L., Solopov, P., Dimitropoulou, C., Gregory, B., Day, T., and Catravas, J. D. (2022). The heat shock protein 90 inhibitor, AT13387, protects the alveolo-capillary barrier and prevents HCl-induced chronic lung injury and pulmonary fibrosis. *Cells* 11 (6), 1046. doi:10.3390/cells11061046

Colunga Biancatelli, R. M. L., Solopov, P., Gregory, B., and Catravas, J. D. (2021). The HSP90 inhibitor, AUY-922, protects and repairs human lung microvascular endothelial cells from hydrochloric acid-induced endothelial barrier dysfunction. *Cells* 10 (6), 1489. doi:10.3390/cells10061489

Dimitropoulou, C., Barabutis, N., Birmpas, H., and Catravas, J. (2013). Post-treatment with the heat shock protein 90 (hsp90) inhibitor, AUY-922, reduces lung hsp90 tyrosine (Y) phosphorylation and pulmonary inflammation in LPS-induced acute lung injury (ALI) in mice. *Eur. Respir. J.* 42 (57), P3933. doi:10.1080/01902148.2020.1764148

Doi, T., Kurokawa, Y., Sawaki, A., Komatsu, Y., Ozaka, M., Takahashi, T., et al. (2019). Efficacy and safety of TAS-116, an oral inhibitor of heat shock protein 90, in patients with metastatic or unresectable gastrointestinal stromal tumour refractory to imatinib, sunitinib and regorafenib: A phase II, single-arm trial. *Eur. J. Cancer* 121, 29–39. doi:10.1016/j.ejca.2019.08.009

Dyer, R. F., and Esch, V. H. (1976). Polyvinyl chloride toxicity in fires. Hydrogen chloride toxicity in fire fighters. *Jama* 235 (4), 393–397. doi:10.1001/jama.1976.03260300019022

Honma, Y., Kurokawa, Y., Sawaki, A., Naito, Y., Iwagami, S., Baba, H., et al. (2021). Randomized, double-blind, placebo (PL)-controlled, phase III trial of pimitespib (TAS-116), an oral inhibitor of heat shock protein 90 (HSP90), in patients (pts) with advanced gastrointestinal stromal tumor (GIST) refractory to imatinib (IM), sunitinib (SU) and regorafenib (REG). *J. Clin. Oncol.* 39 (15), 11524. doi:10.1200/jco.2021.39.15_suppl.11524

Hunter, M. C., O'Hagan, K. L., Kenyon, A., Dhanani, K. C. H., Prinsloo, E., and Edkins, A. L. (2014). Hsp90 binds directly to fibronectin (FN) and inhibition reduces the extracellular fibronectin matrix in breast cancer cells. *PLOS ONE* 9 (1), e86842. doi:10.1371/journal.pone.0086842

Izbicki, G., Segel, M. J., Christensen, T. G., Conner, M. W., and Breuer, R. (2002). Time course of bleomycin-induced lung fibrosis. *Int. J. Exp. Pathol.* 83 (3), 111–119. doi:10.1046/j.1365-2613.2002.00220.x

Kawazoe, A., Itahashi, K., Yamamoto, N., Kotani, D., Kuboki, Y., Taniguchi, H., et al. (2021). TAS-116 (pimitespib), an oral HSP90 inhibitor, in combination with nivolumab in patients with colorectal cancer and other solid tumors: An open-label, dose-finding, and expansion phase ib trial (EPOC1704). *Clin. Cancer Res.* 27 (24), 6709–6715. doi:10.1158/1078-0432.CCR-21-1929

Kim, D. S., Collard, H. R., and King, T. E., Jr. (2006). Classification and natural history of the idiopathic interstitial pneumonias. *Proc. Am. Thorac. Soc.* 3 (4), 285–292. doi:10.1513/pats.200601-005TK

Kurokawa, Y., Doi, T., Sawaki, A., Komatsu, Y., Ozaka, M., Takahashi, T., et al. (2017). Phase II study of TAS-116, an oral inhibitor of heat shock protein 90 (HSP90), in metastatic or unresectable gastrointestinal stromal tumor refractory to imatinib, sunitinib and regorafenib. *Ann. Oncol.* 28, v322–v323. doi:10.1093/annonc/mdx387.006

Landolt, L., Spagnoli, G. C., Hertig, A., Brocheriou, I., and Marti, H.-P. (2020). Fibrosis and cancer: Shared features and mechanisms suggest common targeted therapeutic approaches. *Nephrol. Dial. Transplant.* 37, 1024–1032. doi:10.1093/ndt/gfaa301

Le Cras, T. D., Korfhagen, T. R., Davidson, C., Schmidt, S., Fenchel, M., et al. (2010). Inhibition of PI3K by PX-866 prevents transforming growth factor-alpha-induced pulmonary fibrosis. *Am. J. Pathol.* 176 (2), 679–686. doi:10.2353/ajpath.2010.090123

Ma, X., Zhou, Y., Qiao, B., Jiang, S., Shen, Q., Han, Y., et al. (2020). Androgen aggravates liver fibrosis by activation of NLRP3 inflammasome in CCl(4)-induced liver injury mouse model. *Am. J. Physiol. Endocrinol. Metab.* 318 (5), E817–E829. doi:10.1152/ajpendo.00427.2019

Marinova, M., Solopov, P., Dimitropoulou, C., Colunga Biancatelli, R. M. L., and Catravas, J. D. (2019). Acute exposure of mice to hydrochloric acid leads to the development of chronic lung injury and pulmonary fibrosis. *Inhal. Toxicol.* 31 (4), 147–160. doi:10.1080/08958378.2019.1624895

Marinova, M., Solopov, P., Dimitropoulou, C., Colunga Biancatelli, R. M. L., and Catravas, J. D. (2020). Post-treatment with a heat shock protein 90 inhibitor prevents chronic lung injury and pulmonary fibrosis, following acute exposure of mice to HCl. *Exp. Lung Res.* 46 (6), 203–216. doi:10.1080/01902148.2020.1764148

National Research Council (US) Committee on Acute Exposure Guideline Levels (2010). *Acute exposure guideline levels for selected airborne chemicals*. Washington (DC): National Academies Press US.

Occupational exposures to mists and vapours from strong inorganic acids and other industrial chemicals. Working Group views and expert opinions, Lyon, 15-22 October 1991. *IARC Monogr. Eval. Carcinog. Risks Hum.*, 1992. 54: p. 1–310.

Ohkubo, S., Kodama, Y., Muraoka, H., Hitotsumachi, H., Yoshimura, C., Kitade, M., et al. (2015). TAS-116, a highly selective inhibitor of heat shock protein 90α and β, demonstrates potent antitumor activity and minimal ocular toxicity in preclinical models. *Mol. Cancer Ther.* 14 (1), 14–22. doi:10.1158/1535-7163.MCT-14-0219

Parambil, J. G., Myers, J. L., and Ryu, J. H. (2005). Histopathologic features and outcome of patients with acute exacerbation of idiopathic pulmonary fibrosis undergoing surgical lung biopsy. *Chest* 128 (5), 3310–3315. doi:10.1378/chest.128.5.3310

Piersma, B., Hayward, M. K., and Weaver, V. M. (2020). *Fibrosis and cancer: A strained relationship*. *Biochim. Biophys. Acta. Rev. Cancer* 1873 (2), 188356. doi:10.1016/j.bbcan.2020.188356

Plantier, L., Cazes, A., Dinh-Xuan, A.-T., Bancal, C., Marchand-Adam, S., and Crestani, B. (2018). Physiology of the lung in idiopathic pulmonary fibrosis. *Eur. Respir. Rev.* 27 (147), 170062. doi:10.1183/16000617.0062-2017

Ranta-aho, S., Piippo, N., Korhonen, E., Kaarniranta, K., Hytti, M., and Kauppinen, A. (2021). TAS-116, a well-tolerated Hsp90 inhibitor, prevents the activation of the NLRP3 inflammasome in human retinal pigment epithelial cells. *Int. J. Mol. Sci.* 22 (9), 4875. doi:10.3390/ijms22094875

Saito, Y., Takahashi, T., Obata, Y., Nishida, T., Ohkubo, S., Nakagawa, F., et al. (2020). TAS-116 inhibits oncogenic KIT signalling on the Golgi in both imatinib-naïve and imatinib-resistant gastrointestinal stromal tumours. *Br. J. Cancer* 122 (5), 658–667. doi:10.1038/s41416-019-0688-y

Sanchez, J., Carter, T. R., Cohen, M. S., and Blagg, B. S. J. (2020). Old and new approaches to target the Hsp90 chaperone. *Curr. Cancer Drug Targets* 20 (4), 253–270. doi:10.2174/1568009619666191202101330

Schopf, F. H., Biebl, M. M., and Buchner, J. (2017). The HSP90 chaperone machinery. *Nat. Rev. Mol. Cell Biol.* 18 (6), 345–360. doi:10.1038/nrm.2017.20

Solopov, P., Colunga Biancatelli, R. M., Dimitropoulou, C., and Catravas, J. D. (2021). Dietary phytoestrogens ameliorate hydrochloric acid-induced chronic lung injury and pulmonary fibrosis in mice. *Nutrients* 13 (10), 3599. doi:10.3390/nu13103599

Solopov, P., Marinova, M., Dimitropoulou, C., Colunga Biancatelli, R. M. L., and Catravas, J. D. (2020). Development of chronic lung injury and pulmonary fibrosis in mice following acute exposure to nitrogen mustard. *Inhal. Toxicol.* 32 (4), 141–154. doi:10.1080/08958378.2020.1757791

Sontake, V., Wang, Y., Kasam, R. K., Sinner, D., Reddy, G. B., Naren, A. P., et al. (2017). Hsp90 regulation of fibroblast activation in pulmonary fibrosis. *JCI Insight* 2 (4), e91454. doi:10.1172/jci.insight.91454

Trepel, J., Mollapour, M., Giaccone, G., and Neckers, L. (2010). Targeting the dynamic HSP90 complex in cancer. *Nat. Rev. Cancer* 10 (8), 537–549. doi:10.1038/nrc2887

Wong, M. Y., Doan, N. D., DiChiara, A. S., Papa, L. J., 3rd, Cheah, J. H., Soule, C. K., et al. (2018). A high-throughput assay for collagen secretion suggests an unanticipated role for Hsp90 in collagen production. *Biochemistry* 57 (19), 2814–2827. doi:10.1021/acs.biochem.8b00378

Yoshida, K., Kuwano, K., Hagimoto, N., Watanabe, K., Matsuba, T., Fujita, M., et al. (2002). MAP kinase activation and apoptosis in lung tissues from patients with idiopathic pulmonary fibrosis. *J. Pathol.* 198 (3), 388–396. doi:10.1002/path.1208

frontiers | Frontiers in Pharmacology

TYPE Review
PUBLISHED 15 November 2022
DOI 10.3389/fphar.2022.1059434

OPEN ACCESS

EDITED BY
Wenjun Li,
Yantai Institute of Coastal Zone Research (CAS), China

REVIEWED BY
Fardous El-Senduny,
Mansoura University, Egypt
Feng Zhang,
Nanjing University of Chinese Medicine, China

*CORRESPONDENCE
Xiaodong Song,
songxd71@163.com
Hongbo Li,
lihongbo0516@sina.com

SPECIALTY SECTION
This article was submitted to Respiratory Pharmacology, a section of the journal Frontiers in Pharmacology

RECEIVED 01 October 2022
ACCEPTED 01 November 2022
PUBLISHED 15 November 2022

CITATION
Zhang T, Zhang J, Lv C, Li H and Song X (2022), Senescent AECII and the implication for idiopathic pulmonary fibrosis treatment.
Front. Pharmacol. 13:1059434.
doi: 10.3389/fphar.2022.1059434

Senescent AECII and the implication for idiopathic pulmonary fibrosis treatment

Tingwei Zhang[1], Jinjin Zhang[2], Changjun Lv[1], Hongbo Li[1]* and Xiaodong Song[2]*

[1]Department of Respiratory and Critical Care Medicine, Binzhou Medical University Hospital, Binzhou Medical University, Binzhou, China, [2]Department of Cellular and Genetic Medicine, School of Pharmaceutical Sciences, Binzhou Medical University, Yantai, China

Idiopathic pulmonary fibrosis (IPF) is a chronic and lethal lung disease with limited treatment options. The onset of IPF increases with age, indicating that aging is a major risk factor for IPF. Among the hallmarks of aging, cellular senescence is the primordial driver and primary etiological factor for tissue and organ aging, and an independent risk factor for the progression of IPF. In this review, we focus on the senescence of alveolar type II epithelial cells (AECIIs) and systematically summarize abnormal changes in signal pathways and biological process and implications of senescent AECIIs during IPF progression. Meanwhile, we objectively analyze current medications targeting the elimination of senescent cells or restoration of vitality such as senolytics, senomorphics, autophagy regulators, and stem cell therapy. Finally, we dialectically discuss the feasibility and limitation of targeting senescent AECIIs for IPF treatment. We hope that the understanding will provide new insights to the development of senescent AECII-based approaches for the prevention and mitigation of IPF.

KEYWORDS

alveolar type II epithelial cells (AECIIs), cell senescence, idiopathic pulmonary fibrosis, senescence-associated secretory phenotype, senescenceassociated differentiation disorder

Introduction

Idiopathic pulmonary fibrosis (IPF) is an irreversible fibrotic disease in the lungs and is the most common form of idiopathic interstitial pneumonia and idiopathic fibrotic lung disorder (Moss et al., 2022). Its biological process is defined as an abnormal repair response to repeated alveolar epithelial cells (AEC) damage and fibroblast-to-myofibroblast differentiation and characterized by the excessive disordered deposition of collagen in the extra- and intra-cellular matrix (Liu and Liu, 2020). Several potential risk factors, such as aging, genetic predisposition, chemical, environmental exposure, and bioenvironmental factor (bacteria and virus), can act on various types of lung cells and enhance the risk of developing IPF (Noble et al., 2012; Moore and Moore, 2015; Sheng et al., 2020; Parimon et al., 2021). Of these risk factors, aging is considered an independent risk factor. Even in patients with a genetic predisposition, the onset of IPF seldom occurs

before the sixth decade, and the incidence increases exponentially with advancing age (Raghu et al., 2006). A longitudinal cohort study identifying independent risk factors for the progression of interstitial lung disease has shown that the risk of IPF in people aged 70 or over is 6.9 times that in people aged over 40 (Choi et al., 2018), confirming that IPF is an age-related disease.

Cell senescence and stem cell exhaustion are the hallmarks of all age-related diseases, as in IPF. Alveolar type II epithelial cells (AECIIs) are the stem cells for the lungs and play a role in maintaining intrapulmonary homeostasis, immunity, and regeneration in the alveoli. Senescent AECIIs secrete high levels of interleukin, interferon, tumor necrosis factor, colony-stimulating factors, growth factors, and chemotactic cytokines, which promote fibroblast-to-myofibroblast differentiation and persistent tissue remodeling (Abbadie et al., 2017; Liu and Liu, 2020). A recent study has uncovered that pulmonary fibrosis after coronavirus disease 2019 (COVID-19) may be caused by virus-induced AECII senescence (Lee et al., 2021; Michalski et al., 2022; Sinha et al., 2022). Preventing AECII senescence or targeting senescent cells in patients with COVID-19 can reduce the risk of pulmonary fibrosis (Hong et al., 2022). Moimas et al. detected that AECII exhibited high levels of the senescence markers p21 and p16 from patients with IPF (Moimas et al., 2019). Other numerous studies have shown that AECII senescence promotes the occurrence of IPF (Naikawadi et al., 2016; Parimon et al., 2020; Yao et al., 2021; Hong et al., 2022). However, pathological mechanisms underlying AECII senescence and specific effects of targeting senescent AECIIs on IPF remain unclear. This review will discuss the mechanism of AECII senescence, which drives the onset and progression of IPF, and highlights the advantages and disadvantages of targeting senescent AECIIs for IPF.

Cellular senescence is a risk factor for idiopathic pulmonary fibrosis

Cellular senescence

Cellular senescence is irreversible cell cycle arrest, characterized by morphological flattening and expansion, resistance to apoptosis, altered gene expression and chromatin structure, expression of senescence-associated β-galactosidase (SA-β-gal) and acquisition of a senescence-associated secretory phenotype (SASP) (Mohamad et al., 2020). Often caused by persistent DNA damage. It is worth mentioning that during cellular senescence, an increase in SA-β-gal was exhibited, which was the first marker for *in situ* detection of senescence cellular in tissues (Kurz et al., 2000). Cellular senescence on an organism has three adverse effects: First, the degenerative physiological function of senescent cells and their accumulation disrupt tissue and organ functions, thereby leading to the aging of the body. Second, accumulated senescent cells secrete a variety of proteins such as inflammatory cytokines, chemokines, growth factors and matrix metalloproteinases. This phenomenon is known as the senescence-associated secretory phenotype (SASP), SASP affects the physiological functions of normal cells in the surrounding microenvironment in an autocrine or paracrine manner, causing the dysfunction of tissues and organs and participating in senescence-associated diseases (Childs et al., 2015). Third, stem cells are gradually exhausted during the aging process. When tissues and organs function abnormally, stem cells cannot be repaired in time, thus affecting the physiological functions of the body (Korolchuk et al., 2017; Parimon et al., 2021). Accompanied by the adverse effects of cellular senescence on an organism, abnormal changes arise in biological processes, such as telomere attrition, DNA damage, epigenetic modifications, abnormal protein homeostasis, mitochondrial dysfunction, and impaired autophagy (Korfei et al., 2020; Duckworth et al., 2021; Kellogg et al., 2021).

The regulatory pathways of cellular senescence mainly include cell cycle and SASP regulation (Parimon et al., 2021). Cell cycle blockade is induced by cyclin-dependent kinase (CDK) inhibitors $p16^{Ink4a}$ or $p53/p21^{Cip1/Waf1}$ (Lomas et al., 2012). Persistent DNA damage induces the expression of p16 through the transcription factor Ets and causes the stabilization of transcription factor p53, which induces the expression of p21. P16 and P21 respectively inhibit the cyclin cyclin-dependent kinase 4/6 (CDK4/6) complex and cyclin-dependent kinase 2 (CDK2). Both CDK inhibitors activate the Rb protein, which blocks the cell cycle and leads to cellular senescence (Ohtani et al., 2001; Takahashi et al., 2006; Yasuda et al., 2021). Therefore, $p16^{INK4a}$ and $p21^{WAF1}$ are considered to be important markers of cellular senescence. However, no specific marker for cellular senescence has been identified. The study shown that senescent cells synthesize many oxidized lipids, a class of bioactive lipids derived from the oxidation of polyunsaturated fatty acids. Dihomo-15-deoxy-delta-12,14-prostaglandin J2 (dihomo-15d-PGJ2) as an oxygenated lipid that promotes senescence and secretion of SASP by activating RAS/mitogen activated protein kinase (RAS/MAPK) pathway. It is produced and accumulated in senescent cells, released upon senescent cell lysis, and detected in urine and blood. Wiley et al. (2021) confirmed dihomo-15d-PGJ2 as a potential biomarker for validating the performance of aging drugs. Therefore, it may become the first biomarker of aging, or even a therapeutic target in the near future. Several studies have shown that cellular senescence mediates IPF, targeting senescence can alleviate fibrosis and extend the life spans of experimental animals (Baker et al., 2016; Schafer et al., 2017; Hohmann et al., 2019; Rhinn et al., 2019; Omori et al., 2020). However, little is known about the mechanisms by which senescence leads to IPF.

Cellular senescence in idiopathic pulmonary fibrosis

The human lung, the organ with the largest surface area in the body, represents a unique interface with the external environment. Lung maturation and function peak around 25 years of age, remain steady until 35 years of age, and gradually decline with structural remodeling thereafter (Ruaro et al., 2021; Schneider et al., 2021), which characterized by enlarged alveolar size and signifies increased mechanical force (Schiller et al., 2019). The progressive increase in alveolar size as the lungs senescence partially explains why the elderly are more likely to suffer from IPF in terms of mechanical force. In recent years, developments in mechanics and mechanical force, including mechanical stiffness, stretch, adhesion, density and tension, have been thought to be the key factors in IPF remodeling (Chilosi et al., 2013). They not only induce cellular senescence but also promote AECII proliferation, differentiation, and alveolar regeneration by regulating multiple signaling pathways (Wu et al., 2021). Elevated mechanical tension can activate TGF-β signaling loop in AECIIs, which drives the periphery-to-center progression of lung fibrosis (Gonzalez-Garcia et al., 2018; Wu et al., 2021). Transforming growth factor β (TGF-β) is a multifunctional cytokine that controls growth, proliferation, differentiation and apoptosis in many cell types. It includes TGF-β isoforms (TGF-β1, TGF-β2 and TGF-β3) and other signaling proteins (Meng et al., 2016; Morikawa et al., 2016). Numerous studies have demonstrated a significant increase in TGF-β1 gene and protein expression in fibrotic lung tissue (Bellaye et al., 2018; Boutanquoi et al., 2020; Lee et al., 2020; Lv et al., 2020). In IPF, TGF-β leads to increased ECM production mainly through induction of fibroblast activation and myofibroblast differentiation (Liu et al., 2021). Circular RNA (circRNA) is found to be associated with pulmonary fibrosis (Zhou et al., 2022). It produces from pre-mRNA back splicing, is a kind of endogenous noncoding RNA. A total of 67 significantly dysregulated circRNAs were identified in the plasma of IPF patients by using a circRNA microarray, including 38 upregulated-circRNAs and 29 downregulated-circRNAs (Li et al., 2018; Li et al., 2019). Among these circRNAs, the upregulated has-circ-100906, termed circANKRD42 because it is derived from its host gene Ankyrin repeat domain 42 (ANKRD42), increases with age in healthy people. It can accelerate IPF by mediating the crosstalk between mechanical stiffness and biochemical signal (Xu et al., 2022). Mechanistic studies reveal that circANKRD42 sponges miR-324-5p and miR-136-5p to promote the expression of yes-associated protein 1 (YAP1). Accumulating YAP1 in nucleus bound to tea domain transcription factor (TEAD), which initiates the transcription of genes related to mechanical stiffness.

In IPF, cellular senescence can lead to stem cell failure, SASP secretion, impaired myofibroblast apoptosis (Liu and Liu, 2020), and senescence-associated differentiation disorder (SADD), manifested by reduced tissue regeneration and excessive cellular matrix deposition. Impaired myofibroblast apoptosis, excessive deposition at an injury site, and continuous response are also considered the base for the continuous IPF process (Liu and Liu, 2020; Wei et al., 2021). Studies confirmed that targeting senescence cells is effective in alleviating IPF and senescence-related diseases (Lehmann et al., 2017; Merkt et al., 2020). Therefore, further exploring cellular senescence mechanisms and the involvement of senescent cells in the pathogenesis of IPF can facilitate the discovery of novel therapies for IPF treatment and other senescence-related diseases.

Senescent AECIIs promote idiopathic pulmonary fibrosis development

Role of AECIIs

AECs are composed of alveolar type I epithelial cells (AECIs) and AECIIs. They are separated from one another by interalveolar septa. AECIs are differentiated cells with a thin and flat shape and cover over 90% of the alveolar surface area, facilitating contact among alveolar endothelial cells and promoting gas exchange. AECIIs are small and cuboidal cells covering the remaining 10% of the alveolar surface area. Their primary function is to reduce surface tension by secreting surfactants (Confalonieri et al., 2022). When lung tissues are damaged, AECIIs can differentiate into AECIs, which are involved in epithelial repair (Barkauskas et al., 2013). In recurrent micro-injuries, dysfunctional AECIIs not only fail to maintain physiological lung regeneration but also promote abnormal epithelial–mesenchymal crosstalk, which lead to fibrosis rather than regeneration (Confalonieri et al., 2022). Mature AECIIs have heterogeneity, telomerase activity, and proliferative and differentiation potential. They respond to various cellular signals during senescence (Chen et al., 2017), and are among the major effector cells in the evolution of IPF. Therefore, understanding the mechanisms involved in the involvement of AECII as stem cells in lung repair is of great importance in delaying or treating pulmonary fibrosis. Their quiescence, proliferation, and differentiation are regulated by a combination of signaling pathways, including Notch, Hippo/Yap, and TGF-β1 pathways (Aumiller et al., 2013; Wu and Song, 2020).

The Hippo/YAP kinase cascade reaction promotes alveolar regeneration induced by proliferation of lung parenchymal cells. It comprises a large protein network, whose central components can be divided into two modules: the regulatory kinase module in the cytoplasm and the transcription module in the nucleus (Sun et al., 2021). The kinase module mainly comprises mammalian Ste20-like serine/threonine protein kinase 1 and 2 (MST1/2) and the large tumor suppressor kinase 1 and 2 (LATS1/2) axis (Moya

and Halder, 2019). They interact with the scaffolding protein Salvador (SAV1) and ultimately phosphorylate Yap and its homologue TAZ in the transcriptional module to prevent nuclear localization. Most importantly, activation of the upstream kinase module hinders the downstream transcription module (Sun et al., 2021). When in the absence of this phosphorylation cascade, YAP/TAZ localizes to the nucleus to regulate gene transcription associated with cell migration and proliferation. Nuclear translocation of YAP/TAZ can promote AECII differentiation into AECI. Studies shown that non-cell-specific YAP/TAZ RNA interference can exacerbate bleomycin-induced pulmonary fibrosis in mice by blocking alveolar regeneration (Haak et al., 2019).

There have been conflicting reports on the relationship between TGF-β signaling and alveolar epithelial cells. For example, when IL-33 was transferred into Treg-depleted mice during the study of ARDS, Treg cell recovery and a significant increase in TGF-β1 secretion were observed, and lung regeneration was promoted by accelerating the recovery of AECII, presumably IL-33-dependent Tregs accumulation may accelerate lung epithelial regeneration in a TGF-β1-dependent manner (Tan et al., 2021). This validates that TGF-β1 promotes regeneration of alveolar epithelial cells. In addition, single-cell RNA sequencing also identified TGF-β signaling as a key factor in lipopolysaccharide (LPS)-induced regeneration after lung injury in mice (Riemondy et al., 2019). However, it has also been demonstrated that TGF-β1 promotes lung fibrosis by inducing apoptosis in AECII. Recent studies have found that in bleomycin-induced lung fibrosis, the early production of TGF-β and platelet derived growth factor subunit A (PDGFA) by senescent AECII may directly promote fibroblast activation and collagen production, which in turn promotes fibrosis (Yamada et al., 2022). In addition to the above signaling pathways, growth factors produced by different neighboring cells, intercellular contacts, immune cells, and the extracellular matrix also regulate the state of AECIIs (Wu and Song, 2020).

Pro-fibrotic role of senescent AECII

AECII senescence promotes IPF (Parimon et al., 2020), and the senescent phenotypes of AECIIs are detected in fibrotic areas in the lungs of patients with IPF. These features confirm that senescent AECIIs have capacities for incomplete repair and can promote fibroproliferation (Wiley et al., 2021). To study the role of AECII senescence in IPF, Yao et al. (2021) established a mouse model with a conditional deletion of Sin3a in AECIIs and found that conditionally induced AECII senescence leads to progressive fibrosis and removing senescent AECIIs from the lungs of Sin3a LOF mice prevents progressive fibrosis, suggesting that targeting senescent AECIIs can prevent progressive fibrosis. Moreover, a study has confirmed that targeting senescent AECIIs can stabilize epithelial cell phenotype and reduce fibrosis markers (Lehmann et al., 2017).

Telomere is a ribonucleoprotein complex at the end of a cell's chromosome, consisting of an oligonucleotide sequence and a corresponding protein, which is essential for chromosome stability (Rossiello et al., 2022). Telomere is highly susceptible to various stresses. Cellular stress signals trigger glycogen synthase kinase-3β targeting the telomere protection protein complex, inducing the telomerase recruitment protein tripeptidyl peptidase I (TPP1) phosphorylation, and promoting TPP1 multisite polyubiquitination and degradation, resulting in telomere uncapping, which in turn activates protein kinase inhibitors (Razdan et al., 2018; Hong et al., 2022). H_2O_2-induced AECII model, bleomycin-treated mice and IPF patients samples show that AECIIs exhibit abnormal shortening of telomeres. In addition to this, incomplete replication of chromosome ends can lead to telomere shortening (Pineiro-Hermida et al., 2022). Recently, Pineiro-Hermida et al. (2022) studied the telomeres of different cell types in the lung by controlling the TRF1 gene and confirmed that fibrosis only occurs when telomeres are disrupted in AECII, and telomere shortening can be compensated by the telomerase reverse transcriptase (TERT) and telomerase RNA component (TERC) (Pineiro-Hermida et al., 2022). Thus, preventing stress-induced telomere damage may prevent cells from entering replicative senescence and fibrosis. Targeting senescent AECII or using inhibitors of telomere dysfunction to prevent senescence is a promising strategy for IPF intervention (Wang et al., 2020; Hong et al., 2022). Peptidomimetic telomere dysfunction inhibitor TELODIN, a newly discovered 8-mer peptide with TPP1 protective function that can reduce telomere uncapping and shortening, thereby expanding the alveolar AECII stem cell population in mice and preventing chronic stress-induced premature lung senescence and fibrosis, thus serving as a novel tool for disrupting pulmonary fibrosis (Wang et al., 2021). Long noncoding RNA (lncRNA) is usually unable to code protein and has a length more than 200 nt, which can inhibit or promote lung fibrogenesis and is becoming a promising new target (Song et al., 2014a; Zhang B et al., 2021). lncRNA telomeric repeat-containing RNA (lncTERRA) is a physiological indicator of aging for IPF. Gao et al. (2017) found that RNA interference on lncTERRA can ameliorate the functions of telomeres, thereby alleviating the symptoms of pulmonary fibrosis such as forced vital capacity.

As AECIIs become senescent, their stem cell potential is gradually exhausted. This effect not only cause impaired self-proliferation but also hamper the differentiation of AECIIs into AECIs, which leaves AECIIs in an intermediate or partially differentiated state, also known as the pre-alveolar type I transitional cell state or alveolar differentiation intermediate, resulting in SADD. When AECIIs are in a state of transition or partial differentiation, they can promote the proliferation of

myofibroblasts in a low-inflammation environment created by SASP, which promote the development of IPF (Hong et al., 2022). Watanabe et al. (2021) has confirmed that the incomplete conversion of AECs from AECIIs into AECIs can lead to the development of pulmonary fibrosis. During the differentiation of AECIIs into AECIs, AECIIs undergo dramatic cell shape changes (Wu et al., 2021). When SADD occurs in senescent AECIIs, it not only promotes aberrant trans-differentiation but also leads to impaired AECII regeneration during the repair of AECs. Impaired regeneration results in the exposure of AECIIs to continuously elevated mechanical force caused by cytoskeleton rearrangement (Wu et al., 2021). Thus, SADD should be used as an entry point for the detection of premature lung failure and the early stages of fibrosis. Single-AECII populations can be sequenced for the differentiation of the gene profile of AECII senescence and differentiation status, identification of structural modifications after gene transcription, and decoding of compromised protective complexes. An in-depth study of the mechanisms that promote lung regeneration and reduce elevated mechanical forces caused by impaired alveolar regeneration may improve interventions for IPF. The Notch signaling pathway plays an important role in the differentiation of AECII into AECI, it is activated in AECII early in alveolar repair but is inhibited by the Notch ligand deltalike 1 homolog (Dlk1) late in repair after Notch activation has reached its peak. Dlk1 controls Notch signaling after lung injury and promotes AECII to AECI conversion and alveolar epithelial repair. Lack of Dlk1 in AECII results in continued activation of Notch signaling in AECII, which prevents AECII from differentiating to AECI, resulting in incomplete alveolar repair. It suggesting that Dlk1 and the Notch signaling system may be potential therapeutic targets for alveolar epithelial repair (Liu et al., 2010; Finn et al., 2019). In-depth study of the Notch signaling pathway to facilitate the conversion of AECII to AECI, thus avoiding the development of SADD-induced IPF is a possible direction for future research.

Senescent AECII and senescence-associated secretory phenotype

During AECII senescence, a specific phenotype is acquired, which is known as the SASP, which is characterized by replication arrest and the abnormal secretion of pro-fibrosis and pro-inflammatory senescence-related factors (Munoz-Espin and Serrano, 2014; Lehmann et al., 2017; Hansel et al., 2020). Proinflammatory and matrix-degradation factors are the most important ones (Coppe et al., 2008). SASP can lead to cellular dysfunction and impaired immune function and reacts on senescent cells and their neighbors, accelerating the aging process and thus creating a vicious cycle that maintains inflammation in the lungs. SASP acts as a trigger and effector molecule for the advancement of IPF (Rana et al., 2020). Studies have confirmed that KDM4, a key regulator of SASP, can selectively target SASP to inhibit AECII senescence while maintaining cell cycle arrest to manipulate senescent AECII, thereby maintaining homeostasis within tissues and organs and controlling organismal senescence (Zhang S et al., 2021). By contrast, the human protein 12S rRNA-c, encoded by mitochondrial DNA, and the mitochondrial open reading frame induce the production of specific SASP factors in azithromycin-induced and replicative cellular senescence (Kim et al., 2018). Therefore, targeting mitochondria to inhibit SASP may be a potential strategy for the treatment of IPF. Furthermore, the expression of noncoding RNAs is significantly up-regulated during cellular senescence. Further analysis has shown that human satellite II (hSATII) RNA interferes with the staining of certain SASP gene regions by impairing the function of CCCTC-binding factor. Pericentromeric hSATII RNA can promote SASP-Like inflammatory gene expression in senescent cells, thereby up-regulating the expression of SASP-like inflammatory genes (Miyata et al., 2021). In addition, studies have shown that telomere-mediated AECII senescence can lead to cell-autonomous defects and upregulation of secondary paracrine signaling, which can induce inflammation and mesenchymal abnormalities associated with altered intracellular gene expression and SASP (Alder et al., 2015). SASP affects its surrounding non-senescent cells through autocrine and paracrine functions and mediate the exacerbation of cellular senescence (De Cecco et al., 2019).

In IPF, SASP regulates senescence mainly through nuclear factor kappa-B (NF-κB), CCAAT-enhancer-binding protein beta (CEBPβ), and tumor protein p53 (TP53). All three of these transcription factors have a common characteristic which is their redox-dependent regulation. Among them, NF-κB is the main regulator of SASP, which is maintained in an autocrine manner by the SASP factor interleukin Iα (IL-Iα) (Nelson et al., 2012; Salminen et al., 2012). Secretion of IL-1α and signaling cascade of the p38 mitogen-activated protein kinase (p38MAPK) can active NF-κB, thereby promoting SASP expression (Orjalo et al., 2009; Amaya-Montoya et al., 2020). C/EBPβ mainly regulates the expression of various SASP factors. Its activation is a key event in the transition of cells to the terminal senescent state (Hoare et al., 2016). TP53 plays a key role in cellular stress response and senescence by regulating multiple antioxidant genes to maintain cellular redox homeostasis. It can promote p38MAPK phosphorylation and downstream NF-κB activation when p53 inactivated, thereby establishing an irreversible senescence phenotype (Freund et al., 2011). TGF-β is one of the secreted factors of SASP. When TGF-β signaling is activated in an autocrine or paracrine manner, it induces SASP and thus induces and maintains the aging phenotype. Interestingly, spectral tracing in mice has shown that AECIIs undergo aberrant cellular remodeling during

increased TGF-β and TP53 signaling. This effect is accompanied by morphological changes associated with the replicative senescence characteristics of SADD (Yang et al., 2020).

Senescent AECIIs propagate senescence signals to surrounding cells by secreting SASP, which not only leads to persistent inflammation, tissue remodeling, and fibrotic phenotypic changes but also creates senescence-associated low-grade inflammation, leading to SADD that promotes myofibroblast proliferation under SALI (Acosta et al., 2013; Kobayashi et al., 2020) and further promoting IPF. In conclusion, a causal relationship among senescent AECIIs, SASP, and SADD was found, which synergistically promotes the occurrence and progression of IPF. Therefore, preventing premature pulmonary failure or clearing senescent AECIIs and blocking its related SASP secretion can be effective measures for IPF treatment.

Senescent AECII and autophagy

Autophagy, a highly selective cellular clearance pathway associated with the maintenance of cellular tissue homeostasis, is an evolutionarily conserved degradation system in which cellular contents, such as proteins, organelles, and lipids are degraded in a lysosome-dependent manner (Kirkin, 2020). Autophagy inhibits senescence-associated inflammation, maintains genomic integrity, and preserves cellular and tissue homeostasis and the regenerative capacity of stem cells; the core processes are initiated by inhibiting mammalian target of rapamycin (mTOR) or activating Adenosine monophosphate (AMP)-activated protein kinase (AMPK) (Rubinsztein et al., 2011; Hansen et al., 2018). Studies show a decrease in AMPK phosphorylation and an increase in mTORC1 signaling and metabolic reprogramming in IPF (Hansen et al., 2018; Rangarajan et al., 2018). mTOR, a mammalian target of rapamycin, forms two complexes, mTORC1 and mTORC2. They have distinct effector proteins that are activated by multiple upstream inputs and trigger distinct downstream cellular responses (Plate et al., 2020). Among them, mTORC1 regulates autophagy and senescence by promoting *ab initio* lipid synthesis through sterol response element binding protein (SREBP), protein synthesis through phosphorylation of the eukaryotic translation initiation factor 4E-binding protein 1 (4E-BP1), and in the absence of glucose, the key energy sensor AMPK promotes autophagy through direct activation of unc-51-like kinase 1 (ULK1). Under nutrient-sufficient conditions, mTORC1 phosphorylates ULK1, preventing its activation and disrupting its interaction with AMPK to prevent autophagy (Kim et al., 2011).

Impaired autophagy is one of the hallmarks of senescence (Aman et al., 2021), and inflammation caused by its impairment is a major driver of senescence-induced tissue damage (Lopez-Otin et al., 2013; Franceschi et al., 2018). In addition, autophagy plays an important role in the control and treatment of COVID-19 (Brest et al., 2020; Mijaljica and Klionsky, 2020; Shojaei et al., 2020). The autophagic pathway is tightly regulated by multimolecular pathways, such as AMPK and mTORC1, and deacetylases (sirtuins) (Rubinsztein et al., 2011), and mTOR signaling is a central part of TGF-β1-mediated fibrosis (Laplante and Sabatini, 2012; Zhai et al., 2017). Severe deficiencies in autophagy levels in lung tissues during the IPF cause AEC senescence and damage, leading to abnormal epithelial–mesenchymal crosstalk and promoting fibroblast-to-myofibroblast differentiation. Meanwhile, restoring autophagy inhibits transformation and reduces collagen deposition, thereby inhibiting IPF formation (Araya et al., 2013; Margaritopoulos et al., 2013). Therefore, promoting autophagy to slow down senescence and regulating the IPF process through the disruption of typical molecular pathways is a promising therapeutic option. lncIAPF (lncRNA inhibit autophagy in pulmonary fibrogenesis) is identified as a profibrotic factor to promote pulmonary fibrosis. Mechanistically, lncIAPF forms a RNA-protein complex with human antigen R (HuR) to block autophagy by controlling the stability of the target genes EZH2 (enhancer of zeste 2 polycomb repressive complex 2 subunit), STAT1 (signal transducer and activators of transcription 1) and FOXK1 (forkhead box K1). Zhang et al. have provided preclinical evidence from the mouse models of lung fibrosis and patient samples and proposed pharmacological approaches for inhibiting lncIAPF related to autophagy; these approaches represent promising therapeutic options for IPF (Zhang et al., 2022). However, numerous questions need to be answered. For example, given that reduction in autophagy in IPF can lead to AEC senescence and the accumulation of inflammatory factors, and excessive autophagy can lead to lung atrophy, how autophagy balance can be achieved? What is the threshold for autophagy balance? How autophagy regulators can be delivered to specific cells at the right time? In the future, changes in AECII autophagy in IPF, the role and regulatory mechanism of autophagy in IPF, and whether AECII stem cell properties can be restored through autophagy for the conversion of AECIIs into AECIs and alleviation of SADD should be investigated.

Medication

IPF is a serious lung disease with poor prognosis and without effective treatment. Anti-inflammatory drugs, corticosteroids and immunosuppressants have been used in the treatment of IPF over the past decades based on the assumption that inflammation is the main mechanism of pulmonary fibrosis (Hewlett et al., 2018). However, a multicentre randomised trial showed that the combination of corticosteroids, azathioprine and N-acetylcysteine increased mortality and hospitalisation rates (Raghu et al., 2012). As a

result, this combination was discontinued. Only pirfenidone and nintedanib are currently approved for clinical use. In placebo-controlled, randomised phase 3 studies, pirfenidone and nitisinib effectively slowed disease progression, but did not improve survival or reverse pulmonary fibrosis (Lomas et al., 2012; King et al., 2014; Richeldi et al., 2014). Recent advances in understanding the pathogenesis of IPF are multifaceted and have led to the exploration and development of therapeutic agents for IPF. AECII, as stem cells of the alveolar epithelium, play an important role in the development of IPF due to the positive feedback loop caused by their senescence (Parimon et al., 2020; Kellogg et al., 2021; Parimon et al., 2021). Hashimoto et al. (2016) provided striking evidence that cellular senescence is a relevant target for lung functional improvement. Thus, one of the therapeutic strategies for IPF is to target senescent cells mainly through the elimination of senescent cells or restoration of their vitality. The following section will focus on three therapies targeting senescent AECIIs. Senotherapeutics, which is a new class of antisenescence agents designed to eliminate or delay the adverse effects of cellular senescence containing senolytics (selectively removes senescent cells) and senomorphics (acts as SASP inhibitors without killing cells) (Lagoumtzi and Chondrogianni, 2021), autophagy regulators, and stem cell therapy.

Senolytics

Senolytics are agents that target senescent cells through senescence-associated anti-apoptotic pathways (Lagoumtzi and Chondrogianni, 2021). Kim et al. have summarized seven classes of antisenescence agents, namely, natural compounds, kinase inhibitors, Bcl-2 family inhibitors/Bcl-2 homolog 3 (BH3) mimetics, MDM2/p53 interaction inhibitors, Hsp90 inhibitors, p53 binding inhibitors, and HDAC inhibitors (Kim and Kim, 2019). The combination of quercetin and dasatinib (DQ therapy) can alleviate experimental pulmonary fibrosis by targeting senescent cells. The first human trial conducted on patients with IPF has validated the safety of DQ therapy (Justice et al., 2019). The AECII pathology-driven features in COVID-19 are similar to those in IPF (Sinha et al., 2022). Tests on mice infected with SARS-CoV-2 showed that DQ therapy or ABT-263 have targeted the elimination of virus-induced senescence and alleviation of COVID-19-related pulmonary symptoms. Further clinical trials conducted on COVID-19 patients have found that quercetin significantly improve pulmonary symptoms (Lee et al., 2021), but DQ therapy dose-dependently cleared senescent cells while damaging proliferating cells. The inhibition of Bcl-2/xl by ABT-263 can selectively target senescent AECIIs and reverses persistent pulmonary fibrosis in mice. However, it also results in the removal of normally proliferating or dormant cells from organs (off-target effect) (Pan et al., 2017). Research should further explore the key molecules and signaling pathways involved in AECII senescence causing IPF to preserve AECII population with differentiation potential in tissues and prevent the off-target effect. Damage to the stem cell characteristics of AECIIs in the microenvironment, which can lead to impaired differentiation and renewal and repair of tissues, should be prevented.

Senomorphics

Senomorphics target SASP by inhibiting SASP-expression-related pathways or inhibit specific SASP factors and neutralizing specific antibodies. Senomorphics contain JAK inhibitors (ruxolitinib), NF-κB inhibitors (resveratrol and apigenin), mTOR kinase inhibitors (rapamycin and everolimus) and antibodies against specific SASP factor (Song et al., 2020). Metformin, ruxolitinib and glucocorticoids have been currently approved by the FDA as potential anti-aging drugs (Laberge et al., 2012; Lagoumtzi and Chondrogianni, 2021). Other reports have suggested that the Ca^{2+} channel blockers loperamide and niguldipine, the ataxia telangiectasia-mutated (ATM) kinase inhibitor KU-60019, and the IKK peptide inhibitor NBD have potential antisenescence activities (Kang et al., 2017; Song et al., 2020; Lagoumtzi and Chondrogianni, 2021). However, their targeting and efficacy have not yet been systematically and comprehensively elucidated.

Procyanidin C1 (PCC1), a polyphenolic component of grape seed extract (GSE), is the main substance mediating the senolytic effect of GSE. It can increase the accumulation of ROS in the cytoplasm of senescent cells and induce a continuous decrease in the mitochondrial membrane potential of senescent cells followed by the release of mitochondrial cytochrome c, resulting in the abnormal cleavage of caspase 3 and ultimately causing senescent cell apoptosis. In contrast to other traditional senolytics, PCC1 has a dual function of inhibiting SASP and targeting senescent cells (Xu et al., 2021). Its efficacy and safety in antisenescence has been demonstrated in animal studies. Moreover, the concentration of PCC1 *in vivo* varies among organs, and their local concentration may not achieve antisenescence effects in some tissue types. As phenolic compounds in grapes generally have disadvantages, such as poor water solubility and oral bioavailability. However, the use of solid lipid nanoparticle drug delivery systems to encapsulate GSE containing proanthocyanidins not only alleviates these problems but also greatly reduces oxidative stress and inflammation (Castellani et al., 2018). Astaxanthin works in the same manner as PCC1, which can ameliorate IPF through the ROS-dependent mitochondrial signaling pathway in AECIIs (Song et al., 2014b). However, the

TABLE 1 Autophagy regulators.

Compounds	Mechanism of action	Experimental models	References
Rapamycin	inhibit the mTOR pathway; reduce protein synthesis; promote autophagy	human; mice; yeast	Menzies et al. (2017); Rubinsztein et al. (2012); Powers et al. (2006)
Ouabain	inhibit mTOR kinases; facilitate the clearance of endogenous tau; induce autophagic lysosomes; promote cells repair	flies; human; mice	Song et al. (2019)
Fisetin	inhibit mTOR kinases; facilitate the clearance of endogenous tau *via* TFEB and Nrf2 activation; activate sirtuins	flies; mice; worms; yeast	Kim et al. (2016); Yousefzadeh et al. (2018)
Spermidine	inhibit the EP300 acetyltransferase; promote autophagy; anti-inflammation	flies; human; worms; yeast	Pietrocola et al. (2015); Freitag et al. (2022)
Resveratrol	NAD + -dependent; NF	flies, mice, worms, yeast	Morselli et al. (2011); Wang Z et al. (2021)
Metformin	mTOR-independent; act the AMPK pathway; promote autophagy	human; mice	Menzies et al. (2017)
Trehalose	mTOR-independent; activate AMPK pathway; activate TFEB; promote autophagy	human; mice; worms	Menzies et al. (2015); Sharma et al. (2018)
Urolithin A	mitophagy-dependent (pink-1, pdr-1 or dct-1); inhibit amyloid β and tau C	mice; worms	D'Amico et al. (2021); Ryu et al. (2016)
KU-60019	inhibit ATM kinase; restore mitochondrial function; promote autophagy	mice	Kang et al. (2017)
NAD^+	mitophagy-dependent; NAD+–SIRT axis; activate sirtuins; inhibit the deacetylation of mTOR pathways and autophagy proteins	humans, mice	Lautrup et al. (2019); Lee et al. (2008)
nicotinamide riboside	mitophagy-dependent; NAD+ precursors; activate mitophagy	humans, mice	Fang et al. (2019); Mitchell et al. (2018)
lncIAPF	block autophagy by controlling the stability of the target genes EZH2, STAT1 and FOXK1	cell, human, mice	Zhang et al. (2022)

therapeutic role of PCC1 and astaxanthin in IPF should be further investigated.

Aging is an irreversible process. Senescent cells are the sources of SASP, so SASP cannot be permanently eliminated. Therefore, senomorphics need to be taken for a long period to achieve maximum intervention, and the potential risks and adverse effects of senomorphics are greater than those of senolytics (Song et al., 2020). Antisenescence agents exert a positive effect on the treatment of IPF by modulating the activities of senescent cells, as demonstrated in a mouse model (Wiley et al., 2019). However, whether its long-term application promotes the proliferation of adjacent cells, accelerate telomere shortening, and thus promote aging is unclear. Therefore, long-term preclinical trials on the efficacy of antisenescence agents for patients with IPF are needed (Lagoumtzi and Chondrogianni, 2021).

Autophagy regulators

The mechanism of impaired autophagy in IPF is unclear. Not only it can trigger fibrosis due to inadequate mitochondrial quality control but also it can lead to abnormal NF-κB signaling through p62 accumulation (Patel et al., 2012; Hill et al., 2019; Sharma et al., 2021). Autophagy regulators include the mTOR pathway-dependent inhibitors (rapamycin, torin-1, PP242h) and the direct activators of AMPK (metformin and alginate), as well as the regulators of the acetylation pathway (spermidine and resveratrol), and also classical autophagy-inducing factors such as transcription factor EB (TFEB) (Rubinsztein et al., 2012; Menzies et al., 2017; Aman et al., 2021). It was found that metformin accelerated the regression of experimental fibrosis in an AMPK-dependent manner. Mechanistically, metformin not only promoted autophagy and reduced collagen production (Kheirollahi et al., 2019), but also prevented the production of α-SMA and ECM after TGF-β1 stimulation (Rangarajan et al., 2018). The ATM kinase inhibitor KU-60019 induces the functional recovery of an autophagic system and restores mitochondrial function and metabolic reprogramming. Autophagy modulators not only promote autophagy to prevent AEC senescence and inhibit senescence-associated inflammation but also directly reduce collagen deposition (Kang et al., 2017). Thus, the modulation of autophagic pathways holds great promise in the therapeutic exploration of IPF. The compounds of autophagic regulators are listed in Table 1.

Stem cell therapy

Mesenchymal stem cells (MSCs) have great therapeutic potential in IPF due to their powerful paracrine, anti-inflammatory, anti-apoptotic, and immunomodulatory capabilities. MSCs can inhibit AECII senescence by regulating NAMPT-mediated nicotinamide adenine dinucleotide (NAD^+) metabolism and attenuating fibrosis, as demonstrated in animal

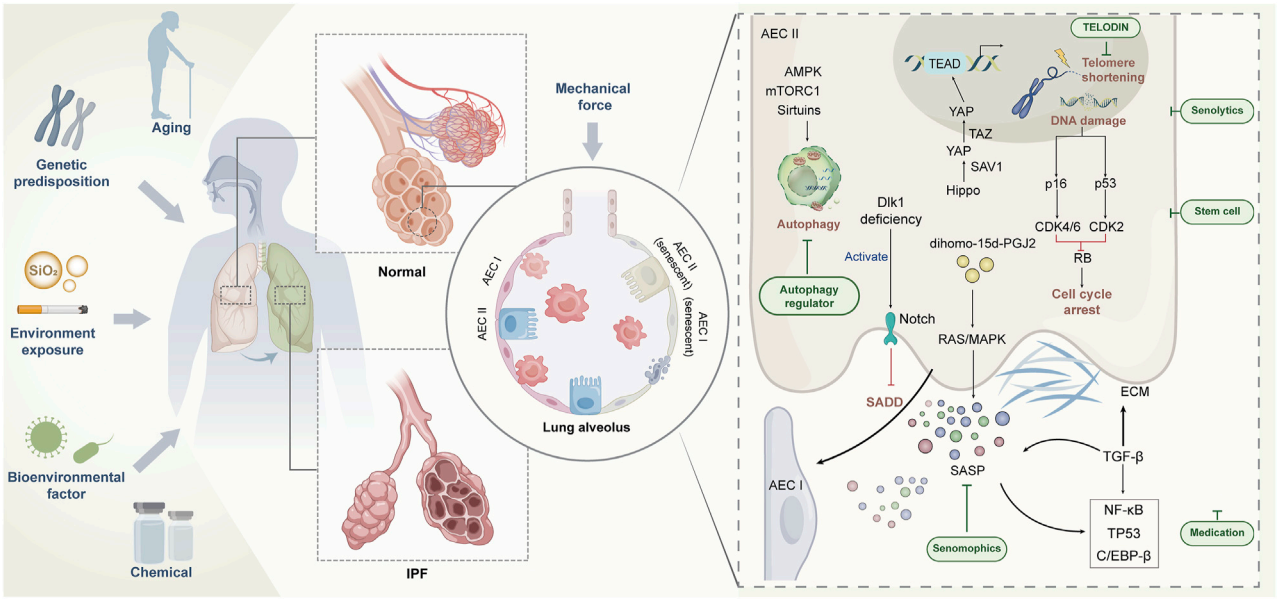

FIGURE 1
Regulation of AECII senescence and strategy of targeting senescent AECII for IPF treatment.

models (Lai et al., 2022). Thus, NAD^+ homeostasis may be responsible for the control of IPF by MSCs. Studies on animal models have found that supplementation with NAD+ precursors, such as nicotinamide riboside (NR) and nicotinamide mononucleotide (NM) can promote autophagy and have significant anti-aging effects (Verdin, 2015; Lautrup et al., 2019; Ruaro et al., 2021). According to preclinical studies on different sources of MSCs in IPF models, human Wharton jelly-derived mesenchymal stem cells may offer prospects for stem cell therapy for pulmonary fibrosis (Saleh et al., 2022).

Stem cell therapy has promising clinical applications, but high labor costs and tumorigenesis and immunological risks limit its application. Dinh et al. (2020) have proposed that the inhalation of lung spheroid cell secretome (LSC-Sec) and exosomes (LSC-Exo) is more therapeutic and has fewer side effects. Monocyte chemotactic protein 1 (MCP-1), also known as chemokine (C-C motif) ligand 2, is down-regulated in sera from animals treated with LSC-Sec and LSC-Exo. MCP-1 plays a key role in lung inflammation, and increase in its level represents poor prognosis in patients with IPF. Hence, the nebulized inhalation of LSC-Sec and LSC-Exo not only offers an opportunity for the treatment of IPF but also provides a reliable way for assessing its prognosis. However, current researches on these compounds have found many limitations in terms of dose response, route of administration, and secretome isolation. Selecting the right stem cell dose and injection method and establishing precise isolation protocols are challenges in stem cell therapy. Rejuvenating strategies for stem-cell-based therapies for aging should be explored.

Conclusion

AECII senescence is one of the key drivers of IPF pathogenesis (Parimon et al., 2020; Yao et al., 2021). Senescent AECII-associated SADD and SASP act together as triggers and effector molecules to promote the IPF process. How senescent AECIIs act on IPF, how it alters the lung microenvironment, and how it mediates persistent and progressive fibrosis are unclear. The role of AECIIs in IPF should be explored in depth, and *in vivo* models should be conducted for the senescent AECII population.

The evolution of IPF is a dynamic process with complex etiology and unknown mechanisms. A large number of studies have revealed the complex pathophysiological basis of IPF, including genetics, epigenetics, metabolomics, and interaction with environment (Figure 1). Single-cell RNA sequencing data have shown that senescence markers are up-regulated in AECIIs in IPF (Xu et al., 2016; Mora et al., 2017; Adams et al., 2020), suggesting that impaired self-differentiation and profibrotic and low-inflammation environment caused by AECII senescence are important risk factors for IPF. Targeting senescence is expected to improve the health of patients with IPF. However, no research has confirmed that targeting senescence agents can completely remove senescent cells. However, numerous studies have shown that even partial elimination of senescent cells can cause a remission of the aging phenotype (Lehmann et al., 2017). In addition to using TELODIN and autophagy modulators in preventing AECII senescence (Hong et al., 2022), we can further investigate the selection of antisenescence agents to

target senescent AECIIs or selectively block the damaging effects of SASP, thus minimizing the drive of senescence on IPF. For the acceleration of the process for targeting senescent AECIIs in the treatment of IPF, at least three issues need to be addressed: whether the progression of IPF can be terminated by targeting senescent AECIIs, whether AECII senescence can be selectively and safely targeted by some drugs without affecting normal cells, and whether clearance senescent AECIIs can reverse or even counteract the pathological features of IPF. The resolution of these issues can facilitate the design of highly effective drugs or development of novel therapies that can target senescent AECIIs and promote the restoration of the original function of senescent lung cells. In conclusion, combating or reversing lung aging by targeting senescent AECIIs is a demanding challenge. The implications of inhibiting the deterioration of IPF by medical means are objectively complex and are the subject of continued exploration in the future.

Author contributions

This work was designed and drafted by TZ and XS. HL, JZ and CL reviewed and edited the manuscript.

Funding

This work was supported by the National Natural Science Foundation of China (82170085, 81970064, 81870001, 81670064, and 31670365), the Natural Science Foundation of Shandong Province (ZR2020MH009 and ZR2020MH010).

Conflict of interest

The authors declare that the research was conducted in the absence of any commercial or financial relationships that could be construed as a potential conflict of interest.

Publisher's note

References

Abbadie, C., Pluquet, O., and Pourtier, A. (2017). Epithelial cell senescence: An adaptive response to pre-carcinogenic stresses? *Cell. Mol. Life Sci.* 74 (24), 4471–4509. doi:10.1007/s00018-017-2587-9

Acosta, J. C., Banito, A., Wuestefeld, T., Georgilis, A., Janich, P., Morton, J. P., et al. (2013). A complex secretory program orchestrated by the inflammasome controls paracrine senescence. *Nat. Cell. Biol.* 15 (8), 978–990. doi:10.1038/ncb2784

Adams, T. S., Schupp, J. C., Poli, S., Ayaub, E. A., Neumark, N., Ahangari, F., et al. (2020). Single-cell RNA-seq reveals ectopic and aberrant lung-resident cell populations in idiopathic pulmonary fibrosis. *Sci. Adv.* 6 (28), eaba1983. doi:10.1126/sciadv.aba1983

Alder, J. K., Barkauskas, C. E., Limjunyawong, N., Stanley, S. E., Kembou, F., Tuder, R. M., et al. (2015). Telomere dysfunction causes alveolar stem cell failure. *Proc. Natl. Acad. Sci. U. S. A.* 112 (16), 5099–5104. doi:10.1073/pnas.1504780112

Aman, Y., Schmauck-Medina, T., Hansen, M., Morimoto, R. I., Simon, A. K., Bjedov, I., et al. (2021). Autophagy in healthy aging and disease. *Nat. Aging* 1 (8), 634–650. doi:10.1038/s43587-021-00098-4

Amaya-Montoya, M., Perez-Londono, A., Guatibonza-Garcia, V., Vargas-Villanueva, A., and Mendivil, C. O. (2020). Cellular senescence as a therapeutic target for age-related diseases: A review. *Adv. Ther.* 37 (4), 1407–1424. doi:10.1007/s12325-020-01287-0

Araya, J., Kojima, J., Takasaka, N., Ito, S., Fujii, S., Hara, H., et al. (2013). Insufficient autophagy in idiopathic pulmonary fibrosis. *Am. J. Physiol. Lung Cell. Mol. Physiol.* 304 (1), L56–L69. doi:10.1152/ajplung.00213.2012

Aumiller, V., Balsara, N., Wilhelm, J., Gunther, A., and Konigshoff, M. (2013). WNT/β-catenin signaling induces IL-1β expression by alveolar epithelial cells in pulmonary fibrosis. *Am. J. Respir. Cell. Mol. Biol.* 49 (1), 96–104. doi:10.1165/rcmb.2012-0524OC

Baker, D. J., Childs, B. G., Durik, M., Wijers, M. E., Sieben, C. J., Zhong, J., et al. (2016). Naturally occurring p16(Ink4a)-positive cells shorten healthy lifespan. *Nature* 530 (7589), 184–189. doi:10.1038/nature16932

Barkauskas, C. E., Cronce, M. J., Rackley, C. R., Bowie, E. J., Keene, D. R., Stripp, B. R., et al. (2013). Type 2 alveolar cells are stem cells in adult lung. *J. Clin. Invest.* 123 (7), 3025–3036. doi:10.1172/JCI68782

Bellaye, P. S., Yanagihara, T., Granton, E., Sato, S., Shimbori, C., Upagupta, C., et al. (2018). Macitentan reduces progression of TGF-β1-induced pulmonary fibrosis and pulmonary hypertension. *Eur. Respir. J.* 52 (2), 1701857. doi:10.1183/13993003.01857-2017

Boutanquoi, P. M., Burgy, O., Beltramo, G., Bellaye, P. S., Dondaine, L., Marcion, G., et al. (2020). TRIM33 prevents pulmonary fibrosis by impairing TGF-β1 signalling. *Eur. Respir. J.* 55 (6), 1901346. doi:10.1183/13993003.01346-2019

Brest, P., Benzaquen, J., Klionsky, D. J., Hofman, P., and Mograbi, B. (2020). Open questions for harnessing autophagy-modulating drugs in the SARS-CoV-2 war: Hope or hype? *Autophagy* 16 (12), 2267–2270. doi:10.1080/15548627.2020.1779531

Castellani, S., Trapani, A., Spagnoletta, A., di Toma, L., Magrone, T., Di Gioia, S., et al. (2018). Nanoparticle delivery of grape seed-derived proanthocyanidins to airway epithelial cells dampens oxidative stress and inflammation. *J. Transl. Med.* 16 (1), 140. doi:10.1186/s12967-018-1509-4

Chen, Q., Suresh, K. V., Finn, J., Jiang, D., Liang, J., Zhao, Y. Y., et al. (2017). CD44(high) alveolar type II cells show stem cell properties during steady-state alveolar homeostasis. *Am. J. Physiol. Lung Cell. Mol. Physiol.* 313 (1), L41–L51. doi:10.1152/ajplung.00564.2016

Childs, B. G., Durik, M., Baker, D. J., and van Deursen, J. M. (2015). Cellular senescence in aging and age-related disease: From mechanisms to therapy. *Nat. Med.* 21 (12), 1424–1435. doi:10.1038/nm.4000

Chilosi, M., Carloni, A., Rossi, A., and Poletti, V. (2013). Premature lung aging and cellular senescence in the pathogenesis of idiopathic pulmonary fibrosis and COPD/emphysema. *Transl. Res.* 162 (3), 156–173. doi:10.1016/j.trsl.2013.06.004

Choi, W. I., Dauti, S., Kim, H. J., Park, S. H., Park, J. S., and Lee, C. W. (2018). Risk factors for interstitial lung disease: A 9-year Nationwide population-based study. *BMC Pulm. Med.* 18 (1), 96. doi:10.1186/s12890-018-0660-2

Confalonieri, P., Volpe, M. C., Jacob, J., Maiocchi, S., Salton, F., Ruaro, B., et al. (2022). Regeneration or repair? The role of alveolar epithelial cells in the pathogenesis of idiopathic pulmonary fibrosis (IPF). *Cells* 11 (13), 2095. doi:10.3390/cells11132095

Coppe, J. P., Patil, C. K., Rodier, F., Sun, Y., Munoz, D. P., Goldstein, J., et al. (2008). Senescence-associated secretory phenotypes reveal cell-nonautonomous functions of oncogenic RAS and the p53 tumor suppressor. *PLoS Biol.* 6 (12), 2853–2868. doi:10.1371/journal.pbio.0060301

D'Amico, D., Andreux, P. A., Valdes, P., Singh, A., Rinsch, C., and Auwerx, J. (2021). Impact of the natural compound urolithin A on health, disease, and aging. *Trends Mol. Med.* 27 (7), 687–699. doi:10.1016/j.molmed.2021.04.009

De Cecco, M., Ito, T., Petrashen, A. P., Elias, A. E., Skvir, N. J., Criscione, S. W., et al. (2019). L1 drives IFN in senescent cells and promotes age-associated inflammation. *Nature* 566 (7742), 73–78. doi:10.1038/s41586-018-0784-9

Dinh, P. C., Paudel, D., Brochu, H., Popowski, K. D., Gracieux, M. C., Cores, J., et al. (2020). Inhalation of lung spheroid cell secretome and exosomes promotes lung repair in pulmonary fibrosis. *Nat. Commun.* 11 (1), 1064. doi:10.1038/s41467-020-14344-7

Duckworth, A., Gibbons, M. A., Allen, R. J., Almond, H., Beaumont, R. N., Wood, A. R., et al. (2021). Telomere length and risk of idiopathic pulmonary fibrosis and chronic obstructive pulmonary disease: A mendelian randomisation study. *Lancet. Respir. Med.* 9 (3), 285–294. doi:10.1016/S2213-2600(20)30364-7

Fang, E. F., Hou, Y., Lautrup, S., Jensen, M. B., Yang, B., Sengupta, T., et al. (2019). NAD(+) augmentation restores mitophagy and limits accelerated aging in Werner syndrome. *Nat. Commun.* 10 (1), 5284. doi:10.1038/s41467-019-13172-8

Finn, J., Sottoriva, K., Pajcini, K. V., Kitajewski, J. K., Chen, C., Zhang, W., et al. (2019). Dlk1-Mediated temporal regulation of Notch signaling is required for differentiation of alveolar type II to type I cells during repair. *Cell. Rep.* 26 (11), 2942–2954. e5. doi:10.1016/j.celrep.2019.02.046

Franceschi, C., Garagnani, P., Parini, P., Giuliani, C., and Santoro, A. (2018). Inflammaging: A new immune-metabolic viewpoint for age-related diseases. *Nat. Rev. Endocrinol.* 14 (10), 576–590. doi:10.1038/s41574-018-0059-4

Freitag, K., Sterczyk, N., Wendlinger, S., Obermayer, B., Schulz, J., Farztdinov, V., et al. (2022). Spermidine reduces neuroinflammation and soluble amyloid beta in an Alzheimer's disease mouse model. *J. Neuroinflammation* 19 (1), 172. doi:10.1186/s12974-022-02534-7

Freund, A., Patil, C. K., and Campisi, J. (2011). p38MAPK is a novel DNA damage response-independent regulator of the senescence-associated secretory phenotype. *EMBO J.* 30 (8), 1536–1548. doi:10.1038/emboj.2011.69

Gao, Y., Zhang, J., Liu, Y., Zhang, S., Wang, Y., Liu, B., et al. (2017). Regulation of TERRA on telomeric and mitochondrial functions in IPF pathogenesis. *BMC Pulm. Med.* 17 (1), 163. doi:10.1186/s12890-017-0516-1

Gonzalez-Garcia, C., Cantini, M., Ballester-Beltran, J., Altankov, G., and Salmeron-Sanchez, M. (2018). The strength of the protein-material interaction determines cell fate. *Acta Biomater.* 77, 74–84. doi:10.1016/j.actbio.2018.07.016

Haak, A. J., Kostallari, E., Sicard, D., Ligresti, G., Choi, K. M., Caporarello, N., et al. (2019). Selective YAP/TAZ inhibition in fibroblasts via dopamine receptor D1 agonism reverses fibrosis. *Sci. Transl. Med.* 11 (516), eaau6296. doi:10.1126/scitranslmed.aau6296

Hansel, C., Jendrossek, V., and Klein, D. (2020). Cellular senescence in the lung: The central role of senescent epithelial cells. *Int. J. Mol. Sci.* 21 (9), E3279. doi:10.3390/ijms21093279

Hansen, M., Rubinsztein, D. C., and Walker, D. W. (2018). Autophagy as a promoter of longevity: Insights from model organisms. *Nat. Rev. Mol. Cell. Biol.* 19 (9), 579–593. doi:10.1038/s41580-018-0033-y

Hashimoto, M., Asai, A., Kawagishi, H., Mikawa, R., Iwashita, Y., Kanayama, K., et al. (2016). Elimination of p19(ARF)-expressing cells enhances pulmonary function in mice. *JCI Insight* 1 (12), e87732. doi:10.1172/jci.insight.87732

Hewlett, J. C., Kropski, J. A., and Blackwell, T. S. (2018). Idiopathic pulmonary fibrosis: Epithelial-mesenchymal interactions and emerging therapeutic targets. *Matrix Biol.* 71-72, 112–127. doi:10.1016/j.matbio.2018.03.021

Hill, C., Li, J., Liu, D., Conforti, F., Brereton, C. J., Yao, L., et al. (2019). Autophagy inhibition-mediated epithelial-mesenchymal transition augments local myofibroblast differentiation in pulmonary fibrosis. *Cell. Death Dis.* 10 (8), 591. doi:10.1038/s41419-019-1820-x

Hoare, M., Ito, Y., Kang, T. W., Weekes, M. P., Matheson, N. J., Patten, D. A., et al. (2016). NOTCH1 mediates a switch between two distinct secretomes during senescence. *Nat. Cell. Biol.* 18 (9), 979–992. doi:10.1038/ncb3397

Hohmann, M. S., Habiel, D. M., Coelho, A. L., Verri, W. J., and Hogaboam, C. M. (2019). Quercetin enhances ligand-induced apoptosis in senescent idiopathic pulmonary fibrosis fibroblasts and reduces lung fibrosis *in vivo*. *Am. J. Respir. Cell. Mol. Biol.* 60 (1), 28–40. doi:10.1165/rcmb.2017-0289OC

Hong, X., Wang, L., Zhang, K., Liu, J., and Liu, J. P. (2022). Molecular mechanisms of alveolar epithelial stem cell senescence and senescence-associated differentiation disorders in pulmonary fibrosis. *Cells* 11 (5), 877. doi:10.3390/cells11050877

Justice, J. N., Nambiar, A. M., Tchkonia, T., Lebrasseur, N. K., Pascual, R., Hashmi, S. K., et al. (2019). Senolytics in idiopathic pulmonary fibrosis: Results from a first-in-human, open-label, pilot study. *EBioMedicine* 40, 554–563. doi:10.1016/j.ebiom.2018.12.052

Kang, H. T., Park, J. T., Choi, K., Kim, Y., Choi, H., Jung, C. W., et al. (2017). Chemical screening identifies ATM as a target for alleviating senescence. *Nat. Chem. Biol.* 13 (6), 616–623. doi:10.1038/nchembio.2342

Kellogg, D. L., Kellogg, D. J., Musi, N., and Nambiar, A. M. (2021). Cellular senescence in idiopathic pulmonary fibrosis. *Curr. Mol. Biol. Rep.* 7 (3), 31–40. doi:10.1007/s40610-021-00145-4

Kheirollahi, V., Wasnick, R. M., Biasin, V., Vazquez-Armendariz, A. I., Chu, X., Moiseenko, A., et al. (2019). Metformin induces lipogenic differentiation in myofibroblasts to reverse lung fibrosis. *Nat. Commun.* 10 (1), 2987. doi:10.1038/s41467-019-10839-0

Kim, E. C., and Kim, J. R. (2019). Senotherapeutics: Emerging strategy for healthy aging and age-related disease. *BMB Rep.* 52 (1), 47–55. doi:10.5483/bmbrep.2019.52.1.293

Kim, J., Kundu, M., Viollet, B., and Guan, K. L. (2011). AMPK and mTOR regulate autophagy through direct phosphorylation of Ulk1. *Nat. Cell. Biol.* 13 (2), 132–141. doi:10.1038/ncb2152

Kim, S., Choi, K. J., Cho, S. J., Yun, S. M., Jeon, J. P., Koh, Y. H., et al. (2016). Fisetin stimulates autophagic degradation of phosphorylated tau via the activation of TFEB and Nrf2 transcription factors. *Sci. Rep.* 6, 24933. doi:10.1038/srep24933

Kim, S. J., Mehta, H. H., Wan, J., Kuehnemann, C., Chen, J., Hu, J. F., et al. (2018). Mitochondrial peptides modulate mitochondrial function during cellular senescence. *Aging (Albany NY)* 10 (6), 1239–1256. doi:10.18632/aging.101463

King, T. J., Bradford, W. Z., Castro-Bernardini, S., Fagan, E. A., Glaspole, I., Glassberg, M. K., et al. (2014). *A phase 3 trial of pirfenidone in patients.*

Kirkin, V. (2020). History of the selective autophagy research: How did it begin and where does it stand today? *J. Mol. Biol.* 432 (1), 3–27. doi:10.1016/j.jmb.2019.05.010

Kobayashi, Y., Tata, A., Konkimalla, A., Katsura, H., Lee, R. F., Ou, J., et al. (2020). Persistence of a regeneration-associated, transitional alveolar epithelial cell state in pulmonary fibrosis. *Nat. Cell. Biol.* 22 (8), 934–946. doi:10.1038/s41556-020-0542-8

Korfei, M., Mackenzie, B., and Meiners, S. (2020). The ageing lung under stress. *Eur. Respir. Rev.* 29 (156), 200126. doi:10.1183/16000617.0126-2020

Korolchuk, V. I., Miwa, S., Carroll, B., and von Zglinicki, T. (2017). Mitochondria in cell senescence: Is mitophagy the weakest link? *EBioMedicine* 21, 7–13. doi:10.1016/j.ebiom.2017.03.020

Kurz, D. J., Decary, S., Hong, Y., and Erusalimsky, J. D. (2000). Senescence-associated (beta)-galactosidase reflects an increase in lysosomal mass during replicative ageing of human endothelial cells. *J. Cell. Sci.* 113 (20), 3613–3622. doi:10.1242/jcs.113.20.3613

Laberge, R. M., Zhou, L., Sarantos, M. R., Rodier, F., Freund, A., de Keizer, P. L., et al. (2012). Glucocorticoids suppress selected components of the senescence-associated secretory phenotype. *Aging Cell.* 11 (4), 569–578. doi:10.1111/j.1474-9726.2012.00818.x

Lagoumtzi, S. M., and Chondrogianni, N. (2021). Senolytics and senomorphics: Natural and synthetic therapeutics in the treatment of aging and chronic diseases. *Free Radic. Biol. Med.* 171, 169–190. doi:10.1016/j.freeradbiomed.2021.05.003

Lai, X., Huang, S., Lin, S., Pu, L., Wang, Y., Lin, Y., et al. (2022). mTOR inhibition improves the immunomodulatory properties of human bone marrow mesenchymal stem cells by inducing COX-2 and PGE2. *Stem Cell. Res. Ther.* 13 (1), 292. doi:10.1186/s13287-017-0744-6

Laplante, M., and Sabatini, D. M. (2012). mTOR signaling in growth control and disease. *Cell.* 149 (2), 274–293. doi:10.1016/j.cell.2012.03.017

Lautrup, S., Sinclair, D. A., Mattson, M. P., and Fang, E. F. (2019). NAD(+) in brain aging and neurodegenerative disorders. *Cell. Metab.* 30 (4), 630–655. doi:10.1016/j.cmet.2019.09.001

Lee, I. H., Cao, L., Mostoslavsky, R., Lombard, D. B., Liu, J., Bruns, N. E., et al. (2008). A role for the NAD-dependent deacetylase Sirt1 in the regulation of autophagy. *Proc. Natl. Acad. Sci. U. S. A.* 105 (9), 3374–3379. doi:10.1073/pnas.0712145105

Lee, S., Yu, Y., Trimpert, J., Benthani, F., Mairhofer, M., Richter-Pechanska, P., et al. (2021). Virus-induced senescence is a driver and therapeutic target in COVID-19. *Nature* 599 (7884), 283–289. doi:10.1038/s41586-021-03995-1

Lee, T. H., Yeh, C. F., Lee, Y. T., Shih, Y. C., Chen, Y. T., Hung, C. T., et al. (2020). Fibroblast-enriched endoplasmic reticulum protein TXNDC5 promotes pulmonary fibrosis by augmenting TGFβ signaling through TGFBR1 stabilization. *Nat. Commun.* 11 (1), 4254. doi:10.1038/s41467-020-18047-x

Lehmann, M., Korfei, M., Mutze, K., Klee, S., Skronska-Wasek, W., Alsafadi, H. N., et al. (2017). Senolytic drugs target alveolar epithelial cell function and attenuate experimental lung fibrosis *ex vivo*. *Eur. Respir. J.* 50 (2), 1602367. doi:10.1183/13993003.02367-2016

Li, C., Wang, Z., Zhang, J., Zhao, X., Xu, P., Liu, X., et al. (2019). Crosstalk of mRNA, miRNA, lncRNA, and circRNA and their regulatory pattern in pulmonary fibrosis. *Mol. Ther. Nucleic Acids* 18, 204–218. doi:10.1016/j.omtn.2019.08.018

Li, R., Wang, Y., Song, X., Sun, W., Zhang, J., Liu, Y., et al. (2018). Potential regulatory role of circular RNA in idiopathic pulmonary fibrosis. *Int. J. Mol. Med.* 42 (6), 3256–3268. doi:10.3892/ijmm.2018.3892

Liu, G., Philp, A. M., Corte, T., Travis, M. A., Schilter, H., Hansbro, N. G., et al. (2021). Therapeutic targets in lung tissue remodelling and fibrosis. *Pharmacol. Ther.* 225, 107839. doi:10.1016/j.pharmthera.2021.107839

Liu, J., Sato, C., Cerletti, M., and Wagers, A. (2010). Notch signaling in the regulation of stem cell self-renewal and differentiation. *Curr. Top. Dev. Biol.* 92, 367–409. doi:10.1016/S0070-2153(10)92012-7

Liu, R. M., and Liu, G. (2020). Cell senescence and fibrotic lung diseases. *Exp. Gerontol.* 132, 110836. doi:10.1016/j.exger.2020.110836

Lomas, N. J., Watts, K. L., Akram, K. M., Forsyth, N. R., and Spiteri, M. A. (2012). Idiopathic pulmonary fibrosis: Immunohistochemical analysis provides fresh insights into lung tissue remodelling with implications for novel prognostic markers. *Int. J. Clin. Exp. Pathol.* 5 (1), 58–71.

Lopez-Otin, C., Blasco, M. A., Partridge, L., Serrano, M., and Kroemer, G. (2013). The hallmarks of aging. *Cell.* 153 (6), 1194–1217. doi:10.1016/j.cell.2013.05.039

Lv, Q., Wang, J., Xu, C., Huang, X., Ruan, Z., and Dai, Y. (2020). Pirfenidone alleviates pulmonary fibrosis *in vitro* and *in vivo* through regulating Wnt/GSK-3β/β-catenin and TGF-β1/Smad2/3 signaling pathways. *Mol. Med.* 26 (1), 49. doi:10.1186/s10020-020-00173-3

Margaritopoulos, G. A., Tsitoura, E., Tzanakis, N., Spandidos, D. A., Siafakas, N. M., Sourvinos, G., et al. (2013). Self-eating: Friend or foe? The emerging role of autophagy in idiopathic pulmonary fibrosis. *Biomed. Res. Int.* 2013, 420497. doi:10.1155/2013/420497

Meng, X. M., Nikolic-Paterson, D. J., and Lan, H. Y. (2016). TGF-B: The master regulator of fibrosis. *Nat. Rev. Nephrol.* 12 (6), 325–338. doi:10.1038/nrneph.2016.48

Menzies, F. M., Fleming, A., Caricasole, A., Bento, C. F., Andrews, S. P., Ashkenazi, A., et al. (2017). Autophagy and neurodegeneration: Pathogenic mechanisms and therapeutic opportunities. *Neuron* 93 (5), 1015–1034. doi:10.1016/j.neuron.2017.01.022

Menzies, F. M., Fleming, A., and Rubinsztein, D. C. (2015). Compromised autophagy and neurodegenerative diseases. *Nat. Rev. Neurosci.* 16 (6), 345–357. doi:10.1038/nrn3961

Merkt, W., Bueno, M., Mora, A. L., and Lagares, D. (2020). Senotherapeutics: Targeting senescence in idiopathic pulmonary fibrosis. *Semin. Cell. Dev. Biol.* 101, 104–110. doi:10.1016/j.semcdb.2019.12.008

Michalski, J. E., Kurche, J. S., and Schwartz, D. A. (2022). From ARDS to pulmonary fibrosis: The next phase of the COVID-19 pandemic? *Transl. Res.* 241, 13–24. doi:10.1016/j.trsl.2021.09.001

Mijaljica, D., and Klionsky, D. J. (2020). Autophagy/virophagy: A "disposal strategy" to combat COVID-19. *Autophagy* 16 (12), 2271–2272. doi:10.1080/15548627.2020.1782022

Mitchell, S. J., Bernier, M., Aon, M. A., Cortassa, S., Kim, E. Y., Fang, E. F., et al. (2018). Nicotinamide improves aspects of healthspan, but not lifespan, in mice. *Cell. Metab.* 27 (3), 667–676. e4. doi:10.1016/j.cmet.2018.02.001

Miyata, K., Imai, Y., Hori, S., Nishio, M., Loo, T. M., Okada, R., et al. (2021). Pericentromeric noncoding RNA changes DNA binding of CTCF and inflammatory gene expression in senescence and cancer. *Proc. Natl. Acad. Sci. U. S. A.* 118 (35), e2025647118. doi:10.1073/pnas.2025647118

Mohamad, K. N., Safuan, S., Shamsuddin, S., and Foroozandeh, P. (2020). Aging of the cells: Insight into cellular senescence and detection Methods. *Eur. J. Cell. Biol.* 99 (6), 151108. doi:10.1016/j.ejcb.2020.151108

Moimas, S., Salton, F., Kosmider, B., Ring, N., Volpe, M. C., Bahmed, K., et al. (2019). miR-200 family members reduce senescence and restore idiopathic pulmonary fibrosis type II alveolar epithelial cell transdifferentiation. *ERJ Open Res.* 5, 00138-2019. doi:10.1183/23120541.00138-2019

Moore, B. B., and Moore, T. A. (2015). Viruses in idiopathic pulmonary fibrosis. Etiology and exacerbation. *Ann. Am. Thorac. Soc.* 12 (2), S186–S192. doi:10.1513/AnnalsATS.201502-088AW

Mora, A. L., Rojas, M., Pardo, A., and Selman, M. (2017). Emerging therapies for idiopathic pulmonary fibrosis, a progressive age-related disease. *Nat. Rev. Drug Discov.* 16 (11), 755–772. doi:10.1038/nrd.2017.170

Morikawa, M., Derynck, R., and Miyazono, K. (2016). TGF-Beta and the TGF-beta family: Context-dependent roles in cell and tissue physiology. *Cold Spring Harb. Perspect. Biol.* 8 (5), a021873. doi:10.1101/cshperspect.a021873

Morselli, E., Marino, G., Bennetzen, M. V., Eisenberg, T., Megalou, E., Schroeder, S., et al. (2011). Spermidine and resveratrol induce autophagy by distinct pathways converging on the acetylproteome. *J. Cell. Biol.* 192 (4), 615–629. doi:10.1083/jcb.201008167

Moss, B. J., Ryter, S. W., and Rosas, I. O. (2022). Pathogenic mechanisms underlying idiopathic pulmonary fibrosis. *Annu. Rev. Pathol.* 17, 515–546. doi:10.1146/annurev-pathol-042320-030240

Moya, I. M., and Halder, G. (2019). Hippo-YAP/TAZ signalling in organ regeneration and regenerative medicine. *Nat. Rev. Mol. Cell. Biol.* 20 (4), 211–226. doi:10.1038/s41580-018-0086-y

Munoz-Espin, D., and Serrano, M. (2014). Cellular senescence: From physiology to pathology. *Nat. Rev. Mol. Cell. Biol.* 15 (7), 482–496. doi:10.1038/nrm3823

Naikawadi, R. P., Disayabutr, S., Mallavia, B., Donne, M. L., Green, G., La, J. L., et al. (2016). Telomere dysfunction in alveolar epithelial cells causes lung remodeling and fibrosis. *JCI Insight* 1 (14), e86704. doi:10.1172/jci.insight.86704

Nelson, G., Wordsworth, J., Wang, C., Jurk, D., Lawless, C., Martin-Ruiz, C., et al. (2012). A senescent cell bystander effect: Senescence-induced senescence. *Aging Cell.* 11 (2), 345–349. doi:10.1111/j.1474-9726.2012.00795.x

Noble, P. W., Barkauskas, C. E., and Jiang, D. (2012). Pulmonary fibrosis: Patterns and perpetrators. *J. Clin. Invest.* 122 (8), 2756–2762. doi:10.1172/JCI60323

Ohtani, N., Zebedee, Z., Huot, T. J., Stinson, J. A., Sugimoto, M., Ohashi, Y., et al. (2001). Opposing effects of Ets and Id proteins on p16INK4a expression during cellular senescence. *Nature* 409 (6823), 1067–1070. doi:10.1038/35059131

Omori, S., Wang, T. W., Johmura, Y., Kanai, T., Nakano, Y., Kido, T., et al. (2020). Generation of a p16 reporter mouse and its use to characterize and target p16(high) cells *in vivo*. *Cell. Metab.* 32 (5), 814–828. e6. doi:10.1016/j.cmet.2020.09.006

Orjalo, A. V., Bhaumik, D., Gengler, B. K., Scott, G. K., and Campisi, J. (2009). Cell surface-bound IL-1alpha is an upstream regulator of the senescence-associated IL-6/IL-8 cytokine network. *Proc. Natl. Acad. Sci. U S A.* 106 (40), 17031–17036. doi:10.1073/pnas.0905299106

Pan, J., Li, D., Xu, Y., Zhang, J., Wang, Y., Chen, M., et al. (2017). Inhibition of bcl-2/xl with ABT-263 selectively kills senescent type II pneumocytes and reverses persistent pulmonary fibrosis induced by ionizing radiation in mice. *Int. J. Radiat. Oncol. Biol. Phys.* 99 (2), 353–361. doi:10.1016/j.ijrobp.2017.02.216

Parimon, T., Hohmann, M. S., and Yao, C. (2021). Cellular senescence: Pathogenic mechanisms in lung fibrosis. *Int. J. Mol. Sci.* 22 (12), 6214. doi:10.3390/ijms22126214

Parimon, T., Yao, C., Stripp, B. R., Noble, P. W., and Chen, P. (2020). Alveolar epithelial type II cells as drivers of lung fibrosis in idiopathic pulmonary fibrosis. *Int. J. Mol. Sci.* 21 (7), E2269. doi:10.3390/ijms21072269

Patel, A. S., Lin, L., Geyer, A., Haspel, J. A., An, C. H., Cao, J., et al. (2012). Autophagy in idiopathic pulmonary fibrosis. *PLoS One* 7 (7), e41394. doi:10.1371/journal.pone.0041394

Pietrocola, F., Lachkar, S., Enot, D. P., Niso-Santano, M., Bravo-San, P. J., Sica, V., et al. (2015). Spermidine induces autophagy by inhibiting the acetyltransferase EP300. *Cell. Death Differ.* 22 (3), 509–516. doi:10.1038/cdd.2014.215

Pineiro-Hermida, S., Martinez, P., Bosso, G., Flores, J. M., Saraswati, S., Connor, J., et al. (2022). Consequences of telomere dysfunction in fibroblasts, club and basal cells for lung fibrosis development. *Nat. Commun.* 13 (1), 5656. doi:10.1038/s41467-022-32771-6

Plate, M., Guillotin, D., and Chambers, R. C. (2020). The promise of mTOR as a therapeutic target pathway in idiopathic pulmonary fibrosis. *Eur. Respir. Rev.* 29 (157), 200269. doi:10.1183/16000617.0269-2020

Powers, R. R., Kaeberlein, M., Caldwell, S. D., Kennedy, B. K., and Fields, S. (2006). Extension of chronological life span in yeast by decreased TOR pathway signaling. *Genes. Dev.* 20 (2), 174–184. doi:10.1101/gad.1381406

Raghu, G., Anstrom, K. J., King, T. J., Lasky, J. A., and Martinez, F. J. (2012). Prednisone, azathioprine, and N-acetylcysteine for pulmonary fibrosis. *N. Engl. J. Med.* 366 (21), 1968–1977. doi:10.1056/NEJMoa1113354

Raghu, G., Weycker, D., Edelsberg, J., Bradford, W. Z., and Oster, G. (2006). Incidence and prevalence of idiopathic pulmonary fibrosis. *Am. J. Respir. Crit. Care Med.* 174 (7), 810–816. doi:10.1164/rccm.200602-163OC

Rana, T., Jiang, C., Liu, G., Miyata, T., Antony, V., Thannickal, V. J., et al. (2020). PAI-1 regulation of TGF-β1-induced alveolar type II cell senescence, SASP secretion, and SASP-mediated activation of alveolar macrophages. *Am. J. Respir. Cell. Mol. Biol.* 62 (3), 319–330. doi:10.1165/rcmb.2019-0071OC

Rangarajan, S., Bone, N. B., Zmijewska, A. A., Jiang, S., Park, D. W., Bernard, K., et al. (2018). Metformin reverses established lung fibrosis in a bleomycin model. *Nat. Med.* 24 (8), 1121–1127. doi:10.1038/s41591-018-0087-6

Razdan, N., Vasilopoulos, T., and Herbig, U. (2018). Telomere dysfunction promotes transdifferentiation of human fibroblasts into myofibroblasts. *Aging Cell.* 17 (6), e12838. doi:10.1111/acel.12838

Rhinn, M., Ritschka, B., and Keyes, W. M. (2019). Cellular senescence in development, regeneration and disease. *Development* 146 (20), dev151837. doi:10.1242/dev.151837

Richeldi, L., du Bois, R. M., Raghu, G., Azuma, A., Brown, K. K., Costabel, U., et al. (2014). Efficacy and safety of nintedanib in idiopathic pulmonary fibrosis. *N Engl. J. Med.* 370 (22), 2071–2082. doi:10.1056/NEJMoa1402584

Riemondy, K. A., Jansing, N. L., Jiang, P., Redente, E. F., Gillen, A. E., Fu, R., et al. (2019). Single cell RNA sequencing identifies TGFβ as a key regenerative cue following LPS-induced lung injury. *JCI Insight* 5, 123637. doi:10.1172/jci.insight.123637

Rossiello, F., Jurk, D., Passos, J. F., and D'Adda, D. F. F. (2022). Telomere dysfunction in ageing and age-related diseases. *Nat. Cell. Biol.* 24 (2), 135–147. doi:10.1038/s41556-022-00842-x

Ruaro, B., Salton, F., Braga, L., Wade, B., Confalonieri, P., Volpe, M. C., et al. (2021). The history and mystery of alveolar epithelial type II cells: Focus on their physiologic and pathologic role in lung. *Int. J. Mol. Sci.* 22 (5), 2566. doi:10.3390/ijms22052566

Rubinsztein, D. C., Codogno, P., and Levine, B. (2012). Autophagy modulation as a potential therapeutic target for diverse diseases. *Nat. Rev. Drug Discov.* 11 (9), 709–730. doi:10.1038/nrd3802

Rubinsztein, D. C., Marino, G., and Kroemer, G. (2011). Autophagy and aging. *Cell.* 146 (5), 682–695. doi:10.1016/j.cell.2011.07.030

Ryu, D., Mouchiroud, L., Andreux, P. A., Katsyuba, E., Moullan, N., Nicolet-Dit-Felix, A. A., et al. (2016). Urolithin A induces mitophagy and prolongs lifespan in *C. elegans* and increases muscle function in rodents. *Nat. Med.* 22 (8), 879–888. doi:10.1038/nm.4132

Saleh, M., Fotook, K. S., and Kavianpour, M. (2022). Application of Wharton jelly-derived mesenchymal stem cells in patients with pulmonary fibrosis. *Stem Cell. Res. Ther.* 13 (1), 71. doi:10.1186/s13287-022-02746-x

Salminen, A., Kauppinen, A., and Kaarniranta, K. (2012). Emerging role of NF-κB signaling in the induction of senescence-associated secretory phenotype (SASP). *Cell. Signal.* 24 (4), 835–845. doi:10.1016/j.cellsig.2011.12.006

Schafer, M. J., White, T. A., Iijima, K., Haak, A. J., Ligresti, G., Atkinson, E. J., et al. (2017). Cellular senescence mediates fibrotic pulmonary disease. *Nat. Commun.* 8, 14532. doi:10.1038/ncomms14532

Schiller, H. B., Montoro, D. T., Simon, L. M., Rawlins, E. L., Meyer, K. B., Strunz, M., et al. (2019). The human lung cell atlas: A high-resolution reference map of the human lung in health and disease. *Am. J. Respir. Cell. Mol. Biol.* 61 (1), 31–41. doi:10.1165/rcmb.2018-0416TR

Schneider, J. L., Rowe, J. H., Garcia-De-Alba, C., Kim, C. F., Sharpe, A. H., and Haigis, M. C. (2021). The aging lung: Physiology, disease, and immunity. *Cell.* 184 (8), 1990–2019. doi:10.1016/j.cell.2021.03.005

Sharma, J., di Ronza, A., Lotfi, P., and Sardiello, M. (2018). Lysosomes and brain health. *Annu. Rev. Neurosci.* 41, 255–276. doi:10.1146/annurev-neuro-080317-061804

Sharma, P., Alizadeh, J., Juarez, M., Samali, A., Halayko, A. J., Kenyon, N. J., et al. (2021). Autophagy, apoptosis, the unfolded protein response, and lung function in idiopathic pulmonary fibrosis. *Cells* 10 (7), 1642. doi:10.3390/cells10071642

Sheng, G., Chen, P., Wei, Y., Yue, H., Chu, J., Zhao, J., et al. (2020). Viral infection increases the risk of idiopathic pulmonary fibrosis: A meta-analysis. *Chest* 157 (5), 1175–1187. doi:10.1016/j.chest.2019.10.032

Shojaei, S., Suresh, M., Klionsky, D. J., Labouta, H. I., and Ghavami, S. (2020). Autophagy and SARS-CoV-2 infection: Apossible smart targeting of the autophagy pathway. *Virulence* 11 (1), 805–810. doi:10.1080/21505594.2020.1780088

Sinha, S., Castillo, V., Espinoza, C. R., Tindle, C., Fonseca, A. G., Dan, J. M., et al. (2022). COVID-19 lung disease shares driver AT2 cytopathic features with Idiopathic pulmonary fibrosis. *bioRxiv.* 28, 470269. doi:10.1101/2021.11.28.470269

Song, H. L., Demirev, A. V., Kim, N. Y., Kim, D. H., and Yoon, S. Y. (2019). Ouabain activates transcription factor EB and exerts neuroprotection in models of Alzheimer's disease. *Mol. Cell. Neurosci.* 95, 13–24. doi:10.1016/j.mcn.2018.12.007

Song, S., Tchkonia, T., Jiang, J., Kirkland, J. L., and Sun, Y. (2020). Targeting senescent cells for a healthier aging: Challenges and opportunities. *Adv. Sci.* 7 (23), 2002611. doi:10.1002/advs.202002611

Song, X., Cao, G., Jing, L., Lin, S., Wang, X., Zhang, J., et al. (2014a). Analysing the relationship between lncRNA and protein-coding gene and the role of lncRNA as ceRNA in pulmonary fibrosis. *J. Cell. Mol. Med.* 18 (6), 991–1003. doi:10.1111/jcmm.12243

Song, X., Wang, B., Lin, S., Jing, L., Mao, C., Xu, P., et al. (2014b). Astaxanthin inhibits apoptosis in alveolar epithelial cells type II *in vivo* and *in vitro* through the ROS-dependent mitochondrial signalling pathway. *J. Cell. Mol. Med.* 18 (11), 2198–2212. doi:10.1111/jcmm.12347

Sun, M., Sun, Y., Feng, Z., Kang, X., Yang, W., Wang, Y., et al. (2021). New insights into the Hippo/YAP pathway in idiopathic pulmonary fibrosis. *Pharmacol. Res.* 169, 105635. doi:10.1016/j.phrs.2021.105635

Takahashi, A., Ohtani, N., Yamakoshi, K., Iida, S., Tahara, H., Nakayama, K., et al. (2006). Mitogenic signalling and the p16INK4a-Rb pathway cooperate to enforce irreversible cellular senescence. *Nat. Cell. Biol.* 8 (11), 1291–1297. doi:10.1038/ncb1491

Tan, W., Zhang, B., Liu, X., Zhang, C., Liu, J., and Miao, Q. (2021). Interleukin-33-Dependent accumulation of regulatory T cells mediates pulmonary epithelial regeneration during acute respiratory distress syndrome. *Front. Immunol.* 12, 653803. doi:10.3389/fimmu.2021.653803

Verdin, E. (2015). NAD^+ in aging, metabolism, and neurodegeneration. *Science* 350 (6265), 1208–1213. doi:10.1126/science.aac4854

Wang, L., Chen, R., Li, G., Wang, Z., Liu, J., Liang, Y., et al. (2020). FBW7 mediates senescence and pulmonary fibrosis through telomere uncapping. *Cell. Metab.* 32 (5), 860–877. e9. doi:10.1016/j.cmet.2020.10.004

Wang, L., Wang, Z., and Liu, J. P. (2021). Identification of peptidomimetic telomere dysfunction inhibitor (TELODIN) through telomere dysfunction-induced foci (TIF) assay. *Star. Protoc.* 2 (3), 100620. doi:10.1016/j.xpro.2021.100620

Wang, Z., Li, X., Chen, H., Han, L., Ji, X., Wang, Q., et al. (2021). Resveratrol alleviates bleomycin-induced pulmonary fibrosis via suppressing HIF-1α and NF-κB expression. *Aging (Albany NY)* 13 (3), 4605–4616. doi:10.18632/aging.202420

Watanabe, S., Markov, N. S., Lu, Z., Piseaux, A. R., Soberanes, S., Runyan, C. E., et al. (2021). Resetting proteostasis with ISRIB promotes epithelial differentiation to attenuate pulmonary fibrosis. *Proc. Natl. Acad. Sci. U. S. A.* 118 (20), e2101100118. doi:10.1073/pnas.2101100118

Wei, Y., Tanaka, M., Sakurai, T., Kamiyoshi, A., Ichikawa-Shindo, Y., Kawate, H., et al. (2021). Adrenomedullin ameliorates pulmonary fibrosis by regulating TGF-ß-smads signaling and myofibroblast differentiation. *Endocrinology* 162 (8), bqab090. doi:10.1210/endocr/bqab090

Wiley, C. D., Brumwell, A. N., Davis, S. S., Jackson, J. R., Valdovinos, A., Calhoun, C., et al. (2019). Secretion of leukotrienes by senescent lung fibroblasts promotes pulmonary fibrosis. *JCI Insight* 4 (24), 130056. doi:10.1172/jci.insight.130056

Wiley, C. D., Sharma, R., Davis, S. S., Lopez-Dominguez, J. A., Mitchell, K. P., Wiley, S., et al. (2021). Oxylipin biosynthesis reinforces cellular senescence and allows detection of senolysis. *Cell. Metab.* 33 (6), 1124–1136.e5. e5. doi:10.1016/j.cmet.2021.03.008

Wu, A., and Song, H. (2020). Regulation of alveolar type 2 stem/progenitor cells in lung injury and regeneration. *Acta Biochim. Biophys. Sin.* 52 (7), 716–722. doi:10.1093/abbs/gmaa052

Wu, H., Yu, Y., Huang, H., Hu, Y., Fu, S., Wang, Z., et al. (2021). Progressive pulmonary fibrosis is caused by elevated mechanical tension on alveolar stem cells. *Cell.* 184 (3), 845–846. doi:10.1016/j.cell.2021.01.020

Xu, P., Zhang, J., Wang, M., Liu, B., Li, R., Li, H., et al. (2022). hnRNPL-activated circANKRD42 back-splicing and circANKRD42-mediated crosstalk of mechanical stiffness and biochemical signal in lung fibrosis. *Mol. Ther.* 30 (6), 2370–2387. doi:10.1016/j.ymthe.2022.01.045

Xu, Q., Fu, Q., Li, Z., Liu, H., Wang, Y., Lin, X., et al. (2021). The flavonoid procyanidin C1 has senotherapeutic activity and increases lifespan in mice. *Nat. Metab.* 3 (12), 1706–1726. doi:10.1038/s42255-021-00491-8

Xu, Y., Mizuno, T., Sridharan, A., Du, Y., Guo, M., Tang, J., et al. (2016). Single-cell RNA sequencing identifies diverse roles of epithelial cells in idiopathic pulmonary fibrosis. *JCI Insight* 1 (20), e90558. doi:10.1172/jci.insight.90558

Yamada, Z., Nishio, J., Motomura, K., Mizutani, S., Yamada, S., Mikami, T., et al. (2022). Senescence of alveolar epithelial cells impacts initiation and chronic phases of murine fibrosing interstitial lung disease. *Front. Immunol.* 13, 935114. doi:10.3389/fimmu.2022.935114

Yang, J., Pan, X., Wang, L., and Yu, G. (2020). Alveolar cells under mechanical stressed niche: Critical contributors to pulmonary fibrosis. *Mol. Med.* 26 (1), 95. doi:10.1186/s10020-020-00223-w

Yao, C., Guan, X., Carraro, G., Parimon, T., Liu, X., Huang, G., et al. (2021). Senescence of alveolar type 2 cells drives progressive pulmonary fibrosis. *Am. J. Respir. Crit. Care Med.* 203 (6), 707–717. doi:10.1164/rccm.202004-1274OC

Yasuda, T., Baba, H., and Ishimoto, T. (2021). Cellular senescence in the tumor microenvironment and context-specific cancer treatment strategies. *FEBS J.* doi:10.1111/febs.16231

Yousefzadeh, M. J., Zhu, Y., Mcgowan, S. J., Angelini, L., Fuhrmann-Stroissnigg, H., Xu, M., et al. (2018). Fisetin is a senotherapeutic that extends health and lifespan. *EBioMedicine* 36, 18–28. doi:10.1016/j.ebiom.2018.09.015

Zhai, X. X., Tang, Z. M., Ding, J. C., and Lu, X. L. (2017). Expression of TGF-beta1/mTOR signaling pathway in pathological scar fibroblasts. *Mol. Med. Rep.* 15 (6), 3467–3472. doi:10.3892/mmr.2017.6437

Zhang, B., Long, Q., Wu, S., Xu, Q., Song, S., Han, L., et al. (2021). KDM4 orchestrates epigenomic remodeling of senescent cells and potentiates the senescence-associated secretory phenotype. *Nat. Aging* 1 (5), 454–472. doi:10.1038/s43587-021-00063-1

Zhang, J., Wang, H., Chen, H., Li, H., Xu, P., Liu, B., et al. (2022). ATF3 -activated accelerating effect of LINC00941/lncIAPF on fibroblast-to-myofibroblast differentiation by blocking autophagy depending on ELAVL1/HuR in pulmonary fibrosis. *Autophagy* 18, 2636–2655. doi:10.1080/15548627.2022.2046448

Zhang, S., Chen, H., Yue, D., Blackwell, T. S., Lv, C., and Song, X. (2021). Long non-coding RNAs: Promising new targets in pulmonary fibrosis. *J. Gene Med.* 23 (3), e3318. doi:10.1002/jgm.3318

Zhou, J., Chen, Y., He, M., Li, X., and Wang, R. (2022). Role of circular RNAs in pulmonary fibrosis. *Int. J. Mol. Sci.* 23 (18), 10493. doi:10.3390/ijms231810493

frontiers | Frontiers in Pharmacology

TYPE Original Research
PUBLISHED 18 November 2022
DOI 10.3389/fphar.2022.1039103

OPEN ACCESS

EDITED BY
Jian Gao,
Shanghai Children's Medical Center, China

REVIEWED BY
Venkata Ramireddy Narala,
Yogi Vemana University, India
Gary C. Mouradian,
Medical College of Wisconsin, United States
Chung-Ming Chen,
Taipei Medical University, Taiwan

*CORRESPONDENCE
Lina Qiao,
iaqiao@163.com
Zhongwei Cao,
zhongweicao@scu.edu.cn

†These authors share first authorship

SPECIALTY SECTION
This article was submitted to Respiratory Pharmacology, a section of the journal Frontiers in Pharmacology

RECEIVED 07 September 2022
ACCEPTED 02 November 2022
PUBLISHED 18 November 2022

CITATION
Long Y, Chen H, Deng J, Ning J, Yang P, Qiao L and Cao Z (2022), Deficiency of endothelial FGFR1 alleviates hyperoxia-induced bronchopulmonary dysplasia in neonatal mice.
Front. Pharmacol. 13:1039103.
doi: 10.3389/fphar.2022.1039103

Deficiency of endothelial FGFR1 alleviates hyperoxia-induced bronchopulmonary dysplasia in neonatal mice

Yanrong Long†, Hongbin Chen†, Junchao Deng, Junjie Ning, Pengbo Yang, Lina Qiao* and Zhongwei Cao*

Key Laboratory of Birth Defects of MOE, State Key Laboratory of Biotherapy, West China Second University Hospital, Sichuan University, Chengdu, China

Disrupted neonatal lung angiogenesis and alveologenesis often give rise to bronchopulmonary dysplasia (BPD), the most common chronic lung disease in children. Hyperoxia-induced pulmonary vascular and alveolar damage in premature infants is one of the most common and frequent factors contributing to BPD. The purpose of the present study was to explore the key molecules and the underlying mechanisms in hyperoxia-induced lung injury in neonatal mice and to provide a new strategy for the treatment of BPD. In this work, we reported that hyperoxia decreased the proportion of endothelial cells (ECs) in the lungs of neonatal mice. In hyperoxic lung ECs of neonatal mice, we detected upregulated fibroblast growth factor receptor 1 (FGFR1) expression, accompanied by upregulation of the classic downstream signaling pathway of activated FGFR1, including the ERK/MAPK signaling pathway and PI3K-Akt signaling pathway. Specific deletion of *Fgfr1* in the ECs of neonatal mice protected the lungs from hyperoxia-induced lung injury, with improved angiogenesis, alveologenesis and respiratory metrics. Intriguingly, the increased *Fgfr1* expression was mainly attributed to aerosol capillary endothelial (aCap) cells rather than general capillary endothelial (gCap) cells. Deletion of endothelial *Fgfr1* increased the expression of gCap cell markers but decreased the expression of aCap cell markers. Additionally, inhibition of FGFR1 by an FGFR1 inhibitor improved alveologenesis and respiratory metrics. In summary, this study suggests that in neonatal mice, hyperoxia increases the expression of endothelial FGFR1 in lung ECs and that deficiency of endothelial *Fgfr1* can ameliorate hyperoxia-induced BPD. These data suggest that FGFR1 may be a potential therapeutic target for BPD, which will provide a new strategy for the prevention and treatment of BPD.

KEYWORDS

bronchopulmonary dysplasia (BPD), hyperoxia, endothelial cells (ECs), FGFR1, neonatal

Introduction

In neonates, especially premature infants, the premature developing lungs are often susceptible to damage from many factors, such as hyperoxia, which often results in bronchopulmonary dysplasia (BPD). It is the most common chronic lung disease in preterm birth and is mainly characterized by simplified vascularization and alveolarization and even fibrosis in severe cases (Northway et al., 1967; Thébaud et al., 2019; Sahni and Mowes, 2022). As a consequence of BPD, residual pulmonary dysfunction and cardiovascular sequelae in adolescence and adulthood may occur (Islam et al., 2015; DeMauro, 2018; Tracy and Berkelhamer, 2019).

The development of the mammalian lung is broadly divided into two phases: prenatal phase and postnatal phase. During the prenatal phase, the core lung structure containing the branching conducting airways with their attendant vasculature develops, while the alveolarization and the maturation of pulmonary microvasculature are mainly completed at the postnatal phase (Warburton et al., 2005; Chang et al., 2013; Silva et al., 2015; Schittny, 2017). The two phases of lung development are intimately coordinated, and being disturbed at any phase may provoke lung disease (Chang et al., 2013). BPD is thought to be the result of an abnormal reparative response to both antenatal injury and repetitive postnatal injury to the developing lungs (Thébaud et al., 2019). Endothelial cells (ECs) play an important role in angiogenesis, which fundamentally contributes to lung development, homeostasis, and injury repair (Ding et al., 2011; Miller and Sewell-Loftin, 2021; Filippini et al., 2022; Zhou et al., 2022). There is complicated reciprocal signaling between ECs and epithelial cells, which regulates the formation of an extensive capillary network to support lung development (Ren et al., 2019).

General capillary endothelial cells (gCap cells) and aerosol capillary endothelial cells (aCap cells) are two subpopulations of ECs that make up the alveolar endothelium. gCap cells are specialized to regulate vasomotor tone and are considered as stem/progenitor cells in capillary homeostasis and repair, while aCap cells are specialized for gas exchange and trafficking of leukocytes (Gillich et al., 2020). Prior studies showed that adoptively transferred *c-kit*$^+$ ECs (gCap cells) increased lung angiogenesis and prevented alveolar simplification in neonatal mice exposed to hyperoxia (Ren et al., 2019). Furthermore, it was previously reported that after acute lung injury, *Car4*-high ECs (aCap cells) are preferentially localized in regenerating regions of the alveolus and contribute to alveolar revascularization (Niethamer et al., 2020). Although previous studies have reported that ECs and their subpopulations play an important role in impaired lung repair, the underlying mechanisms by which ECs and their subpopulations act in BPD are unclear.

Here, we detected the alterations in ECs and their subpopulations in hyperoxia-impaired neonatal lungs by scRNA-seq and RNA-seq. We found that endothelial fibroblast growth factor receptor 1 (FGFR1), a member of the fibroblast growth factor receptor (FGFR) family, may play an important role in hyperoxia-induced BPD. FGF/FGFR signaling was reported to be crucial for many physiological activities, such as embryonic development, organogenesis, and tissue maintenance (Dow and deVere White, 2000; Bates, 2011; Goetz and Mohammadi, 2013; Yu et al., 2017; Kurowski et al., 2019). Some scholars believe that FGF/FGFR signaling plays a proangiogenic role in physiological or pathological conditions (Yanagisawa-Miwa et al., 1992; Deng et al., 1994; Compagni et al., 2000; De Smet et al., 2014). In addition, it was previously found that FGFR1 is the key inhibitor of endothelial-to-mesenchymal transition (EndMT) and is important in combating EndMT-associated fibrotic disorders (Li et al., 2017). Nevertheless, scholars have reported that FGF/FGFR signaling is not essential for angiogenesis and injured vessel repair (Ortega et al., 1998; Zhou et al., 1998; Miller et al., 2000; Ong et al., 2000). Exaggerated FGF2/FGFR1 signaling caused by SUMOylation-defective mutation of FGFR1 suppressed VEGFA/VEGFR2 signaling and the angiogenic capabilities of ECs (Zhu et al., 2022). Additionally, it was previously reported that continuous activation of endothelial FGFR1 can promote the formation of profibrotic vascular niche, which would facilitate fibrosis in chronic liver injury (Ding et al., 2014). Moreover, there is another point of view that endothelial FGFR1 is necessary for pathological neovascularization after injury but not for physiological vascular development and vascular homeostasis (Oladipupo et al., 2014; House et al., 2016). These studies indicated that FGFR1 performs different and potentially important functions in different physiological situations. In this work, we found that hyperoxia increased the expression of endothelial FGFR1, which indicated that endothelial FGFR1 may be a key regulatory molecules in hyperoxia-induced BPD. However, the role of FGFR1 in hyperoxia-induced BPD have not been reported. Therefore, it is meaningful to throw light on this question.

To mimic lung injuries in patients with BPD, firstly, wild-type (WT) neonatal mice were exposed to hyperoxia (80% O_2) to induce a BPD-like lung phenotype, which was suggested to be an ideal model to identify and study pivotal developmental steps of lung injury and repair (Nardiello et al., 2017; Surate Solaligue et al., 2017; Ito et al., 2022). Mice reared in room air were used as controls. Consistent with previous studies (Nardiello et al., 2017; Ito et al., 2022). We observed that hyperoxia exposure resulted in abnormal angiogenesis and disrupted alveologenesis, the prominent features of BPD, in neonatal mice. Next, single-cell RNA sequencing (scRNA-seq) was performed to investigate the cellular and molecular changes in hyperoxia-damaged lungs. The results of scRNA-seq analysis suggested that hyperoxia decreased the proportion of ECs in the lungs of neonatal mice. Then, we employed whole transcriptome sequencing (RNA-seq) to further explore and confirm the molecular changes in ECs during the occurrence and development of hyperoxia-based BPD. We found that hyperoxia increased the expression of endothelial FGFR1.

Therefore, using the same hyperoxia procedure, we used a genetically modified mouse in which *Fgfr1* was conditionally deleted specifically in ECs ($Fgfr1^{i\Delta EC/i\Delta EC}$) to investigate the role of FGFR1 in hyperoxia-induced lung injury and repair.

Materials and methods

Mice and neonatal hyperoxia

The WT C57BL/6J mice were obtained from the Model Animal Research Center of Nanjing University. Floxed *Fgfr1* ($Fgfr1^{fl/fl}$) C57BL/6J mice were generously provided by Dr. Shahin Rafii. Mice expressing EC-specific *VE-Cadherin-(PAC)-Cre*^{ERT2} were obtained from Taconic Biosciences. $Fgfr1^{i\Delta EC/i\Delta EC}$ mice were generated by crossing $Fgfr1^{fl/fl}$ mice with *VE-Cadherin-(PAC)-Cre*^{ERT2} mice. From the day of birth (P0) to postnatal day (P)2, $Fgfr1^{i\Delta EC/i\Delta EC}$ mice were intraperitoneally treated with tamoxifen (50 μg/mouse/day) to induce endothelial-specific deletion of *Fgfr1*. The neonatal hyperoxia exposure was performed to develop the BPD mouse model according to previously described protocols (Silva et al., 2015; Nardiello et al., 2017; Cheon et al., 2018; Willis et al., 2018). At P0, neonatal mouse pups delivered on the same day were randomly divided into equal-sized litters around six pups nursed by each dam. Then, following randomization, mouse cages were either maintained in room air (21% O_2) or in hyperoxia (80% O_2) from P0 to P14. Lungs of mouse pups were harvested for testing at P14. The hyperoxic environment was maintained in sealed Plexiglas chambers, which contained sodium bicarbonate as an odor adsorbent and sodium hydroxide as an H_2O adsorbent. The chamber contained a continuous oxygen monitoring system (ProOX-100HE, TOW-INT TECH) and was attached to a medical oxygen source. To avoid oxygen toxicity, nursing dams were rotated between normoxic and hyperoxic groups every 24 h. All mice were housed under SPF conditions (12/12 h light/dark cycle, 50%–70% relative humidity, temperature was maintained between 26°C and 28°C) and with access to *ad libitum* feeding. All mouse pups were euthanized at P14 to harvest lungs for testing.

FGFR1 inhibitor (AZD4547) injection

The FGFR1 inhibitor (AZD4547) was generously provided by Dr. Tinghong Ye. For *in vivo* efficacy studies, neonatal mice were randomly divided into three groups: room air + vehicle, hyperoxia + vehicle or hyperoxia + inhibitor. From P0 to P5, neonatal mice were daily treated with vehicle or inhibitor (5 μg inhibitor dissolved in 20 μL vehicle: 5% DMSO + 40% PEG 400 + 55% saline) by intragastric injection through the abdominal wall according the dose used in a previously reported study (Gudernova et al., 2016). Each mouse was injected with 20 μL vehicle or 5 μg inhibitor/20 μL vehicle by using a 50-ml Hamilton microsyringe. The hyperoxia exposure and feeding management protocols were the same as those described above. All mouse pups were euthanized at P14 to harvest lungs for testing.

Histology

At P14, the lungs were inflated with 20 ml 4% paraformaldehyde in PBS under constant pressure of 20 cm H_2O and allowed to fix for 24 h. After being fixed with 4% paraformaldehyde, the tissues were dehydrated with an ethanol series, embedded in paraffin and sectioned. Hematoxylin and eosin (H&E) staining was performed for tissue morphology examination and mean linear intercept (MLI) and radial alveolar count (RAC) measurement. Analysis of sections was recorded with an Olympus BX51 microscope (Olympus America). The MLI and RAC were measured following a previously described protocol (Cooney and Thurlbeck, 1982; Ashour et al., 2006). For each animal, one lung sections was prepared on a slide, and 5 randomized microscopic fields in each section were selected for MLI or RAC measurement. The average value of the 5 microscopic fields was calculated to represent the results for individual mouse.

Immunofluorescence

At P14, after the mice being sacrificed, the lungs were inflated with 20 ml PBS under constant pressure of 20 cm H_2O from the left atrium. Then, lung tissues were embedded in Optimum Cutting Temperature (OCT) and made into cryosections. Briefly, at first, each lung was slowly filled with 50 μL OCT: PBS (1:1) mixture from the trachea. Secondly, the lungs were removed from the chest cavity and placed into tissue embedding cassettes with the maximum side down and carefully filled with OCT into the cassettes. Placed the filled cassettes containing embedded tissues onto the flat surface and quickly placed them into a -80°C refrigerator to freeze the embedded tissue. Next, cryosections were made from the frozen embedded tissue for immunofluorescence (IF) analysis. Six-millimeter-thick tissue cryosections were blocked (5% donkey serum/0.3% Triton X-100) and incubated in primary antibodies at 4°C overnight (anti-VE-cadherin antibody, R&D Systems, #AF1002). After incubation with primary antibodies, slides were washed three times with PBS, followed by incubation in fluorophore-conjugated secondary antibodies (Jackson ImmunoResearch), and nuclear staining was carried out with DAPI by using Prolong Gold Anti-fade Reagent (Invitrogen). Finally, fluorescent images were recorded on an AxioVert LSM980 confocal microscope (Zeiss) for analysis. ImageJ (version: 2.0.0-rc-69/1.52p) was used for fluorescent image

analysis following a previously described protocol (Zhou et al., 2021). For each animal, one lung section was prepared on a slide and 5 randomized microscopic fields in each section were selected for fluorescence analysis. The average value of the 5 microscopic fields was calculated to represent the results for individual mouse.

Respiratory metrics testing

The respiratory metrics were quantified by whole-body plethysmography (WBP, DSI Buxco) at P14. Mice were examined in a calibrated WBP chamber, and the manufacturer software was used to calculate respiratory measures. After the respiratory data stabilized, data were recorded for 5 min per mouse. The average was calculated to represent the results for individual mouse.

Single-cell RNA sequencing

Single-cell suspension was prepared following a previously described protocol (Zepp et al., 2017). Briefly, lungs were perfused with PBS, minced with scissors and digested in an enzymatic mixture (dispase II: 200 μg/ml, collagenase I: 200 μg/ml, DNase I: 40 μg/ml) for 35 min at 37°C. Following enzymatic digestion, the samples were filtered, and red blood cells were lysed. Then, single cells were resuspended in MACS buffer (DPBS + 0.1% BSA + 2 mM EDTA). Ensure cell viability exceeded 80% as determined by AO/PI reagent staining. The following sequencing steps were performed by 10X Genomics. The scRNA-seq profiles of 17,320 cells from 16 normoxic and hyperoxic mouse lungs were generated with 150 G sequencing depth. Single-cell suspensions were loaded into 10x Chromium to capture 10,000 single cells according to the manufacturer's instructions of the 10X Genomics Chromium Single-Cell 3′ Kit (V3). Using microfluidic techniques, gel beads with barcodes and primers were wrapped in oil droplets (GEMs) with individual cells. Then the gel beads were dissolved and the cells were lysed to release the mRNA. cDNA with barcode and UMI information for sequencing was generated by reverse transcription of the mRNA. The cDNA amplification and library construction steps were performed according to the standard protocol. Libraries were sequenced on an Illumina NovaSeq 6,000 sequencing system (paired-end multiplexing run, 150 bp). Sequencing results were converted to FASTQ format using Illumina bcl2fastq software (version 2.20). Cell Ranger pipelin (version 6.1.1) was used for sample demultiplexing, barcode processing and gene counting, and scRNA-seq data were aligned to the reference genome (Transcriptome: mm10–1.2.0). Seurat (Version 4.0) was used for dimensional reduction, clustering and analysis of scRNA-seq data. Each group contained eight mice mixed into one sample for scRNA-seq.

iDISCO (ace) procedure

The iDISCO (ace) procedure was performed according to the previously described protocol (Liu et al., 2020). The VE-cadherin antibody conjugated with Alexa Fluor™ 647 (VE-cadherin antibody, Biolegend, #138002. Alexa Fluor™ 647 dye, Thermo Fisher, #A20006) was diluted 1:1000 for use. After immunolabeling with Alexa Fluor dye-conjugated VE-Cadherin antibody, the tissues were washed directly with PBS/0.1% Tween 20/heparin (10 μg/ml) at room temperature for 24 h following the protocol described. The lung tissues processed by the iDISCO (ace) procedure were imaged on an Andor Dragonfly 200 Confocal Imaging System, with a ×10 objective, a step size of 8μm, 250 ms exposure time. About 1200-μm-thick optical stack of signal were acquired for each lung tissue. Imaris (version 9.9) was used to reconstruct the image stacks obtained from the confocal imaging to perform whole-tissue 3D assessment of the vasculature. AngioTool (version 0.6a) was used for vessels percentage area and total number of junctions analysis (Zudaire et al., 2011).

Vascular leakage experiment

After being euthanasiaed, the mice were treated with FITC-dextran (Sigma, #R9379-250 MG, 50 mg/ml, 25 μL/mouse) via lateral tail vein injection. 30 min after FITC-dextran injection, the mice were sacrificed to harvest the lung tissues. After the mice being sacrificed, skipping the step of inflating with PBS, lung tissues were removed from the chest cavity and directly embedded in OCT according to the protocol described above and then made into cryosections. Nuclear staining with DAPI was performed according to the IF protocol described above. Finally, the tissue sections were imaged on an AxioVert LSM980 confocal microscope (Zeiss) for analysis. The fluorescence analysis protocol was the same as that for IF described above.

Whole transcriptome sequencing (RNA-seq)

Single-cell suspensions were prepared as described above. Next, the single-cell suspension was incubated with CD45-coated beads for 30 min at 4°C, the bead-bound cells were removed using a magnet, and the unbound cell suspension was collected, followed by incubation with CD31-coated beads for 30 min at 4°C. The CD31-coated bead-bound cells were collected and washed 5 times with PBS/0.1% BSA/2 mM EDTA. Purified Rat Anti-Mouse CD31 (#553370) and Purified Rat Anti-Mouse CD45 (#553076) were obtained from BD Biosciences, and Dynabeads Sheep anti-Rat IgG (#11035) was obtained from ThermoFisher Scientific. Total RNA was prepared from the

collected ECs using TRIzol (ThermoFisher, #15596018) following the manufacturer's procedure. Then the 2 × 150 bp paired-end sequencing (PE150) was performed on an Illumina NovaseqTM 6,000 following the vendor's recommended protocol. Count data for genes were analyzed in R using the DESeq2 software package (version 1.30.1).

Quantitative RT–PCR

ECs were isolated as described above. Total RNA was prepared from lung ECs using TRIzol following the manufacturer's procedure. Complementary DNAs (cDNA) were synthesized from the total RNA using the PrimeScript RT Reagent Kit (TaKaRa, #RR0447A), and qPCR was performed on a CFX96 Real-Time PCR Detection System (Bio-Rad). Gene mRNA expression was quantified using SYBR green technology, with *β-actin* and *Gapdh* used as internal controls. Primer sequences are available upon request.

Western blot

Protein was extracted from lung ECs isolated as described above. Equal amounts of protein were separated in a 10% gel and transferred to nitrocellulose membranes. The membranes were incubated overnight with primary anti-FGFR1 antibody (1:1000; Cell Signaling Technology, #9740). Gapdh (1:1000, Santa Cruz #sc-32233) was used as an internal control. Signals were detected using corresponding horseradish peroxidase-conjugated secondary antibodies (1:5000, Abcam, #ab205719, #ab6721) and enhanced chemiluminescence (ThermoFisher, #34095).

Quantification and statistical analysis

Calculations were carried out with the Excel and Prism nine software packages (Version 9.1.1). One-way ANOVA followed by Tukey's test was employed to determine statistical significance. All data are presented as means ± standard error of means (SEMs). Error bar shows SEMs and center shows means. $p < 0.05$ was considered statistically significant.

Results

Neonatal hyperoxic lung injury results in disrupted alveolar development, respiratory dysfunction and abnormal vascular development

WT neonatal mice were exposed to hyperoxia (80% O_2) for 14 days to develop a mouse model of BPD, while the mice living in room air were used as controls (Figure 1A). Hyperoxia interrupted lung development in neonatal mice, resulting in enlarged alveoli and reduced alveolar numbers (Figures 1B–D). Mice from the hyperoxia group had an increased mean linear intercept (MLI) (Figure 1C) and a decreased radial alveolar count (RAC) (Figure 1D). Compared with mice from the room air group. The results of respiratory metrics measurement showed a significant decrease in minute ventilation (MVb), tidal volume breathing (TVb) and peak expiratory flow (PEFb) in hyperoxic mice compared to normoxic mice (Figures 1E–G), but a significant increase in Rpef, the ratio of time to peak expiratory flow (PEF) relative to total expiratory time (Te) (Figure 1H). These data mainly show that hyperoxia provokes disrupted alveologenesis, a prominent phenotype of BPD, as well as respiratory dysfunction in neonatal mice.

Next, we detected the influence of hyperoxia on pulmonary vascular development. The iDISCO (ace) tissue clearing procedure followed by immunofluorescence staining was employed to assess the development of pulmonary vasculature. The results showed that hyperoxia-exposed mice had reduced vascular branching and density (Figures 1I–K). The total number of junctions and vessels percentage area were reduced significantly in hyperoxic lungs (Figures 1J,K). Moreover, the results of IF staining showed that the expression of vascular endothelial cadherin (VE-Cad), a marker of endothelial cells, was lower in lungs developed in hyperoxia than in lungs developed in normoxia (Figures 1L, N). We further performed a FITC-dextran leakage experiment to evaluate the barrier function of blood vessels, which indicated that hyperoxia increased vascular leakage (Figures 1M, O). These results confirmed that hyperoxia results in abnormal vascular development, which thought to be one of the main mechanisms contributing to disrupted alveologenesis.

Hyperoxia induces ECs loss and upregulates the expression of endothelial FGFR1 and the classic FGFR1 signaling pathways in ECs

To investigate the cellular and molecular changes resulting from neonatal lung injury induced by hyperoxia, scRNA-seq was performed on a 10X genomics platform to generate scRNA-seq profiles of WT mice reared in normoxia or hyperoxia (Figure 2A). Five major cell lineages (lymphocytes, endothelial cells, stromal cells, epithelial cells and myeloid cells) corresponded by 19 cell clusters were identified by the expression of marker genes (Figures 2B–D; Table 1). We noted that the frequency of ECs decreased in the hyperoxia-impaired lungs (Figures 2E,F), which is consistent with the results obtained by analyzing the raw data from Thébaud who generated scRNA-seq profiles of 66,200 cells from normally (21% O_2-exposed from P0-P14) and aberrantly (85% O_2-exposed from

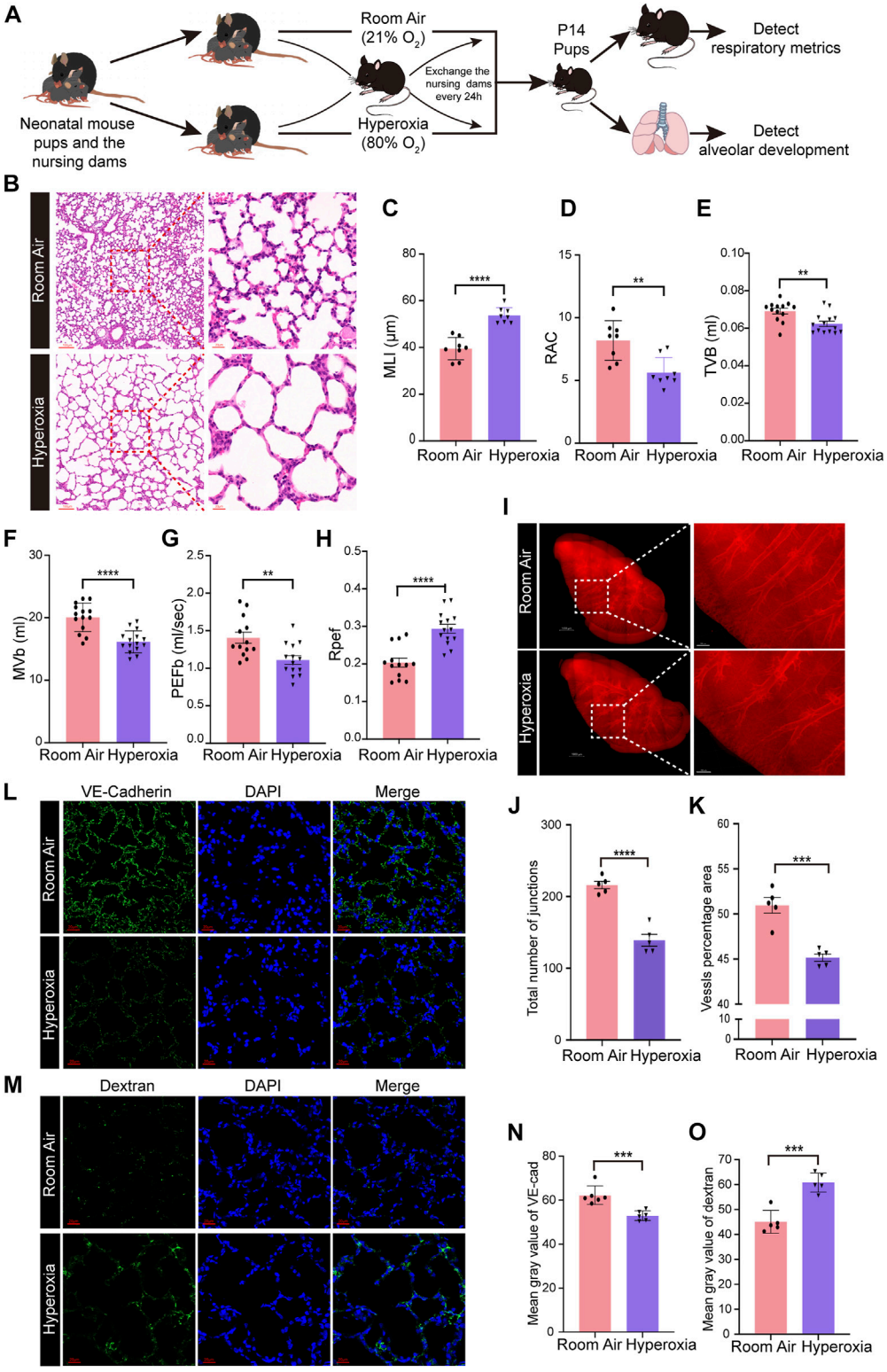

FIGURE 1
Hyperoxia disrupted angiogenesis and alveologenesis and resulted in respiratory dysfunction inneonatal mice. **(A)** Approach to develop a mouse model of BPD. Mouse pups were exposed to room air (21% O_2) or hyperoxia (80% O_2) from the day of birth (P0) to postnatal days (P)14. After measuring the respiratory metrics at P14, lungs were harvested for detection. **(B)** Representative images of H&E-stained lungs. The left panel shows low-magnification (scale bar = 100 μm) images, and the right panel shows higher-magnification (scale bar = 20 μm) images. **(C,D)**

(*Continued*)

FIGURE 1 (Continued)
Quantification of MLI (C) and RAC (D) based on the data in (B). Data are shown as the means ± SEMs. n = 8 per group. $^{**}p < 0.01$, $^{****}p < 0.0001$. **(E–H)** Results of respiratory metrics measurement. Data are shown as the means ± SEMs. n = 13 or 14 per group. $^{**}p < 0.01$, $^{****}p < 0.0001$. **(I–K)** Whole-tissue 3D assessment of vasculature in normal and hyperoxia-impaired lungs. 3D volume fluorescence images of VE-cadherin (VE-Cad)-stained lungs. The left panel shows low-magnification (scale bar = 1000 μm) images, and the right panel shows higher-magnification (scale bar = 200 μm) images (I). Quantification of the total number of junctions (J) and vessels percentage area (K) based on the data in (I). Data are shown as means ± SEMs. n = 5 per group. $^{***}p < 0.001$, $^{****}p < 0.0001$. (**L**) Representative images of IF staining for VE-Cad in lung sections. Magnification: ×40. Scale bar = 20 μm. **(N)** Mean gray value of VE-Cad based on the data in (L). Data are shown as means ± SEMs. n = 6 per group. $^{***}p < 0.001$. **(M)** Representative images of FITC-dextran leakage from mice reared in room air or hyperoxia. Magnification: ×40. Scale bar = 20 μm. **(O)** Mean gray value of dextran based on the data in (M). Data are shown as means ± SEMs. n = 5 per group. $^{***}p < 0.001$.

P0-P14) developing mouse lungs at P14 (Supplementary Figure S1D,E). Gene ontology (GO) enrichment analysis of the endothelial cell population suggested that the pathways associated with angiogenesis were impacted by hyperoxia exposure (Figure 2G). Furthermore, the GO enrichment analysis showed that hyperoxia impacted the signaling pathways associated with epithelial cell migration (Figure 2G). In addition, the results of scRNA-seq analysis showed an increase in the expression of *Fgfr1* in ECs from hyperoxic lungs (Figure 2H) and that the proportion of *Fgfr1*-positive ($Fgfr1^{+}$) ECs increased in hyperoxic lungs (Figure 2I).

Next, we performed RNA-seq to further verify the key molecular changes in ECs during the occurrence and development of hyperoxia-induced BPD. The results revealed that the expression of endothelial *Fgfr1* was increased in hyperoxic lungs (Figures 3A,B). Furthermore, the enrichment analysis of differentially expressed genes (DEGs) showed that hyperoxia upregulated the downstream signaling pathways of activated FGFR1, including the ERK/MAPK signaling pathway and PI3K-Akt signaling pathway (Figures 3C–E). Notably, hyperoxia also affected the signaling pathways associated with epithelial cell proliferation and epithelial tube morphogenesis (Figure 3C). Consistent with the results of sequencing, the results of qPCR and WB also showed that the expression of FGFR1 was significantly increased in ECs from hyperoxic lungs (Figures 3F,G). We also detected the expression of endothelial FGFR2, another major FGFR expressed by ECs in addition to FGFR1. The results showed that there was no significant difference in endothelial FGFR2 expression between normoxic and hyperoxic neonatal lungs (Supplementary Figures S2A–C). We speculate that this may be attributed to that in neonatal lung, endothelial FGFR1 may be more sensitive to hyperoxia exposure than endothelial FGFR2. These data suggest that hyperoxia upregulates endothelial FGFR1 expression and that the upregulated endothelial FGFR1 may play a vital role in hyperoxia-induced BPD.

Deficiency of endothelial FGFR1 improves alveologenesis, respiratory function and angiogenesis in hyperoxia-exposed mice

To dissect the functional contribution of FGFR1 in hyperoxia-induced BPD, we generated the genetically modified mouse in which *Fgfr1* was conditionally deleted specifically in ECs ($Fgfr1^{i\Delta EC/i\Delta EC}$) by crossing $Fgfr1^{fl/fl}$ mice with *VE-Cadherin-(PAC)-*Cre^{ERT2} mice (Figure 4A). The results of qPCR verification showed that the endothelial *Fgfr1* was knockout efficiently (Supplementary Figures S3A–C). Wild-type mice ($Fgfr1^{+/+}$) were used as controls. We found that deletion of *Fgfr1* improved the alveologenesis of neonatal mice upon hyperoxia (Figures 4B–D). After hyperoxia exposure, the MLI of mice from the $Fgfr1^{i\Delta EC/i\Delta EC}$ group was significantly decreased, and the RAC was significantly increased compared to mice from the $Fgfr1^{+/+}$ group (Figures 4C,D). Next, we measured the respiratory metrics of $Fgfr1^{+/+}$ and $Fgfr1^{i\Delta EC/i\Delta EC}$ mice. Unsurprisingly, deficiency of FGFR1 in ECs improved the respiratory function of neonatal mice upon hyperoxia, with TVb, MVb and PEFb increasing markedly and Rpef decreasing markedly in $Fgfr1^{i\Delta EC/i\Delta EC}$ mice (Figures 4E–H). After hyperoxia exposure, the expression of VE-Cad increased in lungs from $Fgfr1^{i\Delta EC/i\Delta EC}$ mice compared to that in lungs from $Fgfr1^{+/+}$ mice by detecting with IF staining (Figures 4I,K). The results of FITC-dextran leakage experiment indicated that the vascular leakage of $Fgfr1^{i\Delta EC/i\Delta EC}$ mice was decreased in hyperoxia (Figures 4J,L). There were no significant differences observed between normoxia-exposed $Fgfr1^{+/+}$ mice and the normoxia-exposed $Fgfr1^{i\Delta EC/i\Delta EC}$ mice or the hyperoxia-exposed $Fgfr1^{i\Delta EC/i\Delta EC}$ mice. Here, it is demonstrated that deletion of endothelial *Fgfr1* can protect the lungs from hyperoxia-induced lung injury in neonatal mice.

Hyperoxia triggers up-expression of FGFR1 in aCap cells rather than in gCap cells

To shed light on the underlying regulatory mechanisms of endothelial FGFR1 in hyperoxia-induced lung injury, we analyzed the alteration of EC subpopulations by scRNA-seq. Five distinct EC subpopulations, including gCap, aCap, Artery, Vein and Lymph, were identified based on their expression profiles (Figures 5A–C; Table 1). Hyperoxia reduced the frequency of gCap cells while increasing the frequency of aCap cells, which is consistent with the results obtained by analyzing the raw data from Thébaud (Figure 5D, Supplementary Figures S4D–E). Corresponding to the changes

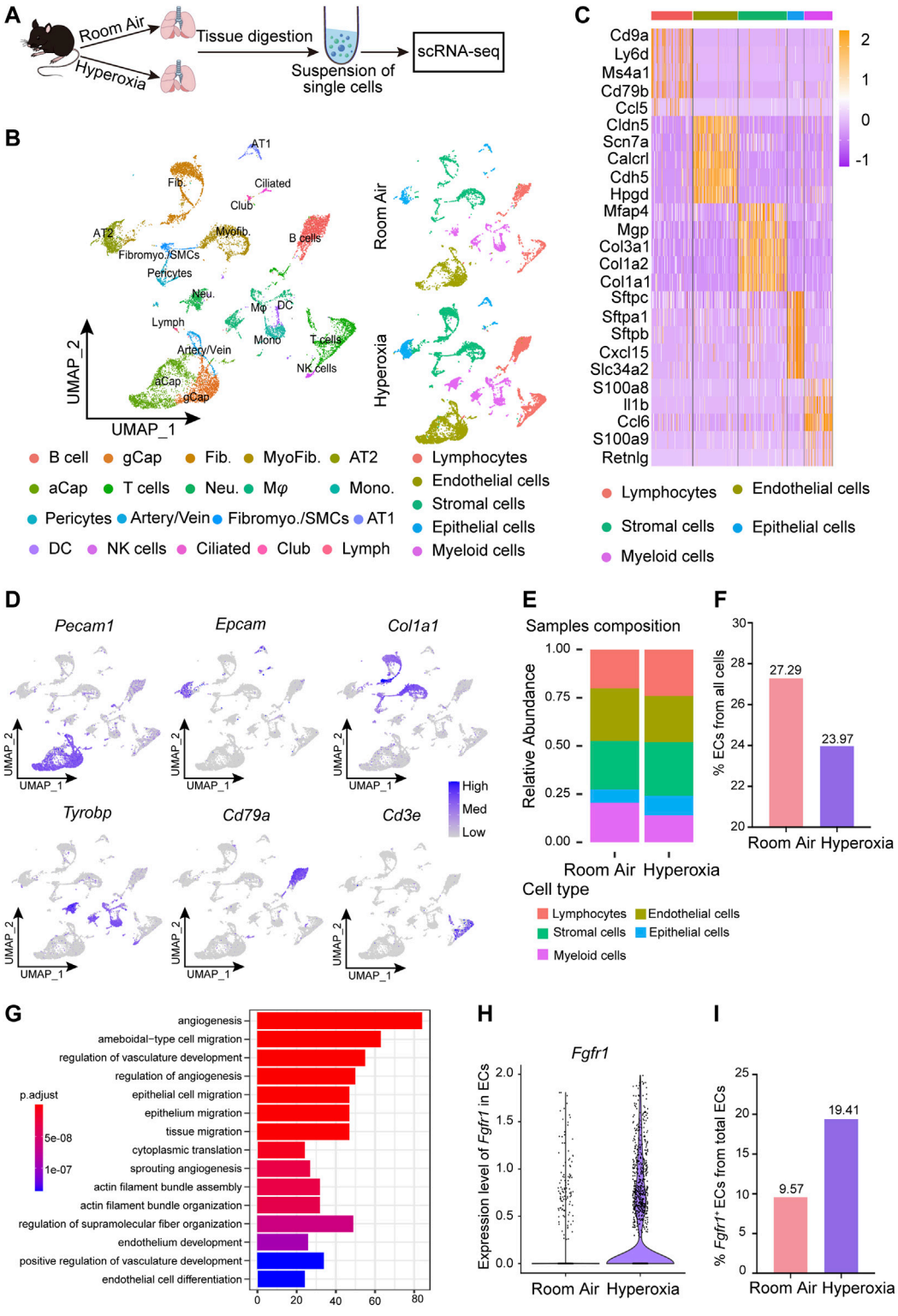

FIGURE 2
scRNA-seq analysis of lungs from normoxia- and hyperoxia-reared mice. **(A)** Approach to generate a single-cell atlas. **(B)** UMAP plot of all scRNA-seq data, showing a total of 19 distinct cell types corresponding to 5 major cell groups. Cell populations are colored as indicated by the legend. **(C)** Heatmap of the top 5 most differentially expressed genes across 5 major cell types. The intensity of expression is indicated as specified by the color legend. **(D)** Feature plots showing the expression of principal identifiers of epithelial cells, endothelial cells, stromal cells, myeloid cells, lymphocytes (B cells) and lymphocyte (T cells) populations. **(E)** Cellular compositions are colored as indicated by the legend in normal and hyperoxia-

(*Continued*)

FIGURE 2 (Continued)
impaired lungs. **(F)** The relative proportion of endothelial cells from all cells in normal and hyperoxia-impaired lungs. **(G)** Hyperoxia-impacted signaling pathways in ECs, as identified by GO enrichment analysis of biological processes. **(H)** Violin plot showing the expression of *Fgfr1* in ECs. **(I)** *Fgfr1*$^{+}$ ECs in total ECs.

TABLE 1 Identified cell populations.

Abbreviation	Cell type	Abbreviation	Cell type
aCap	Aerocyte capillary endothelial cells	Fib	Fibroblasts
Artery	Arterial endothelial cells	Myofib	Myofibroblasts
gCap	General capillary endothelial cells	Fibromyo./SMCs	Fibromyocytes/Smooth muscle cells
Lymph	Lymphatic endothelial cells	Pericyte	Pericyte
Vein	Venous endothelial cells	Neu	Neutrophils
AT1	Alveolar type I cells	MΦ	Macrophages
AT2	Alveolar type II cells	T cells	T cells
Ciliated	Ciliated cells	B cells	B cells
Club	Club cells	Mono.	Monocytes
DC	Dendritic cells		

in cell proportion, in hyperoxia-impaired lung, the expression of gCap cell markers, *Gpihpb1*, *Aplnr* and *Kit* were decreased, while the expression of aCap cell markers, *Ednrb*, *Apln* and *Car4* were increased (Figure 5E).

To determine whether FGFR1 results in these changes, we first analyzed the expression patterns of *Fgfr1* in gCap cells and aCap cells. Interestingly, hyperoxia increased the frequency of *Fgfr1*$^{+}$ aCap cells, and *Fgfr1*$^{+}$ aCap cells accounted for the majority of *Fgfr1*$^{+}$ ECs in hyperoxia (Figure 5F). Additionally, the increment of *Fgfr1* expression was mainly observed in aCap cells rather than in gCap cells (Figure 5G). Next, we found that in hyperoxic lung ECs, *Fgfr1*$^{i\Delta EC/i\Delta EC}$ mutant increased the mRNA expression of gCap cell marker, *Aplnr*, while decreased the mRNA expression of aCap cell markers, *Apln* and *Car4* (Figure 5H). These data indicate that FGFR1 may be pivotal in maintaining the proportion and cellular function of gCap cells and aCap cells upon hyperoxia.

Inhibition of endothelial FGFR1 ameliorates hyperoxia-induced alveolar damage and respiratory dysfunction

To verify whether FGFR1 could be a potential therapeutic target for BPD, the effects of the FGFR1 inhibitor (AZD4547) on hyperoxia-induced BPD was evaluated. The results showed that inhibition of FGFR1 by AZD4547 also improved the alveologenesis of neonatal mice upon hyperoxia (Figure 6A). AZD4547 treatment significantly decreased the MLI of hyperoxia-exposed mice, while significantly increased the RAC of hyperoxia-exposed mice (Figures 6B,C). In addition, the results of respiratory metrics measurement showed that after hyperoxia exposure, mice from AZD4547 treated group had increased TVb, MVb and PEFb, while had decreased Rpef (Figures 6D–G). Consistent with the results of the *Fgfr1* genetic deficiency model, these data demonstrated that FGFR1 may be a potential therapeutic target for BPD.

Discussion

Oxygen supplementation is the most common treatment in newborns. However, hyperoxic damage is one of the main factors that blunts normal lung alveologenesis and the development of pulmonary microvasculature. In this work, neonatal mice exposed to hyperoxia ultimately exhibited simplified alveolarization and enlarged alveolar cavity, the prominent features of BPD. Additionally, we reported a decrease in MVb and TVb in mice with BPD, which indicates the destruction of respiratory function in mice. The worsening of PEFb and Rpef, reference indicators of airflow restriction, perhaps suggested decreased respiratory muscle strength and increased airway obstruction (Menachery et al., 2015; Ramírez-Ramírez et al., 2017). These data suggest that neonatal hyperoxia exposure disrupted alveologenesis and ultimately led to obstructed respiratory function, which indicated that we established the hyperoxia-induced BPD mouse model successfully and stably.

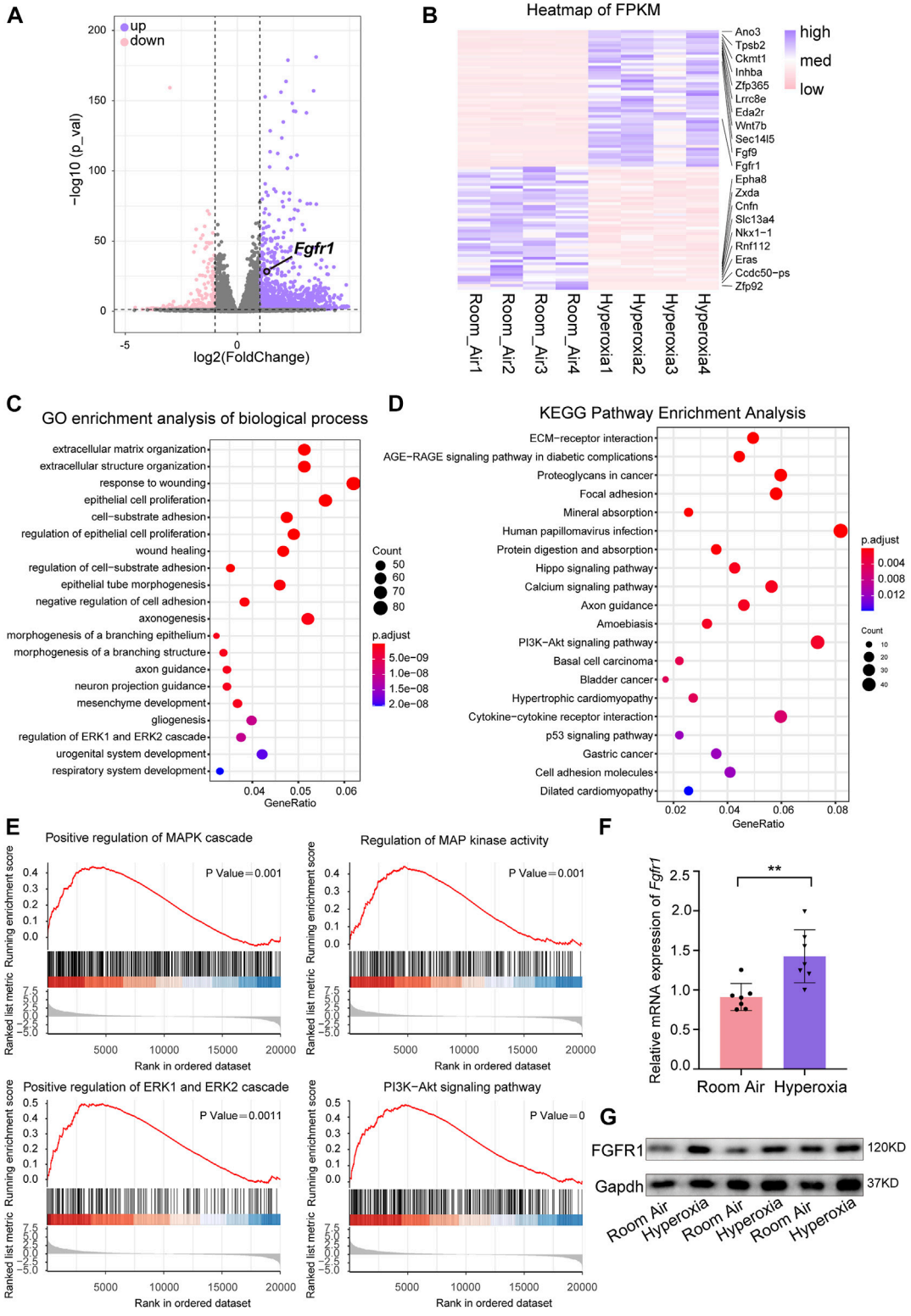

FIGURE 3
RNA-seq analysis of differentially expressed genes (DEGs) and hyperoxia-impacted signaling pathways in ECs from normal and hyperoxia-impaired lungs. **(A)** Volcano plot showing upregulated and downregulated transcript levels of DEGs, p-value < 0.05, |log2FoldChange|≥1. **(B)** Heatmap of the top 50 upregulated DEGs and top 50 downregulated DEGs. **(C)** Hyperoxia-impacted signaling pathways in ECs as identified by GO enrichment analysis of biological processes. All terms shown are significantly enriched (p-value < 0.05). **(D)** Hyperoxia-impacted signaling pathways in ECs as identified by KEGG pathway enrichment analysis. All terms shown are significantly enriched (p-value < 0.05). **(E)** Upregulated downstream pathways of activated FGFR1 as revealed by Gene Set Enrichment Analysis, all terms shown are significantly enriched (p-value < 0.05). **(F)** qPCR of *Fgfr1* expression in ECs of normoxic or hyperoxic lungs. $n = 7$ per group. Data are shown as means ± SEMs. $^{**}p < 0.01$. **(G)** Western blot examining the expression of FGFR1 in ECs of normoxic or hyperoxic lung, Gapdh as negative control.

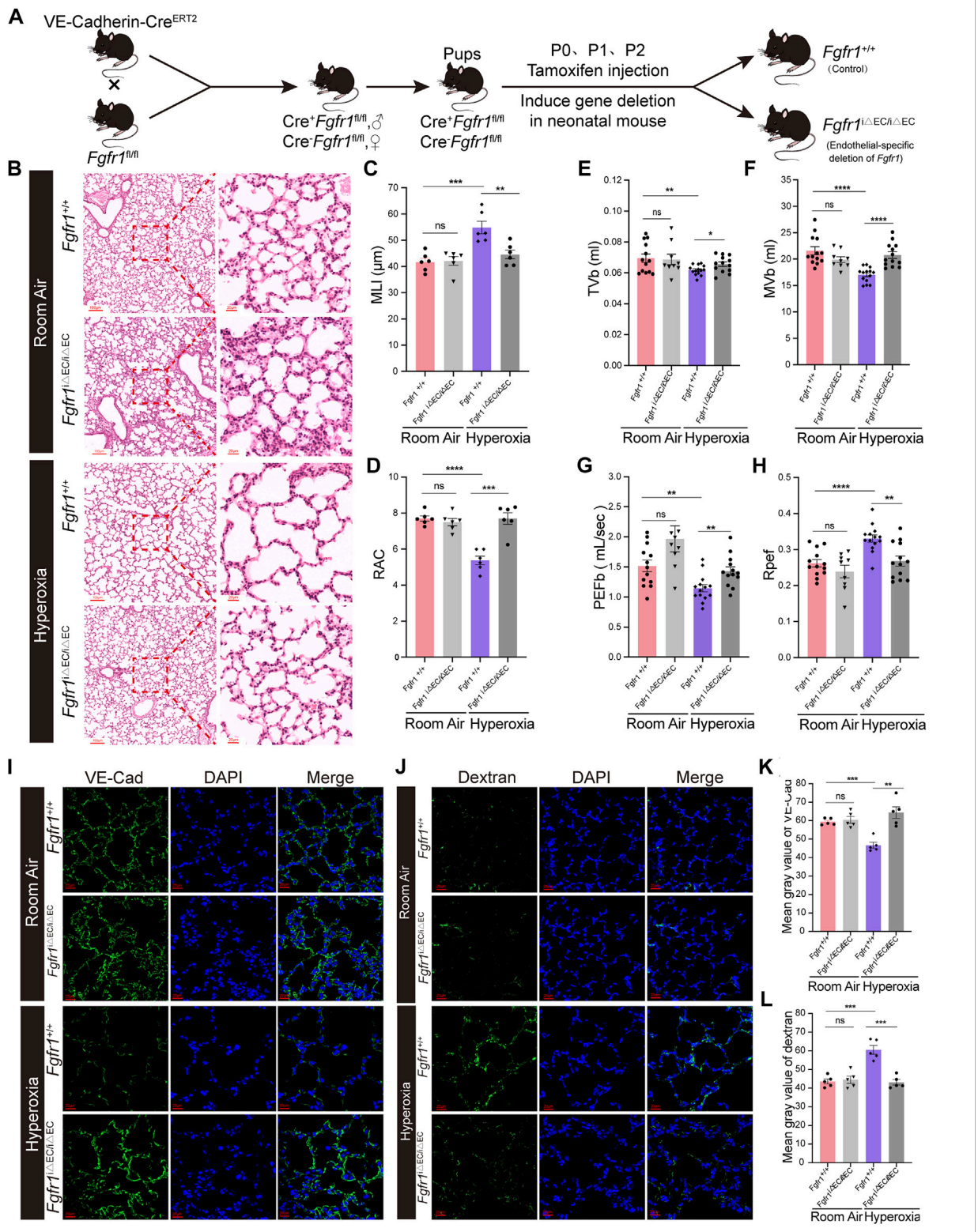

FIGURE 4
Deletion of endothelial *Fgfr1* improved alveolar development and respiratory metrics and angiogenesis in mice upon hyperoxia. **(A)** Schematic representation of EC-specific inducible deletion of *Fgfr1* in neonatal mice. **(B)** Representative images of H&E-stained lungs from *Fgfr1* $^{+/+}$ and *Fgfr1*$^{i\Delta EC/i\Delta EC}$ mice reared in room air or hyperoxia. The top panel shows low-magnification (scale bar = 100 μm) images, and the bottom panel shows higher-magnification (scale bar = 20 μm) images. **(C,D)** Quantification of MLI (C) and RAC (D) based on the data in (B). Data are shown as
(*Continued*)

FIGURE 4 (Continued)
means ± SEMs. n = 6 per group. $^{**}p < 0.01$, $^{***}p < 0.001$. **(E–H)** Results of respiratory metrics measurement. Data are shown as means ± SEMs. n = 9, 13 or 14 per group. $^{*}p < 0.05$, $^{**}p < 0.01$, $^{****}p < 0.0001$. **(I)** Representative images of IF staining for VE-Cad in lung sections. Magnification: ×40. Scale bar = 20 μm. **(K)** Mean gray value of VE-Cad based on the data in (I). Data are shown as means ± SEMs. n = 5 per group. $^{**}p < 0.01$, $^{***}p < 0.001$. **(J)** Representative images of FITC-dextran leakage from mice reared in room air or hyperoxia. Magnification: ×40. Scale bar = 20 μm. **(L)** Mean gray value of dextran based on the data in (J). Data are shown as means ± SEMs. n = 5 per group. $^{***}p < 0.001$.

We observed that hyperoxic mice exhibited abnormal vascular development and mice from hyperoxia group had reduced vascular branching and density. Additionally, the increased leakage of vasculature also suggested that hyperoxia disrupted blood vessels. Disruption of lung angiogenesis is a key mechanism through which hyperoxia leads to alveolar simplification in BPD (Ren et al., 2019). Previous studies have shown that ECs play a critical role in organ injury and repair (Cao et al., 2016; Gladka et al., 2021; Li et al., 2022), so does in hyperoxia-induced lung injury. It was reported that hyperoxia specifically decreased fatty acid oxidation (FAO) in ECs, which induced apoptosis and simplified alveolarization and vascularization in the lungs of mice (Yao et al., 2019). Exposure of human microvascular endothelial cells to hyperoxia decreased cell viability and proliferation (Attaye et al., 2017). Moreover, it was previously found that hyperoxia could evoke mitochondrial DNA damage and mitochondrial fragmentation in pulmonary endothelial cells, which would result in pulmonary endothelial cell dysfunction (Ma et al., 2018). These data demonstrateed that ECs are crucial to the hyperoxia-induced lung injury response.

We further investigated the cellular and molecular changes resulting from hyperoxia-induced lung injury by performing scRNA-seq analysis of normal and hyperoxia-injured lungs and RNA-seq analysis of ECs in lungs from normal mice and hyperoxia-exposed BPD mice. We reported that hyperoxia decreased the proportion of ECs in lungs of neonatal mice. FGFR1 was upregulated in ECs of the hyperoxia-damaged lungs, which was also confirmed in the results of qPCR and WB. Nevertheless, we did not observe significant difference in the expression of endothelial FGFR2. We hypothesized that perhaps endothelial FGFR1 was more sensitive to hyperoxia exposure than endothelial FGFR2. A previous study showed that FGFR1 and FGFR2 were the dominant FGFRs in ECs (Presta et al., 2005) and were autophosphorylated and activated upon the binding of FGF ligands, such as FGF1 and FGF2 (Goetz and Mohammadi, 2013; Xie et al., 2020). In some studies, endothelial FGF/FGFR signals have been reported as facilitative for angiogenesis under physiological or pathological states (Tsuboi et al., 1992; Yanagisawa-Miwa et al., 1992; Compagni et al., 2000; Murakami and Simons, 2009; De Smet et al., 2014). Nevertheless, other findings reported that FGF/FGFR signaling is not essential for angiogenesis. Mice with deficiency of FGF1 or FGF2, even deficiency of FGF1 and FGF2 together had few angiogenesis abnormalities (Ortega et al., 1998; Zhou et al., 1998; Miller et al., 2000). Moreover, there is another point of view that endothelial FGFR1 and FGFR2 are necessary for pathological neovascularization after injury but not for physiological vascular development and vascular homeostasis (Oladipupo et al., 2014; House et al., 2016). Interestingly, studies reported that overactivated FGFR1 could suppress angiogenesis and promote fibrosis. A previous study reported that exaggerated endothelial FGF2/FGFR1 signaling caused by SUMOylation-defective mutation of FGFR1 suppressed VEGFA/VEGFR2 signaling and the angiogenic capabilities of ECs (Zhu et al., 2022). In another study, it was reported that overactivation of FGFR1 contributed to the occurrence of fibrosis (Ding et al., 2014), a prominent feature of severe BPD. The present study, as well as previous studies, demonstrated that in different situations, balancing the level of FGFR1 is important for physiological or pathological activities. The upregulation of the downstream signaling pathways of activated FGFR1 further demonstrated that hyperoxia activated FGFR1 signaling pathways. These data suggested that hyperoxia-induced upregulation of endothelial FGFR1 expression may be a key factor in hyperoxia-induced abnormal vascular development and ultimately result in interrupted alveologenesis and pulmonary dysfunction.

Therefore, we treated the *Fgfr1*$^{i\Delta EC/i\Delta EC}$ mice with the same hyperoxia exposure protocol to further address the role of FGFR1 in hyperoxia-induced lung injury and repair. We found that deletion of endothelial *Fgfr1* protected the lungs from hyperoxia-induced lung injury in neonatal mice. After hyperoxia exposure, mice from *Fgfr1*$^{i\Delta EC/i\Delta EC}$ group had improved angiogenesis, alveologenesis and respiratory metrics. The results of scRNA-seq analysis suggested that hyperoxia decreased the frequency of gCap cells but increased the frequency of aCap cells. Consistently, downregulation of gCap cell markers and upregulation of aCap cell markers were detected in hyperoxic lungs. The *c-Kit*$^{+}$ endothelial cells (gCap) were reported to be capillary progenitors, which could enhance lung angiogenesis and prevent alveolar simplification in neonatal mice exposed to hyperoxia (Miranda et al., 2013; Ren et al., 2019). In addition, gCap cells were shown to be critical for normal neonatal lung angiogenesis (Wang et al., 2022). Thus, it makes sense to believe that the reduction in gCap cells caused by hyperoxia may be crucial to disrupted vascular development in newborn mice. On the other hand, previously published data showed that the number of aCap cells increased after hyperoxia exposure, accompanied by

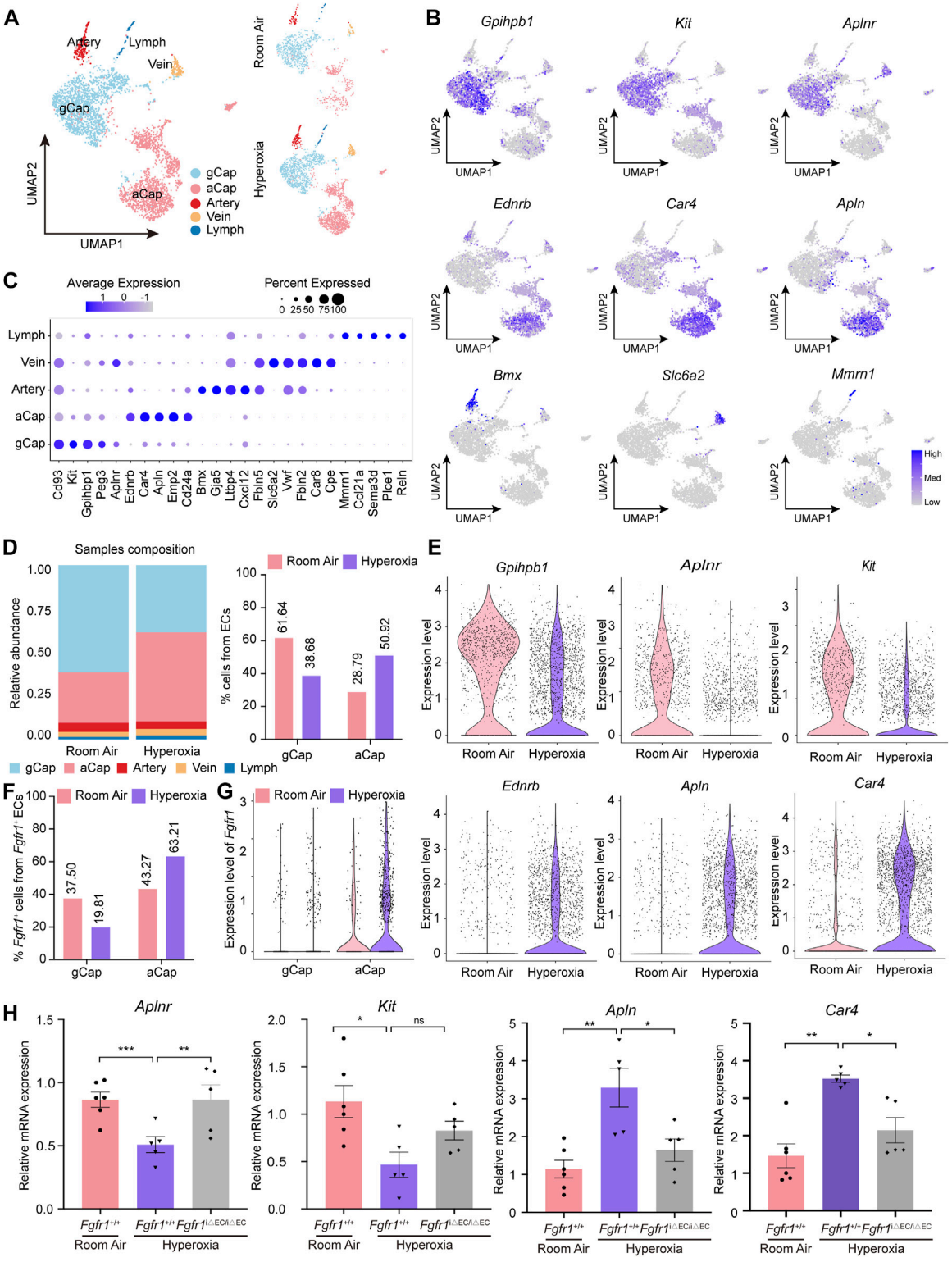

FIGURE 5
Hyperoxia induced upregulation of FGFR1 mainly in aCap cells rather than in gCap cells. **(A)** A total of 5 clusters of ECs were identified. Cell populations are colored as indicated by the legend. **(B)** Feature plots showing the expression of principal identifiers of general capillary endothelial cells (gCap), aerocyte capillary endothelial cells (aCap), arterial endothelial cells (Artery), venous endothelial cells (Vein) and lymphatic endothelial cells (Lymph). **(C)** Dotplot depicting the top 5 most differentially expressed genes across endothelial clusters. The intensity of expression is

(*Continued*)

FIGURE 5 (Continued)
indicated as specified by the color legend. **(D)** Alteration of the relative proportion of gCap cells and aCap cells. The right panel shows the cellular compositions of ECs, colored as indicated by the legend, and the left panel shows the relative proportion of gCap cells and aCap cells from ECs. **(E)** Violin plots displaying the expression patterns of gCap cell and aCap cell markers. **(F)** Column chart showing *Fgfr1*$^{+}$ gCap cells and *Fgfr1*$^{+}$ aCap cells from total *Fgfr1*$^{+}$ ECs. **(G)** Violin plots displaying the expression patterns of *Fgfr1* in gCap cells and aCap cells. **(H)** qPCR of gCap cell markers, *Aplnr* and *Kit* expression and aCap cell markers, *Apln* and *Car4* expression in ECs of lung from *Fgfr1*$^{+/+}$ and *Fgfr1*$^{i\Delta EC/i\Delta EC}$ mice reared in room air or hyperoxia. n = 5 or 6 per group. Data are shown as means ± SEMs. ^{ns}no significant, *p < 0.05, **p < 0.01, ***p < 0.001.

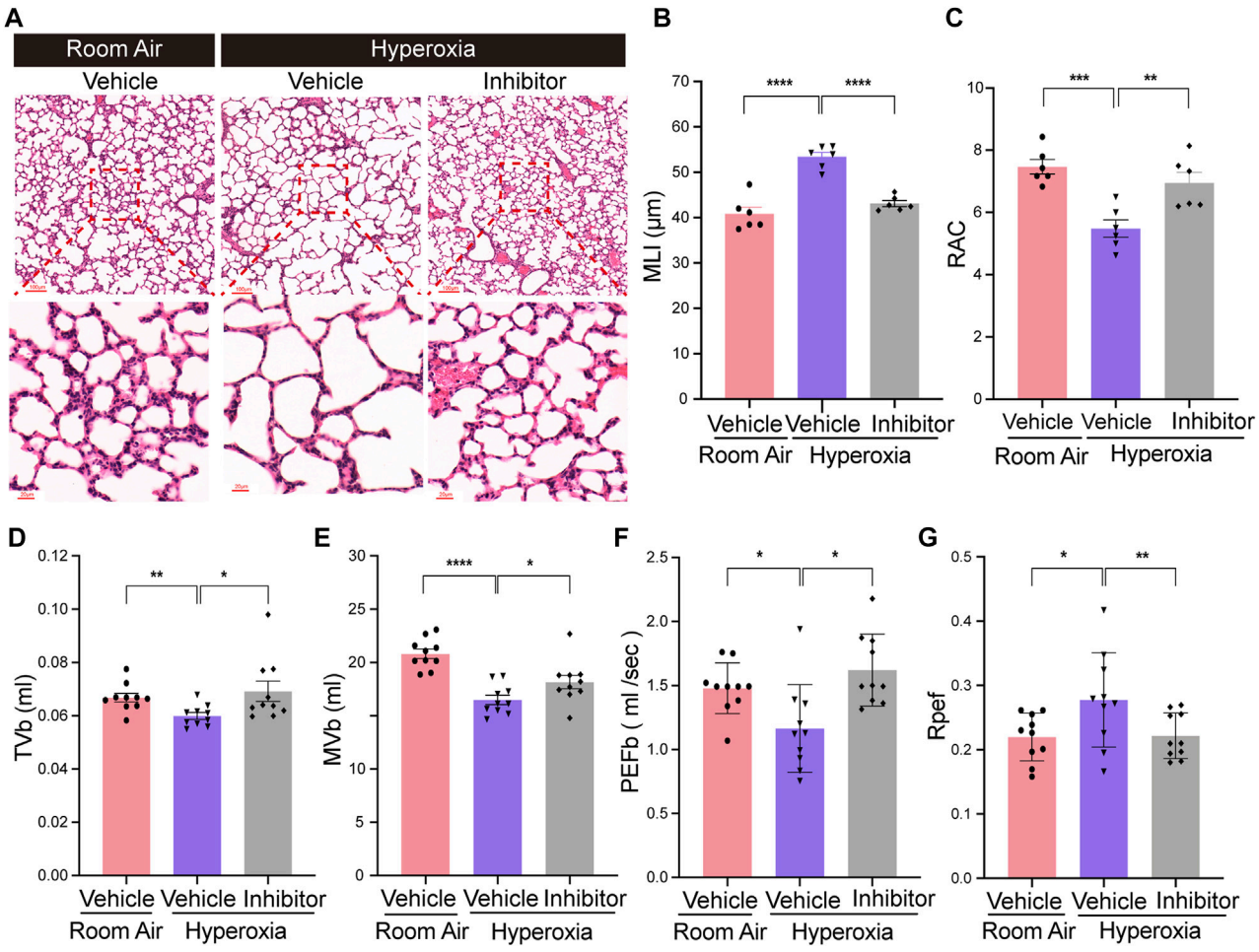

FIGURE 6
Inhibition of endothelial Fgfr1 improved alveolar development and respiratory metrics in neonatal mice in hyperoxia. **(A)** Representative images of H&E-stained lungs from vehicle or FGFR1 inhibitor treated mice. The top panel shows low-magnification (scale bar = 100 μm) images, and the bottom panel shows higher-magnification (scale bar = 20 μm) images. **(B,C)** Quantification of MLI (B) and RAC (C) based on the data in (A). Data are shown as means ± SEMs. n = 6 per group. **p < 0.01, ***p < 0.001, ****p < 0.0001. **(D–G)** Results of respiratory metrics measurement. Data are shown as means ± SEMs. n = 10 per group. *p < 0.05, **p < 0.01, ****p < 0.0001.

upregulation of inflammatory genes and antiangiogenic genes, which contribute to BPD (Hurskainen et al., 2021). The other point of view supports that *Car4*$^{+}$ capillary endothelial cells (aCap) are important for normal alveolar development by interacting with AT1 cells through VEGFA and contribute to alveolar revascularization postinjury (Niethamer et al., 2020; Vila Ellis et al., 2020). Consequently, we hypothesize that the hyperoxia-induced increase in aCap cells resulting in upregulation of the expression of some unfriendly genes (such as inflammatory genes and antiangiogenic genes), through which

aCap cells interact with other cells (such as AT1 cells), may be a major factor in disrupting lung development and regeneration in neonatal mice.

Interestingly, scRNA-seq analysis revealed that the upregulated expression of endothelial *Fgfr1* was mainly found in aCap cells rather than in gCap cells. We validated the correlation of endothelial FGFR1 deficiency with the expression of gCap cell markers and aCap cell markers upon hyperoxia. We observed that deletion of *Fgfr1* increased the expression of gCap cell markers but decreased the expression of aCap cell markers in hyperoxic lung ECs. Thus, we speculate that the upregulated FGFR1 in aCap may affect the cellular proportion and function of gCap cells and aCap cells upon hyperoxia. In the future, further researches are needed to determine their regulatory relationships and the underlying mechanisms.

Finally, to mimic the clinical treatment method, we treated neonatal mice with FGFR1 inhibitor by intragastric injection of AZD4547 to induce FGFR1 deficiency. Consistent with the results of the *Fgfr1* genetic deficiency model, inhibition of FGFR1 by AZD4547 also showed protective function against hyperoxia-induced lung injury in neonatal mice. After hyperoxia exposure, mice from inhibitor treated group had improved alveologenesis and respiratory metrics. These data suggest that FGFR1 may be a potential therapeutic target for BPD.

In summary, the present study shows that hyperoxia upregulates the expression of FGFR1 and FGFR1 signaling pathways in lung ECs of neonatal mice. Deletion of endothelial *Fgfr1* can protect lung from hyperoxia-induced lung injury in neonatal mice, which may be attributed to the regulation of FGFR1 on gCap cells and aCap cells. The results of the present research suggest that FGFR1 is a potential therapeutic target for BPD, which has considerable clinical value.

Data availability statement

All sequencing data, including raw fastq sequencing files, gene expression matrices, and associated metadata generated in this study have been deposited in the NCBI's Gene Expression Omnibus (GEO) database under accession number GSE217489 (https://www.ncbi.nlm.nih.gov/geo/query/acc.cgi?acc?GSE217489). Further inquiries can be directed to the corresponding author.

Ethics statement

The animal study was reviewed and approved by Institutional Animal Care and Use Committee of West China Second University Hospital.

Author contributions

ZC and LQ conceived the project, designed and supervised the experiments. YL and PY designed the experiments. YL, HC, JD, and JN performed all of the experiments. YL and HC analyzed the data. YL wrote the manuscript with input from all the authors. ZC and PY revised the manuscript. All authors contributed to the article reading and approved the final manuscript.

Funding

This work was supported by the National Natural Science Foundation of China (82125002, 81941007).

Acknowledgments

We are grateful to thank Shahin Rafii for providing the *Fgfr1*$^{fl/fl}$ mice and Tinghong Ye for providing the FGFR1 inhibitor. We would like to thank Chuan Wu, Chengju Xiao, and Liyin Zhang for helping in data analysis. We would also like to thank Tianci Zhong for English language checking.

Conflict of interest

The authors declare that the research was conducted in the absence of any commercial or financial relationships that could be construed as a potential conflict of interest.

Publisher's note

All claims expressed in this article are solely those of the authors and do not necessarily represent those of their affiliated organizations, or those of the publisher, the editors and the reviewers. Any product that may be evaluated in this article, or claim that may be made by its manufacturer, is not guaranteed or endorsed by the publisher.

Supplementary material

The Supplementary Material for this article can be found online at: https://www.frontiersin.org/articles/10.3389/fphar.2022.1039103/full#supplementary-material.

References

Ashour, K., Shan, L., Lee, J. H., Schlicher, W., Wada, K., Wada, E., et al. (2006). Bombesin inhibits alveolarization and promotes pulmonary fibrosis in newborn mice. *Am. J. Respir. Crit. Care Med.* 173 (12), 1377–1385. doi:10.1164/rccm.200507-1014OC

Attaye, I., Smulders, Y. M., de Waard, M. C., Oudemans-van Straaten, H. M., Smit, B., Van Wijhe, M. H., et al. (2017). The effects of hyperoxia on microvascular endothelial cell proliferation and production of vaso-active substances. *Intensive Care Med. Exp.* 5 (1), 22. doi:10.1186/s40635-017-0135-4

Bates, C. M. (2011). Role of fibroblast growth factor receptor signaling in kidney development. *Pediatr. Nephrol.* 26 (9), 1373–1379. doi:10.1007/s00467-010-1747-z

Cao, Z., Lis, R., Ginsberg, M., Chavez, D., Shido, K., Rabbany, S. Y., et al. (2016). Targeting of the pulmonary capillary vascular niche promotes lung alveolar repair and ameliorates fibrosis. *Nat. Med.* 22 (2), 154–162. doi:10.1038/nm.4035

Chang, D. R., Martinez Alanis, D., Miller, R. K., Ji, H., Akiyama, H., McCrea, P. D., et al. (2013). Lung epithelial branching program antagonizes alveolar differentiation. *Proc. Natl. Acad. Sci. U. S. A.* 110 (45), 18042–18051. doi:10.1073/pnas.1311760110

Cheon, I. S., Son, Y. M., Jiang, L., Goplen, N. P., Kaplan, M. H., Limper, A. H., et al. (2018). Neonatal hyperoxia promotes asthma-like features through IL-33-dependent ILC2 responses. *J. Allergy Clin. Immunol.* 142 (4), 1100–1112. doi:10.1016/j.jaci.2017.11.025

Compagni, A., Wilgenbus, P., Impagnatiello, M. A., Cotten, M., and Christofori, G. (2000). Fibroblast growth factors are required for efficient tumor angiogenesis. *Cancer Res.* 60 (24), 7163–7169.

Cooney, T. P., and Thurlbeck, W. M. (1982). The radial alveolar count method of emery and mithal: A reappraisal 1--postnatal lung growth. *Thorax* 37 (8), 572–579. doi:10.1136/thx.37.8.572

De Smet, F., Tembuyser, B., Lenard, A., Claes, F., Zhang, J., Michielsen, C., et al. (2014). Fibroblast growth factor signaling affects vascular outgrowth and is required for the maintenance of blood vessel integrity. *Chem. Biol.* 21 (10), 1310–1317. doi:10.1016/j.chembiol.2014.07.018

DeMauro, S. B. (2018). The impact of bronchopulmonary dysplasia on childhood outcomes. *Clin. Perinatol.* 45 (3), 439–452. doi:10.1016/j.clp.2018.05.006

Deng, C. X., Wynshaw-Boris, A., Shen, M. M., Daugherty, C., Ornitz, D. M., and Leder, P. (1994). Murine FGFR-1 is required for early postimplantation growth and axial organization. *Genes Dev.* 8 (24), 3045–3057. doi:10.1101/gad.8.24.3045

Ding, B. S., Cao, Z., Lis, R., Nolan, D. J., Guo, P., Simons, M., et al. (2014). Divergent angiocrine signals from vascular niche balance liver regeneration and fibrosis. *Nature* 505 (7481), 97–102. doi:10.1038/nature12681

Ding, B. S., Nolan, D. J., Guo, P., Babazadeh, A. O., Cao, Z., Rosenwaks, Z., et al. (2011). Endothelial-derived angiocrine signals induce and sustain regenerative lung alveolarization. *Cell* 147 (3), 539–553. doi:10.1016/j.cell.2011.10.003

Dow, J. K., and deVere White, R. W. (2000). Fibroblast growth factor 2: Its structure and property, paracrine function, tumor angiogenesis, and prostate-related mitogenic and oncogenic functions. *Urology* 55 (6), 800–806. doi:10.1016/s0090-4295(00)00457-x

Filippini, A., Tamagnone, L., and D'Alessio, A. (2022). Endothelial cell metabolism in vascular functions. *Cancers (Basel)* 14 (8), 1929. doi:10.3390/cancers14081929

Gillich, A., Zhang, F., Farmer, C. G., Travaglini, K. J., Tan, S. Y., Gu, M., et al. (2020). Capillary cell-type specialization in the alveolus. *Nature* 586 (7831), 785–789. doi:10.1038/s41586-020-2822-7

Gladka, M. M., Kohela, A., Molenaar, B., Versteeg, D., Kooijman, L., Monshouwer-Kloots, J., et al. (2021). Cardiomyocytes stimulate angiogenesis after ischemic injury in a ZEB2-dependent manner. *Nat. Commun.* 12 (1), 84. doi:10.1038/s41467-020-20361-3

Goetz, R., and Mohammadi, M. (2013). Exploring mechanisms of FGF signalling through the lens of structural biology. *Nat. Rev. Mol. Cell Biol.* 14 (3), 166–180. doi:10.1038/nrm3528

Gudernova, I., Vesela, I., Balek, L., Buchtova, M., Dosedelova, H., Kunova, M., et al. (2016). Multikinase activity of fibroblast growth factor receptor (FGFR) inhibitors SU5402, PD173074, AZD1480, AZD4547 and BGJ398 compromises the use of small chemicals targeting FGFR catalytic activity for therapy of short-stature syndromes. *Hum. Mol. Genet.* 25 (1), 9–23. doi:10.1093/hmg/ddv441

House, S. L., Castro, A. M., Lupu, T. S., Weinheimer, C., Smith, C., Kovacs, A., et al. (2016). Endothelial fibroblast growth factor receptor signaling is required for vascular remodeling following cardiac ischemia-reperfusion injury. *Am. J. Physiol. Heart Circ. Physiol.* 310 (5), H559–H571. doi:10.1152/ajpheart.00758.2015

Hurskainen, M., Mižíková, I., Cook, D. P., Andersson, N., Cyr-Depauw, C., Lesage, F., et al. (2021). Single cell transcriptomic analysis of murine lung development on hyperoxia-induced damage. *Nat. Commun.* 12 (1), 1565. doi:10.1038/s41467-021-21865-2

Islam, J. Y., Keller, R. L., Aschner, J. L., Hartert, T. V., and Moore, P. E. (2015). Understanding the short- and long-term respiratory outcomes of prematurity and bronchopulmonary dysplasia. *Am. J. Respir. Crit. Care Med.* 192 (2), 134–156. doi:10.1164/rccm.201412-2142PP

Ito, R., Barnes, E. A., Che, X., Alvira, C. M., and Cornfield, D. N. (2022). SM22α cell-specific HIF stabilization mitigates hyperoxia-induced neonatal lung injury. *Am. J. Physiol. Lung Cell. Mol. Physiol.* 323 (2), L129–l141. doi:10.1152/ajplung.00110.2022

Kurowski, A., Molotkov, A., and Soriano, P. (2019). FGFR1 regulates trophectoderm development and facilitates blastocyst implantation. *Dev. Biol.* 446 (1), 94–101. doi:10.1016/j.ydbio.2018.12.008

Li, J., Shi, S., Srivastava, S. P., Kitada, M., Nagai, T., Nitta, K., et al. (2017). FGFR1 is critical for the anti-endothelial mesenchymal transition effect of N-acetyl-seryl-aspartyl-lysyl-proline via induction of the MAP4K4 pathway. *Cell Death Dis.* 8 (8), e2965. doi:10.1038/cddis.2017.353

Li, L., Mu, J., Zhang, Y., Zhang, C., Ma, T., Chen, L., et al. (2022). Stimulation by exosomes from hypoxia preconditioned human umbilical vein endothelial cells facilitates mesenchymal stem cells angiogenic function for spinal cord repair. *ACS Nano* 16, 10811–10823. doi:10.1021/acsnano.2c02898

Liu, T., Yang, L., Han, X., Ding, X., Li, J., and Yang, J. (2020). Local sympathetic innervations modulate the lung innate immune responses. *Sci. Adv.* 6 (20), eaay1497. doi:10.1126/sciadv.aay1497

Ma, C., Beyer, A. M., Durand, M., Clough, A. V., Zhu, D., Norwood Toro, L., et al. (2018). Hyperoxia causes mitochondrial fragmentation in pulmonary endothelial cells by increasing expression of pro-fission proteins. *Arterioscler. Thromb. Vasc. Biol.* 38 (3), 622–635. doi:10.1161/atvbaha.117.310605

Menachery, V. D., Gralinski, L. E., Baric, R. S., and Ferris, M. T. (2015). New metrics for evaluating viral respiratory pathogenesis. *PLoS One* 10 (6), e0131451. doi:10.1371/journal.pone.0131451

Miller, B., and Sewell-Loftin, M. K. (2021). Mechanoregulation of vascular endothelial growth factor receptor 2 in angiogenesis. *Front. Cardiovasc. Med.* 8, 804934. doi:10.3389/fcvm.2021.804934

Miller, D. L., Ortega, S., Bashayan, O., Basch, R., and Basilico, C. (2000). Compensation by fibroblast growth factor 1 (FGF1) does not account for the mild phenotypic defects observed in FGF2 null mice. *Mol. Cell. Biol.* 20 (6), 2260–2268. doi:10.1128/mcb.20.6.2260-2268.2000

Miranda, L. F., Rodrigues, C. O., Ramachandran, S., Torres, E., Huang, J., Klim, J., et al. (2013). Stem cell factor improves lung recovery in rats following neonatal hyperoxia-induced lung injury. *Pediatr. Res.* 74 (6), 682–688. doi:10.1038/pr.2013.165

Murakami, M., and Simons, M. (2009). Regulation of vascular integrity. *J. Mol. Med.* 87 (6), 571–582. doi:10.1007/s00109-009-0463-2

Nardiello, C., Mižíková, I., Silva, D. M., Ruiz-Camp, J., Mayer, K., Vadász, I., et al. (2017). Standardisation of oxygen exposure in the development of mouse models for bronchopulmonary dysplasia. *Dis. Model. Mech.* 10 (2), 185–196. doi:10.1242/dmm.027086

Niethamer, T. K., Stabler, C. T., Leach, J. P., Zepp, J. A., Morley, M. P., Babu, A., et al. (2020). Defining the role of pulmonary endothelial cell heterogeneity in the response to acute lung injury. *Elife* 9, e53072. doi:10.7554/eLife.53072

Northway, W. H., Jr., Rosan, R. C., and Porter, D. Y. (1967). Pulmonary disease following respirator therapy of hyaline-membrane disease. Bronchopulmonary dysplasia. *N. Engl. J. Med.* 276 (7), 357–368. doi:10.1056/nejm196702162760701

Oladipupo, S. S., Smith, C., Santeford, A., Park, C., Sene, A., Wiley, L. A., et al. (2014). Endothelial cell FGF signaling is required for injury response but not for vascular homeostasis. *Proc. Natl. Acad. Sci. U. S. A.* 111 (37), 13379–13384. doi:10.1073/pnas.1324235111

Ong, S. H., Guy, G. R., Hadari, Y. R., Laks, S., Gotoh, N., Schlessinger, J., et al. (2000). FRS2 proteins recruit intracellular signaling pathways by binding to diverse targets on fibroblast growth factor and nerve growth factor receptors. *Mol. Cell. Biol.* 20 (3), 979–989. doi:10.1128/mcb.20.3.979-989.2000

Ortega, S., Ittmann, M., Tsang, S. H., Ehrlich, M., and Basilico, C. (1998). Neuronal defects and delayed wound healing in mice lacking fibroblast growth factor 2. *Proc. Natl. Acad. Sci. U. S. A.* 95 (10), 5672–5677. doi:10.1073/pnas.95.10.5672

Presta, M., Dell'Era, P., Mitola, S., Moroni, E., Ronca, R., and Rusnati, M. (2005). Fibroblast growth factor/fibroblast growth factor receptor system in

angiogenesis. *Cytokine Growth Factor Rev.* 16 (2), 159–178. doi:10.1016/j.cytogfr.2005.01.004

Ramírez-Ramírez, E., Torres-Ramírez, A., Alquicira-Mireles, J., Cañavera-Constantino, A., Segura-Medina, P., Montaño-Ramírez, M., et al. (2017). Characteristic plethysmographic findings in a Guinea pig model of COPD. *Exp. Lung Res.* 43 (2), 57–65. doi:10.1080/01902148.2017.1294632

Ren, X., Ustiyan, V., Guo, M., Wang, G., Bolte, C., Zhang, Y., et al. (2019). Postnatal alveologenesis depends on FOXF1 signaling in c-KIT(+) endothelial progenitor cells. *Am. J. Respir. Crit. Care Med.* 200 (9), 1164–1176. doi:10.1164/rccm.201812-2312OC

Sahni, M., and Mowes, A. K. (2022). "Bronchopulmonary dysplasia," in *StatPearls* (Treasure island (FL): StatPearls Publishing LLC.).

Schittny, J. C. (2017). Development of the lung. *Cell Tissue Res.* 367 (3), 427–444. doi:10.1007/s00441-016-2545-0

Silva, D. M., Nardiello, C., Pozarska, A., and Morty, R. E. (2015). Recent advances in the mechanisms of lung alveolarization and the pathogenesis of bronchopulmonary dysplasia. *Am. J. Physiol. Lung Cell. Mol. Physiol.* 309 (11), L1239–L1272. doi:10.1152/ajplung.00268.2015

Surate Solaligue, D. E., Rodríguez-Castillo, J. A., Ahlbrecht, K., and Morty, R. E. (2017). Recent advances in our understanding of the mechanisms of late lung development and bronchopulmonary dysplasia. *Am. J. Physiol. Lung Cell. Mol. Physiol.* 313 (6), L1101–l1153. doi:10.1152/ajplung.00343.2017

Thébaud, B., Goss, K. N., Laughon, M., Whitsett, J. A., Abman, S. H., Steinhorn, R. H., et al. (2019). Bronchopulmonary dysplasia. *Nat. Rev. Dis. Prim.* 5 (1), 78. doi:10.1038/s41572-019-0127-7

Tracy, M. K., and Berkelhamer, S. K. (2019). Bronchopulmonary dysplasia and pulmonary outcomes of prematurity. *Pediatr. Ann.* 48 (4), e148–e153. doi:10.3928/19382359-20190325-03

Tsuboi, R., Shi, C. M., Rifkin, D. B., and Ogawa, H. (1992). A wound healing model using healing-impaired diabetic mice. *J. Dermatol.* 19 (11), 673–675. doi:10.1111/j.1346-8138.1992.tb03757.x

Vila Ellis, L., Cain, M. P., Hutchison, V., Flodby, P., Crandall, E. D., Borok, Z., et al. (2020). Epithelial vegfa specifies a distinct endothelial population in the mouse lung. *Dev. Cell* 52 (5), 617–630. e616. doi:10.1016/j.devcel.2020.01.009

Wang, G., Wen, B., Deng, Z., Zhang, Y., Kolesnichenko, O. A., Ustiyan, V., et al. (2022). Endothelial progenitor cells stimulate neonatal lung angiogenesis through FOXF1-mediated activation of BMP9/ACVRL1 signaling. *Nat. Commun.* 13 (1), 2080. doi:10.1038/s41467-022-29746-y

Warburton, D., Bellusci, S., De Langhe, S., Del Moral, P. M., Fleury, V., Mailleux, A., et al. (2005). Molecular mechanisms of early lung specification and branching morphogenesis. *Pediatr. Res.* 57, 26R–37r. doi:10.1203/01.PDR.0000159570.01327.ED

Willis, G. R., Fernandez-Gonzalez, A., Anastas, J., Vitali, S. H., Liu, X., Ericsson, M., et al. (2018). Mesenchymal stromal cell exosomes ameliorate experimental bronchopulmonary dysplasia and restore lung function through macrophage immunomodulation. *Am. J. Respir. Crit. Care Med.* 197 (1), 104–116. doi:10.1164/rccm.201705-0925OC

Xie, Y., Zinkle, A., Chen, L., and Mohammadi, M. (2020). Fibroblast growth factor signalling in osteoarthritis and cartilage repair. *Nat. Rev. Rheumatol.* 16 (10), 547–564. doi:10.1038/s41584-020-0469-2

Yanagisawa-Miwa, A., Uchida, Y., Nakamura, F., Tomaru, T., Kido, H., Kamijo, T., et al. (1992). Salvage of infarcted myocardium by angiogenic action of basic fibroblast growth factor. *Science* 257 (5075), 1401–1403. doi:10.1126/science.1382313

Yao, H., Gong, J., Peterson, A. L., Lu, X., Zhang, P., and Dennery, P. A. (2019). Fatty acid oxidation protects against hyperoxia-induced endothelial cell apoptosis and lung injury in neonatal mice. *Am. J. Respir. Cell Mol. Biol.* 60 (6), 667–677. doi:10.1165/rcmb.2018-0335OC

Yu, P., Wilhelm, K., Dubrac, A., Tung, J. K., Alves, T. C., Fang, J. S., et al. (2017). FGF-dependent metabolic control of vascular development. *Nature* 545 (7653), 224–228. doi:10.1038/nature22322

Zepp, J. A., Zacharias, W. J., Frank, D. B., Cavanaugh, C. A., Zhou, S., Morley, M. P., et al. (2017). Distinct mesenchymal lineages and niches promote epithelial self-renewal and myofibrogenesis in the lung. *Cell* 170 (6), 1134–1148. e1110. doi:10.1016/j.cell.2017.07.034

Zhou, C., Kuang, Y., Li, Q., Duan, Y., Liu, X., Yue, J., et al. (2022). Endothelial S1pr2 regulates post-ischemic angiogenesis via AKT/eNOS signaling pathway. *Theranostics* 12 (11), 5172–5188. doi:10.7150/thno.71585

Zhou, M., Sutliff, R. L., Paul, R. J., Lorenz, J. N., Hoying, J. B., Haudenschild, C. C., et al. (1998). Fibroblast growth factor 2 control of vascular tone. *Nat. Med.* 4 (2), 201–207. doi:10.1038/nm0298-201

Zhou, X., Du, J., Qing, L., Mee, T., Xu, X., Wang, Z., et al. (2021). Identification of sensory and motor nerve fascicles by immunofluorescence staining after peripheral nerve injury. *J. Transl. Med.* 19 (1), 207. doi:10.1186/s12967-021-02871-w

Zhu, X., Qiu, C., Wang, Y., Jiang, Y., Chen, Y., Fan, L., et al. (2022). FGFR1 SUMOylation coordinates endothelial angiogenic signaling in angiogenesis. *Proc. Natl. Acad. Sci. U. S. A.* 119 (26), e2202631119. doi:10.1073/pnas.2202631119

Zudaire, E., Gambardella, L., Kurcz, C., and Vermeren, S. (2011). A computational tool for quantitative analysis of vascular networks. *PLoS One* 6 (11), e27385. doi:10.1371/journal.pone.0027385

frontiers | Frontiers in Pharmacology

TYPE Original Research
PUBLISHED 29 November 2022
DOI 10.3389/fphar.2022.1055702

OPEN ACCESS

EDITED BY
Isaac Kirubakaran Sundar,
University of Kansas Medical Center,
United States

REVIEWED BY
Pavel Solopov,
Old Dominion University, United States
Ruxandra Rajnoveanu,
Iuliu Haţieganu University of Medicine and Pharmacy, Romania

*CORRESPONDENCE
Guojun Zhang,
gjzhangzzu@126.com
Xiaojian Zhang,
zhangxj6686@163.com

†These authors have contributed equally to this work

SPECIALTY SECTION
This article was submitted to Respiratory Pharmacology,
a section of the journal
Frontiers in Pharmacology

RECEIVED 28 September 2022
ACCEPTED 18 November 2022
PUBLISHED 29 November 2022

CITATION
Li H, Yang J, Chen S, Wang P, Yu X, Zhou Q, Zhang X and Zhang G (2022), Analysis of the safety and efficacy of different plasma concentrations of pirfenidone in patients with idiopathic pulmonary fibrosis.
Front. Pharmacol. 13:1055702.
doi: 10.3389/fphar.2022.1055702

Analysis of the safety and efficacy of different plasma concentrations of pirfenidone in patients with idiopathic pulmonary fibrosis

Hui Li[1], Jing Yang[2], Shanshan Chen[1], Peile Wang[2], Xueqing Yu[3], Qingwei Zhou[3], Xiaojian Zhang[2*†] and Guojun Zhang[1*†]

[1]Department of Respiratory Medicine, Henan key Laboratory of Interstitial Lung Diseases and Lung Transplantation Medicine, Henan Respiratory Disease Clinical Medical Research Center, The First Affiliated Hospital of Zhengzhou University, Zhengzhou, China, [2]Department of Pharmacy, Henan Engineering Research Center for Application and Translation of Precision Clinical Pharmacy, The First Affiliated Hospital of Zhengzhou University, Zhengzhou University, Zhengzhou, China, [3]Department of Respiratory Diseases, The First Affiliated Hospital of Henan University of Chinese Medicine, Zhengzhou, China

The high incidence and mortality of idiopathic pulmonary fibrosis (IPF) have led to the widespread use of antifibrotic drugs such as pirfenidone; however, the associated adverse reactions greatly vary among individuals and the dose is not fixed. To date, no reliable blood concentration range of pirfenidone is available to monitor adverse reactions and clinical efficacy. This real study assessed the efficacy and safety of different plasma concentrations of pirfenidone in patients with IPF. The study included 99 patients with IPF orally treated with pirfenidone capsules for at least 52 weeks. Ultra-performance liquid chromatography–mass spectrometry was used to analyze drug plasma concentrations. The annual rate of forced vital capacity (FVC) decline, assessed at week 52, was set as the primary end point. Secondary end points were the change from the baseline in the 6-min walk distance (6 MWD) and the time to the first acute exacerbation of IPF, both of which evaluated over 52 weeks. In the total population, the annual FVC decline in the high-concentration group was −90.0 ml per year versus −260.0 ml per year in the low-concentration group, for a between-group difference of 190.3 ml per year. The proportion of patients treated with high plasma concentrations of pirfenidone who showed an absolute decline of ≥10% in FVC% predicted, with a 6 MWD reduction of ≥50 m, or died, was lower than that of patients treated with low plasma concentrations of pirfenidone. High concentrations of pirfenidone reduced the risk of acute exacerbation in patients with IPF. Considerable differences were not observed for the total St. George's Respiratory Questionnaire score or the rates of death between the high- and low-concentration groups. Mild to moderate adverse events, mainly involving the gastrointestinal system and the skin, were more common in the high-concentration group than in the low-concentration group but did not lead to termination of treatment in most cases. Our results suggest that treatment of IPF with high blood concentration of pirfenidone is both safe and effective. In

the case of tolerable adverse reactions, patients with IPF may benefit from high concentrations of pirfenidone.

KEYWORDS

pirfenidone, idiopathic pulmonary fibrosis, plasma concentration, safety, efficacy

Introduction

Idiopathic pulmonary fibrosis (IPF) is a chronic and progressive fibrotic lung disease with usual interstitial pneumonia (UIP) as the main histopathological and radiological pattern. IPF causes honeycombing, irreversible tissue damage, and respiratory failure, which seriously affect the quality of life of patients and increase the mortality rate. IPF accounts for approximately 20% of all cases of interstitial lung diseases, with approximately 3 million IPF cases globally (Lederer and Martinez, 2018) and a high prevalence among the elderly and males. The survival time varies widely among patients with IPF (Raghu et al., 2011). Advanced age, male, dyspnea, the rapid decline of lung functions in the early stage of the disease (Raghu et al., 2020), and severe pathological injury are all associated with the poor prognosis of patients with IPF. Due to the lack of effective drug treatments, the median survival of transplant-free patients with IPF is 3–5 years, which is less than the survival rate of patients with other malignancies (Mora et al., 2017), with an extremely poor prognosis. Hence, the search for an effective therapeutic strategy for IPF is at the forefront of contemporary research (Collard et al., 2016; Kolb et al., 2017; Richeldi et al., 2017; Lederer and Martinez, 2018; Kondoh, 2019; Kirby, 2021).

The pathogenesis of IPF is extremely complex and hence can be easily misdiagnosed. Studies have shown that the epithelial-mesenchymal transition (Jayachandran et al., 2009; Wilson and Wynn, 2009), abnormal activation of lung fibroblasts (Zhao et al., 2016), and excessive deposition of collagen matrix (Martinez et al., 2017) play a key role in the process of pulmonary fibrosis.

Previous large-scale controlled clinical trial studies of IPF do not recommend the use of the combination of prednisone, azathioprine, and N- acetylcysteine as well as the administration of warfarin and endothelin receptor antagonists (Noth et al., 2012) due to their poor efficacy. The Food and Drug Association (FDA) has approved the antifibrotic drugs pirfenidone (Noble et al., 2011; King et al., 2014) and nintedanib (Richeldi et al., 2014; Bonella et al., 2015; Flaherty et al., 2019) for the treatment of IPF, as they suppress the decline in lung functions and delay disease progression. Pirfenidone, an oral pyridone derivative with anti-inflammatory, antioxidant, and antifibrotic properties (Lee et al., 1998; Schaefer et al., 2011), has been reported to regulate TGF-β expression in animal models of pulmonary fibrosis and can inhibit fibroblast and collagen synthesis (Schaefer et al., 2011).

A study showed that pirfenidone reduced the number of coughs per hour in patients with IPF by 35% and improved subjective cough indicators (van Manen et al., 2017). In addition, pirfenidone could significantly alleviate the deterioration of dyspnea by decreasing the change of FVC decline and the University of California and San Diego Shortness of Breath Questionnaire from baseline to 12 months in the patients with IPF treated with pirfenidone (Glassberg et al., 2019). In a prospective controlled trial, treatment with pirfenidone for 9 months improved vital capacity and significantly reduced the risk of acute exacerbation of IPF (Azuma et al., 2005). A retrospective analysis of ASCEND and CAPACITY004 and 006 studies reported that pirfenidone could reduce the incidence of disease progression events in patients with IPF (FVC% predicted decreased by more than 10%, 6 MWD decreased by more than 50 m, hospitalization and death) (Nathan et al., 2019).

In recent years, more patients with IPF are prescribed pirfenidone by professional respiratory physicians, and the recommended dose is 1,800 mg/d. However, pirfenidone causes side effects, mostly in the gastrointestinal tract (indigestion and loss of appetite) and skin (photosensitivity), and these adverse reactions worsen with dosage increase, resulting in poor compliance of patients. There are highly variable individual differences in adverse reactions, the dosage is not fixed, and there is a lack of a reliable blood concentration range of pirfenidone to monitor adverse reactions and clinical efficacy. In view of this, this study investigates the safety and efficacy of different plasma concentrations of pirfenidone in the treatment of patients with IPF and explores appropriate drug reference for clinical treatment decisions.

Materials and methods

Study design and patients

This study is a multicenter real-world study conducted in 16 centers in Henan Province. The study was approved by the Research and Clinical trial Ethics Committee of the First Affiliated Hospital of Zhengzhou University (Ethical Review No. 2020-KY-257).

The recruitment time was from July 2020 to August 2021, and the eligible patients were 40–85 years old. IPF was diagnosed based on the diagnostic guidelines for IPF by the ATS/ERS/JRS/ALAT in 2018 (Raghu et al., 2018); patients with image findings

suggesting probable UIP were diagnosed by transbronchial lung biopsy or surgical lung biopsy. All the high-resolution computed tomographic images and lung histopathology specimens were reviewed uniformly by at least one expert chest radiologist and one pathologist. The range dose of pirfenidone was 1,200–1,800 mg/d, taken orally *ter in die* (t.i.d., i.e., three times a day). Other eligibility criteria were as follows: 1) An FVC % predicted of 50% or more. 2) A diffusion capacity of the lung for carbon monoxide (DLco) between 30 and 90% predicted. 3) A ratio of the forced expiratory volume in 1 s to the FVC that was equal to or greater than 0.80. 4) A 6-min walk distance (6 MWD) of over 150 m at baseline. Written informed consent was obtained from all patients.

Exclusion criteria were as follows: 1) Use of other antifibrotic drugs, including nintedanib, high-dose prednisone (>10 mg), immunosuppressants, rituximab, and N- acetylcysteine. 2) Participation in any study of IPF drugs during the preceding one month. 3) History of malignant tumors during the preceding 5 years. 4) Patients receiving antineoplastic therapy. 5) Patients suffering from active or latent tuberculosis during the preceding six months. If an acute exacerbation was reported at any time during the trial, the researcher had the choice to either start any other treatment or increase the dose as required.

Treatment regimen

All patients had been treated with an oral pirfenidone capsule with a dose of ≥1,200 mg/d and a maximum dose of 1,800 mg/d. The drug was administered in three equal doses and taken with three meals. Physical examination, clinical laboratory tests, lung function test, 6 MWD test, and the analysis of total St George's Respiratory Questionnaire (SGRQ) score were performed at baseline and at week 52. Telephone follow-up was carried out on the 2nd, 4th, 8th, 13th, 26th, 39th, and 52nd weeks to evaluate exercise tolerance and dyspnea, acute aggravation of symptoms, and hospitalization due to illness. Adverse drug reactions and treatment measures were documented meticulously. We assessed the adequacy and repeatability of all lung function results according to the American Thoracic Society standards (Culver et al., 2017). Safety outcomes were determined from clinical and laboratory evaluations and the records of adverse events that occurred within the 52 weeks and were coded using the Common Toxicity Criteria (CTC) version 2.0 of the National Cancer Institute.

Measurement of pirfenidone plasma concentration

Serial blood samples were collected at the baseline. Peripheral venous blood samples (2 ml) were drawn from each patient prior to dosing and at 1.5, 2, 4, 6, and 8 h post-dosing. All blood samples were collected in EDTA tubes and centrifuged at × 3,500 g for 10 min to isolate the plasma. Ultra-performance liquid chromatography–tandem mass spectrometry (UPLC-MS/MS) was used to analyze the plasma concentrations of pirfenidone. The calibration curve covered the range of 0.2–20.0 mg/L. An analysis of quality control samples indicated good precision (coefficients of variation ≤4.2%) and accuracy (measured concentrations ≤4.7% from target concentrations) (Wang et al., 2021). The area under the curve (AUC) at baseline was evaluated using the linear trapezoidal method, whereas the AUC 8 h was multiplied by 3 to obtain the AUC 24 h.

Outcomes

The primary endpoint was the annual rate of decline in the FVC over the 52-week period. According to the international guidelines (Culver et al., 2017), pulmonary function was measured at the baseline and at the 52nd week. The secondary end points were the assessment of absolute changes in the percentage of predicted FVC, DLco, 6 MWD reduction, and the time to the first confirmed or suspected acute exacerbation of IPF or death from baseline to week 52.

The implementation of the 6-min walk test was defined and controlled according to the standards defined and validated by du (Bois et al., 2011); additional control measures were taken according to the ERS/ATS guidelines for field walking testing (Holland et al., 2014). Disease progression was defined as a decline of greater than 10% in the absolute FVC % predicted, hospitalization due to respiratory diseases, or a drop of 50 m or more in the 6 MWD compared with the baseline measurement. Acute exacerbation of IPF was defined as the acute clinically significant deterioration of respiratory functions characterized by new evidence of extensive alveolar abnormalities, which met the following diagnostic criteria (Collard et al., 2016): 1) The previous or current diagnosis was IPF. 2) Acute deterioration or dyspnea, usually lasting <30 days. 3) Computed tomography showed bilateral ground glass shadows and/or overlapping consolidations of background types consistent with the common type of interstitial pneumonia. 4) A deterioration that does not account completely for heart failure or humoral overload. Cases that are of unknown cause but do not fulfill the criteria listed due to missing computed tomography data and have been termed "suspected acute exacerbations of IPF." Additional secondary endpoints included the change in the total SGRQ score measured over the entire treatment period. The SGRQ, which is used to evaluate the quality of life, is a self-administered questionnaire that consists of three different domains (symptoms, activity, and impact). The score of each domain ranges from 0 to 100, and the total score represents the weighted average of the three sub-scores, with higher scores

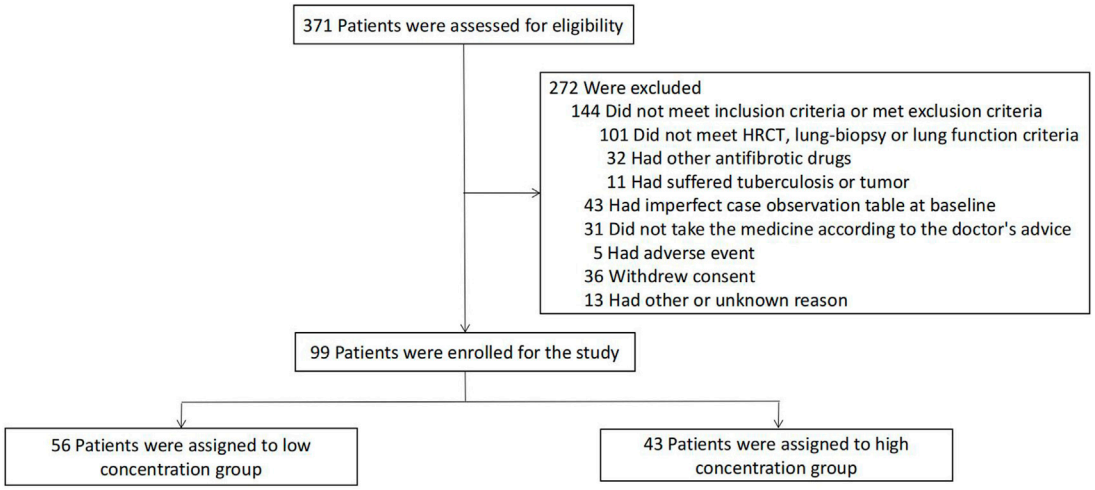

FIGURE 1
Enrollment and Grouped in the Overall Population. Patients could have more than one reason for exclusion. The numbers of patients who withdrew from the study do not include patients who died or underwent lung transplantation. Patients who discontinued the study treatment were included in the analysis of data for patients who completed the study.

corresponding to a poorer quality of life (Jones et al., 1991; Furukawa et al., 2017; Prior et al., 2019).

Statistical analysis

The research data were statistically analyzed using the SPSS25.0 software (IBM Corporation, Armonk, NY, United States). To analyze the mean change, the missing values due to death were assigned the worst result (e.g., FVC = 0). The normal distribution, skewed distribution, and counting data were expressed as average ±standard deviation, median (lower quartile, upper quartile), and frequency (constituent ratio), respectively. The T, $\chi 2$, and Mann-Whitney *U* tests were performed for comparisons among groups. The data were all double-tailed statistics, with an alpha value of 0.05. For time-to-event analyses, the high-concentration group was compared with the low-concentration group using the log-rank test.

Results

Patient characteristics

From July 2020 to August 2021, 405 blood samples were collected from 371 patients treated with pirfenidone (≥1,200 mg/d), of which 31 collected two blood samples and 1 collected four blood samples while adjusting the drug dose. After excluding the patients with inadequate clinical features, test results, pulmonary functions, 6 MWD and SGRQ scores at baseline, and follow-ups within 52 weeks, along with the patients who could not be diagnosed as having IPF by imaging or pathology, 99 patients who completed the visits were finally enrolled in the study (Figure 1).

A UPLC-MS/MS-based method for the simultaneous measurement of pirfenidone and its main metabolites in the plasma of the patients was established in our center. Blood samples were collected for drug concentration determination after repeated administration. The plasma concentration of pirfenidone in patients with IPF was 112.8 ± 65.5 mg h/L. Upon viewing the AUC of the receiver operating characteristic curve (Figure 2A), we found that pirfenidone exposure was strongly correlated with the progression of the disease, and the cut-off value was 104.483 mg h/L; the patients were assigned into two different plasma concentration groups: the low-concentration group (AUC lower than 100 mg h/L) and the high concentration group (AUC ≥100 mg h/L). The distribution of pirfenidone plasma concentrations showed considerable differences between the two groups (Figure 2B).

Overall, the two study groups were similar in terms of demographic and baseline characteristics (Table 1). Most enrolled patients in the low- and high-concentration groups were males (80.4%and 76.7%, respectively), with a median age and smoking history of 64 and 67 years and 66.1 and 58.1%, respectively. Most patients were diagnosed within the preceding 3 years, with 80.4% in the low-concentration group and 79.1% in the high-concentration group. The mean (±SD) baseline FVC of the predicted value was 78.6% ± 16.7% in the low-concentration group and 74.4% ± 18.5% in the high-concentration group. The baseline values of the 6 MWD were 452.5 (388.5–505.0) m in the low-concentration group and 415.0 (385.0–465.0) m in the high-

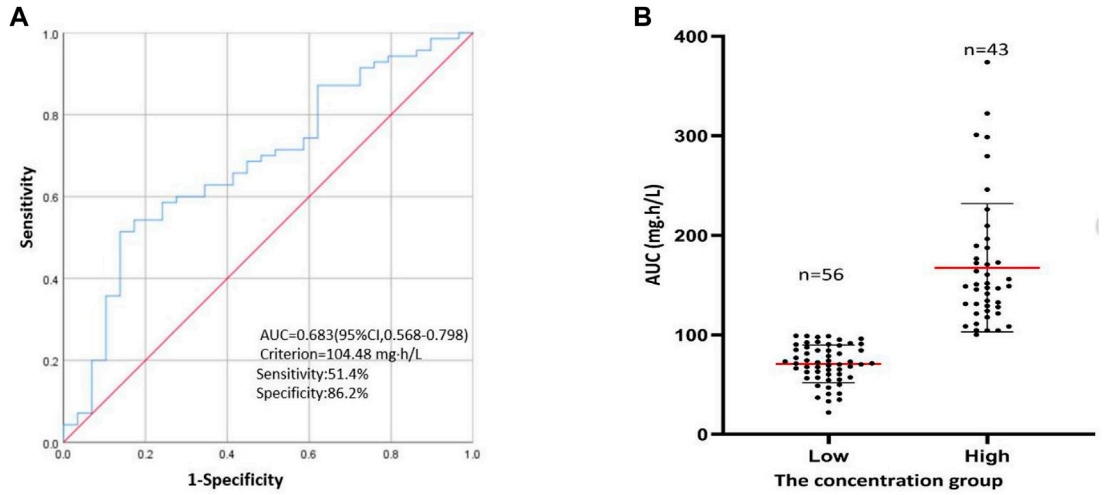

FIGURE 2
The concentration group. **(A)** ROC curve for values of pirfenidone plasma concentration to predict the progression in IPF patients. **(B)** The distribution for the two different concentrations, the horizontal red lines represent the mean value and the lower and upper black lines represent the S = D value, respectively.

concentration group; the percentage of predicted DLco was 53.6% ± 12.2% and 53.7% ± 14.9%, respectively.

Plasma concentration and clinical outcomes of treatment

After treatment with pirfenidone capsules, the adjusted annual rate of decline in the FVC (the primary end point) was −90.0 ml per year in the high-concentration group as compared with −260.0 ml per year in the low concentration group, with a difference of 190.3 ml per year (95% CI, 109.2–280.0; $p < 0.001$) (Table 2; Figure 3B).

The FVC % predicted changed significantly during the 52-week treatment period between the two different plasma concentration groups ($p < 0.001$) (Table 2). The proportion of patients with a decline of ≥10% in the absolute FVC % predicted or who had died at week 52 was less in the high-concentration group than in the low concentration group (9.3% vs. 33.9%, $p = 0.004$) (Figure 3A). The high-concentration group showed a significantly lower decline over the 52-week period in the 6 MWD than the low concentration group (−15.0 m and −40.0 m, respectively, between-group difference, 23 m; 95% CI, 5.0–35.0; $p = 0.006$) (Table 2). At week 52, five patients (11.63%) in the high-concentration group and 21 patients (37.5%) in the low-concentration group had a 6 MWD reduction of more than 50 m or died, for a relative decrease of 28.6% in the high concentration group (Figure 3C).

During the assessment of changes in the percentage of predicted DLco from the baseline to week 52, the high- and low-concentration groups showed a decrease of −5.3 and −7.9% in DLco, respectively (between-group difference, 2.5%; 95% CI, −0.3 to 5.6; $p = 0.078$) (Table 2). At week 52, no significant difference in the average change in the total SGRQ score was observed between the two groups (2.7 and 2.9 in the high- and low-concentration groups, respectively; between-group difference, −0.3; 95% CI, −2.1–1.6; $p = 0.764$) (Table 2).

In the analyses of the time to the first acute exacerbation, a significant increase was observed in the high-concentration group compared with that in the low-concentration group (hazard ratio, 0.30; 95% CI, 0.11–0.82; $p = 0.046$) (Figure 3D); the percentage of patients with an acute exacerbation of IPF was lower in the high-concentration group than in the low-concentration group (7.0% vs. 21.4%) (Table 3). The all-cause mortality analysis showed two deaths (4.7%) over the 52-week period in the high-concentration group and three deaths (5.4%) in the low-concentration group; no significant difference was observed between the two groups (hazard ratio, 0.85; 95% CI, 0.14–5.09; $p = 0.860$) (Table 3). Similarly, the percentage of patients who died from IPF in the high-concentration group was lower than that in the low-concentration group, although the difference was not significant ($p = 0.461$) (Table 3).

Plasma concentration and adverse events

Table 4 summarizes the adverse events associated with oral administration of pirfenidone in patients within the 52 weeks. In the overall population, the most common adverse events

TABLE 1 Characteristics of the patients at baseline.

Characteristic	Low concentration group (n = 56)	High concentration group (n = 43)	*p*-value
Male sex-- no. (%)	45 (80.4)	33 (76.7)	0.663
Age-- years	64.0 (60.8–70.0)	67.0 (64.0–73.0)	0.129
Height (cm)	166.5 ± 6.3	165.1 ± 8.1	0.289
Body weight (kg)	70.8 ± 11	68.7 ± 12.9	0.404
Smoking history-- no. (%)	37 (66.1)	25 (58.1)	0.419
Time since first diagnosis years-- no. (%)	56	43	0.987
<1	17 (30.4)	13 (30.2)	
1–3	28 (50.0)	21 (48.8)	
≥3	11 (19.6)	9 (20.9)	
Diagnostic mode-- no. (%)	56	43	0.469
HRCT	52 (92.9)	37 (86.0)	
transbronchial lung biopsy	2 (3.6)	2 (4.7)	
Surgical lung biopsy	2 (3.6)	4 (9.3)	
Hypertension disease-- no. (%)	16 (28.6)	13 (30.2)	0.857
Diabetes-- no. (%)	8 (14.3)	6 (14.0)	0.962
Coronary artery disease-- no. (%)	8 (14.3)	4 (9.3)	0.451
Chronic gastritis-- no. (%)	1 (1.8)	1 (2.3)	0.850
PPI-- no. (%)	5 (8.9)	6 (14.0)	0.430
Antihypertensive drug-- no. (%)	9 (16.1)	11 (25.6)	0.243
Hypoglycemic-- no. (%)	6 (10.7)	3 (7.0)	0.521
Antiplatelet medicines-- no. (%)	5 (8.9)	3 (7.0)	0.724
Lipid-lowering drugs-- no. (%)	7 (12.5)	3 (7.0)	0.366
Drugs for control hepatitis-- no. (%)	0 (0.0)	1 (2.3)	0.251
Glucocorticoid-- no. (%)	9 (16.1)	2 (4.7)	0.073
Use of supplemental oxygen-- no. (%)	18 (32.1)	13 (30.2)	0.839
Total SGRQ score	34.2 ± 14.0	36.8 ± 11.6	0.326
6 MWD(m)	452.5 (388.5–505.0)	415.0 (385.0–465.0)	0.128
FVC(L)	2.8 (2.0–3.3)	2.4 (1.8–3.2)	0.105
FVC%	78.6 ± 16.7	74.4 ± 18.5	0.229
DLco (mmol/min/kPa)	4.3 ± 1.0	4.1 ± 1.1	0.267
Dlco%	53.6 ± 12.2	53.7 ± 14.9	0.995

HRCT, High-Resolution Computed tomography; PPI, proton pump inhibitors; SGRQ, St George's Respiratory Questionnaire. 6 MWD, 6-min walk distance; FVC, forced vital capacity. FVC %, the percentage of the predicted FVC. DLco, diffusion capacity of the lung for carbon monoxide. Dlco %, the percentage of the predicted DLco.

TABLE 2 Efficacy endpoints.

End point	Low concentration group (n = 56)	High concentration group (n = 43)	Difference, high vs. low (95%CI)	*p*-value
ΔFVC(mL)	−260.0 (−390.0 to−120.0)	−90.0 (−190.0 to 80.0)	190.3 (109.2–280.0)	0.000
ΔFVC %	−7.6 (−11.4 to −3.0)	−2.5 (−5.4 to 3.0)	5.9 (3.2–8.6)	0.000
ΔDlco %	−7.9 (−12.8 to −4.1)	−5.3 (−9.0 to −2.0)	2.5 (−0.3–5.6)	0.078
Δ6MWD(m)	−40.0 (−70.0 to −15.0)	−15.0 (−40.0 to −5.0)	23 (5.0–35.0)	0.006
ΔTotal SGRQ score	2.9 (−1.8–5.6)	2.7 (0.8–4.4)	−0.3 (−2.1 to 1.6)	0.764

ΔFVC, the annual rate of decline in the FVC, from baseline to week 52. ΔFVC %, the absolute change in the percentage of the predicted FVC, from baseline to week 52. ΔDlco %, the absolute change in the percentage of the predicted Dlco from baseline to week 52. Δ6MWD, the absolute change in 6-min walk distance from baseline to week 52. ΔTotal SGRQ, score, the change from baseline to week 52 in the total score on the St. George's Respiratory Questionnaire.

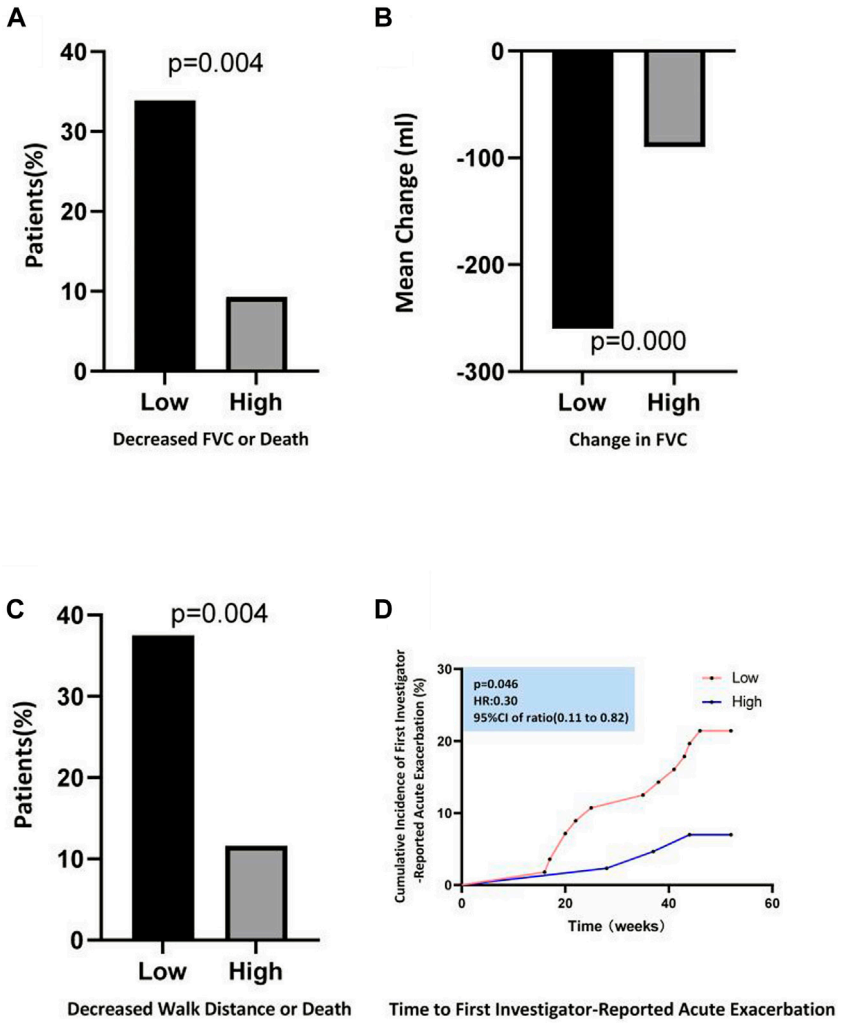

FIGURE 3
Efficacy Outcomes during the 52-Week Study Period. **(A)** Shows the proportion of patients who had a decreased percentage of the predicted FVC≥ 10% or who died. **(B)** Shows the mean change from baseline in FVC. **(C)** Shows the proportion of patients who had a decline of 6-min walk distance≥ 50 m or who died. **(D)** Shows the Kaplan–Meier distribution for the probability of time to first investigator-reported Acute Exacerbation.

TABLE 3 Outcomes of the trial.

Outcomes	Low concentration group (n = 56)	High concentration group (n = 43)	Hazard ratio (95% CI)	p-value
Acute exacerbation of IPF at Week 52-- no. (%)	12 (21.4)	3 (7.0)	0.30 (0.11–0.82)	0.046
Death from any cause-- no. (%)	3 (5.4)	2 (4.7)	0.85 (0.14–5.09)	0.860
Death related to IPF-- no. (%)	3 (5.4)	1 (2.3)	0.43 (0.04–4.10)	0.461

IPF, idiopathic pulmonary fibrosis.

associated with oral pirfenidone were digestive tract-related adverse reactions such as nausea, vomiting, abdominal pain, diarrhea, dyspepsia, gastroesophageal reflux, weight loss, and rash. The total number of adverse events was 37 (86.0%) in the high-concentration group and 35 (62.5%) in the low-concentration group. There was a significant difference in the total incidence of adverse effects between the different concentration groups (p = 0.009).

TABLE 4 Adverse events in the overall population.

Event	Low concentration group (n = 56)	High concentration group (n = 43)	p-value
	no. of patients (%)		
Any	35 (62.5)	37 (86.0)	0.009
Nausea	20 (35.7)	27 (62.8)	0.007
Vomiting	5 (8.9)	9 (20.9)	0.089
Diarrhea, abdominal pain	2 (3.6)	6 (14.0)	0.060
Dyspepsia	19 (33.9)	24 (55.8)	0.029
Gastroesophageal reflux	23 (41.1)	20 (46.5)	0.588
Headache	4 (7.1)	7 (16.3)	0.152
Dizziness	2 (3.6)	3 (7.0)	0.443
Nasopharyngitis	0 (0.0)	2 (4.7)	0.103
Insomnia	5 (8.9)	8 (18.6)	0.158
Decrease in weight	14 (25.0)	19 (44.2)	0.045
arthritis	0 (0.0)	4 (9.3)	0.020
Rash	14 (25.0)	21 (48.8)	0.014
Allergy	5 (8.9)	7 (16.3)	0.267
Elevated bilirubin	1 (1.8)	0 (0.0)	0.378
Elevated transaminase	1 (1.8)	0 (0.0)	0.378
Elevated creatinine	1 (1.8)	0 (0.0)	0.378

In the high-concentration group, adverse events related to nausea, dyspepsia, weight loss, arthritis, and rash were more common compared with those in the low-concentration group. In the low-concentration group, one patient (1.8%) had grade 3 gastrointestinal adverse events, and two patients (3.6%) had grade 3 weight loss adverse events. One patient (2.3%) in the high-concentration group showed grade 4 skin-related adverse effects, while another (1.8%) in the low-concentration group showed grade 3 skin-related adverse effects. The adverse events were mostly mildly to moderately severe, easy to occur in the early stage of oral drug increment, and could be gradually tolerated or significantly relieved by drug treatment (such as proton pump inhibitors) or adjustment of living habits. In this study, liver-related adverse reactions were very rare. Only one patient (1.0%) had alanine or aspartate aminotransferase levels at least three times higher than the upper normal limit in the total population; the total bilirubin level of this patient increased to more than double the upper normal limit. However, the liver injury was reversible, and liver functions were restored after treatment with hepatoprotective drugs.

Discussion

The recommended initial dosage for oral administration of pirfenidone capsules for patients with IPF is 200 mg thrice daily, and has been incrementally increased. The dosage of pirfenidone capsules is maintained at 600 mg per dose (1,800 mg daily). However, in clinical setting, patients with IPF are more susceptible to adverse events such as gastrointestinal reactions and skin rashes upon oral administration of 1,200 mg/day and these adverse reactions worsen as the dosage increase, and so does the cost of treatment, thereby causing financial burden on patients and affecting the incremental use of drug. Thus, it is pertinent to find an effective and safe blood concentration range of pirfenidone in patients with IPF. When we collated the data in the early stages, we found that ingesting higher doses of pirfenidone would increase the blood drug concentration in the same patient. However, no apparent correlation was observed between the dose and blood drug concentration in the overall population. Accordingly, it can be inferred that increasing the oral pirfenidone dose may increase the blood concentration of pirfenidone, resulting in a better therapeutic outcome.

In a multicenter clinical trial in Japan (Taniguchi et al., 2010), significant differences were observed in the vital capacity decline and progression-free survival (PFS) between the high-dose and placebo groups, but not between the high-dose (1,800 mg/d) and low-dose (1,200 mg/d) groups. The Ascend study (Richeldi et al., 2014) found that the annual FVC decline was 428 ml in the placebo group versus 235 ml in the pirfenidone group. At week 52, treatment with pirfenidone led to a markedly lower reduction in the 6 MWD and an improvement in the PFS. In this study, we found that the annual FVC decline (the main endpoint)

was −90 ml in the high-concentration group and −260 ml in the low-concentration group. Additionally, the number of patients who showed a reduction of more than 10% in the absolute FVC % predicted, had a 6 MWD decrease of more than 50 m, or died at week 52 was considerably lower in the high-concentration group than in the low-concentration group. We found that the high plasma concentration of pirfenidone was beneficial in hindering the annual FVC decline and reducing the progression of the disease.

In previous clinical studies, it had been proved that pirfenidone had a positive effect on the decline of pulmonary function in the treatment of IPF, which not only reduced the annual decline rate of FVC but also slowed down the decline of DLCO (Feng et al., 2020; Krauss et al., 2020). In addition, DLCO decline of ≥10% shows potential as a mortality predictor in IPF patients on pirfenidone during follow-up examinations (Zurkova et al., 2019). Health-related quality of life (HRQL), often measured using the SGRQ is impaired in patients with IPF. This study showed no significant differences between the two different concentration groups regarding the changes in the percentage of predicted DLco (p = 0.078) or the total SGRQ score (p = 0.764) from the baseline to week 52. This may be because high-and low-concentration groups do not meet the differences in these indicators, and we need to enroll more patients to confirm these results.

Previous studies (Taniguchi et al., 2010; Noble et al., 2011; Richeldi et al., 2014) reported limited effects of pirfenidone on reducing the risk of acute exacerbation of IPF compared with that in the placebo group. However, the high plasma concentration of pirfenidone was beneficial in prolonging the time to the first acute exacerbation and reducing the risk of acute exacerbations, thus providing more evidence emphasizing the importance of monitoring the blood levels of pirfenidone.

A comprehensive analysis of data from three phase III clinical trials (Nathan et al., 2019) showed a significant reduction in the overall number of deaths (p = 0.01) and IPF-related deaths (p = 0.006) in the pirfenidone group compared with the placebo group. However, this study showed no significant differences between the two different concentration groups regarding the change in the overall deaths (p = 0.860), or deaths related to IPF (p = 0.461). This may be due to the low mortality rate in patients participating in IPF clinical trials, resulting in a small sample size not sufficient to acquire an accurate estimate of the therapeutic effect. Generally, pirfenidone capsule intake was safe. However, it was associated with some adverse events, the most common being digestive tract-related adverse events, weight loss, and rashes, which is consistent with the previous research findings (Wilson and Wynn, 2009; Raghu et al., 2011; Kolb et al., 2017; Martinez et al., 2017). The total incidence of adverse events in the high-concentration group (86.0%) was higher than that in the low-concentration group (62.5%). Adverse events (mostly mild to moderate) related to nausea, indigestion, weight loss, arthritis, and rash were more common in the high-concentration group than in the low-concentration group, but did not result in discontinuation of the drug.

This study has some limitations. 1) Its realistic design that did not alter the clinical treatment decisions of patients and the lack of a blank control group for comparison. 2) Relatively small sample size. 3) Patients with mild to moderate physical injuries were included. 4) The study groups were not divided by sex. IPF is a sex-dependent disease, and men and women could react to the treatment differently. 5) Some patients were on a long-term treatment of chronic diseases and had different lifestyles, which made it a tedious process to accurately evaluate the adverse reactions attributed to pirfenidone.

Despite these limitations, our multicenter study confirmed the advantages of the high plasma concentration of pirfenidone in the treatment of patients with IPF, such as delaying the annual decline rate of FVC, reducing the decline of 6 MWD, attenuating disease progression and the risk of acute exacerbation. Moreover, Treatment with pirfenidone capsules containing high plasma concentrations was generally safe, with tolerable side effects.

It is expected to carry out prospective researches and find a therapeutic window of the pirfenidone to monitor adverse reactions and clinical efficacy. It may achieve personalized medication of pirfenidone in the treatment of patients with IPF in the future.

Data availability statement

The raw data supporting the conclusion of this article will be made available by the authors, without undue reservation.

Ethics statement

The studies involving human participants were reviewed and approved by the Human Research Ethics Committee of The First Affiliated Hospital of Zhengzhou University. The patients/participants provided their written informed consent to participate in this study. Written informed consent was obtained from the individual(s) for the publication of any potentially identifiable images or data included in this article.

Author contributions

GZ and XZ conceived and designed the study, critically revised the manuscript, and were responsible for the funding. HL, JY, SC, PW, XY, and QZ acquired and interpreted the data, and drafted and critically revised the manuscript. All authors have read and approved the final manuscript.

Funding

Supported by the China National Natural Science Foundation Project (grant number 81874042) and the China National Key Research and Development Program (grant number 2020YFC2008304).

Acknowledgments

The authors are grateful to Huaqi Wang (First Affiliated Hospital of Zhengzhou University), Zheng Wang (Henan Provincial People's Hospital), Qiang Dang (Nanyang Central Hospital), Xin Liu (Xuchang Central Hospital), Haitao Hu (Xinyang Central Hospital), Zhuyun Duan (Sanmenxia Central Hospital), Feng Wang (The first People's Hospital of Shangqiu), Qingwei Li (Central Hospital of Jiaozuo Coal Industry Group), Qiang Peng (Henan Provincial Chest hospital), Fangfang Zhang (The People's Hospital of Anyang city), Beibei Kang (Zhoukou Central Hospital), Zhanyi Zhai (Zhumadian Central Hospital), Yudong Xie (Zhoukou Central Hospital), Gongxing Li (The fourth People's Hospital of Shangqiu), Junhong Ding (The first People's Hospital of Pingdingshan) for their support with data collection.

Conflict of interest

The authors declare that the research was conducted in the absence of any commercial or financial relationships that could be construed as a potential conflict of interest.

Publisher's note

All claims expressed in this article are solely those of the authors and do not necessarily represent those of their affiliated organizations, or those of the publisher, the editors and the reviewers. Any product that may be evaluated in this article, or claim that may be made by its manufacturer, is not guaranteed or endorsed by the publisher.

References

Azuma, A., Nukiwa, T., Tsuboi, E., Suga, M., Abe, S., Nakata, K., et al. (2005). Double-blind, placebo-controlled trial of pirfenidone in patients with idiopathic pulmonary fibrosis. *Am. J. Respir. Crit. Care Med.* 171(9), 1040–1047. doi:10.1164/rccm.200404-571OC

Bois, R. M., Weycker, D., Albera, C., Bradford, W. Z., Costabel, U., Kartashov, A., et al. (2011). Six-minute-walk test in idiopathic pulmonary fibrosis: Test validation and minimal clinically important difference. *Am. J. Respir. Crit. Care Med.* 183(9), 1231–1237. doi:10.1164/rccm.201007-1179OC

Bonella, F., Stowasser, S., and Wollin, L. (2015). Idiopathic pulmonary fibrosis: Current treatment options and critical appraisal of nintedanib. *Drug Des. devel. Ther.* 9, 6407–6419. doi:10.2147/DDDT.S76648

Collard, H. R., Ryerson, C. J., Corte, T. J., Jenkins, G., Kondoh, Y., Lederer, D. J., et al. (2016). Acute exacerbation of idiopathic pulmonary fibrosis. An international working group report. *Am. J. Respir. Crit. Care Med.* 194(3), 265–275. doi:10.1164/rccm.201604-0801CI

Culver, B. H., Graham, B. L., Coates, A. L., Wanger, J., Berry, C. E., Clarke, P. K., et al. (2017). Recommendations for a standardized pulmonary function report. An official American thoracic society technical statement. *Am. J. Respir. Crit. Care Med.* 196(11), 1463–1472. doi:10.1164/rccm.201710-1981ST

Feng, H., Zhao, Y., Li, Z., and Kang, J. (2020). Real-life experiences in a single center: Efficacy of pirfenidone in idiopathic pulmonary fibrosis and fibrotic idiopathic non-specific interstitial pneumonia patients. *Ther. Adv. Respir. Dis.* 14, 1753466620963015. doi:10.1177/1753466620963015

Flaherty, K. R., Wells, A. U., Cottin, V., Devaraj, A., Walsh, S., Inoue, Y., et al. (2019). Nintedanib in progressive fibrosing interstitial lung diseases. *N. Engl. J. Med.* 381(18), 1718–1727. doi:10.1056/NEJMoa1908681

Furukawa, T., Taniguchi, H., Ando, M., Kondoh, Y., Kataoka, K., Nishiyama, O., et al. (2017). The St. George's Respiratory Questionnaire as a prognostic factor in IPF. *Respir. Res.* 18(1), 18. doi:10.1186/s12931-017-0503-3

Glassberg, M. K., Wijsenbeek, M. S., Gilberg, F., Petzinger, U., Kirchgaessler, K. U., and Albera, C. (2019). Effect of pirfenidone on breathlessness in patients with idiopathic pulmonary fibrosis. *Eur. Respir. J.* 54, 1900399(3). doi:10.1183/13993003.00399-2019

Holland, A. E., Spruit, M. A., Troosters, T., Puhan, M. A., Pepin, V., Saey, D., et al. (2014). An official European respiratory society/American thoracic society technical standard: Field walking tests in chronic respiratory disease. *Eur. Respir. J.* 44(6), 1428–1446. doi:10.1183/09031936.00150314

Jayachandran, A., Konigshoff, M., Yu, H., Rupniewska, E., Hecker, M., Klepetko, W., et al. (2009). SNAI transcription factors mediate epithelial-mesenchymal transition in lung fibrosis. *Thorax.* 64(12), 1053–1061. doi:10.1136/thx.2009.121798

Jones, P. W., Quirk, F. H., and Baveystock, C. M. (1991). The St george's respiratory questionnaire. *Respir. Med.* 85 25. doi:10.1016/s0954-6111(06)80166-6

King, T. J., Bradford, W. Z., Castro-Bernardini, S., Fagan, E. A., Glaspole, I., Glassberg, M. K., et al. (2014). A phase 3 trial of pirfenidone in patients with idiopathic pulmonary fibrosis. *N. Engl. J. Med.* 370(22), 2083–2092. doi:10.1056/NEJMoa1402582

Kirby, T. (2021). Living with idiopathic pulmonary fibrosis. *Lancet. Respir. Med.* 9(2), 136–138. doi:10.1016/S2213-2600(20)30562-2

Kolb, M., Bonella, F., and Wollin, L. (2017). Therapeutic targets in idiopathic pulmonary fibrosis. *Respir. Med.* 131, 49–57. doi:10.1016/j.rmed.2017.07.062

Kondoh, Y. (2019). Diagnostic difficulty in idiopathic pulmonary fibrosis. *Respir. Investig.* 57(4), 298–299. doi:10.1016/j.resinv.2019.03.012

Krauss, E., Tello, S., Wilhelm, J., Schmidt, J., Stoehr, M., Seeger, W., et al. (2020). Assessing the effectiveness of pirfenidone in idiopathic pulmonary fibrosis: Long-term, real-world data from European IPF registry (eurIPFreg). *J. Clin. Med.* 9, E3763(11). doi:10.3390/jcm9113763

Lederer, D. J., and Martinez, F. J. (2018). Idiopathic pulmonary fibrosis. *N. Engl. J. Med.* 378(19), 1811–1823. doi:10.1056/NEJMra1705751

Lee, B. S., Margolin, S. B., and Nowak, R. A. (1998). Pirfenidone: A novel pharmacological agent that inhibits leiomyoma cell proliferation and collagen production. *J. Clin. Endocrinol. Metab.* 83(1), 219–223. doi:10.1210/jcem.83.1.4503

Martinez, F. J., Collard, H. R., Pardo, A., Raghu, G., Richeldi, L., Selman, M., et al. (2017). Idiopathic pulmonary fibrosis. *Nat. Rev. Dis. Prim.* 3, 17074. doi:10.1038/nrdp.2017.74

Mora, A. L., Rojas, M., Pardo, A., and Selman, M. (2017). Emerging therapies for idiopathic pulmonary fibrosis, a progressive age-related disease. *Nat. Rev. Drug Discov.* 16(11), 755–772. doi:10.1038/nrd.2017.170

Nathan, S. D., Costabel, U., Glaspole, I., Glassberg, M. K., Lancaster, L. H., Lederer, D. J., et al. (2019). Efficacy of pirfenidone in the context of multiple disease progression events in patients with idiopathic pulmonary fibrosis. *Chest.* 155(4), 712–719. doi:10.1016/j.chest.2018.11.008

Noble, P. W., Albera, C., Bradford, W. Z., Costabel, U., Glassberg, M. K., Kardatzke, D., et al. (2011). Pirfenidone in patients with idiopathic pulmonary fibrosis (CAPACITY): Two randomised trials. *Lancet.* 377(9779), 1760–1769. doi:10.1016/S0140-6736(11)60405-4

Noth, I., Anstrom, K. J., Calvert, S. B., de Andrade, J., Flaherty, K. R., Glazer, C., et al. (2012). A placebo-controlled randomized trial of warfarin in idiopathic pulmonary fibrosis. *Am. J. Respir. Crit. Care Med.* 186(1), 88–95. doi:10.1164/rccm.201202-0314OC

Prior, T. S., Hoyer, N., Shaker, S. B., Davidsen, J. R., Yorke, J., Hilberg, O., et al. (2019). Validation of the IPF-specific version of St. George's respiratory questionnaire. *Respir. Res.* 20(1), 199. doi:10.1186/s12931-019-1169-9

Raghu, G., Collard, H. R., Egan, J. J., Martinez, F. J., Behr, J., Brown, K. K., et al. (2011). An official ATS/ERS/JRS/ALAT statement: Idiopathic pulmonary fibrosis: Evidence-based guidelines for diagnosis and management. *Am. J. Respir. Crit. Care Med.* 183(6), 788–824. doi:10.1164/rccm.2009-040GL

Raghu, G., Ley, B., Brown, K. K., Cottin, V., Gibson, K. F., Kaner, R. J., et al. (2020). Risk factors for disease progression in idiopathic pulmonary fibrosis. *Thorax*. 75(1), 78–80. doi:10.1136/thoraxjnl-2019-213620

Raghu, G., Remy-Jardin, M., Myers, J. L., Richeldi, L., Ryerson, C. J., Lederer, D. J., et al. (2018). Diagnosis of idiopathic pulmonary fibrosis. An official ATS/ERS/JRS/ALAT clinical practice guideline. *Am. J. Respir. Crit. Care Med.* 198(5), e44-e68. doi:10.1164/rccm.201807-1255ST

Richeldi, L., Collard, H. R., and Jones, M. G. (2017). Idiopathic pulmonary fibrosis. *Lancet*. 389(10082), 1941–1952. doi:10.1016/S0140-6736(17)30866-8

Richeldi, L., du Bois, R. M., Raghu, G., Azuma, A., Brown, K. K., Costabel, U., et al. (2014). Efficacy and safety of nintedanib in idiopathic pulmonary fibrosis. *N. Engl. J. Med.* 370(22), 2071–2082. doi:10.1056/NEJMoa1402584

Schaefer, C. J., Ruhrmund, D. W., Pan, L., Seiwert, S. D., and Kossen, K. (2011). Antifibrotic activities of pirfenidone in animal models. *Eur. Respir. Rev.* 20(120), 85–97. doi:10.1183/09059180.00001111

Taniguchi, H., Ebina, M., Kondoh, Y., Ogura, T., Azuma, A., Suga, M., et al. (2010). Pirfenidone in idiopathic pulmonary fibrosis. *Eur. Respir. J.* 35(4), 821–829. doi:10.1183/09031936.00005209

van Manen, M., Birring, S. S., Vancheri, C., Vindigni, V., Renzoni, E., Russell, A. M., et al. (2017). Effect of pirfenidone on cough in patients with idiopathic pulmonary fibrosis. *Eur. Respir. J.* 50, 1701157(4). doi:10.1183/13993003.01157-2017

Wang, P., Sun, T., Gao, M., Zhang, G., Zhang, X., and Yang, J. (2021). UPLC-MS/MS method for determination of pirfenidone and its metabolite in plasma and its application for pharmacokinetics research in patients with idiopathic pulmonary fiber. *Chin. Pharm. J.* 56(8), 675–681. doi:10.11669/cpj.2021.08.012

Wilson, M. S., and Wynn, T. A. (2009). Pulmonary fibrosis: Pathogenesis, etiology and regulation. *Mucosal Immunol.* 2(2), 103–121. doi:10.1038/mi.2008.85

Zhao, H., Bian, H., Bu, X., Zhang, S., Zhang, P., Yu, J., et al. (2016). Targeting of discoidin domain receptor 2 (DDR2) prevents myofibroblast activation and neovessel formation during pulmonary fibrosis. *Mol. Ther.* 24(10), 1734–1744. doi:10.1038/mt.2016.109

Zurkova, M., Kriegova, E., Kolek, V., Lostakova, V., Sterclova, M., Bartos, V., et al. (2019). Effect of pirfenidone on lung function decline and survival: 5-yr experience from a real-life IPF cohort from the Czech EMPIRE registry. *Respir. Res.* 20(1), 16. doi:10.1186/s12931-019-0977-2

frontiers | Frontiers in Pharmacology

TYPE Original Research
PUBLISHED 06 January 2023
DOI 10.3389/fphar.2022.1070736

OPEN ACCESS

EDITED BY
Changjun Lv,
Binzhou Medical University Hospital, China

REVIEWED BY
Pavel Solopov,
Old Dominion University, United States
Ying Meng,
Southern Medical University, China

*CORRESPONDENCE
Ming Liu,
mingliu128@hotmail.com
Shiyue Li,
lishiyue@188.com

†These authors have contributed equally to this work and share first authorship

SPECIALTY SECTION
This article was submitted to Respiratory Pharmacology, a section of the journal Frontiers in Pharmacology

RECEIVED 15 October 2022
ACCEPTED 29 November 2022
PUBLISHED 06 January 2023

CITATION
Chen H, Luo Y, Zhu Y, Ye Y, Chen D, Song X, Xiao Z, Liu M and Li S (2023), Enhanced secretion of hepatocyte growth factor in human umbilical cord mesenchymal stem cells ameliorates pulmonary fibrosis induced by bleomycin in rats.
Front. Pharmacol. 13:1070736.
doi: 10.3389/fphar.2022.1070736

Enhanced secretion of hepatocyte growth factor in human umbilical cord mesenchymal stem cells ameliorates pulmonary fibrosis induced by bleomycin in rats

Huanjie Chen[1†], Yulong Luo[2†], Yiping Zhu[1†], Yongshun Ye[3], Difei Chen[1], Xinyu Song[1], Zhulin Xiao[1], Ming Liu[1*] and Shiyue Li[1*]

[1]State Key Laboratory of Respiratory Disease, National Clinical Research Center for Respiratory Disease, Guangzhou Institute of Respiratory Health, The First Affiliated Hospital of Guangzhou Medical University, Guangzhou, Guangdong, China, [2]Innovation Centre for Advanced Interdisciplinary Medicine, Key Laboratory of Biological Targeting Diagnosis, Therapy and Rehabilitation of Guangdong Higher Education Institutes, The Fifth Affiliated Hospital of Guangzhou Medical University, Guangzhou, Guangdong, China, [3]Huizhou Municipal Central Hospital, Guangzhou, Guangdong, China

Umbilical cord mesenchymal stem cells (UCMSCs) are a reportedly promising choice in the treatment of irreversible pulmonary fibrosis and lethal interstitial lung disease with limited drug treatment options. In this study, we investigated the therapeutic efficacy of UCMSCs overexpressing hepatocyte growth factor (HGF), which is considered one of the main anti-fibrotic factors secreted by MSCs. Adenovirus vector carrying the HGF gene was transfected into UCMSCs to produce HGF-modified UCMSCs (HGF-UCMSCs). Transfection promoted the proliferation of UCMSCs and did not change the morphology, and differentiation ability, or biomarkers. Rats were injected with HGF-UCMSCs on days 7 and 11 after intratracheal administration of bleomycin (10 mg/kg). We performed an analysis of histopathology and lung function to evaluate the anti-fibrotic effect. The results showed that HGF-UCMSCs decreased the Ashcroft scores in hematoxylin and eosin-stained sections, the percentage positive area in Masson trichrome-stained sections, and the hydroxyproline level in lungs. Forced expiratory volume in the first 300 m/forced vital capacity was also improved by HGF-UCMSCs. To explore the possible therapeutic mechanism of HGF-UCMSCs, we detected inflammatory factors in the lungs and performed mRNA sequencing in UCMSCs and HGF-UCMSCs. The data indicated that inhibition of interleukin-17 in the lung may be related to the anti-fibrosis of HGF-UCMSCs, and overexpressed HGF probably played a primary role in the treatment. Collectively, our study findings suggested that the overexpression of HGF may improve the anti-fibrotic effect of UCMSCs through directly or indirectly interacting with interleukin-17-producing cells in fibrotic lungs.

KEYWORDS

umbilical cord, mesenchymal stem cells, pulmonary fibrosis, hepatocyte growth factor, interleukin-17

Introduction

Idiopathic pulmonary fibrosis (IPF) is one of the forms of chronic progressive fibrotic interstitial lung disease (Lederer and Martinez, 2018). Patients with IPF eventually develop and ultimately die of irreversible respiratory failure (Richeldi et al., 2017). The death rate among patients with IPF has gradually increased, with an annually increasing trend (Hutchinson et al., 2014; Raghu et al., 2014; Hutchinson et al., 2015; Dove et al., 2019; Navaratnam and Hubbard, 2019; Tran et al., 2020). At present, the most effective treatment is lung transplantation, but transplant rejection and a lack of donor's lungs make it impossible for more patients to benefit from transplantation (Raghu et al., 2015; George et al., 2019). Although pirfenidone and nintedanib can improve lung function and exercise tolerance to some extent, it is still difficult to prevent IPF from progressing (King Jr et al., 2014; Richeldi et al., 2014). Thus, new curative methods for patients with IPF are urgently needed.

Mesenchymal stem cells (MSCs) have been widely proven to effectively treat pulmonary fibrosis in animals through secreting anti-fibrotic factors (Huang et al., 2015; Kotani et al., 2017; Chen et al., 2018). Given that MSCs were likely an effective way to cure patients with IPF, clinical studies were subsequently conducted. The results showed that MSC administration was safe and could delay the deterioration of pulmonary function over time (Tzouvelekis et al., 2013; Chambers et al., 2014; Glassberg et al., 2017). Nevertheless, the progression of pulmonary fibrosis still cannot be stopped. Therefore, researchers must find ways of enhancing the anti-fibrotic efficacy of MSCs.

Gene modification of anti-fibrotic factors is a valid means to achieve the abovementioned goal (Madrigal et al., 2014; Ocansey et al., 2020). The hepatocyte growth factor (HGF) is a crucial factor in anti-fibrosis (Dong et al., 2015; Cahill et al., 2016). It has been shown that HGF can repair damaged alveolar epithelium and inhibit the profibrotic ability of fibroblasts and myofibroblasts in the lungs (Mizuno et al., 2005; Lee et al., 2008; Shukla et al., 2009). Umbilical cord MSCs (UCMSCs) are most likely the appropriate choice for modification due to their naturally high secretion of HGF, abundant supply, and no invasive extraction or donor site morbidity (Prasanna et al., 2010; Balasubramanian et al., 2012; Han et al., 2013; El Omar et al., 2014; Marmotti et al., 2017; Kim et al., 2018; Al Naem et al., 2020). HGF-modified UCMSCs (HGF-UCMSCs) have been used in the treatment of bronchiolitis obliterans, wound healing, acute kidney injury, and liver fibrosis, among others (Chen et al., 2011; Li et al., 2015; Cao et al., 2016; Yin et al., 2020). However, the application of HGF-UCMSCs in the treatment of bleomycin-induced pulmonary fibrosis has rarely been reported. A comparison of the therapeutic effects between HGF-UCMSCs and identified anti-fibrotic drugs is also needful.

In the present study, we evaluated the therapeutic outcome of HGF-UCMSCs in rats with pulmonary fibrosis induced by bleomycin. The therapeutic mechanism of HGF-UCMSCs was also explored using lung cytokines detection together with mRNA sequencing.

Materials and methods

Isolation and culture of human UCMSCs

Clinical-grade UCMSCs were obtained from Beijing SH Biotechnology (http://www.bjshbio.com/). The isolation and culture of UCMSCs were based on previously described methods (Chu et al., 2019), as follows. The umbilical cord was minced into small pieces then washed thoroughly with phosphate buffer saline (PBS) (Gibco, United States) and digested using collagenase (Gibco, United States) at 37°C for 60 min. The digestion was stopped using an MSCs growth medium (Beijing SH Technology, China), and the digested mixture was passed through a 70-μm cell strainer (BD, United States) to obtain a single-cell suspension. All primary UCMSCs were seeded in flasks at a density of 8,000/cm^2 and cultured at 37°C in a humidified atmosphere containing 5% CO2.

Production of HGF-UCMSCs

The protocol for producing HGF-UCMSCs was referred to in the previous paper (Wang et al., 2013). A replication-defective adenovirus expressing human HGF (Ad-HGF) and a replication-defective adenovirus not carrying exogenous genes (Ad-Null) were constructed with the AdEasy system (Stratagene, United States) and were purified by double cesium chloride density gradient ultracentrifugation. Ad-HGF and Ad-Null dissolved in storage buffer (Hanks' buffer, 10% glycerol) were stored at −80°C. According to the previous protocol, UCMSCs were infected with 150 multiplicities of infection of Ad-Null or Ad-HGF. The cells were collected 48 h post-infection for further usage in vitro and *in vivo* experiments. Before treatment, the conditioned medium of MSCs infected with Ad-Null and Ad-HGF was collected for HGF testing according to the instructions in an HGF ELISA kit (ExCell, China). Medium not used for cell culture was utilized as a negative control in the ELISA reaction.

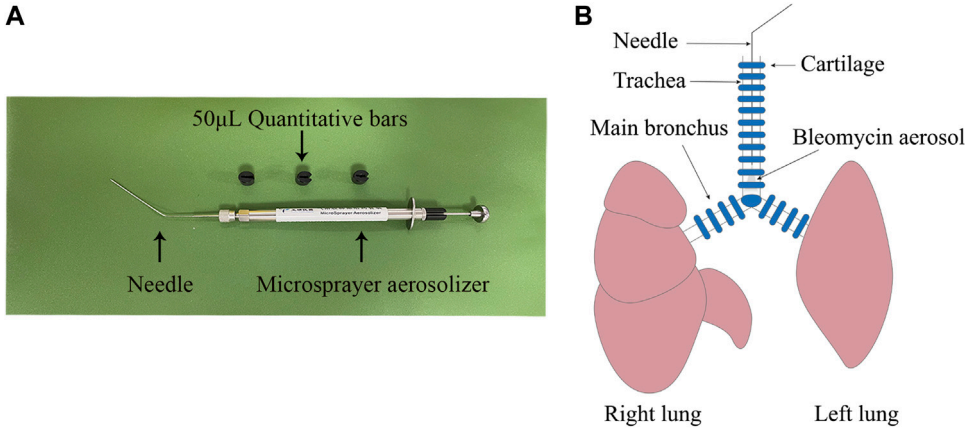

FIGURE 1
Establishment of pulmonary fibrosis model. **(A)** A microsprayer aerosolizer was used to deliver aerosols of PBS or bleomycin into the lungs of rats **(B)** The aerosols were presented in the lower tracheas.

Identification of MSCs

Cultured MSCs were identified for cell morphology and adherence, immune surface markers, and differentiation potential (Nadri et al., 2002; Soleimani and Nadri, 2009). MSCs were photographed for observation using a fluorescence digital microscope BZ-X800 (Keyence, Japan). Immune surface markers (i.e., CD105, CD73, CD90, CD34, CD11b, CD19, CD45, and HLA-DR) were analyzed by flow cytometry using a Human MSC Analysis Kit (BD, United States). For osteogenesis or adipogenesis, MSCs were respectively incubated in an osteogenic or adipogenic medium (Cyagen, China) for 3 weeks, and were then fixed with methanol. A Leica DMI 3000B fluorescence microscope (Leica, Germany) was used for photographs of osteoblasts or adipoblasts stained with alizarin red or Oil Red O, respectively.

Animals and experimental design

Sprague-Dawley rats (6 weeks, 200–220 g) were purchased from Guangdong Medical Laboratory Animal Center (China) and were housed in a specific pathogen-free animal facility. All studies were approved by the Animal Ethics Committee of Guangdong Medical Laboratory Animal Center.

Rats were divided into five groups (six rats per group): a CTRL group, BLM group, UCMSC group, HGF-UCMSC group, and PFD group. A microsprayer aerosolizer (Yuyan Instruments Co., Ltd. China) (Figure 1) was used to deliver sterile PBS or bleomycin into the lungs. On day 0, rats in the CTRL group were instilled intratracheally with sterile PBS; the remaining rats were instilled with 10 mg/kg body weight bleomycin (Hanhui co. LTD., China). From day 7–20, rats in the PFD group were infused orally with 100 mg/kg body weight pirfenidone once a day. The remaining rats were injected with sterile PBS, UCMSCs, or HGF-UCMSCs *via* tail vein on both days 7 and 11, as follows. 1) CTRL group and BLM group: sterile PBS, 400 μL/day per rat; 2) UCMSC group: UCMSCs, 2 * 10^6/400 μL/day per rat; 3) HGF-UCMSC group: HGF-UCMSCs, 2 * 10^6/400 μL/day per rat.

For the collected lungs on day 21, left lungs were inflated and immersed with 4% paraformaldehyde (Biosharp, China), and right lungs were frozen at −80°C in a refrigerator as quickly as possible.

Lung function test

Rats were anesthetized with pentobarbital sodium and endotracheal intubation was performed. The intubated catheter was connected to a Buxco pulmonary function testing system (DSI Buxco, United States) to measure lung function as follows: forced expiratory volume in the first 300 m/forced vital capacity (FEV300/FVC), peak expiratory flow (PEF), chord compliance (Cchord), and total lung capacity.

Hydroxyproline evaluation

The right lung lobes of each rat were ground into a powder in liquid nitrogen and used for hydroxyproline (HYP) detection. To assess the total collagen content of lung tissue, we used an HYP assay kit (Nanjing Jiancheng Bioengineering Institute, China). The experiment was performed according to the manufacturer's instructions.

Cytokine detection

Some lung tissue powder was prepared for cytokine detection, referring to the protocol of the Rat Cytokine/

Chemokine Magnetic Bead Panel (Millipore, United States). Interleukin-17 (IL-17), IL-10, vascular endothelial growth factor (VEGF), and granulocyte-macrophage colony-stimulating factor (GM-CSF) were detected in 96-well plates using MILLIPLEX® MAGPIX with MILLIPLEX Analyst. V5.1 software. Median fluorescence intensity data were analyzed using a five-parameter logistic method for calculating analyte concentrations in samples.

Histopathological analysis

Left lungs were processed by Bios Biological Co. Ltd. (China). For paraffin sections, lungs were dehydrated using gradient ethanol and then embedded in paraffin blocks. The blocks were cut into sections of 3–5 μm thickness; sections were placed on polylysine-coated glass slides and stored at room temperature for further use. Hematoxylin and eosin (H&E) and Masson trichrome staining were performed following the standard protocol. The stained sections were captured, and the pictures were sent to two pathologists for evaluation. The severity of the injury was quantified using the Ashcroft scoring system in H&E-stained lung sections (Ashcroft et al., 1988). The percentage of blue-stained area in Masson trichrome-stained lung sections was quantified using ImageJ (National Institutes of Health, United States).

mRNA sequencing

UCMSCs ($N = 3$) and HGF-UCMSCs ($N = 3$) were lysed and total RNA was extracted using a Trizol reagent kit (Invitrogen, United States), following the manufacturer's protocol. For mRNA sequencing, samples were submitted to Gene Denovo Biotechnology Co. (Guangzhou, China), where RNA quality evaluation, mRNA enrichment, and cDNA library preparation were performed. The cDNA libraries were sequenced on the Illumina sequencing platform Novaseq6000 by Gene Denovo Biotechnology Co., Ltd. (Guangzhou, China). RNA differential expression was analyzed using DESeq2 [7] software. Transcripts with a false discovery rate (FDR) < 0.05 and absolute fold change (FC) ≥ 2 were considered s differentially expressed genes/transcripts. The upregulation or downregulation of genes depended on the change in mean value of Fragments Per Kilobase of transcript per Million mapped reads (FPKM) in HGF-UCMSCs in comparison with UCMSCs. A volcanic map was drawn to display the differentially significant genes.

Statistical analysis

Statistical analysis was performed using GraphPad Prism 8.0 (GraphPad Software, Inc. United States). Two groups were compared using an unpaired *t* test. Comparisons among more than two groups were performed using a one-way analysis of variance, followed by Tukey's multiple comparison test. All values were expressed as the mean ± standard deviation. $P < 0.05$ was considered statistically significant.

Results

Cell identification and quality control

In bright-field microscopy, both UCMSCs and HGF-UCMSCs were plastic-adherent and appeared spindle-shaped (Figure 2A). Ad-HGF transfection hardly changed the morphology of UCMSCs. Cultured in a specific differentiation induction medium, UCMSCs and HGF-UCMSCs differentiated into osteoblasts and adipoblasts (Figure 2A) with no obvious difference between the two groups. To identify MSC biomarkers, we performed flow cytometry. Overexpression of HGF did not alter the size and granularity of UCMSCs (Figures 2B, C). CD73, CD90, and CD105 were all positively expressed and CD34, CD11b, CD19, CD45, and HLA-DR were seldom expressed on the surface of the cells (Figures 2D–2G). Similar to the results of cell differentiation, gene modification did not influence the proportion of the markers mentioned above. To verify whether Ad-HGF transfection was successful, we measured the concentration of HGF in CM. The level of HGF was much higher in the CM of HGF-UCMSCs than that of UCMSCs ($p < 0.0001$) (Figure 2H). Moreover, HGF-UCMSCs proliferated faster than did UCMSCs ($p = 0.0378$) (Figure 2I). Collectively, the transfection of Ad-HGF promoted HGF secretion and cell proliferation without changing the basic characteristics of UCMSCs.

Efficacy of HGF-UCMSCs in lung function

Before euthanizing the rats, we evaluated the physiological function of the lungs. Compared with the CTRL group, FEV300/FVC, PEF, Cchord and TLC in the BLM group decreased significantly ($p < 0.05$) (Figure 3). The PFD, UCMSC and HGF-UCMSC groups alleviated the pulmonary function injury, but the statistical difference was only found between the BLM and HGF-UCMSC group ($p < 0.05$). The therapeutic effect was not present for PEF, Cchord and TLC in the PFD, UCMSC and HGF-UCMSC group ($p > 0.05$).

Effect of HGF-UCMSCs on the improvement of lung structure

The histopathology was analyzed to estimate the improvement effect on lung structure. In H&E-stained sections, pulmonary fibrosis of differing degrees was induced

10.3389/fphar.2022.1070736

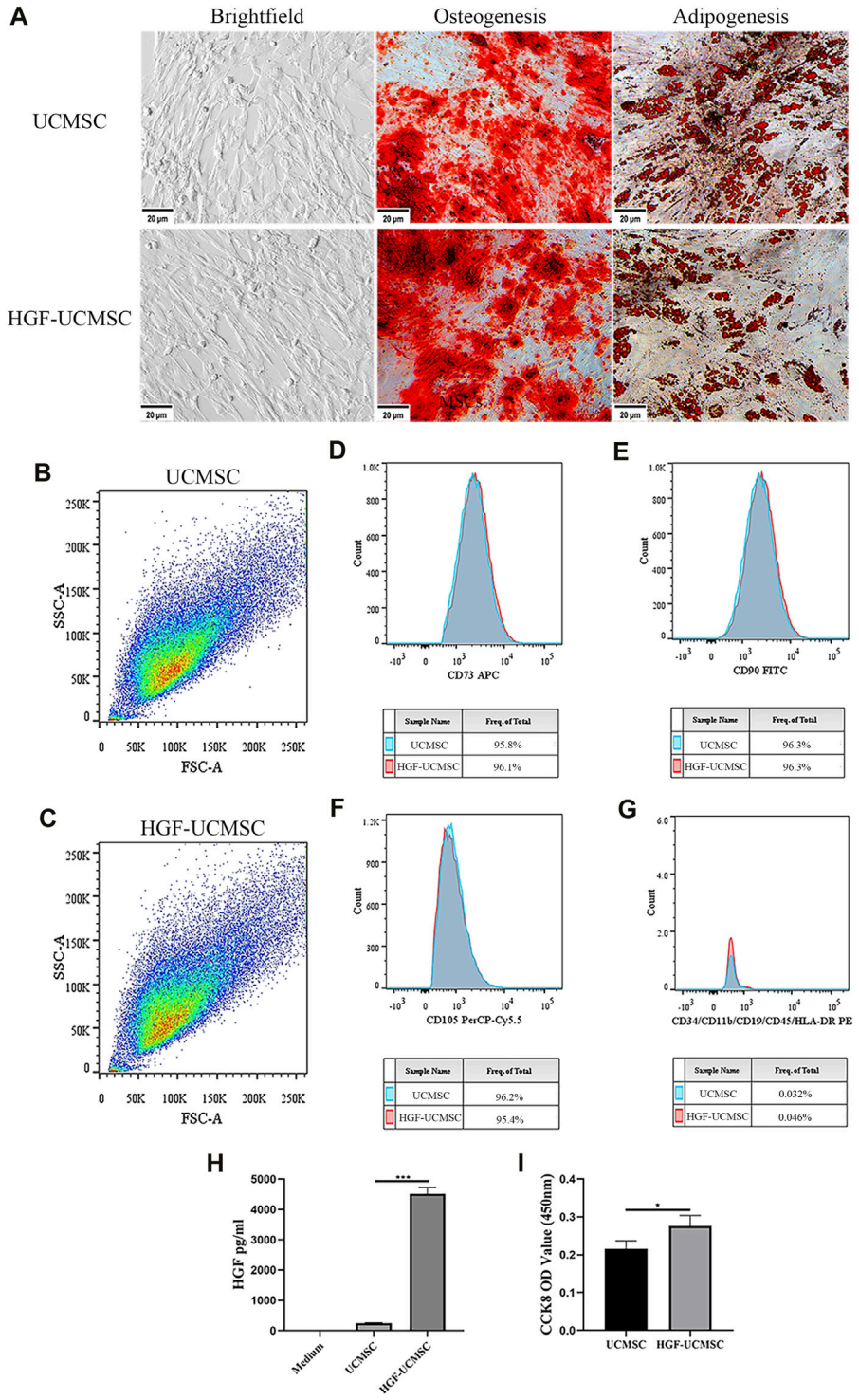

FIGURE 2
Characteristics of UCMSCs and HGF-UCMSCs. **(A)** Regularly cultured MSCs were induced into osteoblasts and adipoblasts stained with alizarin red and Oil Red O, respectively (magnification: ×100). **(B–G)** Flow cytometry was utilized to analyze the physical features and cell surface markers of MSCs **(H)** The concentration of HGF in the conditioned medium was detected using a commercial ELISA kit **(I)** The proliferation of MSCs was assessed by CCK8 assay. Values are presented as mean ± standard deviation. * $p < 0.05$; ** $p < 0.01$; *** $p < 0.001$.

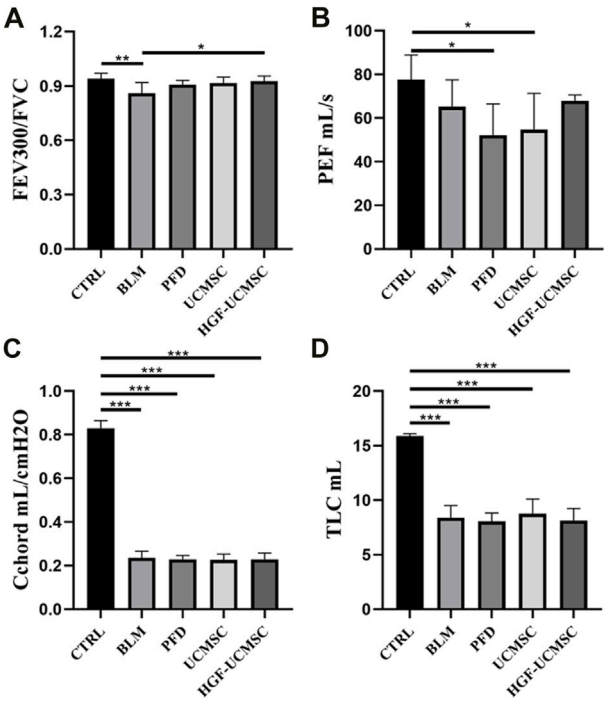

FIGURE 3
Lung function test on day 21 before euthanasia. **(A,B)** Pulmonary ventilatory function: forced expiratory volume in the first 300 m/forced vital capacity (FEV300/FVC); peak expiratory flow (PEF). **(C)** Pulmonary compliance: chord compliance (Cchord). **(D)** Pulmonary volume: total lung capacity (TLC). Values are presented in mean ± standard deviation. * $p < 0.05$; ** $p < 0.01$; *** $p < 0.001$.

in the other groups but was not seen in the CTRL group. The alveolar septum was filled with mesenchymal tissue stained with "acidophilic eosin" (Figure 4A). Ashcroft scores in the BLM group were significantly higher than that in the CTRL group ($p < 0.05$) (Figure 4B). The scores were decreased in all therapeutic groups, in which the PFD group got the lowest scores followed by the HGF-UCMSC group ($p < 0.05$). In sections stained with Masson trichrome, there was a large amount of collagen abnormally present in the interstitial lung tissue (Figure 4A). Similar to the result of Ashcroft scoring, the CTRL group showed significantly less Masson area% than the BLM group ($p < 0.05$) (Figure 4C). In comparison to the BLM group, the PFD, UCMSC and HGF-UCMSC groups significantly decreased the Masson area% ($p < 0.05$). Of note, the HGF-UCMSC group had the lowest p-value among the treatment groups in comparison with the BLM group ($p = 0.0005$). For the evaluation of collagen content, we detected HYP levels in the lungs. A higher level of HYP was present in the BLM group than in the CTRL group ($p < 0.05$) (Figure 4D). The treatment groups had various degrees of inhibitory effect on collagen deposition. HYP was significantly decreased in PFD and HGF-MSC group than the BLM group (PFD vs. BLM, $p = 0.0378$; HGF-UCMSC vs BLM, $p = 0.0088$); the UCMSC group exhibited less HYP, with no statistical significance ($p > 0.05$). Though the statistical difference was not present between the UCMSC and HGF-UCMSC groups, it is likely that HGF modification probably promoted the anti-fibrotic effect of UCMSCs in bleomycin-induced pulmonary fibrosis.

Influence of HGF-UCMSC treatment on lung cytokines

To explain why HGF-UCMSCs had better efficacy than UCMSCs in treating pulmonary fibrosis, cytokines that may be involved were detected according to previous studies (François et al., 2015). The concentration of IL-17 in the BLM group was higher than that in the CTRL group ($p < 0.05$) (Figure 5A). HGF-UCMSCs had significantly decreased levels of IL-17 compared with the BLM, PFD, and UCMSC groups ($p < 0.05$). There was no significance in the PFD and UCMSC group in comparison with the BLM group ($p > 0.05$), although these two groups showed lower levels of IL-17. Compared with the CTRL group, all groups administered with bleomycin exhibited much lower levels of IL-10, and no significance was seen among the bleomycin groups ($p > 0.05$) (Figure 5B). Significantly decreased VEGF and GM-CSF levels were observed in the BLM, PFD, and HGF-UCMSC groups, as compared with the CTRL group ($p < 0.05$) (Figures 5C, D). The UCMSC group had a numerically higher level of VEGF and GM-CSF than did the PFD and HGF-UCMSC groups ($p < 0.05$), although there was no significant difference between the UCMSC and BLM groups ($p > 0.05$). In short, IL-17 may play a role in treatment with respect to HGF-UCMSCs.

Transcriptome difference between UCMSCs and HGF-UCMSCs

Owing to few studies that have depicted the influence of HGF modification on UCMSCs, we conducted mRNA sequencing to uncover the transcriptional change of transfecting Ad-HGF into UCMSCs, thereby ascertaining whether HGF alone participates in treating pulmonary fibrosis. In total, 57% of genes were down-regulated and 43% of genes were up-regulated in all detected genes, without considering the statistical significance (Figure 6A). Among them, three genes (AC092718.2, POC1B-GALNT4 and AC007325.4) were significantly down-regulated, and five genes (HGF, DIO2, IGFBP5, SPTBN2 and SCRG1) were significantly up-regulated, with p values <0.05. (Figure 6B). As shown in Table 1, the log2(FC) value was higher and the FDR value was lower in the HGF gene than in the other genes, which suggested that the anti-fibrotic effect may be primarily owing to HGF.

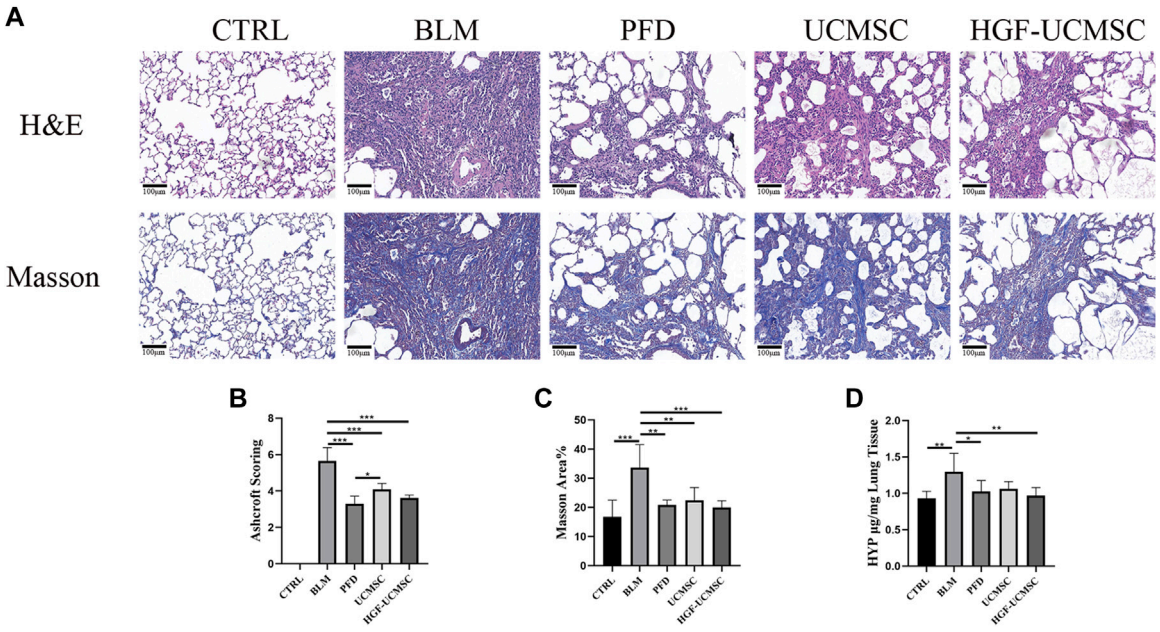

FIGURE 4
Evaluation of pulmonary histopathology. **(A)** Lung sections were stained with H&E or Masson's trichrome (magnification: ×100). **(B)** Ashcroft scoring was performed in H&E-stained sections **(C)** The percentage positive area was calculated in Masson's trichrome-stained sections **(D)** HYP concentrations were detected in the lungs. Values are presented in mean ± standard deviation. * $p < 0.05$; ** $p < 0.01$; *** $p < 0.001$.

Discussion

Gene modification is a promising strategy in the application of MSCs in treating pulmonary fibrosis (Min et al., 2015; Lan et al., 2017). As such, individually designed MSCs may function precisely in the treatment of pulmonary fibrosis. It has been demonstrated that HGF functions as a protective protein in pulmonary fibrosis through binding its receptor, c-met, which is expressed by many types of cells (e.g., epithelial cells, fibroblasts) (Dohi et al., 2000; Watanabe et al., 2005; Gazdhar et al., 2007; Gazdhar et al., 2013; Gazdhar et al., 2018). We therefore performed HGF modification in UCMSCs in order to enhance the anti-fibrotic ability of the cells. Our data showed that the modification improved the anti-fibrotic efficacy of UCMSCs in pulmonary ventilatory function and collagen deposition in the lung.

To explore the possible mechanism of HGF-UCMSCs in treating pulmonary fibrosis, we detected the cytokines that may participate in the process. The results showed that IL-17 may be affected by the treatment of HGF-UCMSCs. Produced by T helper 17 (Th17) cells, IL-17 acts as a driver of pulmonary fibrosis (François et al., 2015; Ting et al., 2017). The deletion of IL-17 in mice ameliorated the severity of pulmonary fibrosis induced by bleomycin (Wilson et al., 2010). In our study, compared with the BLM group, all treatment groups had numerically decreased IL-17 levels but only the HGF-UCMSC group showed a significant inhibitory effect ($p < 0.0001$, Figure 6A). Thus, HGF-UCMSCs may ameliorate pulmonary fibrosis by inhibiting IL-17 in the lung. Our data also showed that significantly lower IL-17 levels were seen in the HGF-UCMSC group than those in the UCMSC group ($p = 0.0285$), which means that the inhibitory effect may be associated with HGF modification. To explore whether other anti-fibrotic factors influenced the inhibition of IL-17 apart from HGF, we performed mRNA sequencing in UCMSCs and HGF-UCMSCs. The data showed that the transcriptional level of HGF was relatively higher than that of other significantly different genes, which suggested that HGF may play the main role in inhibiting IL-17. Interestingly, HGF secreted by MSCs is reported to mediate the differentiation from $CD4^+$ cells to regulatory T cells but not Th17 cells, the IL-17-producing cells (Chen et al., 2020). Therefore, we propose the possible therapeutic mechanism that HGF-UCMSCs may directly or indirectly interact with $CD4^+$ cells or Th17 cells through HGF in fibrotic lungs.

Apart from HGF, the transfection of Ad-HGF also change the transcriptional expression of other genes in UCMSCs. DIO2 acts as an activator of the thyroid hormone, which is critical for the maintenance of cellular homeostasis during stress responses (Sagliocchi et al., 2019). Yu et al. (Yu et al., 2018) reported that DIO2-knockout mice exhibited more severe pulmonary fibrosis.

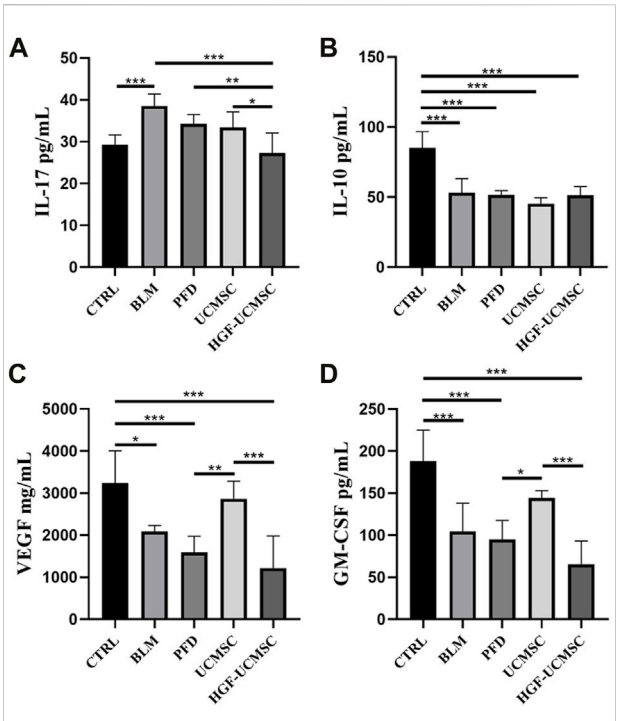

FIGURE 5
Detection of cytokines in the lungs. **(A)** Interleukin-17 (IL-17). **(B)** IL-10 **(C)** Vascular endothelial growth factor (VEGF). **(D)** Granulocyte-macrophage colony-stimulating factor (GM-CSF). Values are presented as mean ± standard deviation. * $p < 0.05$; ** $p < 0.01$; *** $p < 0.001$.

The authors also used thyroid hormone to treat pulmonary fibrosis in mice; their results showed increased survival and resolved lung fibrosis. Insulin-like growth factor binding protein 5 (IGFBP5) was reported as a pro-fibrotic factor in pulmonary fibrosis (Yasuoka et al., 2006). The expression of the human IGFBP5 gene in transgenic mice induced the up-regulation of ECM genes in the lungs (Nguyen et al., 2021). The role of crapie responsive gene 1 (SCRG1) in pulmonary fibrosis is unknown, but it was reported that SCRG1 is associated with the stemness of MSCs (Chosa and Ishisaki, 2018). The relationship between other significantly changed genes and pulmonary fibrosis or MSCs remains unclear in the present.

Our study had some limitations. First, HGF-UCMSCs did not show significantly anti-fibrotic effect in the comparison to UCMSCs, albeit the administration of HGF-UCMSCs but not wild-type UCMSCs significantly improved FEV300/FVC and lung HYP level in our study. This might be attributed to the use of bleomycin in over dosage that is higher than the dosage reported in the published papers (Lee et al., 2010; Rathinasabapathy et al., 2016; Chu et al., 2019). Second, we did not investigate the specific mechanism of the interaction between HGF-UCMSCs and IL-17-producing cells. Thus, *in vitro* and *in vivo* experiments are needed to confirm whether IL-17-producing cells are the targets of HGF and whether IGFBP5 and SCRG1 participate in the treatment of pulmonary fibrosis. Thrid, we did not explore how HGF-UCMSCs function at different stages after treatment and whether there is an

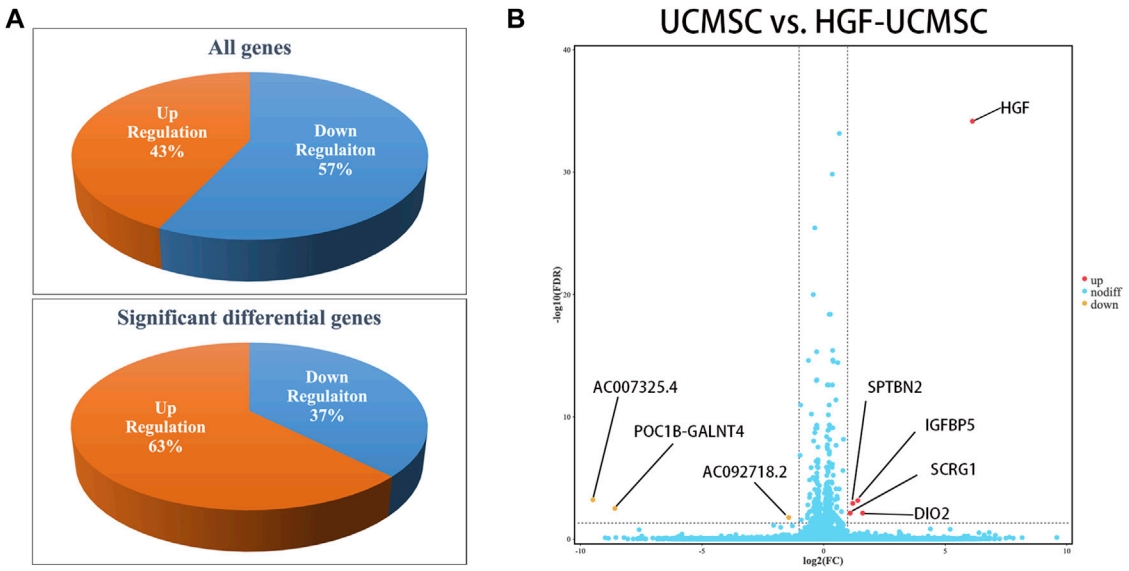

FIGURE 6
Analysis of transcriptional expression of UCMSCs and HGF- UCMSCs. **(A)** The percentage of up-regulated and down-regulated genes was calculated among all genes (upper panel) or the significant differential genes (lower panel) **(B)** Significant differential gene symbols are shown in the volcanic map.

TABLE 1 Statistics for significant differential genes.

Trend	Ensembl ID	Symbol	UCMSC mean FPKM	HGF-UCMSC mean FPKM	log2(FC)	FDR	GO cellular component	GO molecular function	GO biological process
Up regulation	ENSG00000019991	HGF	4.12	288.36	6.1286	0	extracellular region// extracellular space// membrane//. . .	serine-type endopeptidase activity//protein binding//growth factor activity//. . .	MAPK cascade// activation of MAPK activity// mitotic cell cycle//. . .
	ENSG00000211448	DIO2	0.42	1.28	1.6159	0.007803	plasma membrane// membrane// integral component of membrane	thyroxine 5'-deiodinase activity// selenium binding// oxidoreductase activity//. . .	selenocysteine incorporation// thyroid hormone generation//...
	ENSG00000115461	IGFBP5	0.21	0.56	1.415323	0.000722	extracellular region// extracellular space// endoplasmic reticulum lumen//. . .	fibronectin binding// protein binding// insulin-like growth factor binding//. . .	regulation of cell growth// osteoblast differentiation// signal transduction// . . .
	ENSG00000173898	SPTBN2	0.42	0.98	1.210778	0.00125	extracellular space// cytoplasm// cytosol//. . .	actin binding// structural constituent of cytoskeleton// protein binding//. . .	MAPK cascade// ER to Golgi vesicle-mediated transport// cytoskeleton organization// . . .
	ENSG00000164106	SCRG1	0.46	0.99	1.103436	0.007807	extracellular region// extracellular space// cytoplasm//. . .	protein binding	nervous system development// mesenchymal stem cell proliferation
Down regulation	ENSG00000260643	AC092718.2	2.09	0.78	-1.423191	0.017627	mitochondrion// glycine cleavage complex// membrane//. . .		glycine decarboxylation via glycine cleavage system
	ENSG00000259075	POC1B-GALNT4	0.38	0.001	-8.571121	0.003186	Golgi membrane// Golgi apparatus// membrane//. . .	polypeptide N-acetylgalactosaminyltransferase activity// transferase activity// transferase activity, transferring glycosyl groups//. . .	protein glycosylation// protein phosphopantetheinylation
	ENSG00000278817	AC007325.4	0.71	0.001	-9.473706	0.000635			

Abbreviations: HGF, hepatocyte growth factor; DIO2, iodothyronine deiodinase 2; IGFBP5, insulin like growth factor binding protein 5; SPTBN2, spectrin beta, non-erythrocytic 2; SCRG1, stimulator of chondrogenesis 1; POC1B-GALNT4, POC1B-GALNT4 readthrough.

appropriate time window for HGF-UCMSC treatment for better therapeutic efficacy. These may be the keys to reverse fibrosis. Fourth, it remains unclear how the levels of VEGF and GM-CSFin lungs were decreased by HGF-UCMSCs in comparison to UCMSCs. To sample in earlier timing after the administration of HGF-UCMSCs and to determine the main cells secreting VEGF and GM-CSF might be important to reveal the possible mechanism.

Conclusion

In this study, we confirmed that treatment with UCMSCs or HGF-UCMSCs could alleviate pulmonary fibrosis caused by bleomycin in mice. Furthermore, the enhancement of HGF secretion may improve the anti-fibrotic effect of UCMSCs. The improved anti-fibrotic effect may be associated with the inhibition of IL-17 in the lungs.

Data availability statement

The original contributions presented in the study are publicly available. This data can be found here: https://www.ncbi.nlm.nih.gov/sra/PRJNA915313, accession number PRJNA915313.

Ethics statement

The studies involving the isolation of UCMSCs from human participants were reviewed and approved by the Ethics Committee of Beijing 307 Hospital. The participants provided their written informed consent to participate in this study.

Author contributions

HC, YL, SL, and ML contributed to the study design. HC, YL, and YZ performed the experiments and manuscript writing. YY, DC, XS, and ZX participated in the implementation of some experiments and data analysis. All authors contributed to the article and approved the submitted version.

Funding

This research was supported by Innovation team of respiratory diseases and regenerative medicine (2021KCXTD028), Zhongnanshan medical foundation of Guangdong Province (ZNSA-2020013), the Guangzhou Science and Technology Project (202102010358) and Basic Research Foundation of Guangzhou (202102020916).

Acknowledgments

Clinical-grade UCMSCs were shared by Hua Wang, Yuefeng Yang, Chengfeng Sun and Xiaona Zhu from Beijing SH Biotechnology (Beijing, China). MILLIPLEX analysis was performed in Asbio Technology, Inc. (Guangzhou, China). mRNA sequencing and analysis were performed in Gene Denovo Biotechnology Co. (Guangzhou, China). The authors thank all of them for helping.

Conflict of interest

The authors declare that the research was conducted in the absence of any commercial or financial relationships that could be construed as a potential conflict of interest.

Publisher's note

All claims expressed in this article are solely those of the authors and do not necessarily represent those of their affiliated organizations, or those of the publisher, the editors and the reviewers. Any product that may be evaluated in this article, or claim that may be made by its manufacturer, is not guaranteed or endorsed by the publisher.

References

Al Naem, M., Bourebaba, L., Kucharczyk, K., Röcken, M., and Marycz, K. (2020). Therapeutic mesenchymal stromal stem cells: Isolation, characterization and role in equine regenerative medicine and metabolic disorders. *Stem Cell. Rev. Rep.* 16 (2), 301–322. doi:10.1007/s12015-019-09932-0

Ashcroft, T., Simpson, J. M., and Timbrell, V. (1988). Simple method of estimating severity of pulmonary fibrosis on a numerical scale. *J. Clin. Pathol.* 41 (4), 467–470. doi:10.1136/jcp.41.4.467

Balasubramanian, S., Venugopal, P., Sundarraj, S., Zakaria, Z., Majumdar, A. S., and Ta, M. (2012). Comparison of chemokine and receptor gene expression between Wharton's jelly and bone marrow-derived mesenchymal stromal cells. *Cytotherapy* 14 (1), 26–33. doi:10.3109/14653249.2011.605119

Cahill, E. F., Kennelly, H., Carty, F., Mahon, B. P., and English, K. (2016). Hepatocyte growth factor is required for mesenchymal stromal cell protection against bleomycin-induced pulmonary fibrosis. *Stem Cells Transl. Med.* 5 (10), 1307–1318. doi:10.5966/sctm.2015-0337

Cao, X.-P., Han, D.-M., Zhao, L., Guo, Z.-K., Xiao, F.-J., Zhang, Y.-K., et al. (2016). Hepatocyte growth factor enhances the inflammation-alleviating effect of umbilical cord–derived mesenchymal stromal cells in a bronchiolitis obliterans model. *Cytotherapy* 18 (3), 402–412. doi:10.1016/j.jcyt.2015.12.006

Chambers, D. C., Enever, D., Ilic, N., Sparks, L., Whitelaw, K., Ayres, J., et al. (2014). A phase 1b study of placenta-derived mesenchymal stromal cells in patients with idiopathic pulmonary fibrosis. *Respirology* 19 (7), 1013–1018. doi:10.1111/resp.12343

Chen, Q. H., Wu, F., Liu, L., Chen, H. B., Yu, L. N., Wang, H. L., et al. (2020). Mesenchymal stem cells regulate the Th17/Treg cell balance partly through hepatocyte growth factor *in vitro*. *Stem Cell. Res. Ther.* 11 (1), 91. doi:10.1186/s13287-020-01612-y

Chen, S., Cui, G., Peng, C., Lavin, M. F., Sun, X., Zhang, E., et al. (2018). Transplantation of adipose-derived mesenchymal stem cells attenuates pulmonary fibrosis of silicosis via anti-inflammatory and anti-apoptosis effects in rats. *Stem Cell. Res. Ther.* 9 (1), 110–112. doi:10.1186/s13287-018-0846-9

Chen, Y., Qian, H., Zhu, W., Zhang, X., Yan, Y., Ye, S., et al. (2011). Hepatocyte growth factor modification promotes the amelioration effects of human umbilical cord mesenchymal stem cells on rat acute kidney injury. *Stem Cells Dev.* 20 (1), 103–113. doi:10.1089/scd.2009.0495

Chosa, N., and Ishisaki, A. (2018). Two novel mechanisms for maintenance of stemness in mesenchymal stem cells: SCRG1/BST1 axis and cell–cell adhesion through N-cadherin. *Jpn. Dent. Sci. Rev.* 54 (1), 37–44. doi:10.1016/j.jdsr.2017.10.001

Chu, K.-A., Wang, S.-Y., Yeh, C.-C., Fu, T.-W., Fu, Y.-Y., Ko, T.-L., et al. (2019). Reversal of bleomycin-induced rat pulmonary fibrosis by a xenograft of human umbilical mesenchymal stem cells from Wharton's jelly. *Theranostics* 9 (22), 6646–6664. doi:10.7150/thno.33741

Dohi, M., Hasegawa, T., Yamamoto, K., and Marshall, B. C. (2000). Hepatocyte growth factor attenuates collagen accumulation in a murine model of pulmonary fibrosis. *Am. J. Respir. Crit. Care Med.* 162 (6), 2302–2307. doi:10.1164/ajrccm.162.6.9908097

Dong, J., Yu, X., Porter, D. W., Battelli, L. A., Kashon, M. L., and Ma, Q. (2016). Common and distinct mechanisms of induced pulmonary fibrosis by particulate

and soluble chemical fibrogenic agents. *Arch. Toxicol.* 90 (2), 385–402. doi:10.1007/s00204-015-1589-3

Dong, L.-H., Jiang, Y.-Y., Liu, Y.-J., Cui, S., Xia, C.-C., Qu, C., et al. (2015). The anti-fibrotic effects of mesenchymal stem cells on irradiated lungs via stimulating endogenous secretion of HGF and PGE2. *Sci. Rep.* 5 (1), 8713–8810. doi:10.1038/srep08713

Dove, E. P., Olson, A. L., and Glassberg, M. K. (2019). Trends in idiopathic pulmonary fibrosis–related mortality in the United States: 2000–2017. *Am. J. Respir. Crit. Care Med.* 200 (7), 929–931. doi:10.1164/rccm.201905-0958LE

El Omar, R., Beroud, J., Stoltz, J.-F., Menu, P., Velot, E., and Decot, V. (2014). Umbilical cord mesenchymal stem cells: The new gold standard for mesenchymal stem cell-based therapies?*Tissue Eng. Part B Rev.* 20 (5), 523–544. doi:10.1089/ten.teb.2013.0664

François, A., Gombault, A., Villeret, B., Alsaleh, G., Fanny, M., Gasse, P., et al. (2015). B cell activating factor is central to bleomycin-and IL-17-mediated experimental pulmonary fibrosis. *J. Autoimmun.* 56, 1–11. doi:10.1016/j.jaut.2014.08.003

Gazdhar, A., Fachinger, P., van Leer, C., Pierog, J., Gugger, M., Friis, R., et al. (2007). Gene transfer of hepatocyte growth factor by electroporation reduces bleomycin-induced lung fibrosis. *Am. J. Physiol. Lung Cell. Mol. Physiol.* 292, L529–L536. doi:10.1152/ajplung.00082.2006

Gazdhar, A., Fytianos, K., Knudsen, L., Schliep, R., Mueller, S., and Geiser, T. (2018). Electroporation of Hepatocyte growth factor to the lung induces migration of bone marrow mesenchymal stem cells and reduces lung fibrosis. *Eur. Respir. Soc.* doi:10.1183/13993003.congress-2018.PA593

Gazdhar, A., Temuri, A., Knudsen, L., Gugger, M., Schmid, R. A., Ochs, M., et al. (2013). Targeted gene transfer of hepatocyte growth factor to alveolar type II epithelial cells reduces lung fibrosis in rats. *Hum. Gene Ther.* 24 (1), 105–116. doi:10.1089/hum.2012.098

George, P. M., Patterson, C. M., Reed, A. K., and Thillai, M. (2019). Lung transplantation for idiopathic pulmonary fibrosis. *Lancet. Respir. Med.* 7 (3), 271–282. doi:10.1016/S2213-2600(18)30502-2

Glassberg, M. K., Minkiewicz, J., Toonkel, R. L., Simonet, E. S., Rubio, G. A., DiFede, D., et al. (2017). Allogeneic human mesenchymal stem cells in patients with idiopathic pulmonary fibrosis via intravenous delivery (AETHER): a phase I safety clinical trial. *Chest* 151 (5), 971–981. doi:10.1016/j.chest.2016.10.061

Habgood, A. N., Tatler, A. L., Porte, J., Wahl, S. M., Laurent, G. J., John, A. E., et al. (2016). Secretory leukocyte protease inhibitor gene deletion alters bleomycin-induced lung injury, but not development of pulmonary fibrosis. *Lab. Investig.* 96 (6), 623–631. doi:10.1038/labinvest.2016.40

Han, Y.-F., Tao, R., Sun, T.-J., Chai, J.-K., Xu, G., and Liu, J. (2013). Optimization of human umbilical cord mesenchymal stem cell isolation and culture methods. *Cytotechnology* 65 (5), 819–827. doi:10.1007/s10616-012-9528-0

Huang, K., Kang, X., Wang, X., Wu, S., Xiao, J., Li, Z., et al. (2015). Conversion of bone marrow mesenchymal stem cells into type II alveolar epithelial cells reduces pulmonary fibrosis by decreasing oxidative stress in rats. *Mol. Med. Rep.* 11 (3), 1685–1692. doi:10.3892/mmr.2014.2981

Hutchinson, J., Fogarty, A., Hubbard, R., and McKeever, T. (2015). Global incidence and mortality of idiopathic pulmonary fibrosis: A systematic review. *Eur. Respir. J.* 46 (3), 795–806. doi:10.1183/09031936.00185114

Hutchinson, J. P., McKeever, T. M., Fogarty, A. W., Navaratnam, V., and Hubbard, R. B. (2014). Increasing global mortality from idiopathic pulmonary fibrosis in the twenty-first century. *Ann. Am. Thorac. Soc.* 11 (8), 1176–1185. doi:10.1513/AnnalsATS.201404-145OC

Kim, J.-H., Jo, C. H., Kim, H.-R., and Hwang, Y.-i. (2018). Comparison of immunological characteristics of mesenchymal stem cells from the periodontal ligament, umbilical cord, and adipose tissue. *Stem Cells Int.* 2018, 8429042. doi:10.1155/2018/8429042

King, T. E., Jr, Bradford, W. Z., Castro-Bernardini, S., Fagan, E. A., Glaspole, I., Glassberg, M. K., et al. (2014). A phase 3 trial of pirfenidone in patients with idiopathic pulmonary fibrosis. *N. Engl. J. Med.* 370 (22), 2083–2092. doi:10.1056/NEJMoa1402582

Kotani, T., Masutani, R., Suzuka, T., Oda, K., Makino, S., and Ii, M. (2017). Anti-inflammatory and anti-fibrotic effects of intravenous adipose-derived stem cell transplantation in a mouse model of bleomycin-induced interstitial pneumonia. *Sci. Rep.* 7 (1), 14608–14610. doi:10.1038/s41598-017-15022-3

Lan, Y.-W., Theng, S.-M., Huang, T.-T., Choo, K.-B., Chen, C.-M., Kuo, H.-P., et al. (2017). Oncostatin M-preconditioned mesenchymal stem cells alleviate bleomycin-induced pulmonary fibrosis through paracrine effects of the hepatocyte growth factor. *Stem Cells Transl. Med.* 6 (3), 1006–1017. doi:10.5966/sctm.2016-0054

Lederer, D. J., and Martinez, F. J. (2018). Idiopathic pulmonary fibrosis. *N. Engl. J. Med.* 378 (19), 1811–1823. doi:10.1056/NEJMra1705751

Lee, S.-H., Jang, A.-S., Kim, Y.-E., Cha, J.-Y., Kim, T.-H., Jung, S., et al. (2010). Modulation of cytokine and nitric oxide by mesenchymal stem cell transfer in lung injury/fibrosis. *Respir. Res.* 11 (1), 16–14. doi:10.1186/1465-9921-11-16

Lee, Y. H., Suzuki, Y. J., Griffin, A. J., and Day, R. M. (2008). Hepatocyte growth factor regulates cyclooxygenase-2 expression via β-catenin, Akt, and p42/p44 MAPK in human bronchial epithelial cells. *Am. J. Physiol. Lung Cell. Mol. Physiol.* 294 (4), L778–L786. doi:10.1152/ajplung.00410.2007

Li, J., Zheng, C.-Q., Li, Y., Yang, C., Lin, H., and Duan, H.-G. (2015). Hepatocyte growth factor gene-modified mesenchymal stem cells augment sinonasal wound healing. *Stem Cells Dev.* 24 (15), 1817–1830. doi:10.1089/scd.2014.0521

Madrigal, M., Rao, K. S., and Riordan, N. H. (2014). A review of therapeutic effects of mesenchymal stem cell secretions and induction of secretory modification by different culture methods. *J. Transl. Med.* 12 (1), 260–314. doi:10.1186/s12967-014-0260-8

Marmotti, A., Mattia, S., Castoldi, F., Barbero, A., Mangiavini, L., Bonasia, D. E., et al. (2017). Allogeneic umbilical cord-derived mesenchymal stem cells as a potential source for cartilage and bone regeneration: An *in vitro* study. *Stem Cells Int.* 2017, 1732094. doi:10.1155/2017/1732094

Min, F., Gao, F., Li, Q., and Liu, Z. (2015). Therapeutic effect of human umbilical cord mesenchymal stem cells modified by angiotensin-converting enzyme 2 gene on bleomycin-induced lung fibrosis injury. *Mol. Med. Rep.* 11 (4), 2387–2396. doi:10.3892/mmr.2014.3025

Mizuno, S., Matsumoto, K., Li, M.-Y., and Nakamura, T. (2005). HGF reduces advancing lung fibrosis in mice: A potential role for MMP-dependent myofibroblast apoptosis. *Faseb J.* 19 (6), 580–582. doi:10.1096/fj.04-1535fje

Nadri, S., Soleimani, M., Hosseni, R. H., Massumi, M., Atashi, A., and Izadpanah, R. (2002). An efficient method for isolation of murine bone marrow mesenchymal stem cells. *Int. J. Dev. Biol.* 51 (8), 723–729. doi:10.1387/ijdb.072352ns

Navaratnam, V., and Hubbard, R. B. (2019). The mortality burden of idiopathic pulmonary fibrosis in the United Kingdom. *Am. J. Respir. Crit. Care Med.* 200 (2), 256–258. doi:10.1164/rccm.201902-0467LE

Nguyen, X.-X., Renaud, L., and Feghali-Bostwick, C. (2021). Identification of Impacted Pathways and Transcriptomic Markers as Potential Mediators of Pulmonary Fibrosis in Transgenic Mice Expressing Human IGFBP5. *Int. J. Moi. Sci.* 22 (22), 12609. doi:10.3390/ijms222212609

Ocansey, D. K. W., Pei, B., Yan, Y., Qian, H., Zhang, X., Xu, W., et al. (2020). Improved therapeutics of modified mesenchymal stem cells: An update. *J. Transl. Med.* 18 (1), 42–14. doi:10.1186/s12967-020-02234-x

Prasanna, S. J., Gopalakrishnan, D., Shankar, S. R., and Vasandan, A. B. (2010). Pro-inflammatory cytokines, IFNgamma and TNFalpha, influence immune properties of human bone marrow and Wharton jelly mesenchymal stem cells differentially. *PLoS One* 5 (2), e9016. doi:10.1371/journal.pone.0009016

Raghu, G., Chen, S.-Y., Yeh, W.-S., Maroni, B., Li, Q., Lee, Y.-C., et al. (2014). Idiopathic pulmonary fibrosis in US medicare beneficiaries aged 65 years and older: Incidence, prevalence, and survival, 2001–11. *Lancet. Respir. Med.* 2 (7), 566–572. doi:10.1016/S2213-2600(14)70101-8

Raghu, G., Rochwerg, B., Zhang, Y., Garcia, C. A. C., Azuma, A., Behr, J., et al. (2015). An official ATS/ERS/JRS/ALAT clinical practice guideline: Treatment of idiopathic pulmonary fibrosis. An update of the 2011 clinical practice guideline. *Am. J. Respir. Crit. Care Med.* 192 (2), e3–e19. doi:10.1164/rccm.201506-1063ST

Rathinasabapathy, A., Bruce, E., Espejo, A., Horowitz, A., Sudhan, D. R., Nair, A., et al. (2016). Therapeutic potential of adipose stem cell-derived conditioned medium against pulmonary hypertension and lung fibrosis. *Br. J. Pharmacol.* 173 (19), 2859–2879. doi:10.1111/bph.13562

Richeldi, L., Collard, H. R., and Jones, M. G. (2017). Idiopathic pulmonary fibrosis. *Lancet* 389 (10082), 1941–1952. doi:10.1016/S0140-6736(17)30866-8

Richeldi, L., Du Bois, R. M., Raghu, G., Azuma, A., Brown, K. K., Costabel, U., et al. (2014). Efficacy and safety of nintedanib in idiopathic pulmonary fibrosis. *N. Engl. J. Med.* 370 (22), 2071–2082. doi:10.1056/NEJMoa1402584

Sagliocchi, S., Cicatiello, A. G., Di Cicco, E., Ambrosio, R., Miro, C., Di Girolamo, D., et al. (2019). The thyroid hormone activating enzyme, type 2 deiodinase, induces myogenic differentiation by regulating mitochondrial metabolism and reducing oxidative stress. *Redox Biol.* 24, 101228. doi:10.1016/j.redox.2019.101228

Shukla, M. N., Rose, J. L., Ray, R., Lathrop, K. L., Ray, A., and Ray, P. (2009). Hepatocyte growth factor inhibits epithelial to myofibroblast transition in lung cells via Smad7. *Am. J. Respir. Cell. Mol. Biol.* 40 (6), 643–653. doi:10.1165/rcmb.2008-0217OC

Soleimani, M., and Nadri, S. (2009). A protocol for isolation and culture of mesenchymal stem cells from mouse bone marrow. *Nat. Protoc.* 4 (1), 102–106. doi:10.1038/nprot.2008.221

Ting, W., Yuan, L., Jing-Feng, Z., Zhen-Shun, C., and Aamir, A. (2017). Interleukin-17 induces human alveolar epithelial to mesenchymal cell transition

via the TGF-β1 mediated Smad2/3 and ERK1/2 activation. *Plos One* 12 (9), e0183972. doi:10.1371/journal.pone.0183972

Tran, T., Šterclová, M., Mogulkoc, N., Lewandowska, K., Müller, V., Hájková, M., et al. (2020). The European MultiPartner IPF registry (EMPIRE): Validating long-term prognostic factors in idiopathic pulmonary fibrosis. *Respir. Res.* 21 (1), 11–19. doi:10.1186/s12931-019-1271-z

Tzouvelekis, A., Paspaliaris, V., Koliakos, G., Ntolios, P., Bouros, E., Oikonomou, A., et al. (2013). A prospective, non-randomized, no placebo-controlled, phase Ib clinical trial to study the safety of the adipose derived stromal cells-stromal vascular fraction in idiopathic pulmonary fibrosis. *J. Transl. Med.* 11 (1), 1–13. doi:10.1186/1479-5876-11-171

Wang, H., Yang, Y.-F., Zhao, L., Xiao, F.-J., Zhang, Q.-W., Wen, M.-L., et al. (2013). Hepatocyte growth factor gene-modified mesenchymal stem cells reduce radiation-induced lung injury. *Hum. Gene Ther.* 24 (3), 343–353. doi:10.1089/hum.2012.177

Watanabe, M., Ebina, M., Orson, F. M., Nakamura, A., Kubota, K., Koinuma, D., et al. (2005). Hepatocyte growth factor gene transfer to alveolar septa for effective suppression of lung fibrosis. *Mol. Ther.* 12 (1), 58–67. doi:10.1016/j.ymthe.2005.02.019

Wilson, M. S., Madala, S. K., Ramalingam, T. R., Gochuico, B. R., Rosas, I. O., Cheever, A. W., et al. (2010). Bleomycin and IL-1beta-mediated pulmonary fibrosis is IL-17A dependent. *J. Exp. Med.* 207 (3), 535–552. doi:10.1084/jem.20092121

Yasuoka, H., Zhou, Z., Pilewski, J. M., Oury, T. D., Choi, A. M. K., and Feghali-Bostwick, C. A. (2006). Insulin-like growth factor-binding protein-5 induces pulmonary fibrosis and triggers mononuclear cellular infiltration. *Am. J. Pathol.* 169 (5), 1633–1642. doi:10.2353/ajpath.2006.060501

Yin, F., Wang, W.-Y., Mao, L.-C., Cai, Q.-Q., and Jiang, W.-H. (2020). Effect of human umbilical cord mesenchymal stem cells transfected with HGF on TGF-β1/Smad signaling pathway in carbon tetrachloride-induced liver fibrosis rats. *Stem Cells Dev.* 29 (21), 1395–1406. doi:10.1089/scd.2020.0060

Yu, G., Tzouvelekis, A., Wang, R., Herazo-Maya, J. D., Ibarra, G. H., Srivastava, A., et al. (2018). Thyroid hormone inhibits lung fibrosis in mice by improving epithelial mitochondrial function. *Nat. Med.* 24 (1), 39–49. doi:10.1038/nm.4447

frontiers | Frontiers in Pharmacology

TYPE Original Research
PUBLISHED 08 February 2023
DOI 10.3389/fphar.2023.1084617

OPEN ACCESS

EDITED BY
Lie-Fen Shyur,
Academia Sinica, Taiwan

REVIEWED BY
Changzheng Zhou,
Shandong University of Traditional Chinese Medicine, China
Yuqin Chen,
First Affiliated Hospital of Guangzhou Medical University, China

*CORRESPONDENCE
Xuechao Lu,
hospitalbreathing@163.com
Weihong Tao,
qd.thw@163.com
Huantian Cui,
1762316411@qq.com

†These authors share first authorship

SPECIALTY SECTION
This article was submitted to Ethnopharmacology, a section of the journal Frontiers in Pharmacology

RECEIVED 30 October 2022
ACCEPTED 25 January 2023
PUBLISHED 08 February 2023

CITATION
Hu H, Wang F, Han P, Li P, Wang K, Song H, Zhao G, Li Y, Lu X, Tao W and Cui H (2023), Bu-Fei-Huo-Xue capsule alleviates bleomycin-induced pulmonary fibrosis in mice through modulating gut microbiota. *Front. Pharmacol.* 14:1084617. doi: 10.3389/fphar.2023.1084617

Bu-Fei-Huo-Xue capsule alleviates bleomycin-induced pulmonary fibrosis in mice through modulating gut microbiota

Haibo Hu[1†], Fengchan Wang[1†], Ping Han[1†], Peng Li[1], Kun Wang[1], Huan Song[1], Guojing Zhao[1], Yue Li[1], Xuechao Lu[1*], Weihong Tao[1*] and Huantian Cui[2*]

[1]Qingdao Traditional Chinese Medicine Hospital (Qingdao Hiser Hospital), Qingdao University, Qingdao, China, [2]Shandong Provincial Key Laboratory of Animal Cell and Developmental Biology, School of Life Sciences, Shandong University, Jinan, Shandong, China

Introduction: Bu-Fei-Huo-Xue capsule (BFHX) has been used to treat pulmonary fibrosis (PF) in clinic. However, the mechanism of Bu-Fei-Huo-Xue capsule on pulmonary fibrosis remains unclear. Recent studies have shown that the changes in gut microbiota were closely related to the progression of pulmonary fibrosis. Modulating gut microbiota provides new thoughts in the treatment of pulmonary fibrosis.

Methods: In this study,a mouse model of pulmonary fibrosis was induced using bleomycin (BLM) and treated with Bu-Fei-Huo-Xue capsule. We firstly evaluated the therapeutic effects of Bu-Fei-Huo-Xue capsule on pulmonary fibrosis model mice. Besides,the anti-inflammatory and anti- oxidative effects of Bu-Fei-Huo-Xue capsule were evaluated. Furthermore, 16S rRNA sequencing was used to observe the changes in gut microbiota in pulmonary fibrosis model mice after Bu-Fei-Huo-Xue capsule treatment.

Results: Our results showed that Bu-Fei-Huo-Xue capsule significantly reduced the collagen deposition in pulmonary fibrosis model mice. Bu-Fei-Huo-Xue capsule treatment also reduced the levels and mRNA expression of pro-inflammatory cytokines and inhibited the oxidative stress in lung. 16S rRNA sequencing showed that Bu-Fei-Huo-Xue capsule affected the diversity of gut microbiota and the relative abundances of gut microbiota such as *Lactobacillus*, *Lachnospiraceae*_NK4A136_ group, and *Romboutsia*.

Conclusion: Our study demonstrated the therapeutic effects of Bu-Fei-Huo-Xue capsule on pulmonary fibrosis. The mechanisms of Bu-Fei-Huo-Xue capsule on pulmonary fibrosis may be associated with regulating gut microbiota.

KEYWORDS

Bu-Fei-Huo-Xue capsule, pulmonary fibrosis, inflammation, oxidative stress, gut microbiota

Abbreviations: PF, pulmonary fibrosis; TCM, traditional Chinese medicine; ERS, endoplasmic reticulum stress; AECIIs, alveolar epithelial type II cells; XFBD, Xuan-Fei-Bai-Du decoction; BLM, bleomycin; EMT, epithelial-mesenchymal transition; BFHX, Bu-Fei-Huo-Xue capsule; HPLC, high performance liquid chromatography; DXM, dexamethasone; BALF, bronchoalveolar lavage fluid; H&E, hematoxylin and eosin; SOD, superoxide dismutase; GSH-Px, glutathione peroxidase; MDA, malondialdehyde; IL, interleukin; TNF-α, tumor necrosis factor alpha; F to B, Firmicutes/Bacteroidetes.

Introduction

Pulmonary fibrosis (PF) is the final outcome of numerous interstitial lung diseases, and interstitial fibrosis is the most prominent phenotype in most cases. Most patients with interstitial fibrosis of unknown etiology are eventually diagnosed with chronic hypersensitivity pneumonitis, pulmonary sarcoidosis, or idiopathic interstitial pneumonia (Lederer and Martinez, 2018). In spite of the considerable progress in the field of pharmacological treatment in the last 5 years, the high cost of the drugs makes their practical application unsatisfactory. Therefore, continued search for alternative therapeutic drugs is necessary.

Traditional Chinese medicine (TCM) is reported to have a favorable therapeutic effect on PF (Li and Kan, 2017; Zhang et al., 2021). Mai-Men-Dong decoction can improve lung function in rats with PF by reducing the occurrence of endoplasmic reticulum stress (ERS) and apoptosis in alveolar epithelial type II cells (AECIIs) (Shen et al., 2020). Recent studies have reported that SARS-CoV-2 infection can also cause PF (George et al., 2020). Xuan-Fei-Bai-Du decoction (XFBD) has demonstrated remarkable therapeutic effects on COVID-19, and further studies revealed that XFBD improved bleomycin (BLM)-induced PF and reduced collagen deposition in mice. In addition, XFBD improves PF through the inhibition of the IL-6/STAT3 signaling pathway and the regulation of macrophage polarization (Wang et al., 2021; Wang et al., 2022). Qi-Mai-Fei-Luo-Ping decoction inhibits transforming growth factor (TGF)-β-induced proliferation of A549 cells, attenuates epithelial-mesenchymal transition (EMT), and promotes extracellular matrix (ECM) degradation by inhibiting the TGF-β/Smad3 pathway (Yang et al., 2021). Elucidation of the mechanism of action of TCM in the treatment of PF facilitates the modernization of TCM.

Gut microbiota comprise all intestinal microorganisms and contain diverse populations. Each phylum is distributed in different proportions in different parts of the intestine and they maintain the homeostasis of the gut environment (Jandhyala, 2015). With proposal of the concept of "gut-lung axis," the study of lung diseases through gut microbiota has become a new research direction (Dang and Marsland, 2019). In recent years, a correlation between gut microbes and PF has been discovered. Compared to healthy subjects, patients with silicosis and progressive PF showed decreased levels of *Actinobacteria*, along with reduced levels of *Devosia, Clostridiales, Alloprevotella,* and *Rikenellaceae_RC9* (Zhou et al., 2019). A study on the correlation between gut microbiota and PF in mice found that *Alloprevotella, Helicobacter, Rikenella,* and *Rikenllaceae RC9* gut group were negatively correlated with the severity of PF, whereas *Dubosiella* and *Parasutterella* were positively correlated with the outcomes of PF (Gong et al., 2021). Regulating gut microbiota may reportedly provide new therapeutic ideas for treating PF. Anthocyanins modulate radiation-induced disturbances in the lung and gut microbiota of mice and reduce radiation-induced lung inflammation and fibrosis (Li and Kan, 2017; Li et al., 2020; Zhang et al., 2021).

Bu-Fei-Huo-Xue capsule (BFHX) consists of *Astragalus mongholicus* Bunge, *Paeonia anomala subsp. veitchii* (Lynch) D.Y.Hong and K.Y.Pan, and *Cullen corylifolium* (L.) Medik. Clinical studies have shown that BFHX can reduce the secretion of inflammatory cytokines in lung tissue and improve the degree of inflammatory damage and fibrosis-like changes in the lung (Jing et al., 2017). However, the underlying mechanism of action remains unclear.

In the present study, a mouse PF model was established using BLM, which was also treated with BFHX. We first confirmed the therapeutic effects of BFHX on PF and chronic inflammation in PF mice, and then detected changes in gut microbiota diversity and abundance in each group of mice using 16s rRNA sequencing.

Materials and methods

Reagents

The detailed information of reagents used in this study can be found in Supplementary Materials.

Preparation and quality control of BFHX

BFHX was obtained from Guangdong Leiyunshang Pharmaceutical Co., Ltd. (Approval No.: Z20030063). Briefly, 30 g of *A. mongholicus* Bunge, 30 g of *P. anomala subsp. veitchii* (Lynch) D.Y.Hong & K.Y.Pan, and 12 g of *C. corylifolium* (L.) Medik were weighed. The herbs were mixed with 576 mL of distilled water. The mixtures were then decocted for 2 h twice and the water extracts of botanical drugs were filtered and evaporated using a rotary vaporization to obtain the drug powder of BFHX. Each capsule contained 0.35 g of drug powder.

High performance liquid chromatography (HPLC) was conducted for the quality control of the drug powder of BFHX. Psoralenoside, isopsoralenoside, psoralen, angelicin and bakuchiol (purchased from

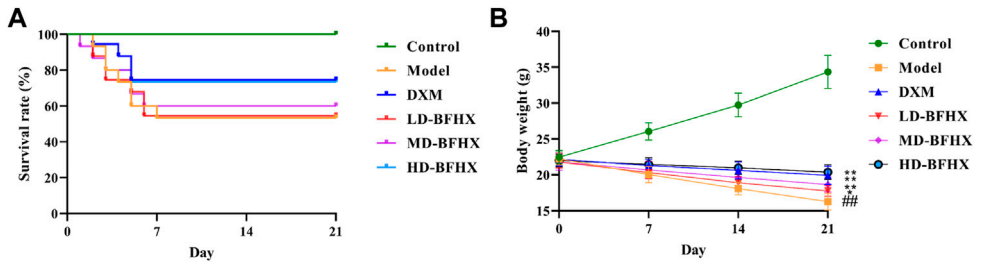

FIGURE 1
(Continued).

10.3389/fphar.2023.1084617

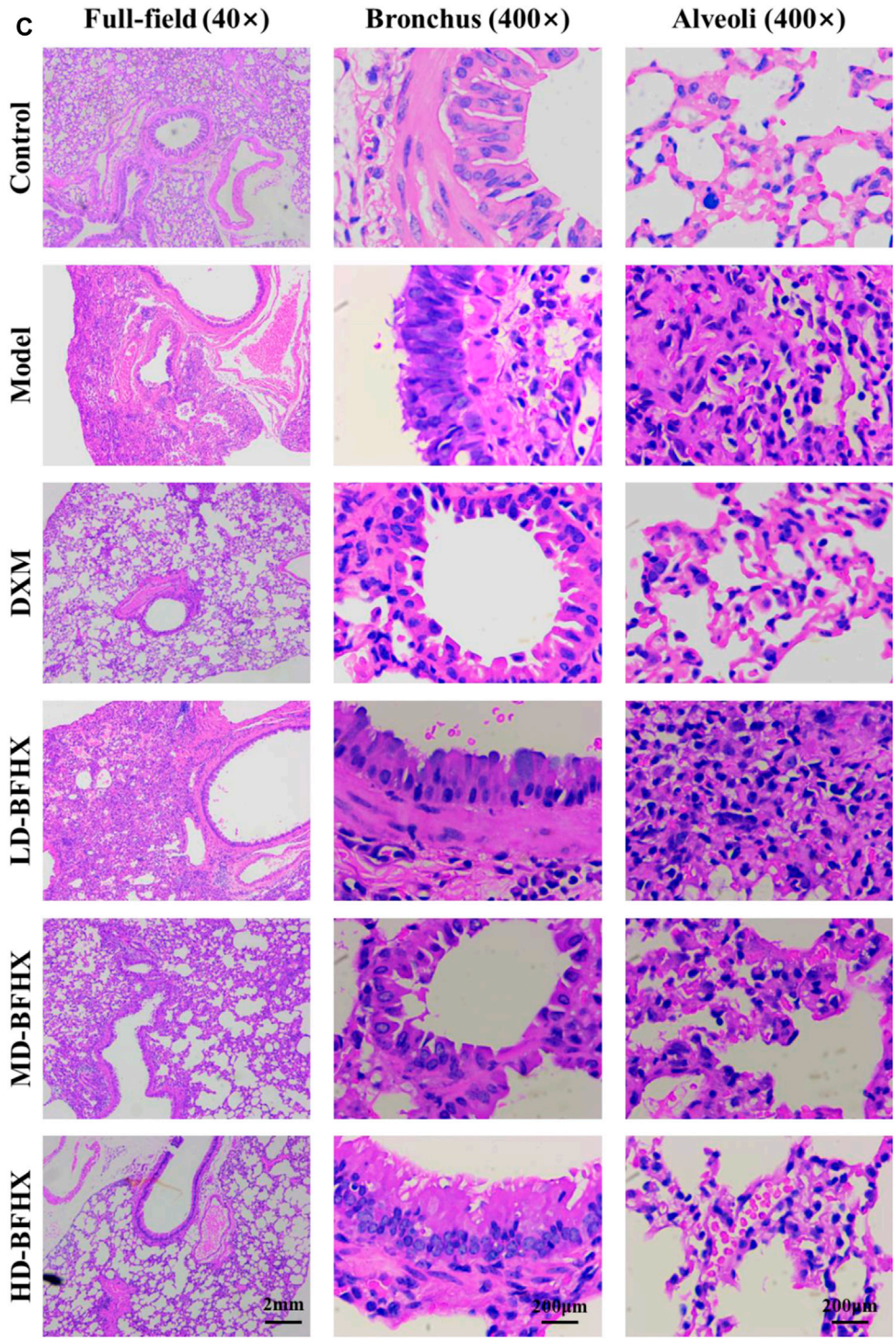

FIGURE 1
(Continued). Bu-Fei-Huo-Xue capsule (BFHX) treatment increased the survival rate, ameliorated the body weight loss and reduced the pathological changes in bleomycin (BLM)-induced pulmonary fibrosis (PF) mice. **(A,B)** The survival rate was increased **(A)** and the body weight loss was reduced **(B)** in PF model mice after treated with BFHX; **(C)** H&E staining indicated that BFHX ameliorated the damage of bronchial epithelial cells, the proliferation of fibrous tissue and the infiltration of inflammatory cells in lung (magnification: ×40 for full-field and 400× for bronchus and alveoli) $^{\#\#}p < 0.01$ compared with the Control group; $^{*}p < 0.05$ compared with the Model group; $^{**}p < 0.01$ compared with the Model group Control group ($n = 15$); Model group ($n = 8$); DXM ($n = 8$); LD-BFHX ($n = 8$); MD-BFHX ($n = 9$); HD-BFHX ($n = 11$).

Yuanye Bio-Technology, Shanghai) were used as the reference standards for quality control. The experimental conditions of HPLC were shown in the supplementary materials (Supplementary Table S1) and the chromatograms of BFHX and reference standards were shown in Supplementary Figure S1. Three different detection parameters (different chromatographic columns, different mobile

10.3389/fphar.2023.1084617

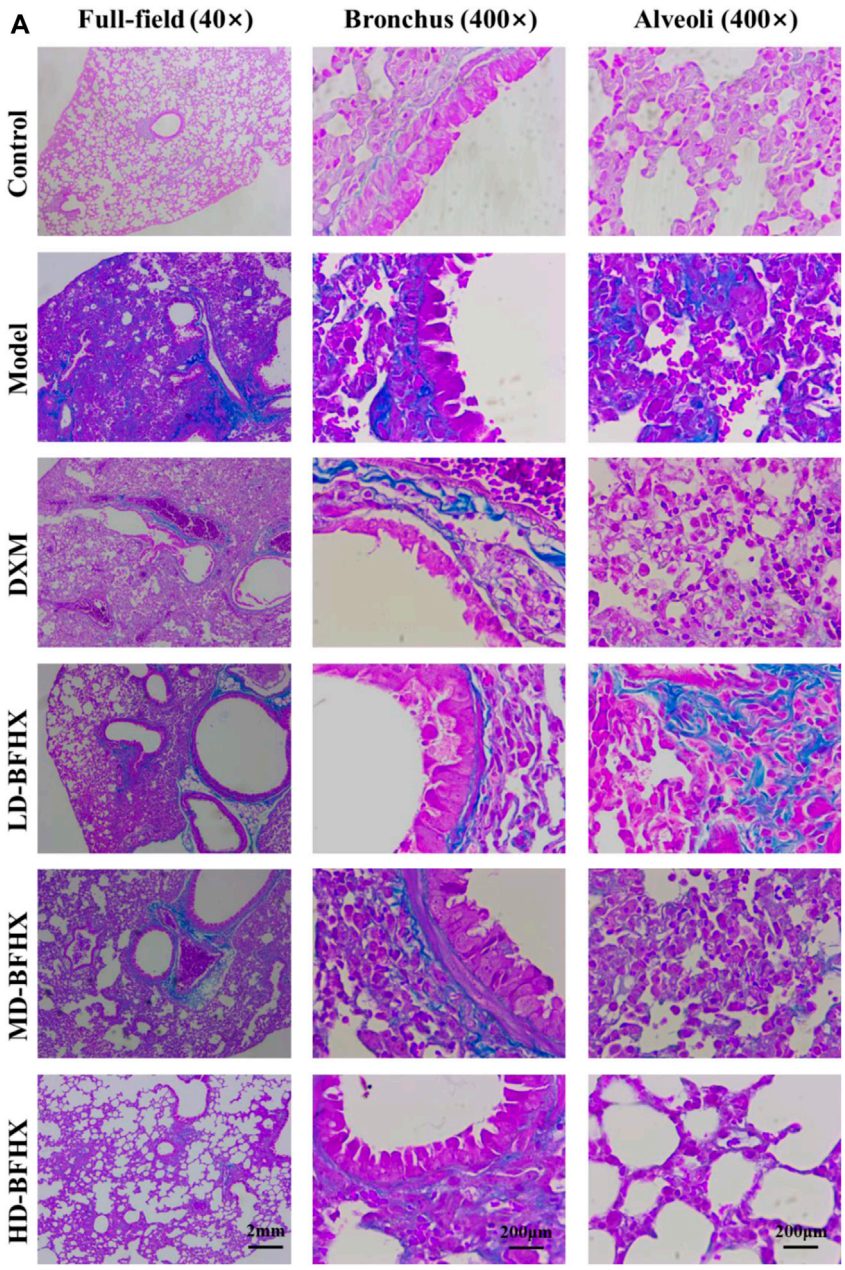

FIGURE 2
(Continued).

phases and different detection wavelengths) within one method were applied to ensure a comprehensive characterization and to countervail the intrinsic limitations of the common fingerprinting methods (Supplementary Tables S2–S5).

Animals

90 male C57BL/6 mice, weighed 18–20 g, were purchased from Beijing Huafukang Co., Ltd. [Certificate of Approval No.: SCXK (Beijing) 2019-0008]. The feeding environment of animals was shown in Supplementary Materials. The animal study was approved by Animal Medicine and Animal Protection Ethics Committee of Qingdao University (approval no. QDU-AEC-202282).

Model construction, grouping, and dosing

90 mice were randomly divided into 6 groups as follows: control, model, DXM, low-dose BFHX (LD-BFHX), medium-dose BFHX (MD-BFHX), and high-dose BFHX (HD-BFHX), with 15 mice in each group. For mice in the model, DXM, LD-BFHX, MD-BFHX, and HD-BFHX groups, PF was induced by a single intratracheal injection

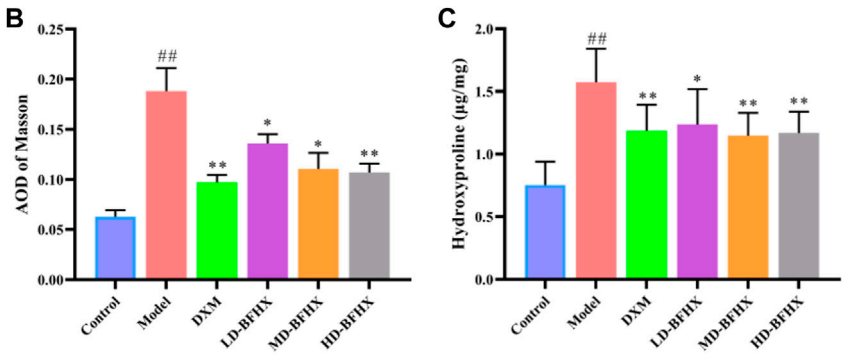

FIGURE 2
(Continued). BFHX treatment decreased the deposition of fibrotic contents in lung in PF model mice. **(A,B)** Masson staining showed that BFHX decreased the accumulation of fibrotic contents in lung (magnification: ×40 for full-field and 400× for bronchus and alveoli); **(C)** BFHX reduced the levels of hydroxyproline in lung tissue homogenates.

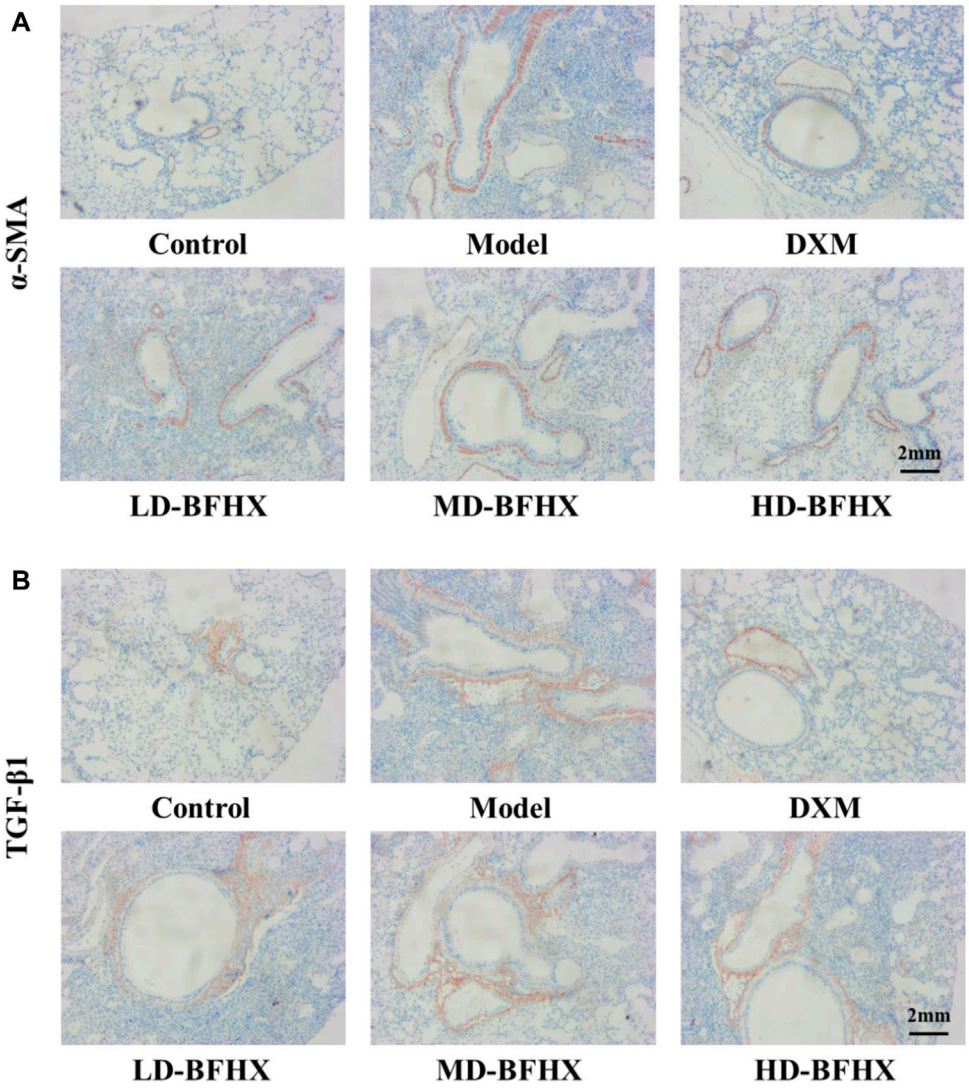

FIGURE 3
(Continued).

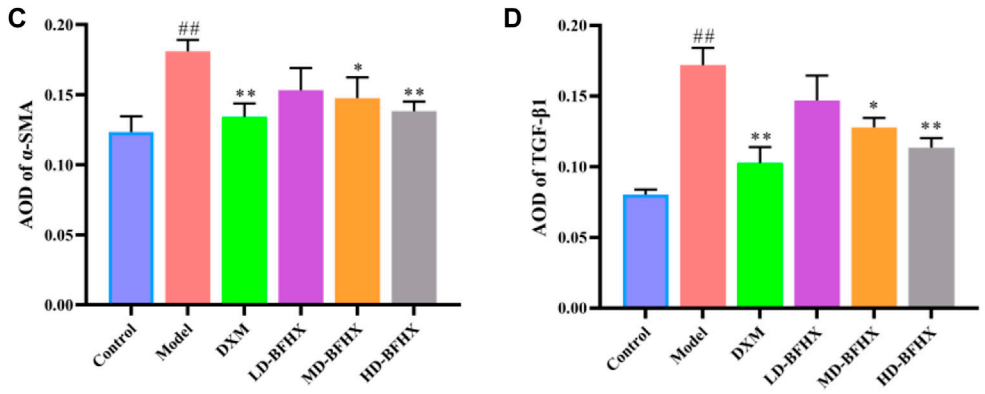

FIGURE 3
(Continued). BFHX treatment decreased the expression of α-SMA and TGF-β1 in lung. **(A,C)** Immunohistochemistry showed that BFHX treatment reduced the expression of α-SMA in lung (magnification: ×40). **(B,D)** Immunohistochemistry showed that BFHX treatment reduced the expression of TGF-β1 in lung (magnification: ×40).

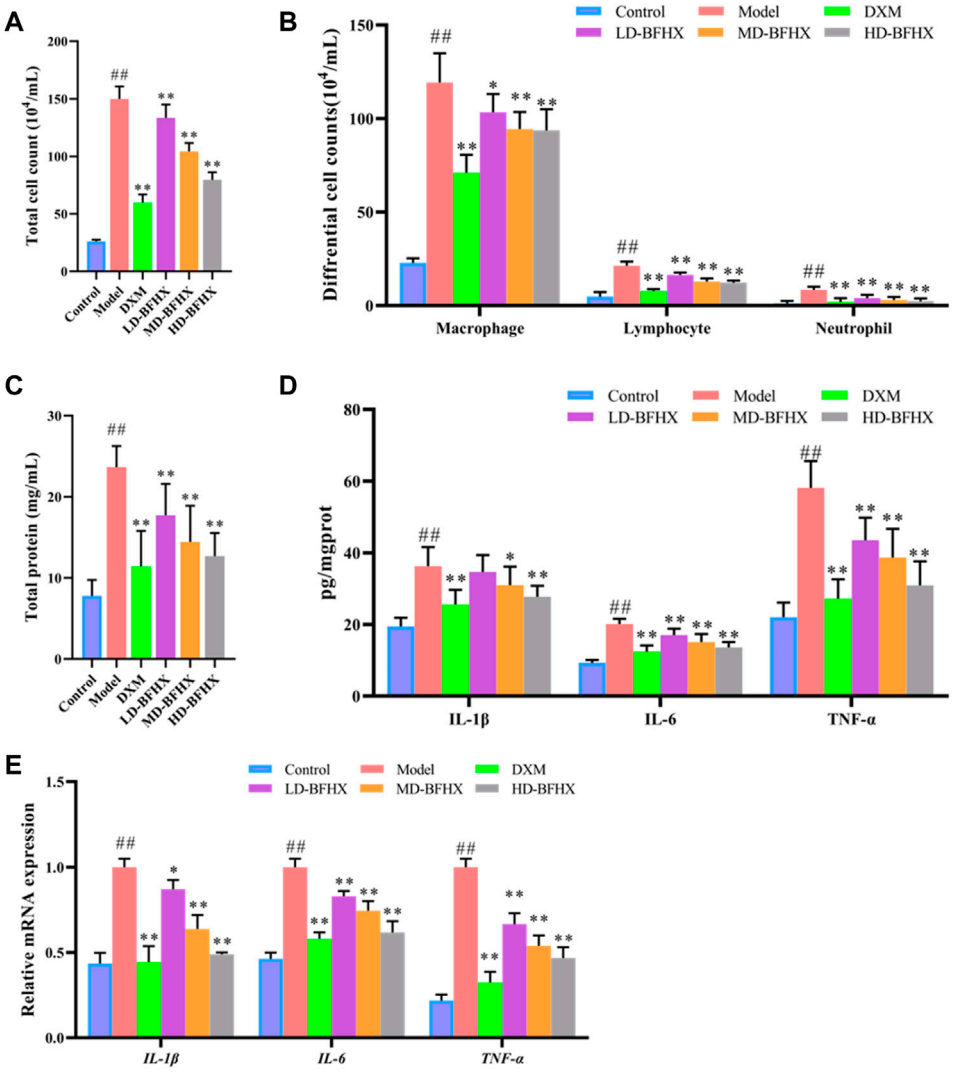

FIGURE 4
Treatment of BFHX alleviated inflammatory response in PF model mice. **(A–C)** BFHX treatment decreased the total cell counts **(A)**, differential cell counts **(B)**, and total protein concentration **(C)** in bronchoalveolar lavage fluid (BALF) in PF model mice. **(D)** The levels of pro-inflammatory cytokines (IL-1β, IL-6, TNF-α) levels in of lung tissue homogenate were decreased in PF model mice after BFHX treatment. **(E)** qPCR results showed that BFHX treatment downregulated the mRNA expression of *IL-6*, *IL-1β* and *TNF-α* in lung.

TABLE 1 Effects of Bu-Fei-Huo-Xue capsule (BFHX) on SOD and GSH-Px activities and MDA levels in lung homogenate.

Group	SOD (U/mg prot)	MDA (nmol/mg prot)	GSH-Px (U/mg prot)
Control	79.93 ± 14.12	1.67 ± 0.25	28.48 ± 7.03
Model	29.88 ± 10.72##	3.03 ± 0.39##	14.84 ± 3.91##
DXM	67.75 ± 13.86**	2.04 ± 0.35**	30.46 ± 4.38**
LD-BFHX	39.50 ± 7.14	2.70 ± 0.49	15.57 ± 5.09
MD-BFHX	60.34 ± 18.01**	2.41 ± 0.30**	19.26 ± 3.67*
HD-BFHX	61.27 ± 8.18**	2.27 ± 0.30**	21.29 ± 4.35**

##$p < 0.01$ compared with the Control group; *$p < 0.05$ compared with the Model group; **$p < 0.01$ compared with the model group. Control group ($n = 15$); model group ($n = 8$); DXM ($n = 8$); LD-BFHX ($n = 8$); MD-BFHX ($n = 9$); HD-BFHX ($n = 11$).

of 2.5 mg/kg of BLM. Meanwhile, mice in the control group received a single intratracheal injection of an equal volume of PBS. Starting on day 1 after intratracheal injection, the DXM group received 2 mg/kg of DXM *via* intragastric administration on daily basis. The LD-BFHX, MD-BFHX, and HD-BFHX groups received 0.32, 0.63, and 1.26 g/kg of BFHX powder by intragastric administration on daily basis, respectively. Briefly, drug powder of BFHX was weighed and diluted into saline to obtain the BFHX mixture, with the final concentration of 32, 63, and 126 mg/mL respectively. The gavage amount of BFHX mixture was 0.1 mL/10 g. The control and model groups received equal volumes of distilled water *via* intragastric administration on daily basis as vehicle (0.1 mL/10 g), and the entire drug administration process lasted for 21 days. During drug administration, the number of surviving mice in each group was counted daily. The mice were also weighed on days 0, 7, 14, and 21 of administration to observe the changes in body weight. On day 22, after intratracheal injection, all mice were sacrificed and samples were collected.

Collection of bronchoalveolar lavage fluid (BALF) and lung tissues

After the mice were sacrificed, the thorax was incised and the cervical trachea was fully exposed. After ligation of the left lung, the right lung was lavaged three times with PBS at 4°C, 0.5 ml each time, and the collected fluid was BALF. The lavaged right lung was removed and stored at −80°C. BALF was then centrifuged at 3,000 rpm for 5 min at 4°C, and the supernatant of the first lavage solution was stored at −80°C and analyzed for total protein content using a protein assay kit. Cell pellets from BALF samples were resuspended in PBS for cell counting, and smears were prepared and then underwent to Wright-Giemsa staining to observe various types of inflammatory cells.

Pathological staining

After BALF collection, the ligated left lung was removed and placed into 4% paraformaldehyde for fixation and embedded in paraffin. The fixed tissue blocks were embedded in paraffin and then cut into 3-μm sections. Hematoxylin and eosin (H&E) staining and Masson's trichrome staining were routinely performed, and the results were observed under a light microscope. The positive expression of Masson staining was quantified using Image Pro Plus 6.0 software and average optical density (AOD) was calculated.

Immunohistochemistry

Paraffin sections were made from fixed lung tissue, and endogenous peroxidase was deactivated using methanol-hydrogen peroxide, followed by clearing using PBS and distilled water. Immunohistochemical staining was carried out after antigen retrieval and blocking. The sections were incubated overnight at 4°C with rabbit anti-smooth muscle actin (α-SMA) (1:100) or rabbit anti-transforming growth factor beta 1 (TGF-β1) (1:100). After that, the sections were washed and incubated with secondary antibody (1:10000), washed again. The sections were then mounted after color development and hematoxylin counterstaining. The α-SMA and TGF-β1 protein expression in lung tissue were observed under a light microscope. The expression in the positive regions was quantitatively analyzed using the Image Pro Plus 6.0 software and AOD was calculated.

Lung tissue biochemical test

We added 100 mg of lung tissue to 900 μL of saline, and homogenized the tissue *via* ultrasonication. The tissue mixture was then centrifuged 3,000 rpm for 15 min at 4°C and the supernatant was collected, where the protein levels in the tissue homogenate were normalized using the BCA kit. Superoxide dismutase (SOD), and glutathione peroxidase (GSH-Px) activities, malondialdehyde (MDA) and hydroxyproline levels were measured in lung tissue using biochemical assay kits. These assays were performed according to the manufacturers' instructions.

Enzyme-linked immunosorbent assay (ELISA)

Quantification of interleukin (IL)-1β, IL-6, and tumor necrosis factor alpha (TNF-α) in lung tissue was performed using mouse ELISA kits. The 10% of the lung homogenate supernatant was added to wells coated with the capture antibody. After washing, biotin-labeled detection antibodies were added to each well. After washing, the color development reaction substrate was added and the reaction

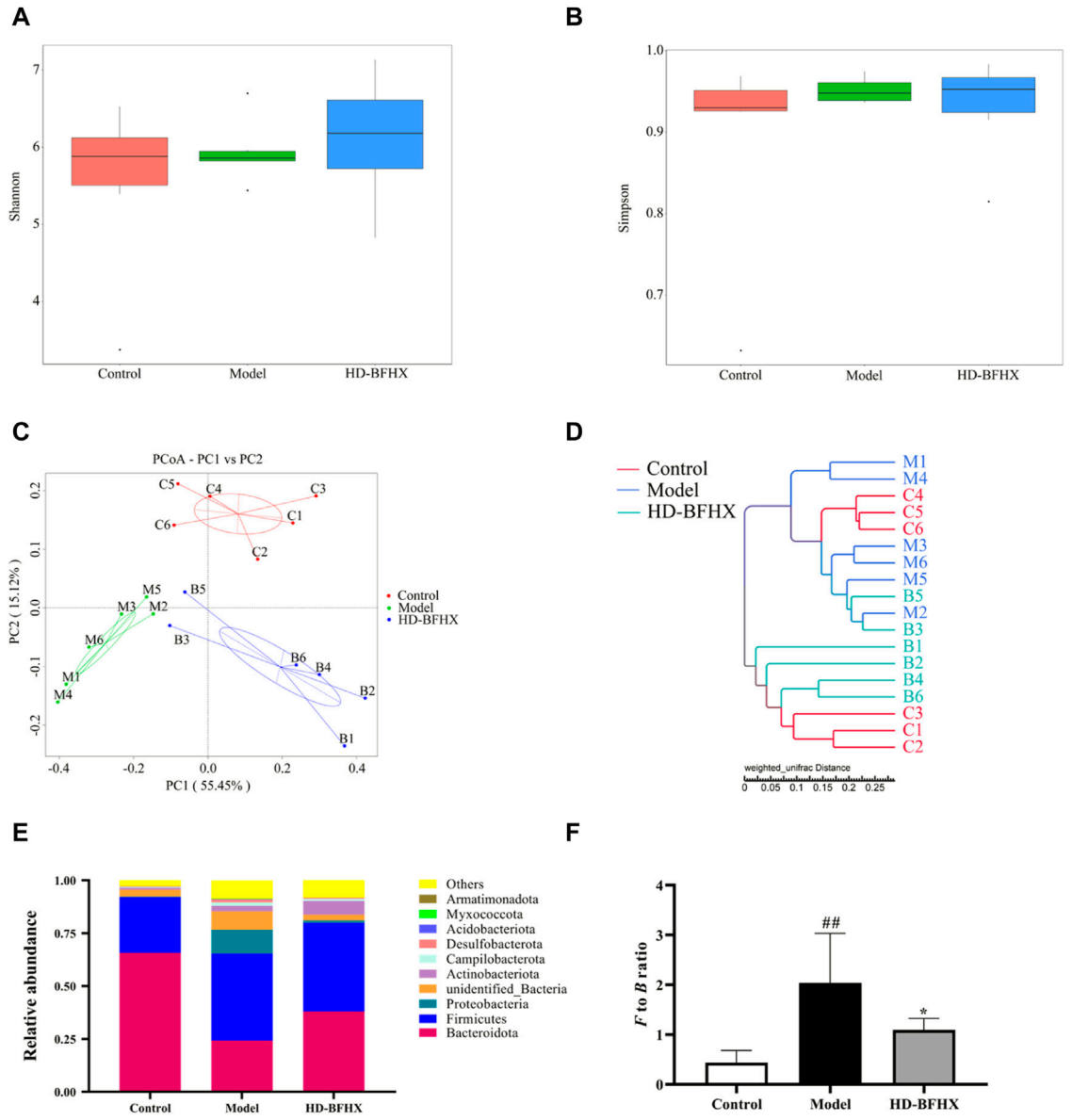

FIGURE 5
(Continued).

was terminated after 15 min. The absorbance was read at 450 nm using a microplate reader and the concentration of the corresponding substance to be measured in the sample was calculated after plotting the standard curve.

Quantitative polymerase chain reaction (qPCR)

RNA extraction kit was used to isolated the total RNA in lung. The purity and concentration of RNA samples were detected by nanodrop. Then the cDNA was synthesized and qPCR was conducted to detect the mRNA expression of *IL-6*, *IL-1β* and *TNF-α*. *Actb* was used as a loading control. $2^{-\triangle\triangle CT}$ method was used to calculate the relative expression. The primer sequence was shown in Supplementary Table S6.

16S rRNA sequencing

Twenty-one days after BFHX treatment, the fecal contents of mice in control, model and HD-BFHX were collected. The total genomic DNA from the fecal contents of the mice was extracted with the cetyltrimethylammonium bromide (CTAB)/sodium dodecyl sulfate (SDS) method, and the DNA concentration and purity were tested using a 1% agarose gel. DNA was diluted to 1 ng/μL with sterile water based on the concentration. The detailed information about PCR and sequencing data analysis were included in Supplementary Material.

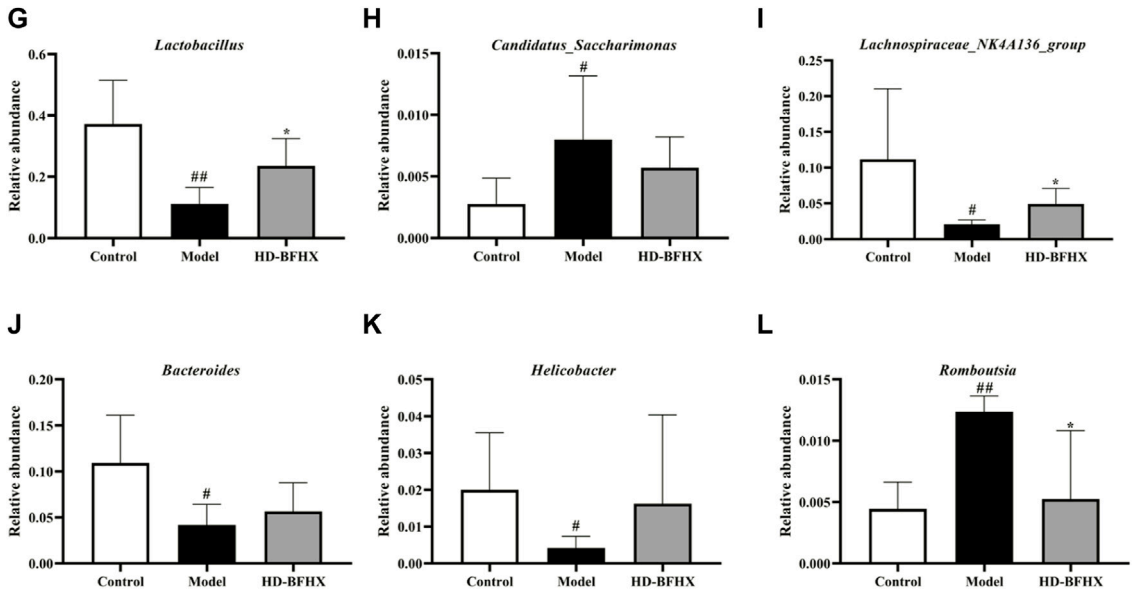

FIGURE 5
(Continued). Treatment of high-dose HD-BFHX affected the gut microbiota community in mice with PF. **(A,B)** Shannon **(A)** and Simpson indexes **(B)** were higher in HD-BFHX group than that in the Model group. **(C,D)** Principal Co-ordinates Analysis (PCoA) score plot **(C)** and UPGMA cluster tree **(D)** indicated more similar beta diversity between HD-BFHX **(B)** and Control **(C)** groups than that between the Model (M) and Control groups. **(E–L)** At the phylum level, BFHX treatment decreased the *F to B* ratio **(E,F)**; At the genus level, the relative abundances of *Lactobacillus* **(G)**, *Candidatus_Saccharimonas* **(H)**, *Lachnospiraceae_NK4A136_group* **(I)**, *Bacteroides* **(J)**, *Helicobacter* **(K)**, and *Romboutsia* **(L)** were changed in PF model mice, BFHX treatment affected the relative abundances of, *Lachnospiraceae_NK4A136_group,* and *Romboutsia* in mice with PF. Control group (n = 6); Model group (n = 6); HD-BFHX (n = 6).

Statistical analysis

All values were expressed as mean ± standard deviation (SD). Statistical analysis was performed using one-way ANOVA for multiple comparisons. In all analyses, a difference with $p < 0.05$ was considered statistically significant.

Results

BFHX improved fibrosis progression in PF mice

After model construction and drug administration, the survival rate was 100% in the control group and 53% in the model group, and DXM and BFHX interventions significantly increased the survival rate of PF mice. The survival rate was 73% in the DXM group, 53% in the LD-BFHX group, 60% in the MD-BFHX group, and 73% in the HD-BFHX group (Figure 1A). Besides, compared with the control group, the body weight of the model group was significantly decreased; compared to the model group, the body weights of mice in the DXM, LD-BFHX, MD-BFHX and HD-BFHX were increased (Figure 1B). H&E staining showed that no alveolar inflammatory exudation and fibrotic lesions were found, and the alveolar structure was clear in the lung tissue of the control group; the structure of bronchial epithelial cells was impaired, the number of interstitial lung cells was increased, fibrous tissue proliferation and fibrosis were present, and alveolar cavity was enlarged and fused in the model group. After the intervention of DXM, LD-BFHX, MD-BFHX and HD-BFHX, lung histopathological changes in mice were reduced, and the lung tissue structure was intact, the alveolar septum was slightly thickened, and inflammatory cell infiltration was reduced (Figure 1C). The results of Masson staining showed that the lung tissues of mice in the control group had normal structural morphology. Compared to the control group, there were significant blue collagen deposits in the interstitium of the model group, which were distributed in large bundles and patches, and the lung tissue fibrosis was severe. Compared to the model group, blue fibrous tissue in the lung tissues of mice was reduced after the intervention of DXM, LD-BFHX, MD-BFHX, and HD-BFHX. The degree of lung tissue fibrosis was significantly improved (Figures 2A, B). The results of hydroxyproline corroborated the degree of pathological changes in lung tissue. Compared to the control group, the model group had significantly higher level of hydroxyproline, and the DXM, LD-BFHX, MD-BFHX, and HD-BFHX groups had lower level of hydroxyproline than the model group (Figure 2C). Besides, immunostaining of lung tissue showed that the expression of α-SMA and TGF-β1 was increased in model group compared with the control, whereas BFHX and DXM treatment reduced the expression of α-SMA and TGF-β1 compared with the model group (Figures 3A–D).

BFHX ameliorated inflammation and oxidative stress in PF mice

The results of BALF total cell count showed that the total cell count in the model group was significantly greater than that in the control group; the total cell count was reduced in the DXM, LD-BFHX, MD-BFHX, and HD-BFHX groups compared to those in the model group (Figure 4A). Wright-Giemsa staining was used to enumerate macrophages, lymphocytes, and neutrophils in BALF of each group of mice, and the results showed that the counts of macrophages,

lymphocytes, and neutrophils were significantly greater in the model group compared to those in the control group. Compared to the model group, the counts of macrophages, lymphocytes, and neutrophils in the DXM, LD-BFHX, MD-BFHX, and HD-BFHX groups and neutrophil counts were reduced (Figure 4B). Total protein quantification showed that total protein concentration in BALF was significantly higher in the model group than in the control group, and DXM, LD-BFHX, MD-BFHX, and HD-BFHX interventions significantly reduced total protein concentration in BALF compared to the model group (Figure 4C). The levels of inflammatory cytokines IL-1β, IL-6, and TNF-α in lung tissue homogenates and BALF were measured using ELISA. The results showed that the levels of inflammatory cytokines, IL-1β, IL-6, and TNF-α, were significantly greater in the lung tissue homogenate in BALF of the model group than in the control group; while IL-1β, IL-6, and TNF-α were decreased in the lung tissue and BALF of DXM, LD-BFHX, MD-BFHX, and HD-BFHX-treated mice, with DXM and HD-BFHX having the most significant reductions (Figure 4D). Moreover, the mRNA expression of *IL-6, IL-1β* and *TNF-α* was upregulated in model group compared with the control group, DXM and BFHX treatment mice showed lower mRNA expression of *IL-6, IL-1β* and *TNF-α* than that in the model group (Figure 4E).

In addition, the effects of BFHX on oxidative stress in PF model mice were evaluated by measuring SOD, GSH-Px activity, and MDA levels in lung tissues of mice in each group. The results showed that the SOD and GSH-Px activities in the lung tissue homogenates of the model group decreased and the MDA level increased compared to the control group; compared to the model group, DXM, MD-BFHX, and HD-BFHX treatment could significantly increase the SOD and GSH-Px activities and decrease the MDA level (Table 1).

In summary, DXM or BFHX treatment improved histopathological changes in the lungs of PF mice, inhibited inflammatory responses, and alleviated oxidative stress. Among the three BFHX groups, the most significant improvement was again seen in the high-dose group. This suggested that BFHX can be a potential therapeutic agent for PF. Therefore, the HD-BFHX group was selected for the subsequent experimental study.

Results of gut microbiota 16S rRNA sequencing

The 16S rRNA sequencing results were used to construct a clustering table with the Amplicon Sequence Variant strategy for subsequent analysis. The *α* diversity of the gut microbial community was assessed by calculating the Shannon and Simpson indices. The results showed that there was no significant difference in Shannon and Simpson indexes in each group (Figures 5A, B). We then calculated the magnitude of differences in the microbial communities between different samples with the Principal Co-ordinates Analysis (PCoA) and UPGMA cluster tree and by assessing their beta diversity. The PCoA and clustering results showed that the sample points of the model group were significantly separated and distant from those of the control group, whereas the sample points of the HD-BFHX group were well separated from those of the model group (Figures 5C, D).

We further compared the relative abundance of gut microbiota to assess microbiota structure. The results showed that *Firmicutes* and *Bacteroidetes* were the dominant taxa in gut microbiota at the phylum level for each group (Figure 5E). The *Firmicutes*/*Bacteroidetes* (*F to B*) ratio was significantly increased in the model group compared to that in the control group, while the *F to B* ratio was significantly decreased after HD-BFHX intervention (Figure 5F). At the genus level, compared to the control group, the relative abundance of *Candidatus_Saccharimonas,* and *Romboutsia* was significantly increased and the relative abundance of *Lactobacillus*, *Lachnospiraceae_NK4A136_group*, *Bacteroides*, and *Helicobacter* was significantly decreased in the model group. Compared to the control group, the relative abundance of *Lactobacillus* and *Lachnospiraceae_NK4A136_group* was significantly increased and the relative abundance of *Romboutsia* was significantly decreased in the HD-BFHX group (Figures 5G–L)

Discussion

In the present study, we established PF model mice by using BLM. BLM is a chemotherapeutic antibiotic that interrupts the cell cycle, leading to a massive production of free radicals, which causes an inflammatory response and pulmonary toxicity, activation of fibroblasts, and subsequent fibrosis. Therefore, it is widely used in the construction of PF animal models (Moeller et al., 2008; Mouratis and Aidinis, 2011). ECM deposition is the basic pathological feature of PF. Collagen is one of the components of ECM and hydroxyproline is the main component of collagen. Pathological staining of the lungs of mice in the model group revealed extensive fibrosis with structural destruction of the lungs and the appearance of striated fibers, as revealed by H&E and Masson staining. Biochemical assays showed a significant increase in hydroxyproline levels. Epithelial cells in the hypoxic environment created by myofibroblasts undergo apoptosis or EMT, which in turn drives the progression of fibrosis (Yang et al., 2021). Therefore, the expression level of α-SMA can be used to determine the progression of fibrosis (Kyung et al., 2018). Our results found that the expression level of α-SMA was significantly higher in the model group of mice than in the normal group, demonstrating the widespread occurrence of fibrosis. Furthermore, immunohistochemistry revealed the presence of large amounts of TGF-β1 in the lungs of PF mice. DXM is a hormonal drug that is commonly used in the clinical treatment of PF and has been used as a positive control drug in many PF animal studies. Our results suggested that no significant difference existed between the BFHX high-dose group and the active control group intervention in terms of improving lung tissue permeability and pathological changes in PF mice, and these suggested that BFHX has therapeutic effect in PF.

In addition, chronic inflammation is one of the important pathological changes in PF (Thannickal et al., 2004; Du et al., 2019). Under chronic inflammatory conditions, fibroblasts synthesize and release large amounts of ECM, which eventually leads to fibrosis and destruction of normal alveolar structure. Previous studies have reported that macrophages play a key role in PF (Kalluri and Weinberg, 2009; Kishore et al., 2021). During the onset of inflammation, macrophages can rapidly migrate to the site of inflammation, secrete a variety of inflammatory mediators, and promote fibroblast activation and proliferation (Buechler et al., 2021; Du et al., 2022). We measured the counts of total cells, macrophages, lymphocytes, and neutrophils in BALF, and found that cell exudation increased significantly in the model group, and the counts of macrophages, lymphocytes, and neutrophils increased to varying degrees, with macrophages occupying a dominant position. ELISA

and qPCR results demonstrated the presence of large amounts of pro-inflammatory cytokines in the lung tissues and BALF of PF model mice than the control group, which is consistent with the results of other studies (Phan and Kunkel, 1992). Our results demonstrated that BFHX reduced the inflammatory response in PF mice.

We also assessed pulmonary oxidative stress by measuring the levels of oxidative stress-related enzyme activities and peroxidation markers. As per our expectations, SOD and GSH-Px activities in the lung tissue of the model group were reduced, whereas MDA levels were increased. This suggested that the lungs were subjected to severe oxidative stress. These sources of stress are associated with several factors besides BLM. Endoplasmic reticulum stress, and peroxisomes are major sources of intracellular reactive oxygen species (ROS); however, macrophages and epithelial cells are the major cellular sources of oxidative stress (Otoupalova et al., 2020). Notably, apoptosis of macrophages releases large amounts of ROS, and this leads to additional macrophage activation and drives PF progression, creating a vicious cycle. Further experiment can be carried out to study the mechanisms of BFHX on PF based on affecting the function of macrophages.

The potential role of gut microbiota in PF has been extensively studied and has been shown to be strongly correlated with inflammation (Bhattacharya et al., 2022). In the present study, the effect of BFHX on the structure and composition of the gut microbiota of PF mice was determined by 16S rRNA sequencing analysis. Alpha diversity of gut microbiota refers to the diversity of microbiota within a specific region or ecosystem and is a comprehensive indicator reflecting the abundance and homogeneity of the microbiota. PF model mice exhibited elevated Shannon and Simpson indices, suggesting elevated alpha diversity in the gut microbiota of PF mice. The beta diversity of mouse gut microbiota was subsequently analyzed using PCoA and cluster analysis, and the overall structure and composition of PF mouse gut microbiota underwent major changes, and BFHX could affect the beta diversity of PF mouse gut microbiota. The results of the analysis of the relative abundance of gut microbiota showed that BFHX could decrease the high *F to B* ratio caused by PF. Changes in the *Firmicutes* to *Bacteroidetes* ratio are intimately associated with many diseases, and *Firmicutes* to *Bacteroidetes* ratio was significantly increased in the PF model. Metabolic disorders and inflammatory responses can be alleviated by decreasing the *F to B* ratio (Trivedi and Barve, 2020; Bhattacharya et al., 2022).

We selected the top few bacteria with the greatest relative total abundance at the genus level for comparison. In PF mice, the relative abundance of *Lactobacillus, Lachnospiraceae_NK4A136_group, Bacteroides,* and *Helicobacter* were significantly decreased, and the relative abundance of *Candidatus_Saccharimonas* and *Romboutsia* were significantly increased. BFHX may have significantly increased the relative abundance of *Lactobacillus, Lachnospiraceae_NK4A136_group* and decreased the relative abundance of *Romboutsia. Lactobacillus,* a natural microorganism with immunomodulatory abilities, has been shown to alleviate respiratory diseases such as asthma in several animal studies and clinical trials (Thannickal et al., 2004; Du et al., 2019). In a previous study, *Lachnospiraceae_NK4A136_group* was significantly and positively correlated with IgE and IL-33 (Wang et al., 2022). However, there was a trend of decreasing abundance of *Lachnospiraceae_NK4A136_group* in the gut microbiota of classical low virulence *Klebsiella pneumoniae* infected mice (Jiang et al., 2022). In a particulate matter-induced lung injury mouse study, the *Lachnospiraceae_NK4A136_group* is likely to be the core gut microorganism playing a protective role (Zhou et al., 2016; Zhao et al., 2021). Our experimental results showed that the relative abundance of *Lachnospiraceae_NK4A136_group* in the gut microbiota of PF mice was significantly reduced, and this was reversed through BFHX intervention. Therefore, the specific role of the *Lachnospiraceae_NK4A136_group* in lung diseases requires further elucidation in the future. *Bacteroides* in gut can metabolize polysaccharides and oligosaccharides to provide nutrients and vitamins to the host and other gut microbiota. However, when *Bacteroides* colonize other sites, they have the potential to become opportunistic pathogens (Zafar and Saier, 2021). *Helicobacter* is a gram-negative spiral bacterium that is closely associated with many gastrointestinal diseases (Graham, 2015). However, controversy exists over the effect of *Helicobacter* on the respiratory system. Some studies have reported a degree of protective effect of *Helicobacter* in the respiratory system; however, other studies have pointed out that there is no negative association between *Helicobacter* and respiratory diseases (Miftahussurur et al., 2017). *Candidatus_Saccharimonas*, a conditional pathogen, was significantly elevated in a colitis-associated carcinogenesis model (Cruzdos et al., 2020). In addition, green tea leaf powder ameliorated high-fat diet-induced abnormalities in lipid metabolism while decreasing its *Candidatus_Saccharimonas* abundance in the gut (Shao et al., 2017). *Romboutsia* was significantly overrepresented in the lung tissue of cancer patients (Ock-Hwa et al., 2022) and positively correlated with the levels of Th2-related factors in the gut microbiota of ovalbumin-induced asthmatic mice, which is consistent with our results and in-depth studies can be conducted using *Romboutsia* as a pathogenic bacterium.

In conclusion, our study demonstrated the therapeutic effects of BFHX on PF. The mechanisms of BFHX on PF may be associated with regulating gut microbiota.

Data availability statement

The datasets presented in this study can be found in online repositories. The names of the repository/repositories and accession number(s) can be found below: NCBI BioProject https://www.ncbi.nlm.nih.gov/bioproject, PRJNA893846.

Ethics statement

The animal study was reviewed and approved by Animal Medicine and Animal Protection Ethics Committee of Qingdao University (approval No. QDU-AEC-202282).

Author contributions

HH, GZ, and KW carried out the experiments and manuscript writing. PH and FW provided experimental help. PL, HS, and YL performed data analysis and result interpretation. XL and WT provided ideas, resources and technical guidance for the whole

work. HC supervised the experiments. All authors contributed to the article and approved the submitted version.

Funding

This work was supported by Qingdao Health Science and Technology Project (2020-WJZD053), Qingdao TCM Science and Technology Project (2021-zyyq03).

Conflict of interest

The authors declare that the research was conducted in the absence of any commercial or financial relationships that could be construed as a potential conflict of interest.

Publisher's note

All claims expressed in this article are solely those of the authors and do not necessarily represent those of their affiliated organizations, or those of the publisher, the editors and the reviewers. Any product that may be evaluated in this article, or claim that may be made by its manufacturer, is not guaranteed or endorsed by the publisher.

Supplementary material

The Supplementary Material for this article can be found online at: https://www.frontiersin.org/articles/10.3389/fphar.2023.1084617/full#supplementary-material

References

Bhattacharya, S. S., Yadav, B., Rosen, L., Nagpal, R., Yadav, H., and Yadav, J. S. (2022). Crosstalk between gut microbiota and lung inflammation in murine toxicity models of respiratory exposure or co-exposure to carbon nanotube particles and cigarette smoke extract. *Toxicol. Appl. Pharmacol.* 447, 116066. doi:10.1016/j.taap.2022.116066

Buechler, M. B., Fu, W., and Turley, S. J. (2021). Fibroblast-macrophage reciprocal interactions in health, fibrosis, and cancer. *Immunity* 54 (5), 903–915. doi:10.1016/j.immuni.2021.04.021

Cruz, B. C., Dos, S., Conceição, L. L., Mendes, T. A., Ferreira, C. L., Gonçalves, R. V., et al. (2020). Use of the synbiotic VSL#3 and yacon-based concentrate attenuates intestinal damage and reduces the abundance of Candidatus Saccharimonas in a colitis-associated carcinogenesis model. *Food Res. Int.* 137, 109721. doi:10.1016/j.foodres.2020.109721

Dang, A. T., and Marsland, B. J. (2019). Microbes, metabolites, and the gut–lung axis. *Mucosal Immunol.* 12 (4), 843–850. doi:10.1038/s41385-019-0160-6

Du, S., Li, C., Lu, Y., Lei, X., Zhang, Y., Li, S., et al. (2019). Dioscin alleviates crystalline silica-induced pulmonary inflammation and fibrosis through promoting alveolar macrophage autophagy. *Theranostics* 9 (7), 1878–1892. doi:10.7150/thno.29682

Du, T., Lei, A., Zhang, N., and Zhu, C. (2022). The beneficial role of probiotic Lactobacillus in respiratory diseases. *Front. Immunol.* 13, 908010. doi:10.3389/fimmu.2022.908010

George, P. M., Wells, A. U., and Jenkins, R. G. (2020). Pulmonary fibrosis and COVID-19: The potential role for antifibrotic therapy. *Lancet Respir. Med.* 8 (8), 807–815. doi:10.1016/s2213-2600(20)30225-3

Gong, G., Song, S., and Su, J. (2021). Pulmonary fibrosis alters gut microbiota and associated metabolites in mice: An integrated 16S and metabolomics analysis. *Life Sci.* 264, 118616. doi:10.1016/j.lfs.2020.118616

Graham, D. Y. (2015). *Helicobacter pylori* update: Gastric cancer, reliable therapy, and possible benefits. *Gastroenterology* 148 (4), 719–731. doi:10.1053/j.gastro.2015.01.040

Jandhyala, S. M., Talukdar, R., Subramanyam, C., Vuyyuru, H., Sasikala, M., and Nageshwar ReDDy, D. (2015). Role of the normal gut microbiota. *World J. Gastroenterology* 21 (29), 8787–8803. doi:10.3748/wjg.v21.i29.8787

Jiang, Q., Xu, Q., Kenéz, Á., Chen, S., and Yang, G. (2022). *Klebsiella pneumoniae* infection is associated with alterations in the gut microbiome and lung metabolome. *Microbiol. Res.* 263, 127139. doi:10.1016/j.micres.2022.127139

Jing, Y., Tang, S., Jin, J., Cao, N., Wang, Y., Liao, Q., et al. (2017). Influence of pulmonary fibrosis in PM2.5 model mice with bufei huoxue capsule. *World J. Intergrated Traditional West. Med.* 12 (06), 774–778. doi:10.13935/j.cnki.sjzx.170610

Kalluri, R., and Weinberg, R. A. (2009). The basics of epithelial-mesenchymal transition. *J. Clin. Investigation* 119 (6), 1420–1428. doi:10.1172/jci39104

Kishore, A., and Petrek, M. (2021). Roles of macrophage polarization and macrophage-derived miRNAs in pulmonary fibrosis. *Front. Immunol.* 12, 678457. doi:10.3389/fimmu.2021.678457

Kyung, S. Y., Kim, D. Y., Yoon, J. Y., Son, E. S., Kim, Y. J., Park, J. W., et al. (2018). Sulforaphane attenuates pulmonary fibrosis by inhibiting the epithelial-mesenchymal transition. *BMC Pharmacol. Toxicol.* 19 (1), 13. doi:10.1186/s40360-018-0204-7

Lederer, D. J., and Martinez, F. J. (2018). Idiopathic pulmonary fibrosis. *N. Engl. J. Med.* 378 (19), 1811–1823. doi:10.1056/nejmra1705751

Li, L.-C., and Kan, L.-D. (2017). Traditional Chinese medicine for pulmonary fibrosis therapy: Progress and future prospects. *J. Ethnopharmacol.* 198, 45–63. doi:10.1016/j.jep.2016.12.042

Li, W., Lu, L., Liu, B., and Qin, S. (2020). Effects of phycocyanin on pulmonary and gut microbiota in a radiation-induced pulmonary fibrosis model. *Biomed. Pharmacother.* 132, 110826. doi:10.1016/j.biopha.2020.110826

Miftahussurur, M., Nusi, I. A., Graham, D. Y., and Yamaoka, Y. (2017). Helicobacter, hygiene, atopy, and asthma. *Front. Microbiol.* 8, 1034. doi:10.3389/fmicb.2017.01034

Moeller, A., Ask, K., Warburton, D., Gauldie, J., and Kolb, M. (2008). The bleomycin animal model: A useful tool to investigate treatment options for idiopathic pulmonary fibrosis? *Int. J. Biochem. Cell Biol.* 40 (3), 362–382. doi:10.1016/j.biocel.2007.08.011

Mouratis, M. A., and Aidinis, V. (2011). Modeling pulmonary fibrosis with bleomycin. *Curr. Opin. Pulm. Med.* 17 (5), 355–361. doi:10.1097/mcp.0b013e328349ac2b

Ock-Hwa, K., Bo-Yun, C., Kwan, K. D., Hyun, K. N., Kyung, R. J., Jun, S. W., et al. (2022). The microbiome of lung cancer tissue and its association with pathological and clinical parameters. *Am. J. Cancer Res.* 12 (5), 2350–2362.

Otoupalova, E., Smith, S., Cheng, G., and Thannickal, V. J. (2020). Oxidative stress in pulmonary fibrosis. *Compr. Physiol.* 10, 509–547. doi:10.1002/cphy.c190017

Phan, S. H., and Kunkel, S. L. (1992). Lung cytokine production in bleomycin-induced pulmonary fibrosis. *Exp. Lung Res.* 18 (1), 29–43. doi:10.3109/01902149209020649

Shao, T., Shao, L., Li, H., Xie, Z., He, Z., and Wen, C. (2017). Combined signature of the fecal microbiome and metabolome in patients with gout. *Front. Microbiol.* 8, 268. doi:10.3389/fmicb.2017.00268

Shen, M., Nan, Y., Zhang, L., Di, L., He, S., Li, Y., et al. (2020). Maimendong decoction improves pulmonary function in rats with idiopathic pulmonary fibrosis by inhibiting endoplasmic reticulum stress in AECIIs. *Front. Pharmacol.* 11, 1262. doi:10.3389/fphar.2020.01262

Thannickal, V. J., Toews, G. B., White, E. S., and Martinez, F. J. (2004). Mechanisms of pulmonary fibrosis. *Annu. Rev. Med.* 55 (1), 395–417. doi:10.1146/annurev.med.55.091902.103810

Trivedi, R., and Barve, K. (2020). Gut microbiome a promising target for management of respiratory diseases. *Biochem. J.* 477 (14), 2679–2696. doi:10.1042/bcj20200426

Wang, J., Lu, H., Yu, L., Cheng, W., Yan, W., and Jing, X. (2021). Aggravation of airway inflammation in RSV-infected asthmatic mice following infection-induced alteration of gut microbiota. *Ann. Palliat. Med.* 10 (5), 5084–5097. doi:10.21037/apm-20-2052

Wang, Y., Sang, X., Shao, R., Qin, H., Chen, X., Xue, Z., et al. (2022). Xuanfei Baidu Decoction protects against macrophages induced inflammation and pulmonary fibrosis via inhibiting IL-6/STAT3 signaling pathway. *J. Ethnopharmacol.* 283, 114701. doi:10.1016/j.jep.2021.114701

Yang, Y., Ding, L., Bao, T., Li, Y., Ma, J., Li, Q., et al. (2021). Network Pharmacology and experimental assessment to explore the pharmacological mechanism of qimai feiluoping decoction against pulmonary fibrosis. *Front. Pharmacol.* 12, 770197. doi:10.3389/fphar.2021.770197

Zafar, H., and Saier, M. H. (2021). Gut Bacteroides species in health and disease. *Gut Microbes* 13 (1), 1–20. doi:10.1080/19490976.2020.1848158

Zhang, Y., Lu, P., Qin, H., Zhang, Y., Sun, X., Song, X., et al. (2021). Traditional Chinese medicine combined with pulmonary drug delivery system and idiopathic pulmonary fibrosis: Rationale and therapeutic potential. *Biomed. Pharmacother.* 133, 111072. doi:10.1016/j.biopha.2020.111072

Zhao, Y., Chen, X., Shen, J., Xu, A., Wang, Y., Meng, Q., et al. (2021). Black tea alleviates particulate matter-induced lung injury via the gut-lung Axis in mice. *J. Agric. Food Chem.* 69 (50), 15362–15373. doi:10.1021/acs.jafc.1c06796

Zhou, W., Mo, X., Cui, W., Zhang, Z., Li, D., Li, L., et al. (2016). Nrf2 inhibits epithelial-mesenchymal transition by suppressing snail expression during pulmonary fibrosis. *Sci. Rep.* 6 (1), 38646. doi:10.1038/srep38646

Zhou, Y., Chen, L., Sun, G., Li, Y., and Huang, R. (2019). Alterations in the gut microbiota of patients with silica-induced pulmonary fibrosis. *J. Occup. Med. Toxicol.* 14 (1), 5. doi:10.1186/s12995-019-0225-1

frontiers | Frontiers in Pharmacology

TYPE Review
PUBLISHED 14 February 2023
DOI 10.3389/fphar.2023.1111393

OPEN ACCESS

EDITED BY
Changjun Lv,
Binzhou Medical University Hospital, China

REVIEWED BY
Pavel Solopov,
Old Dominion University, United States
Hui Huang,
Peking Union Medical College Hospital (CAMS), China

*CORRESPONDENCE
Zhihao Xu,
xuzhihao@zju.edu.cn

SPECIALTY SECTION
This article was submitted to Respiratory Pharmacology, a section of the journal Frontiers in Pharmacology

RECEIVED 29 November 2022
ACCEPTED 03 February 2023
PUBLISHED 14 February 2023

CITATION
Yang X, Xu Z, Hu S and Shen J (2023), Perspectives of PDE inhibitor on treating idiopathic pulmonary fibrosis. *Front. Pharmacol.* 14:1111393. doi: 10.3389/fphar.2023.1111393

Perspectives of PDE inhibitor on treating idiopathic pulmonary fibrosis

Xudan Yang, Zhihao Xu*, Songhua Hu and Juan Shen

Department of Respiratory and Critical Care Medicine, The Fourth Affiliated Hospital, School of Medicine, Zhejiang University, Yiwu, China

Idiopathic pulmonary fibrosis (IPF) is a chronic, progressive interstitial lung disease (ILD) without an identifiable cause. If not treated after diagnosis, the average life expectancy is 3–5 years. Currently approved drugs for the treatment of IPF are Pirfenidone and Nintedanib, as antifibrotic drugs, which can reduce the decline rate of forced vital capacity (FVC) and reduce the risk of acute exacerbation of IPF. However these drugs can not relieve the symptoms associated with IPF, nor improve the overall survival rate of IPF patients. We need to develop new, safe and effective drugs to treat pulmonary fibrosis. Previous studies have shown that cyclic nucleotides participate in the pathway and play an essential role in the process of pulmonary fibrosis. Phosphodiesterase (PDEs) is involved in cyclic nucleotide metabolism, so PDE inhibitors are candidates for pulmonary fibrosis. This paper reviews the research progress of PDE inhibitors related to pulmonary fibrosis, so as to provide ideas for the development of anti-pulmonary fibrosis drugs.

KEYWORDS

pulmonary fibrosis, cAMP, cGMP, PDE inhibitor, anti-fibrosis, senescence

1 Introduction

IPF is a chronic, progressive age-related interstitial lung disease (ILD) of unknown etiology. If not treated after diagnosis, the average life expectancy is 3–5 years (King et al., 2011; Richeldi et al., 2017). Although the understanding of IPF has been significantly improved, the critical pathways of disease still need to be further explored. It is generally believed that environmental stressors and genetic susceptibility are the key factors that activate and promote the development of pulmonary fibrosis (Maher et al., 2007; Margaritopoulos et al., 2012). Genetic, environmental factors (smoking, dust, etc.), infection (EB virus, cytomegalovirus, herpesvirus), aging and other aspects interact to initiate continuous micro-damage of alveolar epithelial cells (Stewart et al., 1999; Lok et al., 2001; Tang et al., 2003; Maher et al., 2007; Richeldi et al., 2017). Alveolar macrophages recognize epithelial injury and amplify inflammatory response, secrete transforming growth factor-β (TGF-β),IL-10, platelet-derived growth factor (PDGF), and other cytokines, recruit fibroblasts to the injured site, transform fibroblasts into myofibroblasts, stimulate alveolar epithelial cells to undergo epithelial-mesenchymal transformation (EMT), and myofibroblasts secrete extracellular matrix components (ECM). It eventually leads to the occurrence, development and maintenance of pulmonary fibrosis (Craig et al., 2015; Pardali et al., 2017; Sgalla et al., 2018; Spagnolo et al., 2018). Many cell types and signaling pathways are involved in disease pathogenesis. The process of pulmonary fibrosis involves epithelial repair disorders, cell senescence, and immune response disorders. Because redundant cell types, growth factors, and fibrosis pathways are involved in the pathogenesis of the disease,

there is still a lack of effective treatment for the progressive stage of IPF (Spagnolo et al., 2018).

Pirfenidone and Nintedanib, the latest two antifibrotic drugs, can significantly reduce the decline rate of forced vital capacity (FVC) within 1 year in IPF patients with mild and moderate lung function impairment. Moreover, it can reduce the risk of acute exacerbation in IPF patients with mild and moderate lung function impairment. Nintedanib is a small molecular tyrosine kinase inhibitor, which can inhibit platelet-derived growth factor receptor (PDGFR), fibroblast growth factor receptor (FGFR) and vascular endothelial growth factor receptor (VEGFR) on the cell surface. It competitively binds to adenosine triphosphate (ATP) binding sites on these intracellular receptor kinase domains, block intracellular signal transduction and inhibit fibroblast proliferation, migration, and transformation (Richeldi et al., 2017). Pirfenidone is a broad-spectrum anti-fibrotic drug with anti-inflammatory and anti-oxidant effects. Its mechanism is not completely clear (Spagnolo et al., 2020). However, the clinical studies had found that neither these two drugs alleviated the IPF-related symptoms nor improved the overall survival rate of IPF patients (Noble et al., 2011; King et al., 2014; Costabel et al., 2016). Furthermore, although Nintedanib and pirfenidone have good safety in clinical trials, there are still a few patients with adverse reactions, including nausea and vomiting, skin photosensitization, dizziness, and liver function damage (Richeldi et al., 2017). Therefore, we hope to explore more effective drugs for IPF. As with other fibrotic diseases, anti-fibrosis therapy focuses on avoiding tissue damage and eliminating remodeling of tissue parenchyma and function decline resulting from ECM deposition. Accumulating evidence suggests that cyclic nucleotides are involved in the regulation of pulmonary fibrosis.

Cyclic nucleotides cAMP and cGMP are typical second messengers. In the classical paradigm, in response to extracellular stimuli, cAMP or cGMP are respectively synthesized by adenylate cyclase (AC) or guanylate cyclase (GC) located on the plasma membrane, and then spread throughout the cell, where they interact with the specific effector proteins that regulate cell function, such as cell proliferation and differentiation, inflammation, apoptosis and metabolic pathways (Bolger, 2021). Phosphodiesterase (PDEs) is involved in cyclic nucleotide metabolism. So exploring the role of cyclic nucleotides and PDEs in the development of pulmonary fibrosis is helpful for developing anti-fibrosis drugs.

2 Mechanism of cyclic nucleotides regulating fibrosis

cAMP is an essential regulator of fibroblast function. The extracellular stimulators bind to the G protein-coupled receptor (GPCRs) on cell membrane, and adenylate cyclase (AC) responds to the activation of GPCRs to produce cAMP. cAMP enables the transmission of extracellular signals into the cell along defined and specific pathways within the network, allowing for signal regulation inside and outside the cell. This process, referred to as Compartmentalization, is a crucial aspect of cAMP signaling (Zuo et al., 2019a). cAMP participates in regulation mainly through four effectors: PKA (protein kinase A protein kinase, PKA), Epac

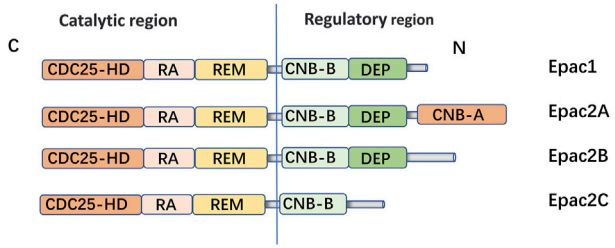

FIGURE 1
Domain architecture of EPAC isoforms: EPAC proteins are single polypeptide molecules which consist of an N-terminal regulatory region and a C-terminal catalytic region. The catalytic region at the C terminus is mainly composed of three structural and: Ras exchange motif (REM), Ras association (RA), CDC25 homology domain [also known as the guanine nucleotide exchange factor for Ras-like small GTPases (RasGEF) domain] responsible for nucleotide exchange activity. The two subtypes had different structures in the N-terminal regulatory region. The Epac2A regulation region contains two CAMP-binding domains, CNB-B and CNB-A. However, Epac1, Epac2A and Epac2B all have Disheveled/Egl-10/pleckstrin (DEP) domains, which are correlated with subcellular localization of Epac. Epac1 is widely expressed in human tissues, such as the hippocampus, thyroid, breast, and lung. EPAC2A is mainly expressed in the central nervous system, pituitary gland and adrenal gland.

(exchange protein activated by cAMP, Epac), cyclic nucleotide-gated (CNG) ion channels, and the Popeye domain-containing protein family (Zuo et al., 2019a). Furthermore, the cAMP/PKA pathway and the cAMP/Epac pathway have been reported the most in pulmonary fibrosis (Liu et al., 2004; Yokoyama et al., 2008; Insel et al., 2012).

The NO-GC-cGMP signaling pathway initiates with the catalytic conversion of arginine and molecular oxygen to NO and citrulline by nitric oxide synthase. After binding of lipophilic NO to sGC in the cytosol, sGC is fully activated and catalyzes the formation of the second messenger cGMP. cGMP can then bind to a variety of effectors to regulate cellular activity.

2.1 The cAMP/Epac pathway

Epac is widely found in lung, brain, and kidneyed. It participates in cAMP-mediated signal transduction by activating Ras-like small GTP enzyme Rap (Kawasaki et al., 1998). In cooperatione with PKA or alone, it undertakes numerous cAMP functions, such as regulating macrophage inflammation, epithelial cell adhesion, fibroblast proliferation, and differentiation. Epac consists of a regulatory region at its N-terminus and a catalytic region at the C-terminus. Based on the differences in the N-terminal regulatory region, Epac can be divided into two subtypes: Epac1 and Epac2 (Figure 1) (Niimura et al., 2009). By comparing pulmonary fibroblasts from normal patients to those from pulmonary fibrotic patients using Western blot, the study demonstrates that Epac1 is primarily expressed in the former group (Huang et al., 2008a). So, Epac1 may be responsible for the anti-fibrosis effect in the lung. Moreover, the lower cAMP concentration prioritizes the Epac pathway's activation (Yokoyama et al., 2008). Based on these findings, Epac appears to be an attractive therapeutic target for the

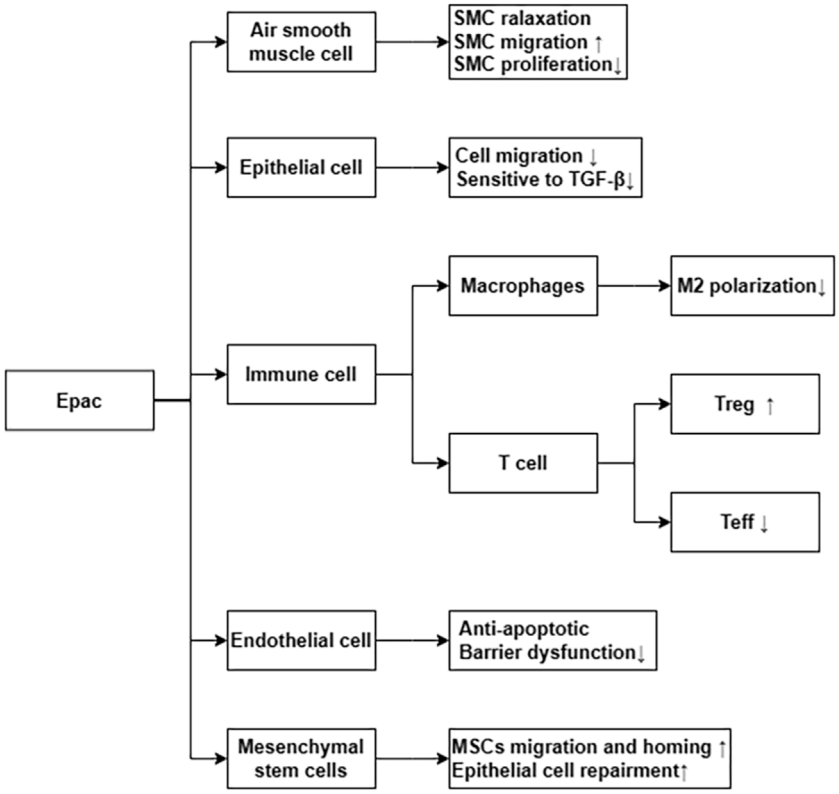

FIGURE 2
Epac *via* differential cellular pathways inhibit the process of IPF. ↑ means increase or upregulated; ↓ means decrease or downregulated.

treatment of pulmonary fibrosis. Epac can regulate the proliferation, migration, and relaxation of airway smooth muscle cells (ASMC) in IPF, thereby correcting dysfunction and retarding the progression of IPF, which may be due to the reduction of RhoA activity by cAMP/Epac/Rap1 signaling (Roscioni et al., 2011; Zieba et al., 2011). Epac agonist promotes endothelial cells (ECs) survival by reducing the activities of pro-apoptotic caspases in a PI3K/Akt and MEK/ERK signalling-dependent manner (Gündüz et al., 2019). Besides, inhibition of MEK/ERK signaling enhances the stabilizing and protective effects of cAMP/Epac activation on endothelial cell barrier, indirectly inhibiting the progression of pulmonary fibrosis (Gündüz et al., 2019). TGF-β is an important profibrotic factor. In lung epithelial cells, EPAC is involved in the inhibition of transforming growth factor-β-dependent cell migration and adhesion, and endogenous TGFRI can form a complex with EPAC1 (Conrotto et al., 2007). In immune cells, Epac also can reverse the polarization of macrophages to pro-fibrotic M2, the mechanism of which remains to be explored (Hartopo et al., 2013). The antifibrotic effect of Epac may be multifaceted. Therefore, the anti-fibrosis mechanism is not well explained (Yokoyama et al., 2008). T cells also play an important role in the development of pulmonary fibrosis. In the early stage of pulmonary fibrosis, the major effector target T cells are regulatory T cells (Tregs). Treg are involved in early pulmonary fibrosis by secreting pro-fibrotic factors such as TGF-β, PDGF (Hou et al., 2017). However, as a homeostatic regulator of the immune response, Tregs can also mediate upstream inflammatory events and indirectly reduce the development of fibrosis by suppressing inflammation and T helper cell responses (Wilson and Wynn, 2009). Therefore, Tregs may have a different role in the process of pulmonary fibrosis at each stage. Epac1 can boosts Treg-mediated suppression effector T-cells (Teffs) while sensitizing Teffs to suppression (Almahariq et al., 2015). So, activation of Treg cells and regulating cAMP/EPAC in T cells may become a new strategy for the prevention and treatment of IPF. Mesenchymal Stem Cells (MSCs) is also involved in pulmonary fibrosis, but the effects are multifaceted. On the one hand, MSCs migrate to sites of lung injury to renew injured epithelial cells (Toonkel et al., 2013). On the other hand, the migration and adhesion of mesenchymal stem cells contribute to their differentiation into myofibroblasts and aggravate pulmonary fibrosis (El Agha et al., 2017). However, MSCs has been suggested as a therapy for the treatment of IPF (Toonkel et al., 2013). cAMP/Epac/Rap1 can promote the homing and migration of MSCs by enhancing stromal cell derived factor 1 (SDF-1), thereby enabling the repair of lung epithelial cells (Toonkel et al., 2013). A summary of the above cell types' correlation with EPAC and IPF is shown in Figure 2.

2.2 The cAMP/PKA pathway

PKA is also involved in the regulation of fibrosis. Endoplasmic reticulum stress (ER stress) contributes to the apoptosis of type II alveolar epithelial cells (AECs), which are involved in the process of

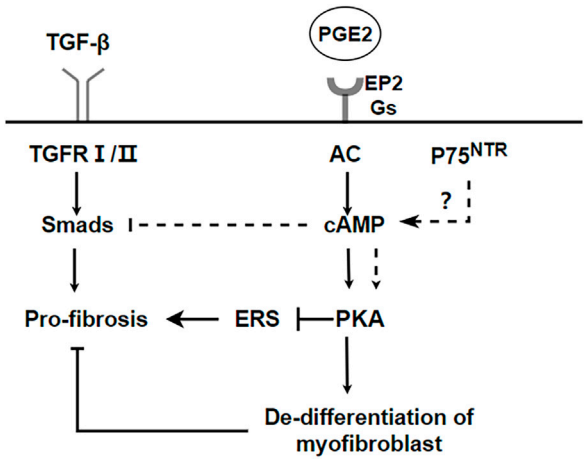

FIGURE 3
PKA pathways inhibit the process of IPF. cAMP/PKA can inhibit endoplasmic reticulum stress and promote dedifferentiation of myofibroblasts to realize anti-fibrosis. $p75^{NTR}$ regulates tissue fibrosis through inhibition of plasminogen activation *via* a PDE4/cAMP/PKA pathway. But it needs to be further verified in pulmonary fibrosis.

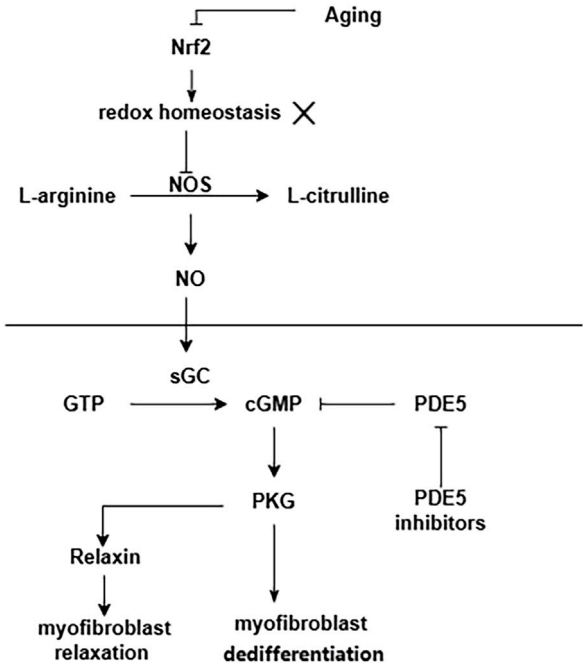

FIGURE 4
NO/sGC-cGMP pathway in pulmonary fibrosis. Aging leads to a decrease in the antioxidant capacity of Nrf2. This pro-oxidant shift results in NOS decoupling and a concurrent decrease in NO signaling and PKG activity.

pulmonary fibrosis (Kropski and Blackwell, 2018; Borok et al., 2020). ER stress stimulates NLRP3 inflammasome activation and promotes the process of lung fibrosis (Stout-Delgado et al., 2016). However, cAMP/PKA is a negative feedback regulator of ER stress-induced NLRP3 inflammasome activation, decreasing ACEⅡ pyroptosis (Hong et al., 2022). Prostaglandin (PG) E2 is a metabolite of arachidonic acid, mainly produced by alveolar epithelial cells and lung fibroblasts (Wilborn et al., 1995). Although it is a proinflammatory factor, it is essential in maintaining lung homeostasis. In the lung, PGE2 inhibits cell migration, proliferation, collagen accumulation, and differentiation into myofibroblasts (Elias et al., 1985; Wilborn et al., 1995; Kohyama et al., 2001). Therefore, PGE2 is considered to be a protective factor in pulmonary fibrosis. The downstream signal transduction of PGE2 is realized by binding to G protein coupled receptor EP1-EP4. However, Gαs-coupled E prostanoid (EP) 2 receptor will lead to an increaseing in cAMP (Huang et al., 2007). Therefore, the antifibrotic effect of PGE2 may be realized by the downstream effect mediated by cAMP.PGE2/Epac1/Rap pathway activation inhibites fibroblast proliferation, whereas PGE2/PKA activation inhibites collagen expression (Huang et al., 2008b). Futhermore, PGE2 can induce de-differentiation of human pulmonary myofibroblasts through cAMP/PKA pathway (Fortier et al., 2021). p75 neurotrophin receptor ($p75^{NTR}$), a TNF receptor superfamily member upregulated after tissue injury, is involved in the regulation of proteolytic activity and fibrin degradation (Sachs et al., 2007). In neuronal tissues, $p75^{NTR}$ regulates tissue fibrosis through inhibition of plasminogen activation *via* a PDE4/cAMP/PKA pathway. However, $p75^{NTR}$ is also expressed in lung inflammation (Renz et al., 2004). Therefore, the $p75^{NTR}$/PDE4/cAMP/PKA pathway it is a potential target for the study of pulmonary fibrosis. Respectively, activating the EPAC and PKA pathways, with the cAMP analogs 8-Me-cAMP and N6-cAMP, can reduce the sensitivity of fibroblasts to TGF-β and the production of myofibroblasts and extracellular matrix (ECM) (Insel et al., 2012). Recently, it has been reported that a new pan-PDE inhibitor shows anti-fibrosis effect in lung tissue by inhibiting the TGF- β signal pathway and activating the cAMP/PKA pathway (Wójcik-Pszczoła et al., 2020). A summary of the above the PKA and IPF is shown in Figure 3.

2.3 NO/SGC-cGMP pathway

cGMP can regulate heart, kidney, and liver fibrosis through the NO/SGC-cGMP pathway (Schinner et al., 2015; Sandner et al., 2017; Flores-Costa et al., 2018; Das et al., 2020). According previous studies, myofibroblasts responsible for lung damage in other ways besides the activity of contraction. The contractile force provides a feedforward mechanism, that maintains the differentiation of myofibroblasts in lung fibrosis. This is accomplished by converting mechanical stimuli into biochemical signals, which drive fibrosis progression (Desmoulière et al., 2005; Hinz, 2007; Wipff et al., 2007; Wynn and Ramalingam, 2012). Relaxin is a peptide hormone that regulates the production and degradation of collagen, and it is responsible for mediating the antifibrotic effects of collagen. Relaxin regulates myosin light chain (MLC20) dephosphorylation and lung myofibroblast contraction through the inactivation of RhoA/Rho-associated protein kinase by a nitric oxide/cGMP/protein kinase G (PKG)—dependent mechanism (Huang et al., 2011). Under conditions of high and persistent guanylyl cyclase activation, the activation of downstream cGMP can also reduce the differentiation of myofibroblasts induced by TGF-β (Dunkern et al., 2007).

TABLE 1 PDE family and Tissue expression.

PDE family	Tissue expression	Disease
PDE1	Significant in cardiac and vascular myocytes, central and peripheral neurons, lymphoid (T and B cells) and myeloid cells Conti and Beavo (2007), Francis et al. (2011), and Keravis and Lugnier (2012)	Alzheimer's disease Cardiovascular disease Le et al. (2022).
PDE2	In the brain, myocytes, liver, adrenal cortex,T cell endothelium and platelets Conti and Beavo (2007), Francis et al. (2011), Keravis and Lugnier (2012), and Michie et al. (1996)	Cardiovascular Diseases Sadek et al. (2020). Cognitive Impairment Abdel-Magid (2017).
PDE3	Cardiac and vascular myocytes, brain, liver, adipose tissues, airway cells Conti and Beavo (2007), Francis et al. (2011), Keravis and Lugnier (2012), and Beute et al. (2018)	Allergic airway inflammation Spagnolo et al. (2018). Age-Related Cognitive Impairment Yanai and Endo (2019) Cardiomyopathy Movsesian (2003).
PDE4	Broad; significant in cells of the cardiovascular, neural, immune and inflammatory systems Conti and Beavo (2007), Francis et al. (2011), and Keravis and Lugnier (2012)	Airway inflammatory diseases: COPD, asthma Phillips (2020). Alzheimer's disease Gurney et al. (2015). Inflammatory bowel disease Li et al. (2022).
PDE5	vascular myocytes, lung, brain, platelets, kidney, gastrointestinal tissues and penis Conti and Beavo (2007), Francis et al. (2011), and Keravis and Lugnier (2012)	Erectile dysfunction Greco et al. (2006). Pulmonary hypertension Barnes et al. (2019). Neurological disorders: Alzheimer's disease Zuccarello et al. (2020), Primary Hippocampal Neuronal Death Xu et al. (2020). Obesity and metabolic syndrome Armani et al. (2011).
PDE6	Photoreceptors and pineal gland Conti and Beavo (2007), Francis et al. (2011), and Keravis and Lugnier (2012)	Retinal diseases Gopalakrishna et al. (2017) and Wang et al. (2018)
PDE7	Spleen, brain, lung and kidney and lymphoid Conti and Beavo (2007), Francis et al. (2011), and Keravis and Lugnier (2012)	Autoimmune Disorders:, autoimmune Hepatitis Świerczek et al. (2021) Central nervous system diseases Chen et al. (2021): Parkinson's disease (PD), Alzheimer's disease (AD), multiple sclerosis (MS),
PDE8	Thyroid, airway smooth muscle, T cell Dong et al. (2006), Conti and Beavo (2007), Francis et al. (2011), Keravis and Lugnier (2012), and Basole et al. (2022)	Inflammatory Dong et al. (2006)
PDE9	Spleen, brain, cardiac, intestinal cells, lower urinary tract, Bender and Beavo (2006), Conti and Beavo (2007), Francis et al. (2011), Keravis and Lugnier (2012), Nagasaki et al. (2012), and Dunkerly-Eyring and Kass (2020)	Obesity and cardiometabolic syndrome Mishra et al. (2021) Alzheimer's Disease Rabal et al. (2019)
PDE10	Brain, pancreatic Conti and Beavo (2007), Francis et al. (2011), and Keravis and Lugnier (2012)	Neurological disorders: Huntington's Disease Models Beaumont et al. (2016), Mental illness: schizophrenia Abdel-Magid (2013)
PDE11	Prostate, testes and salivary and pituitary gland Conti and Beavo (2007), Francis et al. (2011), and Keravis and Lugnier (2012)	Depressive disorder Bollen and Prickaerts (2012)

Senescence is an important factor in the process of pulmonary fibrosis (Schafer et al., 2017; Justice et al., 2019; Otoupalova et al., 2020; Spagnolo et al., 2021a; Yao et al., 2021). Senescent alveolar epithelial cells and lung fibroblasts contribute to pulmonary fibrosis by secreting senescence-associated secretory phenotype (SASP) (Lin and Xu, 2020). Aging is accompanied by the increased oxidative stress and the accumulation of advanced glycation end products (AGEs), both of which are associated with the development of fibrosis (Richter and Kietzmann, 2016). One of the most important regulators of antioxidant genes is NFE2-related factor 2 (Nrf2). The antioxidant capacity of Nrf2 is reduced in the lung fibroblasts of aged mice, which results in a dynamic imbalance of cell redox homeostasis (Hecker et al., 2014). This pro-oxidant shift results in NO synthase (NOS) decoupling and a concurrent decrease in NO signaling and PKG activity (Sampson et al., 2012). Furthermore, in a variety of fibrotic diseases and also during the natural course of aging, NO/cGMP production is low (Sandner et al., 2017). Enhancement of NO/cGMP signaling by sGC stimulators or sGC activators ameliorates the development of fibrosis in various organs and tissues (Sandner et al., 2017). A summary of the above the NO/sGC-cGMP pathway shown in Figure 4.

2.4 Structure and subtype of PDE

PDEs work by hydrolyzing the phosphodiester bonds of the cyclic nucleotides, cyclic adenosine 3′,5′-monophosphate (cAMP) and cyclic guanosine 3′,5′-monophosphate (cGMP), which terminates the downstream signalling of this second messenger. It is subdivided into eleven subtypes based on its diverse structure. Through selective splicing or transcriptional modification of mRNA, these genes produce nearly one hundred PDE isozymes (Azevedo et al., 2014). The structures that make up the PDE superfamily are related but functionally distinct. These differences include tissue distribution, cellular function, primary structure, affinity for cAMP and cGMP, catalytic properties, and responses to specific activators, inhibitors, and effectors and their regulatory mechanisms. PDE4, PDE7, and PDE8 are PDEs that specifically degrade cAMP, while some PDEs specifically degrade cGMP (PDE5, PDE6, and PDE9) (Maurice et al., 2014). Most cells contain more than one PDE family member but in varying amounts, proportions, and subcellular locations. Although PDEs exhibit a broad tissue distribution, some cells are relatively enriched in specific PDEs (Table 1).

PDEs contain two functional regions, regulatory and catalytic. The catalytic region determines the specificity to the substrate or

inhibitor. The amino-terminal regulatory regions of PDEs are highly heterogeneous, reflecting the different cofactors of PDE family members (Maurice et al., 2014). A-kinase anchoring proteins (AKAPs) are anchoring proteins that anchor PKA to specific subcellular sites. AKAPs, PDEs, together, keep cAMP signalling specific and physically compartmentalised. As PDEs are the only route to cyclic nucleotides degradation, the specificity of the temporal and spatial distribution of PDEs ensures the viability of signal transduction. Without PDE-dependent control of local cAMP levels, intracellular cAMP, cGMP would be distributed indiscriminately. As a result, signalling specificity would be lost, as all subpopulations of PKA present in the cell would be activated (Brescia and Zaccolo, 2016). In this scenario, manipulation cyclic nucleotides of levels by specific pharmacological inhibition of individual PDE families is an effective treatment.

3 Studies of different classes of PDE inhibitors in pulmonary fibrosis

3.1 PDE4 inhibitor

PDE4 is a cAMP-specific PDE with relatively high expression levels in cells that regulate immune inflammatory responses and tissue remodeling (Torphy, 1998; Maurice et al., 2014), including macrophage activation (Hertz et al., 2009; Li et al., 2018). Furthermore, primary alveolar A549 cells and human bronchial epithelial (HBE) cells highly express PDE4 (Mata et al., 2005; Oldenburger et al., 2012). The non-selective PDE4 inhibitor Roflusteride is approved for use in severe COPD and acute exacerbations due to its anti-inflammatory properties (Hatzelmann et al., 2010). Studies have shown that PDE4 inhibitors can inhibit the release of fibrogenic factors and alleviate pulmonary fibrosis in a mouse model induced by bleomycin (Cortijo et al., 2009; Udalov et al., 2010; Milara et al., 2015). In transgenic mice expressing diphtheria toxin receptor under the control of the mouse surfactant protein C promoter (a model of pulmonary fibrosis targeting type Ⅱalveolar epithelial injury), PDE4 inhibitor also downregulated plasma levels of selective chemokines, and significantly reduces lung fibrosis induced by targeted type II AEC injury (Sisson et al., 2018). *In vitro*, PDE4 inhibitors inhibites FN-induced aggregation and collagen synthesis of human fetal lung fibroblasts (HFL-1), downregulates the sensitivity of fibroblasts to TGF-β, and promotes the inhibition of fibroblast function by prostaglandin E2 (PGE2) in the presence of PDE4 (Udalov et al., 2010). By decreasing reactive oxygen species, and extracellular signal-regulated kinase phosphorylation, the PDE4 inhibitor Rolipram or PDE4 small interfering RNA effectively inhibits EMT changes in a Smad-independent manner in the human alveolar epithelial type II cell line A549 (Kolosionek et al., 2022). Therefore, PDE4 inhibitors are the potential drug for IPF.

Still, the probability of side effects of non-selective PDE4 inhibitors, such as diarrhea, headache, nausea, and vomiting, makes the use of PDE4 inhibitors in patients limited (Spina, 2008; Maurice et al., 2014). These inhibitors have unfavorable side effects because they inhibit not just one PDE but an entire family of PDEs. It is known as the off-target effect. A coin has two sides, so as the off-target effects. On the one hand, it may increase drug toxicity and cause severe adverse reactions. However, acting with multiple targets may produce synergistic effects that amplify drug effects. For example, methylxanthine theophylline is a purine derivative, and it inhibits almost all types of PDEs. Theophylline can be used in asthma to dilate the bronchi by inhibiting PDE. And its anti-inflammatory actions -- which are mediated *via* inhibition of the nuclear translocation of nuclear factor-κb may be attributed to both PDE inhibition and increased cAMP signaling (Minguet et al., 2005). However, the therapeutic window of theophylline is narrow and toxic symptoms are easy to occur (Jacobs et al., 1976).

According to the difference between the transcriptional initiation site and selective mRNA splice site, PDE4 can be divided into four subtypes of PDE4A-D. In human primary lung fibroblasts (NHLF), PDE4A, B, and D are mainly expressed, while PDE4C is slightly or not present. Knockdown of PDE4B by SiRNA interference resulted in the most significant decrease in overall PDE4 enzyme activity, followed by PDE4A and PDE4D. PDE4B and 4D knockdown can inhibit the expression of α-SMA in TGF-βinduced pulmonary fibroblasts, in which the inhibition of PDE4B knockdown is the most effective, and the effect is similar to the non-selective PDE4 inhibitors (Selige et al., 2011). The adverse effects of PDE4 inhibitors appear to be related to the inhibition of PDE4D (Giembycz, 2001; Maurice et al., 2014). Therefore, PDE4B inhibitors seem to be ideal selective antifibrotic drugs.

BI101550, a PDE4 inhibitor with a high affinity to PDE4B, has anti-inflammatory and anti-fibrosis effects. *In vitro*, BI 1015550 inhibits lipopolysaccharide (LPS) induced TNF-α and phytohemagglutinin induced interleukin-2 synthesis in human peripheral blood mononuclear cells, as well as LPS-induced TNF-α synthesis in human and rat whole blood (Herrmann et al., 2022). In two mouse models of pulmonary fibrosis induced by bleomycin and silica, compared with a low dose (2.5 mg/kg), the higher BI1015550 (12.5 mg/kg b.i.d.) could improve the pulmonary function parameters of mice. High-dose BI1015550 could also significantly improve the content of dense fibrotic tissue in lung tissue. There is a synergistic effect between Nintedanib and BI1015550, which shifts the concentration-response curve to the left (Herrmann et al., 2022). Compared to roflumilast, BI 1015550 seems to be a safer option, and the male *Suncus murinus* is less likely to experience nausea and vomiting as a side effect (Herrmann et al., 2022). In a randomized, double-blind, placebo-controlled study involving 147 patients with IPF, the primary endpoint was the change from baseline in forced vital capacity (FVC) during 12 weeks of treatment with BI1015550 as monotherapy or in combination with antifibrotic background therapy. The trial results showed that BI1015550 at a dose of 18 mg twice daily prevented a decline in lung function in patients with IPF, regardless of background antifibrotic therapy. However, at the same time, the safety of BI1015550 is also of concern, with the most common adverse event being gastrointestinal disease. A case of "suspected IPF exacerbation and suspected vasculitis" was also reported (Richeldi et al., 2022). The adverse reactions need to be further evaluated in subsequent clinical trials. Nevertheless, BI1015550 is currently leading the way in the research and development of new drugs for the treatment of IPF.

There are other types of PDE4 inhibitors reported at present. AA6216 is a novel PDE4 inhibitor. AA6216, also ameliorated pulmonary fibrosis in mice by inhibiting TGF-β release from macrophages. However, in contrast to other PDE4 inhibitors, AA6216 possesses a more potent inhibitory effect with lower risk (Matsuhira et al., 2020). A novel PDE4 inhibitor was obtained by hit-to-lead optimization of natural mangoside based on structure, and its anti-pulmonary fibrosis effect was similar to that of pirfenidone. More importantly, it is safe and has fewer adverse reactions (Huang et al., 2021).

3.2 PDE5 inhibitor

PDE5 hydrolyzes cGMP exclusively. The pharmacological effect of sildenafil, a representative drug of the PDE5 inhibitor, is to increase the intracellular cGMP level by inhibiting cGMP degradation. And then the NO/sGC-cGMP pathway, is used to upregulate potassium channels, inhibit calcium channels, reduce intracellular calcium concentration, and dilate blood vessels. Its clinical indications include pulmonary hypertension (PH) and erectile dysfunction (Giovannoni et al., 2010). Currently, there are many studies on PDE5 inhibitors in pulmonary fibrosis. Due to the degeneration of lung structure that accompanies the progression of pulmonary fibrosis, pulmonary hypertension will eventually develop. In multiple randomized, controlled clinical trials, the addition of sildenafil in the context of antifibrotic agents has not been found to have a significant effect on all-cause mortality, hospitalization, or acute exacerbations (Kolb et al., 2018; Behr et al., 2021; Kang and Song, 2021). But, the efficacy evaluation of sildenafil in IPF is inconsistent (Collard et al., 2007). Since sildenafil improves gas exchange function in patients with severe pulmonary fibrosis by dilating pulmonary vessels, it may be effective in IPF. However, it is still debatable whether pulmonary vessel dilation can improve pulmonary gas exchange function in IPF (Sakao et al., 2019). IPF-related pulmonary arterial hypertension is distinct from idiopathic pulmonary arterial hypertension.

On the one hand, due to the destruction of the alveolar structure, the dysfunction of pulmonary gas exchange results in hypoxic pulmonary vasoconstriction (HPV) (Sylvester et al., 2012; Sakao et al., 2019). Early pulmonary vasoconstriction may be a compensatory mechanism during the development of pulmonary fibrosis. Pulmonary vasoconstriction can maintain the ventilation/perfusion ratio (V/Q) balance. However, continuous pulmonary vasoconstriction will lead to vascular remodeling, resulting in a vicious cycle, which should not be allowed to develop (Sakao et al., 2005; Sakao et al., 2006).

On the other hand, due to the destruction of the alveolar structure in IPF, the respiratory membrane is disordered and thickened, lung diffusion function is decreased, and dilated pulmonary blood vessels will further mismatch V/Q (Sakao et al., 2019). But is it feasible to use PDE5 inhibitors in the early stages of disease, when the structural damage of the lung is not apparent? Due to the insidious onset of IPF, non-specific clinical symptoms, and lack of diagnostic methods with high specificity for early IPF, most patients cannot be correctly diagnosed and treated at an early stage (Spagnolo et al., 2021b). By the time most patients are diagnosed with IPF, there is already apparent structural destruction of the lung. Consequently, there appears to be a lack of research on the potential benefits of initiating PDE5 inhibitor therapy at an early stage of IPF.

Additionally, sildenafil may contribute to pulmonary fibrosis through additional mechanisms. In a rat model of bleomycin-induced pulmonary fibrosis, sildenafil can reduce the oxidative stress level of lung tissue by inhibiting lipid peroxidation, the production and release of cytokines, and the aggregation of neutrophils, so as to achieve the therapeutic effect on pulmonary fibrosis (Yildirim et al., 2010). However, PDE5 inhibitors are not, according to the recommendations of international guidelines, appropriate treatment for IPF (Raghu et al., 2022).

3.3 Non-selective phosphodiesterase inhibitor

Pentoxifylline (PTX) is a methylxanthine derivative and non-selective phosphodiesterase inhibitor. Clinically, it is mainly used to improve peripheral circulation and relieve muscle pain caused by peripheral arterial diseases (Hood et al., 1996; Stevens et al., 2012). Previous studies have demonstrated that PTX can significantly inhibit the secretion of proinflammatory cytokines and the activation of NF-kB, thereby alleviating chronic inflammation (Speer et al., 2017). In RAW264.7 macrophages, the low dose of PTX (10 μg/mL) and the high dose of PTX (300 μg/mL) had different biological effects on cells. Low-dose PTX can reduce endoplasmic reticulum stress (ERS), fibrosis, angiogenesis, and chronic inflammation while promoting RAS/NF-kB signal transduction, proliferation, differentiation, and inflammation. It can also enhance Fas-mediated apoptosis. High doses of PTX, on the other hand, have the opposite effect by preventing RAS/NF-kB signal transduction, which prevents cell proliferation, inflammation, and fibrosis (Seo et al., 2022). It also suggests that PTX is a potential antifibrotic drug. PTX has an anti-fibrosis effect on radiation-induced pulmonary fibrosis by regulating the expression of PKA and PAI-1 (Lee et al., 2017; Wen et al., 2017). Our previous research found that, PTX could influence the expression of fibrosis-related genes in the mouse model of pulmonary fibrosis. In addition, we also found that the expression of senescence-associated secretory phenotype (SASP) decreased in the PTX group (Lin et al., 2022). Therefore, we speculated that PTX might may also alleviate pulmonary fibrosis through anti-aging. mTOR (mechanistic target of rapamycin) is a serine/threonine kinase involved in the integration of multiple metabolic and growth-promoting signals. Accumulating evidence indicates that mTOR activity is necessary for cell senescence (Liu and Sabatini, 2020). A decrease in mTOR activation was also observed after PTX treatment in human melanoma cells (Sharma et al., 2016). So we hypothesized that PTX may achieve its anti-fibrosis effect by affecting the mTOR pathway and changing the autophagy level of senescent cells. But that still needs to be tested. In other fibrosis models, including intestinal fibrosis, hypertrophic scar, and glomerulonephritis, PTX also has an anti-fibrosis effect (Boerma et al., 2008; Ng et al., 2009; Yang et al., 2019; Lee, 2022). The FDA approved PTX in 1984 for the treatment of arteritis. It is currently used to treat stroke because it improves circulation (Bath et al., 2000). So its safety in humans has been verified. “Drug repurposing” is a cost-effective option if the anti-fibrosis ability of PTX can be further developed.

3.4 Pan-PDE inhibitor

Because the antifibrotic effects of inhibitors of specific PDE subtypes are not clearly understood, and given the possible synergistic effects between different subtypes of PDE, the focus of some studies has shifted to dual PDE or pan-PDE inhibitors. Pan-PDE inhibitors represent compounds that can inhibit various isoforms within several PDE classes. Unlike simple PDE inhibitors, pan-PDE can inhibit individual PDE isoforms at the nano and/or micromolar level (Wójcik-Pszczoła et al., 2021). *In vitro* studies have shown that they have promising anti-inflammatory and antifibrotic activities and high inhibitory activity against a selection of PDEs. First, the PAN-PDE has significant inhibitory activity against multiple PDE isoforms, including PDE1, PDE3, PDE4, PDE5, PDE7, and PDE8, which are involved in airway remodeling and the development of pulmonary fibrosis (Wright et al., 1998; Fuhrmann et al., 1999). And next, considering the cAMP signaling compartmentalization during EMT, a different composition of individual isoforms within the cellular compartments cannot be ruled out (Zuo et al., 2019b; Wójcik-Pszczoła et al., 2022). *In vitro*, the pan-PDE inhibitors could inhibit the TGF-β-induced expression of several markers, including vimentin, fibronectin, collagen I, α-smooth muscle actin, N-cadherin, and snail-1 transcription factor in alveolar epithelial type II cells (Wójcik-Pszczoła et al., 2022).

4 Other novel anti-pulmonary fibrosis drugs

At present, there are other types of anti-pulmonary fibrosis drugs under development. The inflammasome NLR Family Pyrin Domain-Containing Protein 3 (NLRP3) is an important regulator of pulmonary inflammation and fibrosis (Colunga Biancatelli et al., 2022). NLRP3 promotes the development of pulmonary fibrosis mainly through the following aspects. Activated NLRP3 promotes fibrosis by producing IL-1 β and IL-18 (Colunga Biancatelli et al., 2022). NLRP3 mediated pyrolysis of csapase-1-dependent alveolar epithelial cells. NLRP3 induced pulmonary mesenchymal stem cells to differentiate into myofibroblasts (Ji et al., 2021). The activation of NLRP3 is increased in pulmonary fibrosis, and inhibition of NLRP3 can effectively delay the progression of pulmonary fibrosis, indicating that targeted NLRP3 may be a new choice for the treatment of pulmonary fibrosis. Although there are several NLRP3 inhibitors in existence, most of these drugs are still in the pre-clinical phase and there is a lack of validated data to confirm that they are indeed effective in pulmonary fibrosis. Furthermore, the indications for NLRP3 inhibitors are unclear. What clinical applications will show the best efficacy for NLRP3-targeting molecules? When, where, how is NLRP3 activated in human disease? To apply NLRP3 to pulmonary fibrosis, these questions need to be addressed.

GSDMD is a key effector of inflammasome signaling, because it controls pyroptosis and the resultant release of proinflammatory cellular contents. Given that GSDMD controls the release of IL-1β downstream of multiple inflammasomes, GSDMD is an attractive target for pulmonary fibrosis. Although, pyroptosis inhibitors will decrease the release of proinflammatory cell contents, they will not block the inflammasome-driven maturation of IL-1β or IL-18. Therefore, its anti-fibrosis effectiveness needs to be further confirmed. Heat-shock protein 90 (HSP) inhibitor, a new drug also developed from the NLRP3 inflammasome. As a multifunctional molecular chaperone, Hsp90 forms a complex with NLRP3 to protect NLRP3 from degrading. In response to stress stimuli, Hsp90 is released, and NLRP3 can be activated to promote inflammation. Hsp90 inhibition block the activation of the NLRP3 inflammasome. Inflammasome blockers show enormous promise as a new generation of anti-inflammatory drugs. However, these treatments are not mature at present, and there is still a long way to go before the real clinical application. Compared with PDEs inhibitors, the PDE inhibitors are more mature. Moreover, there are exact data to prove the effectiveness of PDEs inhibitors in pulmonary fibrosis.

Phosphatidylinositol 3-kinase (PI3K)/protein kinase B (PKB/AKT) signaling pathway plays an important role in IPF. TGF-βand PI3K/AKT promoted the formation of pulmonary fibrosis synergistically. PI3K/AKT can promote pulmonary fibrosis by regulating its downstreams such as mammalian target of rapamycin (mTOR), hypoxia inducible factor-1a (HIF-1a). Therefore, targeting PI3K/AKT has become a new strategy for the treatment of IPF (Conte et al., 2013; Nie et al., 2017). Some PI3K/AKT inhibitors has been investigated in clinical research. Reported treatment-related adverse event mainly include gastrointestinal effects. But for its effectiveness, there is a lack of data at present (Wang et al., 2022). However, PI3K/AKT still considered promising drug candidates for IPF treatment.

5 Discussion

Idiopathic pulmonary fibrosis is the most common type of idiopathic interstitial pneumonia. It is a progressive, irreversible and fatal disease. Its pathological mechanisms are complex and not well understood at present. Therefore, antifibrotic drugs are also limited. Although the current antifibrotic drugs, Pirfenidone and Nintedanib, have a certain therapeutic effect, they do not improve the prognosis of patients. Moreover, their current prices are relatively expensive. Therefore, we need to develop new antifibrotic drugs.

The cAMP signaling pathway is a relatively old signaling pathway, and scientists began to study it as early as 1953 (Zuo et al., 2019b). In the lung, cAMP, and cGMP mainly reduce the sensitivity of fibroblasts to pro-fibrotic factors and decrease the production of myofibroblasts. However, the underlying mechanisms need to be further explored. Our previous study shows that Pentoxifylline can inhibits pulmonary fibrosis by regulating cellular senescence. This suggests that we can study the possible mechanism of cyclic nucleotides against fibrosis from the point of view of aging. In recent years, an increasing number of studies have found that cAMP signalling also plays an important role in age-related cognitive deficits. So, Therefore, studying the role of cyclic nucleotides in pulmonary fibrosis from the perspective of aging may provide new ideas to understand the pathogenesis of pulmonary fibrosis further.

PDEs are involved in the metabolism of cyclic nucleotides, and their inhibitors can increase the intracellular concentration of cyclic nucleotides, thus exerting their anti-fibrotic effects. The “off-target” effect is a problem in the application of drugs, and it is a double-

edged sword. On the one hand, the "off-target" result may have side effects on non-target sites, thus limiting the safe use of the drug. On the other hand, there may be synergistic effects between PDE isoforms, amplifying the drug's therapeutic effects. A novel compound PDE inhibitor, Pan-PDE, is a good example. In contrast, PDE5 inhibitors, although some studies have shown some antifibrotic effects, whether IPF patients really benefit from them needs to be thoroughly evaluated.

Although there are many studies on PDEs inhibitors, most are still in animal experiments, and their effectiveness in humans needs further testing. But it is surprising that BI1O1550, a specific PDE4B inhibitor, has already started clinical trials. This is a big step forward in developing drugs to treat fibrosis.

Author contributions

XY collected the references, and completed the manuscript. SH and JS drew the tables. ZX revised our initial manuscript and provided valuable comments. All authors contributed to the article and approved the submitted version.

Funding

This research was supported by the National Key Research and Development Program of China, grant number 2016YFC1304700.

Conflict of interest

The authors declare that the research was conducted in the absence of any commercial or financial relationships that could be construed as a potential conflict of interest.

Publisher's note

References

Abdel-Magid, A. F. (2013). PDE10 inhibitors as potential treatment for schizophrenia. *ACS Med. Chem. Lett.* 4 (2), 161–162. doi:10.1021/ml4000194

Abdel-Magid, A. F. (2017). Potential treatment of cognitive impairment in schizophrenia by phosphodiesterase 2 (PDE2) inhibitors. *ACS Med. Chem. Lett.* 8 (1), 17–18. doi:10.1021/acsmedchemlett.6b00514

Almahariq, M., Mei, F. C., Wang, H., Cao, A. T., Yao, S., Soong, L., et al. (2015). Exchange protein directly activated by cAMP modulates regulatory T-cell-mediated immunosuppression. *Biochem. J.* 465 (2), 295–303. doi:10.1042/BJ20140952

Armani, A., Marzolla, V., Rosano, G. M. C., Fabbri, A., and Caprio, M. (2011). Phosphodiesterase type 5 (PDE5) in the adipocyte: A novel player in fat metabolism? *Trends Endocrinol. Metab.* 22 (10), 404–411. doi:10.1016/j.tem.2011.05.004

Azevedo, M. F., Faucz, F. R., Bimpaki, E., Horvath, A., Levy, I., de Alexandre, R. B., et al. (2014). Clinical and molecular genetics of the phosphodiesterases (PDEs). *Endocr. Rev.* 35 (2), 195–233. doi:10.1210/er.2013-1053

Barnes, H., Brown, Z., Burns, A., and Williams, T. (2019). Phosphodiesterase 5 inhibitors for pulmonary hypertension. *Cochrane Database Syst. Rev.* 1 (1), Cd012621. doi:10.1002/14651858.CD012621.pub2

Basole, C. P., Nguyen, R. K., Lamothe, K., Billis, P., Fujiwara, M., Vang, A. G., et al. (2022). Treatment of experimental autoimmune encephalomyelitis with an inhibitor of phosphodiesterase-8 (PDE8). *Cells* 11 (4), 660. doi:10.3390/cells11040660

Bath, P. M., Bath, F. J., and Asplund, K. (2000). Pentoxifylline, propentofylline and pentifylline for acute ischaemic stroke. *Pentoxifylline, propentofylline pentifylline acute Ischaem. stroke Cochrane Database Syst Rev* (3), Cd000162. doi:10.1002/14651858.CD000162

Beaumont, V., Zhong, S., Lin, H., Xu, W., Bradaia, A., Steidl, E., et al. (2016). Phosphodiesterase 10A inhibition improves cortico-basal ganglia function in huntington's disease models. *Neuron* 92 (6), 1220–1237. doi:10.1016/j.neuron.2016.10.064

Behr, J., Nathan, S. D., Wuyts, W. A., Mogulkoc Bishop, N., Bouros, D. E., Antoniou, K., et al. (2021). Efficacy and safety of sildenafil added to pirfenidone in patients with advanced idiopathic pulmonary fibrosis and risk of pulmonary hypertension: A double-blind, randomised, placebo-controlled, phase 2b trial. *Lancet. Respir. Med.* 9 (1), 85–95. doi:10.1016/S2213-2600(20)30356-8

Bender, A. T., and Beavo, J. A. (2006). Cyclic nucleotide phosphodiesterases: Molecular regulation to clinical use. *Pharmacol. Rev.* 58 (3), 488–520. doi:10.1124/pr.58.3.5

Beute, J., Lukkes, M., Koekoek, E. P., Nastiti, H., Ganesh, K., de Bruijn, M. J., et al. (2018). A pathophysiological role of PDE3 in allergic airway inflammation. *JCI Insight* 3 (2), e94888. doi:10.1172/jci.insight.94888

Boerma, M., Roberto, K. A., and Hauer-Jensen, M. (2008). Prevention and treatment of functional and structural radiation injury in the rat heart by pentoxifylline and alpha-tocopherol. *Int. J. Radiat. Oncol. Biol. Phys.* 72 (1), 170–177. doi:10.1016/j.ijrobp.2008.04.042

Bolger, G. B. (2021). The PDE-opathies: Diverse phenotypes produced by a functionally related multigene family. *Trends Genet.* 37 (7), 669–681. doi:10.1016/j.tig.2021.03.002

Bollen, E., and Prickaerts, J. (2012). Phosphodiesterases in neurodegenerative disorders. *IUBMB Life* 64 (12), 965–970. doi:10.1002/iub.1104

Borok, Z., Horie, M., Flodby, P., Wang, H., Liu, Y., Ganesh, S., et al. (2020). Grp78 loss in epithelial progenitors reveals an age-linked role for endoplasmic reticulum stress in pulmonary fibrosis. *Am. J. Respir. Crit. Care Med.* 201 (2), 198–211. doi:10.1164/rccm.201902-0451OC

Brescia, M., and Zaccolo, M. (2016). Modulation of compartmentalised cyclic nucleotide signalling via local inhibition of phosphodiesterase activity. *Int. J. Mol. Sci.* 17 (10), 1672. doi:10.3390/ijms17101672

Chen, Y., Wang, H., Wang, W. Z., Wang, D., Skaggs, K., and Zhang, H. T. (2021). Phosphodiesterase 7(PDE7): A unique drug target for central nervous system diseases. *Neuropharmacology* 196, 108694. doi:10.1016/j.neuropharm.2021.108694

Collard, H. R., Anstrom, K. J., Schwarz, M. I., and Zisman, D. A. (2007). Sildenafil improves walk distance in idiopathic pulmonary fibrosis. *Chest* 131 (3), 897–899. doi:10.1378/chest.06-2101

Colunga Biancatelli, R. M. L., Solopov, P. A., and Catravas, J. D. (2022). The inflammasome NLR family Pyrin domain-containing protein 3 (NLRP3) as a novel therapeutic target for idiopathic pulmonary fibrosis. *Am. J. Pathol.* 192 (6), 837–846. doi:10.1016/j.ajpath.2022.03.003

Conrotto, P., Yakymovych, I., Yakymovych, M., and Souchelnytskyi, S. (2007). Interactome of transforming growth factor-beta type I receptor (TbetaRI): Inhibition of TGFbeta signaling by Epac1. *J. Proteome Res.* 6 (1), 287–297. doi:10.1021/pr060427q

Conte, E., Gili, E., Fruciano, M., Korfei, M., Fagone, E., Iemmolo, M., et al. (2013). PI3K p110γ overexpression in idiopathic pulmonary fibrosis lung tissue and fibroblast cells: *In vitro* effects of its inhibition. *Laboratory Investigation; a J. Tech. Methods Pathology* 93 (5), 566–576. doi:10.1038/labinvest.2013.6

Conti, M., and Beavo, J. (2007). Biochemistry and physiology of cyclic nucleotide phosphodiesterases: Essential components in cyclic nucleotide signaling. *Annu. Rev. Biochem.* 76, 481–511. doi:10.1146/annurev.biochem.76.060305.150444

Cortijo, J., IrAnzo, A., Milara, X., Mata, M., Cerda-Nicolas, M., Ruiz-Sauri, A., et al. (2009). Roflumilast, a phosphodiesterase 4 inhibitor, alleviates bleomycin-induced lung injury. *Br. J. Pharmacol.* 156 (3), 534–544. doi:10.1111/j.1476-5381.2008.00041.x

Costabel, U., Inoue, Y., Richeldi, L., Collard, H. R., Tschoepe, I., Stowasser, S., et al. (2016). Efficacy of Nintedanib in idiopathic pulmonary fibrosis across prespecified subgroups in INPULSIS. *Am. J. Respir. Crit. Care Med.* 193 (2), 178–185. doi:10.1164/rccm.201503-0562OC

Craig, V. J., Zhang, L., Hagood, J. S., and Owen, C. A. (2015). Matrix metalloproteinases as therapeutic targets for idiopathic pulmonary fibrosis. *Am. J. Respir. Cell Mol. Biol.* 53 (5), 585–600. doi:10.1165/rcmb.2015-0020TR

Das, S., Neelamegam, K., Peters, W. N., Periyasamy, R., and Pandey, K. N. (2020). Depletion of cyclic-GMP levels and inhibition of cGMP-dependent protein kinase activate p21(Cip1)/p27(Kip1) pathways and lead to renal fibrosis and dysfunction. *Faseb J.* 34 (9), 11925–11943. doi:10.1096/fj.202000754R

Desmoulière, A., Chaponnier, C., and Gabbiani, G. (2005). Tissue repair, contraction, and the myofibroblast. *Wound Repair Regen.* 13 (1), 7–12. doi:10.1111/j.1067-1927.2005.130102.x

Dong, H., Osmanova, V., Epstein, P. M., and Brocke, S. (2006). Phosphodiesterase 8 (PDE8) regulates chemotaxis of activated lymphocytes. *Biochem. Biophys. Res. Commun.* 345 (2), 713–719. doi:10.1016/j.bbrc.2006.04.143

Dunkerly-Eyring, B., and Kass, D. A. (2020). Myocardial phosphodiesterases and their role in cGMP regulation. *J. Cardiovasc Pharmacol.* 75 (6), 483–493. doi:10.1097/FJC.0000000000000773

Dunkern, T. R., Feurstein, D., Rossi, G. A., Sabatini, F., and Hatzelmann, A. (2007). Inhibition of TGF-beta induced lung fibroblast to myofibroblast conversion by phosphodiesterase inhibiting drugs and activators of soluble guanylyl cyclase. *Eur. J. Pharmacol.* 572 (1), 12–22. doi:10.1016/j.ejphar.2007.06.036

El Agha, E., Kramann, R., Schneider, R. K., Li, X., Seeger, W., Humphreys, B. D., et al. (2017). Mesenchymal stem cells in fibrotic disease. *Cell Stem Cell* 21 (2), 166–177. doi:10.1016/j.stem.2017.07.011

Elias, J. A., Rossman, M. D., Zurier, R. B., and Daniele, R. P. (1985). Human alveolar macrophage inhibition of lung fibroblast growth - a prostaglandin-dependent process. *Am. Rev. Respir. Dis.* 131 (1), 94–99. doi:10.1164/arrd.1985.131.1.94

Flores-Costa, R., Alcaraz-Quiles, J., Titos, E., Lopez-Vicario, C., Casulleras, M., Duran-Guell, M., et al. (2018). The soluble guanylate cyclase stimulator IW-1973 prevents inflammation and fibrosis in experimental non-alcoholic steatohepatitis. *Br. J. Pharmacol.* 175 (6), 953–967. doi:10.1111/bph.14137

Fortier, S. M., Penke, L. R., King, D., Pham, T. X., Ligresti, G., and Peters-Golden, M. (2021). Myofibroblast dedifferentiation proceeds via distinct transcriptomic and phenotypic transitions. *JCI Insight* 6 (6), e144799. doi:10.1172/jci.insight.144799

Francis, S. H., Blount, M. A., and Corbin, J. D. (2011). Mammalian cyclic nucleotide phosphodiesterases: Molecular mechanisms and physiological functions. *Physiol. Rev.* 91 (2), 651–690. doi:10.1152/physrev.00030.2010

Fuhrmann, M., Jahn, H. U., Seybold, J., Neurohr, C., Barnes, P. J., HippenStiel, S., et al. (1999). Identification and function of cyclic nucleotide phosphodiesterase isoenzymes in airway epithelial cells. *Am. J. Respir. Cell Mol. Biol.* 20 (2), 292–302. doi:10.1165/ajrcmb.20.2.3140

Giembycz, M. A. (2001). Cilomilast: A second generation phosphodiesterase 4 inhibitor for asthma and chronic obstructive pulmonary disease. *Expert Opin. Investig. Drugs* 10 (7), 1361–1379. doi:10.1517/13543784.10.7.1361

Giovannoni, M. P., Vergelli, C., GrAziAno, A., and Dal Piaz, V. (2010). PDE5 inhibitors and their applications. *Curr. Med. Chem.* 17 (24), 2564–2587. doi:10.2174/092986710791859360

Gopalakrishna, K. N., Boyd, K., and Artemyev, N. O. (2017). Mechanisms of mutant PDE6 proteins underlying retinal diseases. *Cell Signal* 37, 74–80. doi:10.1016/j.cellsig.2017.06.002

Greco, E. A., Spera, G., and Aversa, A. (2006). Combining testosterone and PDE5 inhibitors in erectile dysfunction: Basic rationale and clinical evidences. *Eur. Urol.* 50 (5), 940–947. doi:10.1016/j.eururo.2006.06.049

Gündüz, D., Troidl, C., Tanislav, C., Rohrbach, S., Hamm, C., and Aslam, M. (2019). Role of PI3K/akt and MEK/ERK signalling in cAMP/epac-mediated endothelial barrier stabilisation. *Front. Physiology* 10, 1387. doi:10.3389/fphys.2019.01387

Gurney, M. E., D'Amato, E. C., and Burgin, A. B. (2015). Phosphodiesterase-4 (PDE4) molecular pharmacology and Alzheimer's disease. *Neurotherapeutics* 12 (1), 49–56. doi:10.1007/s13311-014-0309-7

Hartopo, A. B., Emoto, N., Vignon-Zellweger, N., Suzuki, Y., Yagi, K., Nakayama, K., et al. (2013). Endothelin-converting enzyme-1 gene ablation attenuates pulmonary fibrosis via CGRP-cAMP/EPAC1 pathway. *Am. J. Respir. Cell Mol. Biol.* 48 (4), 465–476. doi:10.1165/rcmb.2012-0354OC

Hatzelmann, A., Morcillo, E. J., Lungarella, G., Adnot, S., Sanjar, S., Beume, R., et al. (2010). The preclinical pharmacology of roflumilast--a selective, oral phosphodiesterase 4 inhibitor in development for chronic obstructive pulmonary disease. *Pulm. Pharmacol. Ther.* 23 (4), 235–256. doi:10.1016/j.pupt.2010.03.011

Hecker, L., Logsdon, N. J., Kurundkar, D., Kurundkar, A., Bernard, K., Hock, T., et al. (2014). Reversal of persistent fibrosis in aging by targeting Nox4-Nrf2 redox imbalance. *Sci. Transl. Med.* 6 (231), 231ra47. doi:10.1126/scitranslmed.3008182

Herrmann, F. E., Wollin, L., and Nickolaus, P. (2022). BI 1015550 is a PDE4B inhibitor and a clinical drug candidate for the oral treatment of idiopathic pulmonary fibrosis. *Front. Pharmacol.* 13, 838449. doi:10.3389/fphar.2022.838449

Hertz, A. L., Bender, A. T., Smith, K. C., Gilchrist, M., Amieux, P. S., Aderem, A., et al. (2009). Elevated cyclic AMP and PDE4 inhibition induce chemokine expression in human monocyte-derived macrophages. *Proc. Natl. Acad. Sci. U. S. A.* 106 (51), 21978–21983. doi:10.1073/pnas.0911684106

Hinz, B. (2007). Formation and function of the myofibroblast during tissue repair. *J. Invest. Dermatol* 127 (3), 526–537. doi:10.1038/sj.jid.5700613

Hong, Q., Zhang, Y., Lin, W., Wang, W., Yuan, Y., Lin, J., et al. (2022). Negative feedback of the cAMP/PKA pathway regulates the effects of endoplasmic reticulum stress-induced NLRP3 inflammasome activation on type II alveolar epithelial cell pyroptosis as a novel mechanism of BLM-induced pulmonary fibrosis. *J. Immunol. Res.* 2022, 2291877. doi:10.1155/2022/2291877

Hood, S. C., Moher, D., and Barber, G. G. (1996). Management of intermittent claudication with pentoxifylline: meta-analysis of randomized controlled trials. *Cmaj* 155 (8), 1053–1059.

Hou, Z., Ye, Q., Qiu, M., Hao, Y., Han, J., and Zeng, H. (2017). Increased activated regulatory T cells proportion correlate with the severity of idiopathic pulmonary fibrosis. *Respir. Res.* 18 (1), 170. doi:10.1186/s12931-017-0653-3

Huang, S. K., Wettlaufer, S. H., Chung, J., and Peters-Golden, M. (2008). Prostaglandin E2 inhibits specific lung fibroblast functions via selective actions of PKA and Epac-1. *Am. J. Respir. Cell Mol. Biol.* 39 (4), 482–489. doi:10.1165/rcmb.2008-0080OC

Huang, S. K., Wettlaufer, S. H., Chung, J., and Peters-Golden, M. (2008). Prostaglandin E2 inhibits specific lung fibroblast functions via selective actions of PKA and Epac-1. *Am. J. Respir. Cell Mol. Biol.* 39 (4), 482–489. doi:10.1165/rcmb.2008-0080OC

Huang, S., Wettlaufer, S. H., Hogaboam, C., Aronoff, D. M., and Peters-Golden, M. (2007). Prostaglandin E(2) inhibits collagen expression and proliferation in patient-derived normal lung fibroblasts via E prostanoid 2 receptor and cAMP signaling. *Am. J. Physiology. Lung Cell. Mol. Physiology* 292 (2), L405–L413. doi:10.1152/ajplung.00232.2006

Huang, X., Gai, Y., Yang, N., Lu, B., Samuel, C. S., Thannickal, V. J., et al. (2011). Relaxin regulates myofibroblast contractility and protects against lung fibrosis. *Am. J. Pathology* 179 (6), 2751–2765. doi:10.1016/j.ajpath.2011.08.018

Huang, Y. Y., Deng, J., Tian, Y. J., Liang, J., Xie, X., Huang, Y., et al. (2021). Mangostanin derivatives as novel and orally active phosphodiesterase 4 inhibitors for the treatment of idiopathic pulmonary fibrosis with improved safety. *J. Med. Chem.* 64 (18), 13736–13751. doi:10.1021/acs.jmedchem.1c01085

Insel, P. A., Murray, F., Yokoyama, U., Romano, S., Yun, H., Brown, L., et al. (2012). cAMP and Epac in the regulation of tissue fibrosis. *Br. J. Pharmacol.* 166 (2), 447–456. doi:10.1111/j.1476-5381.2012.01847.x

Jacobs, M. H., Senior, R. M., and Kessler, G. (1976). Clinical experience with theophylline. Relarionships between dosage, serum concentration, and toxicity. *JAMA* 235 (18), 1983–1986. doi:10.1001/jama.235.18.1983

Ji, J., Hou, J., Xia, Y., Xiang, Z., and Han, X. (2021). NLRP3 inflammasome activation in alveolar epithelial cells promotes myofibroblast differentiation of lung-resident mesenchymal stem cells during pulmonary fibrogenesis. *Biochim. Biophys. Acta Mol. Basis Dis.* 1867 (5), 166077. doi:10.1016/j.bbadis.2021.166077

Justice, J. N., Nambiar, A. M., Tchkonia, T., LeBrasseur, N. K., Pascual, R., Hashmi, S. K., et al. (2019). Senolytics in idiopathic pulmonary fibrosis: Results from a first-in-human, open-label, pilot study. *EBioMedicine* 40, 554–563. doi:10.1016/j.ebiom.2018.12.052

Kang, J., and Song, J. W. (2021). Effect of sildenafil added to antifibrotic treatment in idiopathic pulmonary fibrosis. *Sci. Rep.* 11 (1), 17824. doi:10.1038/s41598-021-97396-z

Kawasaki, H., Springett, G. M., Mochizuki, N., Toki, S., Nakaya, M., Matsuda, M., et al. (1998). A family of cAMP-binding proteins that directly activate Rap1. *Sci. (New York, N.Y.)* 282 (5397), 2275–2279. doi:10.1126/science.282.5397.2275

Keravis, T., and Lugnier, C. (2012). Cyclic nucleotide phosphodiesterase (PDE) isozymes as targets of the intracellular signalling network: Benefits of PDE inhibitors in various diseases and perspectives for future therapeutic developments. *Br. J. Pharmacol.* 165 (5), 1288–1305. doi:10.1111/j.1476-5381.2011.01729.x

King, T. E., Bradford, W. Z., Castro-Bernardini, S., Fagan, E. A., Glaspole, I., Glassberg, M. K., et al. (2014). A phase 3 trial of pirfenidone in patients with idiopathic pulmonary fibrosis. *N. Engl. J. Med.* 370 (22), 2083–2092. doi:10.1056/NEJMoa1402582

King, T. E., Pardo, A., and Selman, M. (2011). Idiopathic pulmonary fibrosis. *Lancet* 378 (9807), 1949–1961. doi:10.1016/S0140-6736(11)60052-4

Kohyama, T., Ertl, R. F., Valenti, V., Spurzem, J., KawaMoto, M., Nakamura, Y., et al. (2001). Prostaglandin E-2 inhibits fibroblast chemotaxis. *Am. J. Physiology-Lung Cell. Mol. Physiology* 281 (5), L1257–L1263. doi:10.1152/ajplung.2001.281.5.L1257

Kolb, M., Raghu, G., Wells, A. U., Behr, J., Richeldi, L., Schinzel, B., et al. (2018). Nintedanib plus sildenafil in patients with idiopathic pulmonary fibrosis. *N. Engl. J. Med.* 379 (18), 1722–1731. doi:10.1056/NEJMoa1811737

Kolosionek, E., Savai, R., Ghofrani, H. A., Weissmann, N., Guenther, A., Grimminger, F., et al. (2022). Expression and activity of phosphodiesterase isoforms during epithelial mesenchymal transition: The role of phosphodiesterase 4. *Mol. Biol. Cell* 33 (9), cor2. cor2. doi:10.1091/mbc.E09-01-0019_corr

Kropski, J. A., and Blackwell, T. S. (2018). Endoplasmic reticulum stress in the pathogenesis of fibrotic disease. *J. Clin. Invest.* 128 (1), 64–73. doi:10.1172/JCI93560

Le, M.-L., Jiang, M. Y., Han, C., Yang, Y. Y., and Wu, Y. (2022). PDE1 inhibitors: A review of the recent patent literature (2008-present). *Expert Opin. Ther. Pat.* 32 (4), 423–439. doi:10.1080/13543776.2022.2027910

Lee, H. J. (2022). Therapeutic potential of the combination of pentoxifylline and vitamin-E in inflammatory bowel disease: Inhibition of intestinal fibrosis. *J. Clin. Med.* 11 (16), 4713. doi:10.3390/jcm11164713

Lee, J. G., Shim, S., Kim, M. J., Myung, J. K., Jang, W. S., Bae, C. H., et al. (2017). Pentoxifylline regulates plasminogen activator inhibitor-1 expression and protein kinase A phosphorylation in radiation-induced lung fibrosis. *Biomed. Res. Int.* 2017, 1279280. doi:10.1155/2017/1279280

Li, H., Zhang, Y., Liu, M., Fan, C., Feng, C., Lu, Q., et al. (2022). Targeting PDE4 as a promising therapeutic strategy in chronic ulcerative colitis through modulating mucosal homeostasis. *Acta Pharm. Sin. B* 12 (1), 228–245. doi:10.1016/j.apsb.2021.04.007

Li, H., Zuo, J. P., and Tang, W. (2018). Phosphodiesterase-4 inhibitors for the treatment of inflammatory diseases. *Front. Pharmacol.* 9, 1048. doi:10.3389/fphar.2018.01048

Lin, Y., and Xu, Z. (2020). Fibroblast senescence in idiopathic pulmonary fibrosis. *Front. Cell Dev. Biol.* 8, 593283. doi:10.3389/fcell.2020.593283

Lin, Y., Xu, Z., Zhou, B., Ma, K., and Jiang, M. (2022). Pentoxifylline inhibits pulmonary fibrosis by regulating cellular senescence in mice. *Front. Pharmacol.* 13, 848263. doi:10.3389/fphar.2022.848263

Liu, G. Y., and Sabatini, D. M. (2020). mTOR at the nexus of nutrition, growth, ageing and disease. *Nat. Rev. Mol. Cell Biol.* 21 (4), 183–203. doi:10.1038/s41580-019-0199-y

Liu, X., Ostrom, R. S., and Insel, P. A. (2004). cAMP-elevating agents and adenylyl cyclase overexpression promote an antifibrotic phenotype in pulmonary fibroblasts. *Am. J. Physiology. Cell Physiology* 286 (5), C1089–C1099. doi:10.1152/ajpcell.00461.2003

Lok, S. S., Stewart, J. P., Kelly, B. G., Hasleton, P. S., and Egan, J. J. (2001). Epstein-Barr virus and wild p53 in idiopathic pulmonary fibrosis. *Respir. Med.* 95 (10), 787–791. doi:10.1053/rmed.2001.1152

Maher, T. M., Wells, A. U., and Laurent, G. J. (2007). Idiopathic pulmonary fibrosis: Multiple causes and multiple mechanisms? *Eur. Respir. J.* 30 (5), 835–839. doi:10.1183/09031936.00069307

Margaritopoulos, G. A., RoMagnoli, M., Poletti, V., Siafakas, N. M., Wells, A. U., and Antoniou, K. M. (2012). Recent advances in the pathogenesis and clinical evaluation of pulmonary fibrosis. *Eur. Respir. Rev.* 21 (123), 48–56. doi:10.1183/09059180.00007611

Mata, M., Sarria, B., BuenestAdo, A., CortiJo, J., Cerda, M., and Morcillo, E. J. (2005). Phosphodiesterase 4 inhibition decreases MUC5AC expression induced by epidermal growth factor in human airway epithelial cells. *Thorax* 60 (2), 144–152. doi:10.1136/thx.2004.025692

Matsuhira, T., Nishiyama, O., Tabata, Y., Kaji, C., Kubota-Ishida, N., Chiba, Y., et al. (2020). A novel phosphodiesterase 4 inhibitor, AA6216, reduces macrophage activity and fibrosis in the lung. *Eur. J. Pharmacol.* 885, 173508. doi:10.1016/j.ejphar.2020.173508

Maurice, D. H., Ke, H., Ahmad, F., Wang, Y., Chung, J., and Manganiello, V. C. (2014). Advances in targeting cyclic nucleotide phosphodiesterases. *Nat. Rev. Drug Discov.* 13 (4), 290–314. doi:10.1038/nrd4228

Michie, A. M., Lobban, M., Muller, T., Harnett, M. M., and Houslay, M. D. (1996). Rapid regulation of PDE-2 and PDE-4 cyclic AMP phosphodiesterase activity following ligation of the T cell antigen receptor on thymocytes: Analysis using the selective inhibitors erythro-9-(2-hydroxy-3-nonyl)-adenine (EHNA) and rolipram. *Cell Signal* 8 (2), 97–110. doi:10.1016/0898-6568(95)02032-2

Milara, J., Morcillo, E., Monleon, D., Tenor, H., and Cortijo, J. (2015). Roflumilast prevents the metabolic effects of bleomycin-induced fibrosis in a murine model. *PloS One* 10 (7), e0133453. doi:10.1371/journal.pone.0133453

Minguet, S., Huber, M., Rosenkranz, L., Schamel, W. W. A., Reth, M., and Brummer, T. (2005). Adenosine and cAMP are potent inhibitors of the NF-kappa B pathway downstream of immunoreceptors. *Eur. J. Immunol.* 35 (1), 31–41. doi:10.1002/eji.200425524

Mishra, S., Sadagopan, N., Dunkerly-Eyring, B., Rodriguez, S., Sarver, D. C., Ceddia, R. P., et al. (2021). Inhibition of phosphodiesterase type 9 reduces obesity and cardiometabolic syndrome in mice. *J. Clin. Invest.* 131 (21), e148798. doi:10.1172/JCI148798

Movsesian, M. A. (2003). PDE3 inhibition in dilated cardiomyopathy: Reasons to reconsider. *J. Card. Fail* 9 (6), 475–480. doi:10.1016/s1071-9164(03)00135-0

Nagasaki, S., Nakano, Y., Masuda, M., Ono, K., Miki, Y., Shibahara, Y., et al. (2012). Phosphodiesterase type 9 (PDE9) in the human lower urinary tract: An immunohistochemical study. *BJU Int.* 109 (6), 934–940. doi:10.1111/j.1464-410X.2011.10429.x

Ng, Y. Y., Chen, Y. M., Tsai, T. J., Lan, X. R., Yang, W. C., and Lan, H. Y. (2009). Pentoxifylline inhibits transforming growth factor-beta signaling and renal fibrosis in experimental crescentic glomerulonephritis in rats. *Am. J. Nephrol.* 29 (1), 43–53. doi:10.1159/000150600

Nie, Y., Sun, L., Wu, Y., Yang, Y., Wang, J., He, H., et al. (2017). AKT2 regulates pulmonary inflammation and fibrosis via modulating macrophage activation. *J. Immunol. Baltim. Md, 1950)* 198 (11), 4470–4480. doi:10.4049/jimmunol.1601503

Niimura, M., Miki, T., Shibasaki, T., Fujimoto, W., Iwanaga, T., and Seino, S. (2009). Critical role of the N-terminal cyclic AMP-binding domain of Epac2 in its subcellular localization and function. *J. Cell. Physiology* 219 (3), 652–658. doi:10.1002/jcp.21709

Noble, P. W., Albera, C., Bradford, W. Z., Costabel, U., Glassberg, M. K., Kardatzke, D., et al. (2011). Pirfenidone in patients with idiopathic pulmonary fibrosis (CAPACITY): Two randomised trials. *Lancet* 377 (9779), 1760–1769. doi:10.1016/S0140-6736(11)60405-4

Oldenburger, A., Maarsingh, H., and Schmidt, M. (2012). Multiple facets of cAMP signalling and physiological impact: cAMP compartmentalization in the lung. *Pharm. (Basel)* 5 (12), 1291–1331. doi:10.3390/ph5121291

Otoupalova, E., Smith, S., Cheng, G., and Thannickal, V. J. (2020). Oxidative stress in pulmonary fibrosis. *Compr. Physiol.* 10 (2), 509–547. doi:10.1002/cphy.c190017

Pardali, E., Sanchez-Duffhues, G., Gomez-Puerto, M. C., and Ten Dijke, P. (2017). TGF-beta-Induced endothelial-mesenchymal transition in fibrotic diseases. *Int. J. Mol. Sci.* 18 (10), 2157. doi:10.3390/ijms18102157

Phillips, J. E. (2020). Inhaled phosphodiesterase 4 (PDE4) inhibitors for inflammatory respiratory diseases. *Front. Pharmacol.* 11, 259. doi:10.3389/fphar.2020.00259

Rabal, O., Sanchez-Arias, J. A., Cuadrado-Tejedor, M., de Miguel, I., Perez-Gonzalez, M., Garcia-Barroso, C., et al. (2019). Multitarget approach for the treatment of alzheimer's disease: Inhibition of phosphodiesterase 9 (PDE9) and histone deacetylases (HDACs) covering diverse selectivity profiles. *ACS Chem. Neurosci.* 10 (9), 4076–4101. doi:10.1021/acschemneuro.9b00303

Raghu, G., Remy-Jardin, M., Richeldi, L., Thomson, C. C., Inoue, Y., Johkoh, T., et al. (2022). Idiopathic pulmonary fibrosis (an update) and progressive pulmonary fibrosis in adults: An official ATS/ERS/JRS/ALAT clinical practice guideline. *Am. J. Respir. Crit. Care Med.* 205 (9), e18–e47. doi:10.1164/rccm.202202-0399ST

Renz, H., Kerzel, S., and Nockher, W. A. (2004). The role of neurotrophins in bronchial asthma: Contribution of the pan-neurotrophin receptor p75. *Prog. Brain Res.* 146, 325–333. doi:10.1016/s0079-6123(03)46020-2

Richeldi, L., Azuma, A., Cottin, V., Hesslinger, C., Stowasser, S., Valenzuela, C., et al. (2022). Trial of a preferential phosphodiesterase 4B inhibitor for idiopathic pulmonary fibrosis. *N. Engl. J. Med.* 386, 2178–2187. doi:10.1056/NEJMoa2201737

Richeldi, L., Collard, H. R., and Jones, M. G. (2017). Idiopathic pulmonary fibrosis. *Lancet* 389 (10082), 1941–1952. doi:10.1016/S0140-6736(17)30866-8

Richter, K., and Kietzmann, T. (2016). Reactive oxygen species and fibrosis: Further evidence of a significant liaison. *Cell Tissue Res.* 365 (3), 591–605. doi:10.1007/s00441-016-2445-3

Roscioni, S. S., Maarsingh, H., Elzinga, C. R. S., Schuur, J., Menzen, M., Halayko, A. J., et al. (2011). Epac as a novel effector of airway smooth muscle relaxation. *J. Cell. Mol. Med.* 15 (7), 1551–1563. doi:10.1111/j.1582-4934.2010.01150.x

Sachs, B. D., Baillie, G. S., McCall, J. R., Passino, M. A., Schachtrup, C., Wallace, D. A., et al. (2007). p75 neurotrophin receptor regulates tissue fibrosis through inhibition of plasminogen activation via a PDE4/cAMP/PKA pathway. *J. Cell Biol.* 177 (6), 1119–1132. doi:10.1083/jcb.200701040

Sadek, M. S., Cachorro, E., El-Armouche, A., and Kammerer, S. (2020). Therapeutic implications for PDE2 and cGMP/cAMP mediated crosstalk in cardiovascular diseases. *Int. J. Mol. Sci.* 21 (20), 7462. doi:10.3390/ijms21207462

Sakao, S., Tanabe, N., and Tatsumi, K. (2019). Hypoxic pulmonary vasoconstriction and the diffusing capacity in pulmonary hypertension secondary to idiopathic pulmonary fibrosis. *J. Am. Heart Assoc.* 8 (16), e013310. doi:10.1161/JAHA.119.013310

Sakao, S., Taraseviciene-Stewart, L., Lee, J. D., Wood, K., Cool, C. D., and Voelkel, N. F. (2005). Initial apoptosis is followed by increased proliferation of apoptosis-resistant endothelial cells. *Faseb J.* 19 (9), 1178–1180. doi:10.1096/fj.04-3261fje

Sakao, S., Taraseviciene-Stewart, L., Wood, K., Cool, C. D., and Voelkel, N. F. (2006). Apoptosis of pulmonary microvascular endothelial cells stimulates vascular smooth muscle cell growth. *Am. J. Physiol. Lung Cell Mol. Physiol.* 291 (3), L362–L368. doi:10.1152/ajplung.00111.2005

Sampson, N., Berger, P., and Zenzmaier, C. (2012). Therapeutic targeting of redox signaling in myofibroblast differentiation and age-related fibrotic disease. *Oxidative Med. Cell. Longev.* 2012, 458276. doi:10.1155/2012/458276

Sandner, P., Berger, P., and Zenzmaier, C. (2017). The potential of sGC modulators for the treatment of age-related fibrosis: A mini-review. *Gerontology* 63 (3), 216–227. doi:10.1159/000450946

Schafer, M. J., White, T. A., Iijima, K., Haak, A. J., Ligresti, G., Atkinson, E. J., et al. (2017). Cellular senescence mediates fibrotic pulmonary disease. *Nat. Commun.* 8, 14532. doi:10.1038/ncomms14532

Schinner, E., Wetzl, V., and Schlossmann, J. (2015). Cyclic nucleotide signalling in kidney fibrosis. *Int. J. Mol. Sci.* 16 (2), 2320–2351. doi:10.3390/ijms16022320

Selige, J., Hatzelmann, A., and Dunkern, T. (2011). The differential impact of PDE4 subtypes in human lung fibroblasts on cytokine-induced proliferation and myofibroblast conversion. *J. Cell Physiol.* 226 (8), 1970–1980. doi:10.1002/jcp.22529

Seo, M. H., Kim, D. W., Kim, Y. S., and Lee, S. K. (2022). Pentoxifylline-induced protein expression change in RAW 264.7 cells as determined by immunoprecipitation-based high performance liquid chromatography. *PloS One* 17 (3), e0261797. doi:10.1371/journal.pone.0261797

Sgalla, G., Iovene, B., Calvello, M., Ori, M., Varone, F., and Richeldi, L. (2018). Idiopathic pulmonary fibrosis: Pathogenesis and management. *Respir. Res.* 19, 32. doi:10.1186/s12931-018-0730-2

Sharma, K., Ishaq, M., Sharma, G., Khan, M. A., Dutta, R. K., and Majumdar, S. (2016). Pentoxifylline triggers autophagy via ER stress response that interferes with Pentoxifylline induced apoptosis in human melanoma cells. *Biochem. Pharmacol.* 103, 17–28. doi:10.1016/j.bcp.2015.12.018

Sisson, T. H., Christensen, P. J., Muraki, Y., Dils, A. J., Chibucos, L., Subbotina, N., et al. (2018). Phosphodiesterase 4 inhibition reduces lung fibrosis following targeted type II alveolar epithelial cell injury. *Physiol. Rep.* 6 (12), e13753. doi:10.14814/phy2.13753

Spagnolo, P., Bonella, F., Ryerson, C. J., Tzouvelekis, A., and Maher, T. M. (2020). Shedding light on developmental drugs for idiopathic pulmonary fibrosis. *Expert Opin. Investig. Drugs* 29 (8), 797–808. doi:10.1080/13543784.2020.1782885

Spagnolo, P., Kropski, J. A., Jones, M. G., Lee, J. S., Rossi, G., Karampitsakos, T., et al. (2021). Idiopathic pulmonary fibrosis: Disease mechanisms and drug development. *Pharmacol. Ther.* 222, 107798. doi:10.1016/j.pharmthera.2020.107798

Spagnolo, P., Ryerson, C. J., Putman, R., Oldham, J., Salisbury, M., Sverzellati, N., et al. (2021). Early diagnosis of fibrotic interstitial lung disease: Challenges and opportunities. *Lancet Respir. Med.* 9 (9), 1065–1076. doi:10.1016/S2213-2600(21)00017-5

Spagnolo, P., Tzouvelekis, A., and Bonella, F. (2018). The management of patients with idiopathic pulmonary fibrosis. *Front. Med.* 5, 148. doi:10.3389/fmed.2018.00148

Speer, E. M., Dowling, D. J., Ozog, L. S., Xu, J., Yang, J., Kennady, G., et al. (2017). Pentoxifylline inhibits TLR- and inflammasome-mediated *in vitro* inflammatory cytokine production in human blood with greater efficacy and potency in newborns. *Pediatr. Res.* 81 (5), 806–816. doi:10.1038/pr.2017.6

Spina, D. (2008). PDE4 inhibitors: Current status. *Br. J. Pharmacol.* 155 (3), 308–315. doi:10.1038/bjp.2008.307

Stevens, J. W., Simpson, E., Harnan, S., Squires, H., Meng, Y., ThomaS, S., et al. (2012). Systematic review of the efficacy of cilostazol, naftidrofuryl oxalate and pentoxifylline for the treatment of intermittent claudication. *Br. J. Surg.* 99 (12), 1630–1638. doi:10.1002/bjs.8895

Stewart, J. P., Egan, J. J., Ross, A. J., Kelly, B. G., Lok, S. S., Hasleton, P. S., et al. (1999). The detection of Epstein-Barr virus DNA in lung tissue from patients with idiopathic pulmonary fibrosis. *Am. J. Respir. Crit. Care Med.* 159 (4), 1336–1341. doi:10.1164/ajrccm.159.4.9807077

Stout-Delgado, H. W., Cho, S. J., Chu, S. G., Mitzel, D. N., Villalba, J., El-Chemaly, S., et al. (2016). Age-dependent susceptibility to pulmonary fibrosis is associated with NLRP3 inflammasome activation. *Am. J. Respir. Cell Mol. Biol.* 55 (2), 252–263. doi:10.1165/rcmb.2015-0222OC

Świerczek, A., Plutecka, H., Ślusarczyk, M., Chłoń-Rzepa, G., and Wyska, E. (2021). PK/PD modeling of the PDE7 inhibitor-GRMS-55 in a mouse model of autoimmune hepatitis. *Pharmaceutics* 13 (5), 597. doi:10.3390/pharmaceutics13050597

Sylvester, J. T., Shimoda, L. A., Aaronson, P. I., and Ward, J. P. T. (2012). Hypoxic pulmonary vasoconstriction. *Physiol. Rev.* 92 (1), 367–520. doi:10.1152/physrev.00041.2010

Tang, Y. W., Johnson, J. E., Browning, P. J., Cruz-Gervis, R. A., Davis, A., Graham, B. S., et al. (2003). Herpesvirus DNA is consistently detected in lungs of patients with idiopathic pulmonary fibrosis. *J. Clin. Microbiol.* 41 (6), 2633–2640. doi:10.1128/jcm.41.6.2633-2640.2003

Toonkel, R. L., Hare, J. M., Matthay, M. A., and Glassberg, M. K. (2013). Mesenchymal stem cells and idiopathic pulmonary fibrosis. Potential for clinical testing. *Am. J. Respir. Crit. Care Med.* 188 (2), 133–140. doi:10.1164/rccm.201207-1204PP

Torphy, T. J. (1998). Phosphodiesterase isozymes: Molecular targets for novel antiasthma agents. *Am. J. Respir. Crit. Care Med.* 157 (2), 351–370. doi:10.1164/ajrccm.157.2.9708012

Udalov, S., Dumitrascu, R., Pullamsetti, S. S., Al-tamari, H. M., Weissmann, N., Ghofrani, H. A., et al. (2010). Effects of phosphodiesterase 4 inhibition on bleomycin-induced pulmonary fibrosis in mice. *BMC Pulm. Med.* 10, 26. doi:10.1186/1471-2466-10-26

Wang, J., Hu, K., Cai, X., Yang, B., He, Q., Wang, J., et al. (2022). Targeting PI3K/AKT signaling for treatment of idiopathic pulmonary fibrosis. *Acta Pharm. Sin. B* 12 (1), 18–32. doi:10.1016/j.apsb.2021.07.023

Wang, T., Reingruber, J., Woodruff, M. L., Majumder, A., Camarena, A., Artemyev, N. O., et al. (2018). The PDE6 mutation in the rd10 retinal degeneration mouse model causes protein mislocalization and instability and promotes cell death through increased ion influx. *J. Biol. Chem.* 293 (40), 15332–15346. doi:10.1074/jbc.RA118.004459

Wen, W. X., Lee, S. Y., Siang, R., and Koh, R. Y. (2017). Repurposing pentoxifylline for the treatment of fibrosis: An overview. *Adv. Ther.* 34 (6), 1245–1269. doi:10.1007/s12325-017-0547-2

Wilborn, J., Crofford, L. J., Burdick, M. D., Kunkel, S. L., Strieter, R. M., and Peters-Golden, M. (1995). Cultured lung fibroblasts isolated from patients with idiopathic pulmonary fibrosis have a diminished capacity to synthesize prostaglandin E2 and to express cyclooxygenase-2. *J. Clin. Investigation* 95 (4), 1861–1868. doi:10.1172/JCI117866

Wilson, M. S., and Wynn, T. A. (2009). Pulmonary fibrosis: Pathogenesis, etiology and regulation. *Mucosal Immunol.* 2 (2), 103–121. doi:10.1038/mi.2008.85

Wipff, P. J., Rifkin, D. B., Meister, J. J., and Hinz, B. (2007). Myofibroblast contraction activates latent TGF-beta1 from the extracellular matrix. *J. Cell Biol.* 179 (6), 1311–1323. doi:10.1083/jcb.200704042

Wójcik-Pszczoła, K., Chłoń-Rzepa, G., Jankowska, A., Ferreira, B., Koczurkiewicz-Adamczyk, P., Pękala, E., et al. (2022). Pan-phosphodiesterase inhibitors attenuate TGF-β-induced pro-fibrotic phenotype in alveolar epithelial type II cells by downregulating smad-2 phosphorylation. *Pharm. (Basel, Switz.* 15 (4), 423. doi:10.3390/ph15040423

Wójcik-Pszczoła, K., Chlon-Rzepa, G., Jankowska, A., Slusarczyk, M., Ferdek, P. E., Kusiak, A. A., et al. (2020). A novel, pan-PDE inhibitor exerts anti-fibrotic effects in human lung fibroblasts via inhibition of TGF-β signaling and activation of cAMP/PKA signaling. *Int. J. Mol. Sci.* 21 (11), 4008. doi:10.3390/ijms21114008

Wójcik-Pszczoła, K., Jankowska, A., Ślusarczyk, M., Jakieła, B., Plutecka, H., Pociecha, K., et al. (2021). Synthesis and *in vitro* evaluation of anti-inflammatory, antioxidant, and anti-fibrotic effects of new 8-aminopurine-2,6-dione-based phosphodiesterase inhibitors as promising anti-asthmatic agents. *Bioorg. Chem.* 117, 105409. doi:10.1016/j.bioorg.2021.105409

Wright, L. C., Seybold, J., RobichAud, A., Adcock, I. M., and Barnes, P. J. (1998). Phosphodiesterase expression in human epithelial cells. *Am. J. Physiology-Lung Cell. Mol. Physiology* 275 (4), L694–L700. doi:10.1152/ajplung.1998.275.4.L694

Wynn, T. A., and Ramalingam, T. R. (2012). Mechanisms of fibrosis: Therapeutic translation for fibrotic disease. *Nat. Med.* 18 (7), 1028–1040. doi:10.1038/nm.2807

Xu, F., Lv, C., Deng, Y., Liu, Y., Gong, Q., Shi, J., et al. (2020). Icariside II, a PDE5 inhibitor, suppresses oxygen-glucose deprivation/reperfusion-induced primary hippocampal neuronal death through activating the PKG/CREB/BDNF/TrkB signaling pathway. *Front. Pharmacol.* 11, 523. doi:10.3389/fphar.2020.00523

Yanai, S., and Endo, S. (2019). PDE3 inhibitors repurposed as treatments for age-related cognitive impairment. *Mol. Neurobiol.* 56 (6), 4306–4316. doi:10.1007/s12035-018-1374-4

Yang, F., Chen, E., Yang, Y., Han, F., Han, S., Wu, G., et al. (2019). The Akt/FoxO/p27(Kip1) axis contributes to the anti-proliferation of pentoxifylline in hypertrophic scars. *J. Cell Mol. Med.* 23 (9), 6164–6172. doi:10.1111/jcmm.14498

Yao, C., Guan, X., Carraro, G., Parimon, T., Liu, X., Huang, G., et al. (2021). Senescence of alveolar type 2 cells drives progressive pulmonary fibrosis. *Am. J. Respir. Crit. Care Med.* 203 (6), 707–717. doi:10.1164/rccm.202004-1274OC

Yildirim, A., Ersoy, Y., Ercan, F., Atukeren, P., Gumustas, K., Uslu, U., et al. (2010). Phosphodiesterase-5 inhibition by sildenafil citrate in a rat model of bleomycin-induced lung fibrosis. *Pulm. Pharmacol. Ther.* 23 (3), 215–221. doi:10.1016/j.pupt.2009.11.002

Yokoyama, U., Patel, H. H., Lai, N. C., Aroonsakool, N., Roth, D. M., and Insel, P. A. (2008). The cyclic AMP effector Epac integrates pro- and anti-fibrotic signals. *Proc. Natl. Acad. Sci. U. S. A.* 105 (17), 6386–6391. doi:10.1073/pnas.0801490105

Zieba, B. J., Artamonov, M. V., Jin, L., Momotani, K., Ho, R., Franke, A. S., et al. (2011). The cAMP-responsive Rap1 guanine nucleotide exchange factor, Epac, induces smooth muscle relaxation by down-regulation of RhoA activity. *J. Biol. Chem.* 286 (19), 16681–16692. doi:10.1074/jbc.M110.205062

Zuccarello, E., Acquarone, E., Calcagno, E., Argyrousi, E. K., Deng, S. X., Landry, D. W., et al. (2020). Development of novel phosphodiesterase 5 inhibitors for the therapy of Alzheimer's disease. *Biochem. Pharmacol.* 176, 113818. doi:10.1016/j.bcp.2020.113818

Zuo, H., Cattani-Cavalieri, I., Valenca, S. S., Musheshe, N., and Schmidt, M. (2019). Function of cAMP scaffolds in obstructive lung disease: Focus on epithelial-to-mesenchymal transition and oxidative stress. *Br. J. Pharmacol.* 176 (14), 2402–2415. doi:10.1111/bph.14605

Zuo, H., Cattani-Cavalieri, I., Valenca, S. S., Musheshe, N., and Schmidt, M. (2019). Function of cAMP scaffolds in obstructive lung disease: Focus on epithelial-to-mesenchymal transition and oxidative stress. *Br. J. Pharmacol.* 176 (14), 2402–2415. doi:10.1111/bph.14605

frontiers | Frontiers in Pharmacology

TYPE Original Research
PUBLISHED 14 March 2023
DOI 10.3389/fphar.2023.1141800

OPEN ACCESS

EDITED BY
Wenjun Li,
Yantai Institute of Coastal Zone Research (CAS), China

REVIEWED BY
Pavel Solopov,
Old Dominion University, United States
Yuan Zeli,
Zunyi Medical University, China

*CORRESPONDENCE
Jingyu Chen,
chenjy@wuxiph.com
Juan Li,
juanli0905@163.com

†These authors have contributed equally to this work

SPECIALTY SECTION
This article was submitted to Respiratory Pharmacology, a section of the journal Frontiers in Pharmacology

RECEIVED 10 January 2023
ACCEPTED 28 February 2023
PUBLISHED 14 March 2023

CITATION
Xiong D, Gao F, Shao J, Pan Y, Wang S, Wei D, Ye S, Chen Y, Chen R, Yue B, Li J and Chen J (2023), Arctiin-encapsulated DSPE-PEG bubble-like nanoparticles inhibit alveolar epithelial type 2 cell senescence to alleviate pulmonary fibrosis *via* the p38/p53/p21 pathway. *Front. Pharmacol.* 14:1141800. doi: 10.3389/fphar.2023.1141800

Arctiin-encapsulated DSPE-PEG bubble-like nanoparticles inhibit alveolar epithelial type 2 cell senescence to alleviate pulmonary fibrosis *via* the p38/p53/p21 pathway

Dian Xiong[1†], Fei Gao[2,3†], Jingbo Shao[1], Yueyun Pan[1], Song Wang[4], Dong Wei[1], Shugao Ye[1], Yuan Chen[1], Rui Chen[5], Bingqing Yue[6], Juan Li[7]* and Jingyu Chen[1,6]*

[1]Lung Transplantation Center, Department of Thoracic Surgery, Nanjing Medical University Affiliated Wuxi People's Hospital, Wuxi, China, [2]Department of Emergency, Nanjing Medical University Affiliated Wuxi People's Hospital, Wuxi, China, [3]Department of Emergency, Nanjing General Hospital of Nanjing Military Region, Nanjing, China, [4]Department of Intensive Care Medicine, Nanjing Medical University Affiliated Wuxi People's Hospital, Wuxi, China, [5]Key Laboratory of Clinical Laboratory Diagnostics, Ministry of Education, College of Laboratory Medicine, Chongqing Medical University, Chongqing, China, [6]Department of Lung Transplantation, Second Affiliated Hospital, Zhejiang University School of Medicine, Hangzhou, China, [7]Department of Chemistry, Fudan University, Shanghai, China

Background: Idiopathic pulmonary fibrosis is a severe and deadly form of diffuse parenchymal lung disease and treatment options are few. Alveolar epithelial type 2 (AEC2) cell senescence is implicated in the pathogenies of IPF. A major bioactive compound from the traditional Chinese medicine *Fructus arctii*, arctiin (ARC) has robust anti-inflammatory, anti-senescence, and anti-fibrosis functions. However, the potential therapeutic effects of ARC on IPF and the underlying mechanisms involved are still unknown.

Methods: First of all, ARC was identified as an active ingredient by network pharmacology analysis and enrichment analysis of *F. arctii* in treating IPF. We developed ARC-encapsulated DSPE-PEG bubble-like nanoparticles (ARC@DPBNPs) to increase ARC hydrophilicity and achieve high pulmonary delivery efficiency. C57BL/6 mice were used to establish a bleomycin (BLM)-induced pulmonary fibrosis model for assessing the treatment effect of ARC@DPBNPs on lung fibrosis and the anti-senescence properties of AEC2. Meanwhile, p38/p53 signaling in AEC2 was detected in IPF lungs, BLM-induced mice, and an A549 senescence model. The effects of ARC@DPBNPs on p38/p53/p21 were assessed *in vivo* and *in vitro*.

Results: Pulmonary route of administration of ARC@DPBNPs protected mice against BLM-induced pulmonary fibrosis without causing significant damage to the heart, liver, spleen, or kidney. ARC@DPBNPs blocked BLM-induced

Abbreviations: AEC2, Alveolar epithelial type 2 cells; ARC, Arctiin; ARC@DPBNPs, ARC@DSPE-PEG bubble-like nanoparticles; BLM, Bleomycin; DSPE, 1,2-distearoyl-sn-glycero-3-phosphoethanolamine; HYP, Hydroxyproline; IPF, Idiopathic pulmonary fibrosis; MAPK, Mitogen-activated protein kinase; PEG 2000, Polyethylene glycol 2000; TCM, Traditional Chinese Medicine; SA-β-gal, Senescence-associated beta galactosidase; PBS, Phosphate-buffered saline; PCR, Polymerase chain reaction.

AEC2 senescence *in vivo* and *in vitro*. The p38/p53/p21 signaling axis was significantly activated in the lung tissues of patients with IPF, senescent AEC2, and BLM-induced lung fibrosis. ARC@DPBNPs attenuated AEC2 senescence and pulmonary fibrosis by inhibiting the p38/p53/p21 pathway.

Conclusion: Our data suggest that the p38/p53/p21 signaling axis plays a pivotal role in AEC2 senescence in pulmonary fibrosis. The p38/p53/p21 signaling axis inhibition by ARC@DPBNPs provides an innovative approach to treating pulmonary fibrosis in clinical settings.

KEYWORDS

idiopathic pulmonary fibrosis, alveolar epithelial type 2 cells, cellular senescence, arctiin, nanoparticle, DSPE-PEG, p38/p53/p21 signaling axis, traditional Chinese medicine

1 Introduction

Idiopathic pulmonary fibrosis (IPF) is a progressive, irreversible, and typically fatal lung disease characterized by airway remodeling, inflammation, alveolar destruction, and fibrosis (Wolters et al., 2018). It affects mainly male patients over the age of 60. The median survival of patients after diagnosis is 3–5 years in the absence of lung transplantation (Kropski and Blackwell, 2019); this is comparable to severe cancer disease.

The US Food and Drug Administration approved two medications to treat IPF in 2014: pirfenidone and nintedanib; however, these two therapies did not reduce IPF mortality (King and Nathan, 2015). Furthermore, frequent side effects restrict the clinical application of these antifibrotic drugs. Effective therapies with high accumulation in the lungs and low adverse side effects in other organs and tissues are urgently needed. Local administration of drugs to the lungs is a promising strategy that offers a high-effective dose and prolonged residence in the lungs (da Silva et al., 2017). Recently, nanoparticle drug delivery was used for pulmonary applications due to the increased permeability of the airway mucus layer (Ghumman et al., 2021; Han et al., 2022).

Accumulating evidence demonstrates that the pathogenesis of IPF involves accelerated aging, with senescence of alveolar epithelial type 2 (AEC2) cells playing an important role in this process (Kellogg et al., 2021; Parimon et al., 2021). A single-cell RNA-sequencing study of IPF explant tissues shows regional depletion of AEC2 cells and abnormal activation of multiple pathways related to cellular senescence (Xu et al., 2016). Previous studies (Qiu et al., 2019; Yao et al., 2021) demonstrated that therapies targeting the senescence process in AEC2s could attenuate the progression of pulmonary fibrosis. However, the pathogenesis of AEC2 senescence in IPF remains unclear. The p38 pathway is a major mitogen-activated protein kinase (MAPK) pathway initially discovered to be a mediator of inflammation and stress responses (Ono and Han, 2000). $p38^{MAPK}$ either directly phosphorylates and activates p53 or indirectly phosphorylates p53 through its downstream kinase, casein kinase 2. It was recently discovered that the p38 pathway plays an important role in fibroblast senescence and IPF (Matsuda et al., 2020); however, the role of p38/53 signaling in AEC2 senescence remains largely unknown.

Traditional Chinese Medicine (TCM) has gradually developed an advantage in treating IPF (Zhang et al., 2021). *F. arctii*, one of the most popular TCMs, is officially listed in the Chinese Pharmacopoeia (Li et al., 2022). Arctiin (ARC), isolated from *F. arctii,* is widely investigated for its anti-inflammatory (Lee et al., 2011), antiviral (Hayashi et al., 2010), antiproliferative (Matsuzaki et al., 2008), and anticancer (Hirose et al., 2000) properties. It inhibits hydrogen peroxide-induced senescence in human dermal papilla cells *in vivo* (Bae et al., 2014), suppresses cardiac fibrosis (Li et al., 2017), and attenuates silica-induced lung injury and fibrosis (Liu J. et al., 2021). However, it is unknown whether ARC attenuates bleomycin (BLM)-induced pulmonary fibrosis and AEC2 senescence. After oral administration, most ARC is metabolized to arctigenin. The systemic delivery of ARC has several limitations, including first-pass metabolism, low accumulation in the lungs, and possible adverse side effects in other organs and tissues.

One of the main problems with the inhalation route is the thick mucus layer, which may serve as a barrier to the uptake of active drug particles (Porsio et al., 2018). In this study, our objective was to develop a nanoparticle (ARC@DPBNP) that can be administered by airway delivery to suppress AEC2 senescence for the treatment of pulmonary fibrosis. We chose 1,2-distearoyl-sn-glycero-3-phosphoethanolamine (DSPE)-polyethylene glycol (PEG) 2000 (DSPE-PEG2000) as the main amphiphilic polymer for nanocarrier formation owing to the hydrophobic nature of ARC.

2 Materials and methods

2.1 Studies in humans and animals

All animal experiments complied with the ARRIVE guidelines and were carried out in accordance with the National Research Council's Guide for the Care and Use of Laboratory Animals. The protocol for each experiment was approved by the Research Ethics Committees of Nanjing Medical University Affiliated Wuxi People's Hospital for Animal Research (2022–32). The study has been carried out in accordance with The Code of Ethics of the World Medical Association (Declaration of Helsinki) and was approved by the Research Ethics Committees of Nanjing Medical University Affiliated Wuxi People's Hospital (KY22090). Informed consent was obtained from all participants.

2.2 Reagents

BLM was purchased from MedChemExpress (cat# HY-17565A, China), dissolved in phosphate-buffered saline (PBS) at a concentration of 10 mg/mL, and stored at −80°C in the dark. ARC was purchased from Shanghai Yuanye Bio-Technology Co., Ltd (Shanghai, China), dissolved in DMSO (Biyuntian, China) to a

concentration of 200 mg/mL, and stored at −80°C in the dark. DSPE-PEG2000 was obtained from Ponsure Biological Co. (Shanghai, China). PD 169316 (an inhibitor of $p38^{MAPK}$) was purchased from MedChemExpress (Cat# HY-10570, MCE, China), dissolved in DMSO at a concentration of 10 mM, and stored at −80°C.

2.3 Target fishing and network building

The chemical components of *F. arctii* were categorized using the Traditional Chinese Medicine Systems Pharmacology Database and Analysis Platform (https://tcmspw.com/tcmspsearch.php) (Ru et al., 2014), and those compounds with oral bioavailability ≥30% and drug likeness ≥0.18 were selected as potential active ingredients (Ru et al., 2014). Subsequently, the pharmacological targets of the components were identified and filtered using the Swiss Target Prediction (http://www.swisstargetprediction.ch/) (Gfeller et al., 2013) and ChEMBL databases (https://www.ebi.ac.uk/chembl/) (Gaulton et al., 2017). We searched the GeneCards (https://www.gene-(cards.org/) (Safran et al., 2010), OMIM database (https://www.omim) (Amberger et al., 2015), Drugbank database (https://www.drugbank.ca/) (Wishart et al., 2018) and TTD database (http://bidd.nus.edu.sg/group/cjttd/) (Zhou et al., 2022), using the keywords "idiopathic pulmonary fibrosis" to identify targets related to IPF. The Uniprot database (https://www.uniprot.org/) was used to standardize the target information by including the species information "*homo sapiens*." The STRING database (http://string-db.org) (Szklarczyk et al., 2021) was used to build the protein–protein interactions (PPI) network, and the results were visualized with Cytoscape 3.9.1. Additionally, Cytoscape3.9.1 was adopted for constructing the medicine-ingredients-targets-disease network. The STRING database (http://string-db.org) was employed for Gene Ontology and Kyoto Encyclopaedia of Genes and Genome enrichment analyses, which were performed with Bioinformatics (https://www.bioinformatics.com.cn/).

2.4 Molecular docking

The SDF format file of the three-dimensional structure of ARC was obtained from the PubChem database (https://pubchem.ncbi.nlm.nih.gov/). The small molecule of ARC whose file was subsequently imported into ChemDraw (http://www.perkinelmer.com/tw/category/chemdraw) was processed with minimized energy and saved as a mol2 file. The initial structures of the top 8 potential targets were downloaded from the Protein Data Bank (http://www.rcsb.org/) database and were visualized using PyMoL. The target proteins were then imported into AutoDock MGLTools 1.5.6 (http://mgltools.scripps.edu/documentation/links/autodock), where they were hydrogenated, the charge calculated, and the non-polar hydrogen combination calculated. The results were stored in PDBQT format. Finally, molecular docking simulations were performed using AutoDock Vina 1.1.2, and PyMOL was used to visualize the results.

2.5 Preparation and characterization of ARC@DPBNPs

DSPE-PEG bubble-like nanoparticles (DPBNPs) were used as carriers to encapsulate ARC. DPBNPs were prepared as previously described (Zeng et al., 2012). Briefly, ARC (20 mg) was dissolved in $CHCl_3$ (200 μL) by stirring. DSPE (50 mg, 0.06 mmoL, Ponsure Biological) and PEG 2000 (50 mg, 0.06 mmoL, Ponsure Biological) were dissolved in 200 μL chloroform. The two solutions were mixed in a 1:1 ratio to form a homogeneous organic phase. An additional 1 mL of deionized water was added to the mixture and mixed for 15 min. The solution was sonicated for 10 min using an ultrasonic mixer (Shanghai Bilon Instruments, Shanghai, China). Organic solvents were removed by rotary evaporation under reduced pressure. The deposited nanoparticle film was hydrated with deionized water to obtain a final concentration of 10 mg/mL. The nanoparticles were prepared by extrusion using Avanti mini-extruders (1 or 8 μm membranes). ARC@DPBNP absorbance properties were measured using a Hitachi UH5300 UV spectrophotometer (Tokyo, Japan), and their size was characterized using a Nano ZS zetasizer (Malvern, United Kingdom). The nanoparticle morphology was visualized using transmission electron microscopy (TEM, Tecnai G2-20).

2.6 Cell culture and treatment

The human AEC2 cell line (A549) was acquired from the Shanghai Cell Bank of the Chinese Academy of Sciences (Shanghai, China). A549 cells were grown in Dulbecco's modified Eagle's medium supplemented with 10% fetal bovine serum and 1X penicillin–streptomycin solution (Thermo Fisher Scientific, United States) at 37°C in 5% CO_2. To create a model of cellular senescence, A549 cells were stimulated with particular doses of BLM for 72 h in Dulbecco's modified Eagle's medium supplemented with 5% fetal bovine serum. As described in the figure legends, cells were treated with BLM and/or various concentrations of ARC and ARC@DPBNPs.

2.7 Cell counting kit-8 (CCK-8) assay

In 96-well culture dishes, A549 cells were cultured for various lengths of time in a medium containing various concentrations of BLM, ARC, and ARC@DPBNPs. Each well (containing 100 L of media) received 10 μL of CCK-8 solution (Yesen, Shanghai, China), which was then cultured for 2 h at 37°C. Using a microplate reader (Type:1,510, Thermo Fisher Scientific), the absorbance of each group was determined at 450 nm (n = 5).

Ten microliters of CCK-8 solution (Yesen, Shanghai, China) were added to each well (containing 100 μL medium) and cultured for 2 h at 37°C. The absorbance of each group was measured at 450 nm (n = 5) using a microplate reader (Type:1,510, Thermo Fisher Scientific). The absorbance and number of live cells were directly proportionally related.

2.8 Mice and treatment

Inbred male C57BL/6J mice aged 6–8 weeks were purchased from Changzhou Cavans Animal Experiment Co., Ltd. The mice

TABLE 1 Donor characteristics.

Characteristics	Mean ± SD or n% (n = 15)
Age (years)	42 ± 9.95
Sex: Male (%)	90.3%
Weight (kg)	67.58 ± 9.54
BMI	23.08 ± 2.68
Oxygenation index	420.5 ± 83.86
Ventilation duration (days)	16.03 ± 24.5
DCD	0%
Current smoker	19.4%
Cause of death	
TBI	32.3%
CVA or ICH	67.7%
Others	0%

Abbreviations: BMI, body mass index; CVA, cerebrovascular accident; DCD, donation after circulatory death; ICH, intracerebral hemorrhage; SD, standard deviation; TBI, traumatic brain injury.

TABLE 2 Baseline characteristics of the recipients.

Characteristics	Anterolateral group
	Mean ± SD or n%
Age (years)	52.80 ± 10.30
Sex: Male (%)	66.67%
Weight (kg)	60.79 ± 12.17
BMI	21.93 ± 3.98
Oxygenation index	217.36 ± 58.11
FVC (L)	1.70 ± 0.45
FEV1 (L)	1.44 ± 0.45
6MWT (m)	234.875 ± 109.85
Comorbidities	
Hypertension	3
Diabetes	1
CHD	2
Secondary pulmonary hypertension	6

Abbreviations: BMI, Body mass index; CHD, Coronary heart disease; FVC, Forced vital capacity; FEV1, Forced expiratory volume in 1 s; SD, Standard deviation; 6MWT, 6-minute walk test.

were randomly selected and divided into four groups: PBS (n = 9), ARC@DPBNP (n = 9), BLM (n = 9), and ARC@DPBNP + BLM (n = 9) groups. Pulmonary fibrosis was induced by intranasal administration of 5 mg/kg of BLM on the first day. Mice in the BLM + ARC@DPBNP groups were treated daily with ARC@DPBNPs by transnasal administration for 21 days up to the day before BLM administration. Mice in the PBS and ARC@DPBNP groups were treated with 40 μL PBS or ARC@DPBNPs by using nasal drops for 21 days. The mice were sacrificed on day 21 after treatment with BLM or PBS, and the lung, liver, spleen, heart, and kidney were collected for subsequent experiments.

2.9 Primary tissue sample

Human lung tissue samples were provided by the affiliated hospital. IPF tissues were collected from patients (n = 15; Table 1). Control lung tissues were collected from healthy adult donors (n = 15; Table 2) that were resected based on size incompatibility or deemed unsuitable for lung transplantation.

2.10 Histopathological assessment

Tissues were fixed in 4% paraformaldehyde for 24 h, embedded in paraffin using a paraffin embedding machine (KD-BM, Zhejiang Kedi, China), and cut into 4-μm sections using a Leica RM2016 rotary microtome. Hematoxylin–eosin and Masson's trichrome staining were performed. According to a documented method, the Ashcroft score method was used to blindly score the level of fibrosis in the mouse lung (Porsio et al., 2018). Immunohistochemical techniques were used to identify protein expression in various tissues. The sections were deparaffinized in xylene and rehydrated in graded alcohol (absolute ethyl alcohol, 95% and 80% ethyl alcohol). Endogenous peroxidase activity was quenched with 3% aqueous hydrogen peroxide for 15 min. The tissue sections were blocked with 10% bovine serum albumin (YESEN, Shanghai, China) for 1 h at room temperature, and antigen retrieval was performed with a pressure cooker. Sections were incubated with rabbit antibody against p21 (10355-1-AP; 1:200 dilution; ProteinTech, Wuhan, China), rabbit antibody against P16-InkA (10883-1-AP; 1:1,000 dilution; ProteinTech), rabbit antibody against phospho-$p38^{MAPK}$ (Thr180/Tyr182) (p-$p38^{MAPK}$) (4,511; 1:800 dilution; Cell Signaling Technology, Danvers, United States), rabbit antibody against $p38^{MAPK}$ polyclonal antibody (14064-1-AP, 1:100 dilution; ProteinTech); mouse antibody against p53 (60283-2-Ig, 1:1,000 dilution; ProteinTech) overnight at 4°C, followed by incubation for 1 h at 37°C in the dark with horseradish peroxidase-labeled secondary antibody (Gene Tech; Shanghai, China). Diaminobenzidine (Gene Tech) was used for color development. Finally, the sections were dehydrated and mounted. Collagen area and protein expression levels were independently analyzed by two investigators using ImageJ software (version 1.46; Rawak Software, Inc.).

2.11 Immunofluorescence assay

Immunofluorescence was performed as previously described (Ru et al., 2014). Briefly, fixed A549 cells or deparaffinized sections were stained with respective primary antibodies against p21 (1:100 dilution), p16 (1:200 dilution), p-$p38^{MAPK}$ (Thr180/Tyr182) (1:1,600 dilution), $p38^{MAPK}$ polyclonal antibody (1:50 dilution), and p53 (1:300 dilution) for 12 h at 4°C. The cells or tissue sections were then washed with PBS and incubated with fluorescent-conjugated secondary antibodies for 2 h at room temperature. The nuclei were visualized using 4′, 6-diamidino-2-phenylindole and dihydrochloride (4,083; Cell Signaling Technology). Immunofluorescence images were obtained using a Leica SP8 confocal microscope.

TABLE 3 The top five potential active components of *Fructus Arctii*.

Mol ID	Molecule name	MW	OB%	DL
MOL000522	Arctiin	534.61	34.45	0.84
MOL000358	Beta-sitosterol	414.79	36.91	0.75
MOL000422	Kaempferol	286.25	41.88	0.24
MOL007326	Cynarine	516.49	31.76	0.68
MOL003290	Arctigenin methyl ether	386.48	52.3	0.48

Abbreviation: Mol ID, Molecule identification; MW, Molecule weight; OB, Oral bioavailability.
DL, Drug likeness.

2.12 Quantitative analysis of hydroxyproline (HYP)

Mice were anesthetized with 2% isoflurane and subjected to cardiac perfusion to remove blood from the lungs. Approximately 100 mg of lung tissue sample (stored at −80°C) was hydrolyzed by adding 1 mL of hydrolysate and incubated at 95°C for 20 min (the samples were mixed again after 10 min of incubation). According to the manufacturer's instructions, an HYP kit (Nanjing Jiancheng Bioengineering Institute, Nanjing, China) was used to measure the amount of HYP in the lung tissue.

2.13 RNA isolation and quantitative reverse transcriptase polymerase chain reaction (PCR)

Total RNA was extracted from cultured cells and lung tissues using an RNA extraction kit (R0027; Beyotime, Shanghai, China) according to the manufacturer's instructions. cDNA was synthesized using HiScript III RT SuperMix for qRT-PCR (R323-01, Vazyme, Nanjing, China).

According to the manufacturer's instructions, quantitative real-time PCR was performed using the ChamQ Universal SYBR qPCR master mix (Q711-02, Vazyme, Nanjing, China), and assays were performed using the Applied Biosystems 7,500 Real-time PCR Detection System (ABI, United States).

The internal standard was Glyceraldehyde-3-phosphate dehydrogenase (GADPH). Based on average CT values, mRNA levels were calculated using the GraphPad Prism 7.0 program (GraphPad Software, La Jolla, CA, United States). The following primers were designed: mouse GADPH, forward: 5′-CATCACTGCCACCCAGAAGACTG-3′ and reverse: 5′-ATGCCAGTGAGCTTCCCGTTCAG-3′; human GADPH, forward: 5′- GTCTCCTCTGACTTCAACAGCG-3′ and reverse: 5′-ACCACCCTGTTGCTGTAGCCAA-3′; mouse Col1a1 forward: 5′-CCTCAGGGTATTGCTGGACAAC-3′ and reverse: 5′-CAGAAGGACCTTGTTTGCCAGG-3′; mouse α-SMA forward: 5′- CGAGCGTGAGATTGTCCGT-3′ and reverse: 5′-CCCTGACAGGACGTTGTTAG-3′; human P21 forward: 5′-AGGTGGACCTGGAGACTCTCAG-3′ and reverse: 5′- TCCTCTTGGAGAAGATCAGCCG-3′; and human P16 forward: 5′- CTCGTGCTGATGCTACTGAGGA-3′ and reverse: 5′- GGTCGGCGCAGTTGGGCTCC-3′.

2.14 Western blot analysis

Whole proteins from cell lysates and lung tissues were extracted using RIPA lysis solution (P0013B, Beyotime, Shanghai, China) according to the manufacturer's instructions and measured using a BCA kit (P0009, Beyotime, Shanghai, China). Equal amounts of protein were separated on 8%–12% SDS–PAGE gels (Vazyme, Nanjing, China), blotted onto PVDF membranes (Merck Millipore, Germany), blocked with 5% nonfat milk in Tris-buffered saline with Tween-20 (TBST) (Beyotime, Shanghai, China) for 1 h, and incubated overnight at 4°C in antibody diluent (Beyotime, Shanghai, China) containing the following primary antibodies: rabbit antibody against p21 (1:1,000 dilution), rabbit antibody against p16 (1:1,000 dilution), rabbit antibody against p-p38^{MAPK} (Thr180/Tyr182) (1:1,000 dilution), rabbit antibody against p38^{MAPK} polyclonal antibody (1:1,000 dilution); mouse antibody against p53 (1:5,000 dilution); mouse antibody against GAPDH (60004-1-Ig, 1:50,000 dilution; ProteinTech); and mouse antibody against *ß*-Tubulin (10094-1-AP, 1:2,000 dilution; ProteinTech). The membranes were incubated with horseradish peroxidase-linked secondary antibody (Jackson Labs, United States) for 1 h, and protein expression was detected using ECL (Vazyme, Nanjing, China). Images were captured using the Tanon 5,200 imaging system (Shanghai, China). ImageJ software (version 2.0.0) was used for gray value analysis.

2.15 Measurement of senescence-associated *ß*-galactosidase (SA-β-gal)

According to the manufacturer's instructions, an SA-gal kit (C0602, Beyotime, Shanghai, China) was used for SA-gal staining. Cells on 6-well chamber slides or frozen lung tissue sections were fixed with a fixative solution for 15 min at room temperature, rinsed three times with PBS for 5 min, and incubated with freshly prepared SA-β-gal staining solution at 37°C overnight. The cells or tissue sections were washed twice with PBS for 5 min at room temperature. The tissue sections were counterstained with fast nuclear red staining (Sigma–Aldrich) to clearly observe the alveolar structure. The images were captured using a light microscope equipped with a digital camera (Olympus Imaging System, Tokyo, Japan). At least three fields were obtained for each well of 6-well plates to calculate the SA-β-gal intensity.

10.3389/fphar.2023.1141800

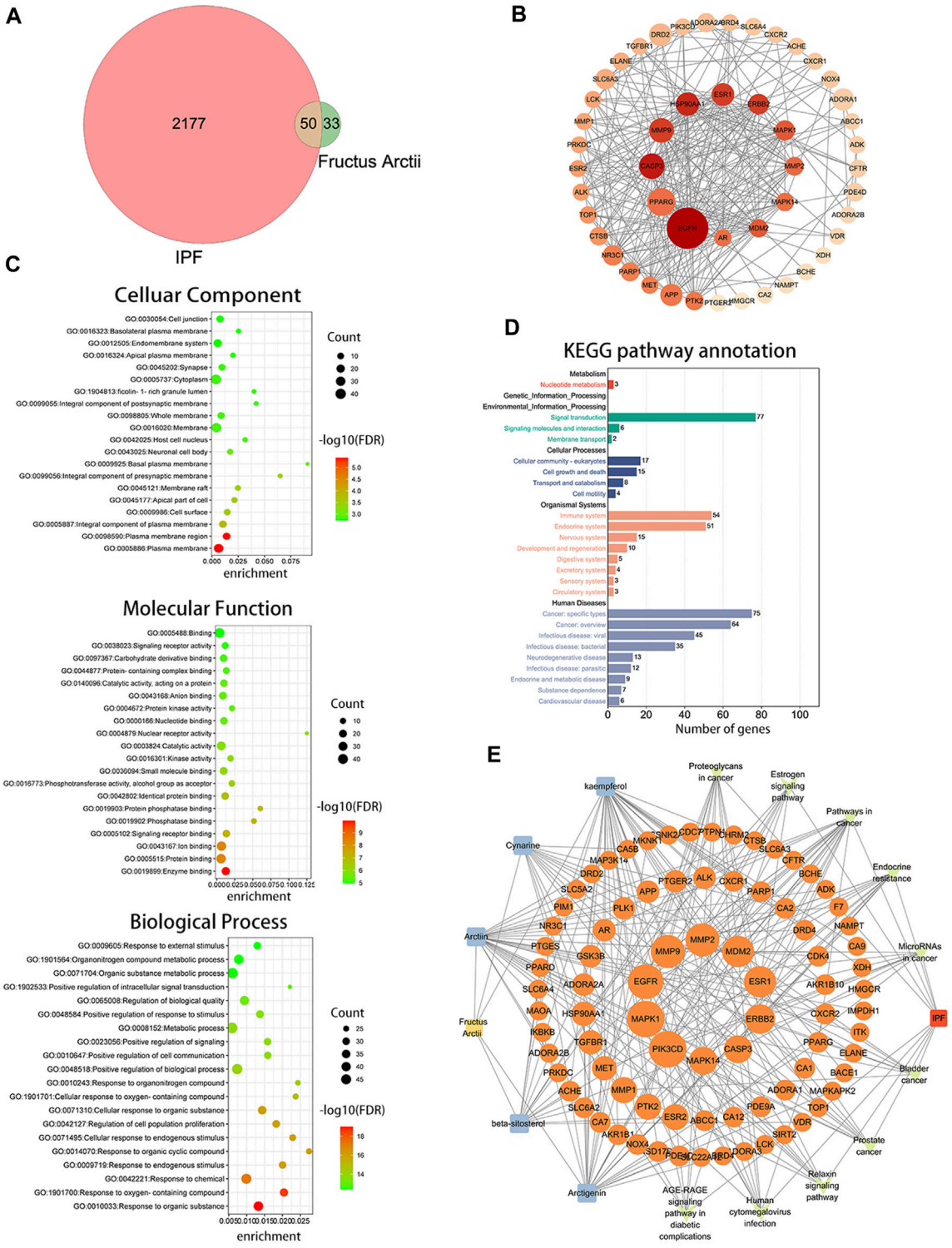

FIGURE 1
Bioinformatics analysis between *Fructus arctii* and idiopathic pulmonary fibrosis (IPF). **(A)** Venn diagram summarizing the intersected gene targets between *Fructus arctii* and the IPF. **(B)** Proteins and protein interaction (PPI) network of the 50 identified targets **(C,D)** The enrichment analysis of *Fructus arctii* targets against IPF by gene Ontology and Kyoto Encyclopaedia of Genes and Genomes analysis of intersections network **(E)** Medicine-Ingredient-Target-Disease network model of *Fructus arctii* and IPF.

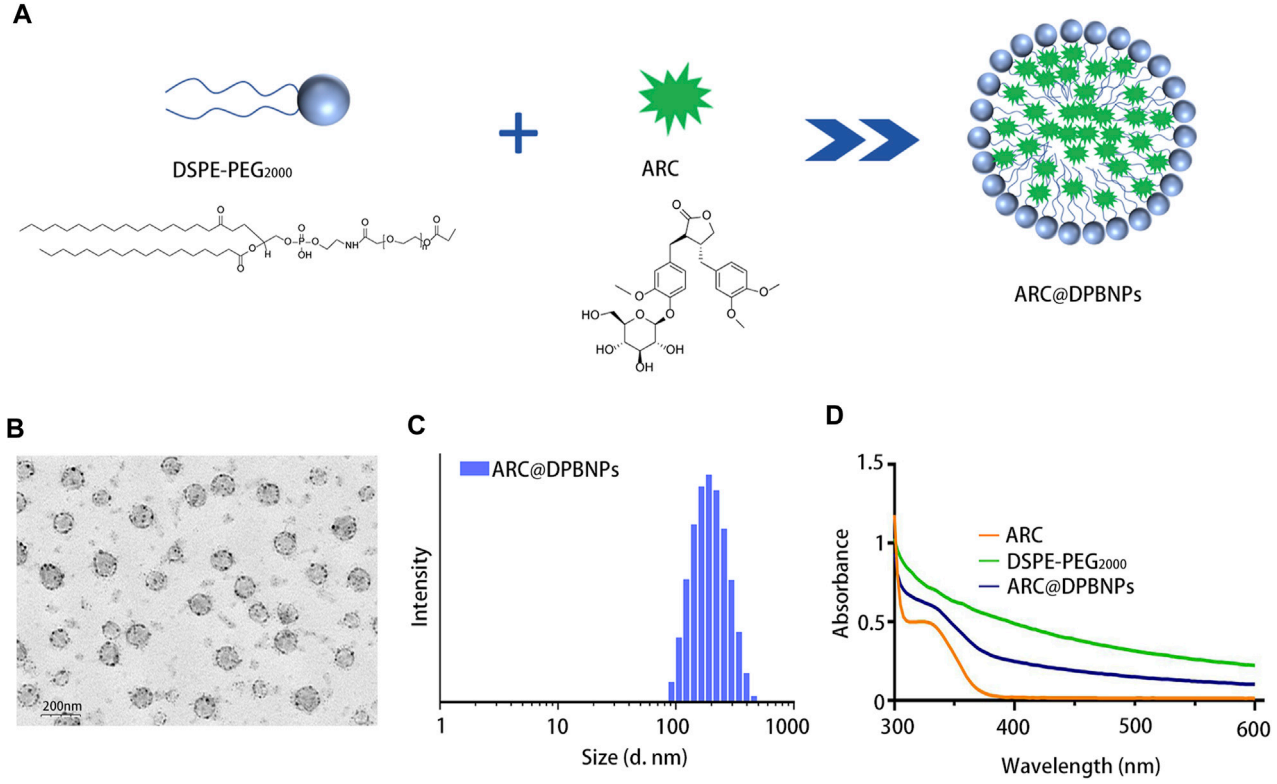

FIGURE 2
Arctiin (ARC)-encapsulated DSPE-PEG bubble-like nanoparticle (ARC@DPBNP) construction and characterization. **(A)** Chemical structures of DSPE-PEG2000 and ARC, and a schematic diagram showing ARC@DPBNP preparation. **(B)** Typical transmission electron microscopy (TEM) images of ARC@DPBNPs, scale bar = 200 nm. **(C)** Size distribution of ARC@DPBNPs according to a Nano ZS zetasizer. **(D)** Ultraviolet-visible absorption spectra of ARC, DPBNP, and ARC@DPBNP solutions.

2.16 Statistical analyses

GraphPad Prism software version 7.0 (La Jolla) was used for statistical analysis. The mean and SEM were used to express the data. A one-way analysis of variance was used to assess differences between two or more groups, and a two-tailed Student's t-test was used to determine differences between the two groups. A *p*-value below 0.05 was accepted as significant.

3 Results

3.1 Bioinformatic analysis between fructus arctii and IPF

ARC is the main bioactive compound of *F. arctii*. We initially investigated the potential mechanisms of *F. arctii* that may contribute to the treatment of IPF. In total, 144 components of *F. arctii* were preliminarily obtained from the Traditional Chinese Medicine Systems Pharmacology Database and Analysis Platform. After screening the active ingredients using the criteria of oral bioavailability ≥30% and drug likeness ≥0:18, 8 compounds were obtained. We removed the duplicated results and filtered the data using the Swiss Target Prediction and ChEMBL databases. 5 active components (ARC, beta-sitosterol, kaempferol, cynarine, and arctigenin methyl ether; Table 3) and 83 potential targets were selected for further analysis. According to methodology in previous literature, targets with a score greater than the median in the Genecards database were selected as potential IPF targets (Oh et al., 2022). After removing the duplicated results and supplementing the database with further data from OMIM, TTD, and Drugbank databases, 2227 IPF-related targets were obtained. The Venn diagram, drawn by Bioinformatics (https://www.bioinformatics.com.cn/), identified 50 potential targets, which were obtained by the intersection of *F. arctii* compound targets and IPF targets (Figure 1A). The PPI network of the 50 intersecting targets was constructed using the STRING database (http://string-db.org) and was visualized with Cytoscape 3.9.1. There were 50 nodes and 254 edges in total, the average node degree was 10.37, and the PPI enrichment *p*-value was <0.001 (Figure 2B). The top 20 screened key targets were based on three major parameters: degree, betweenness, and closeness as shown in (Supplementary Table S1).

The intersection of protein targets was subjected to Gene Ontology and Kyoto Encyclopaedia of Genes and Genome enrichment analyses. The results of the Gene Ontology (biological process) analysis showed that the intersection targets were mostly enriched in response to organic substances, response to oxygen-containing compounds, response to chemicals, etc. The molecular function was mainly involved in enzyme binding,

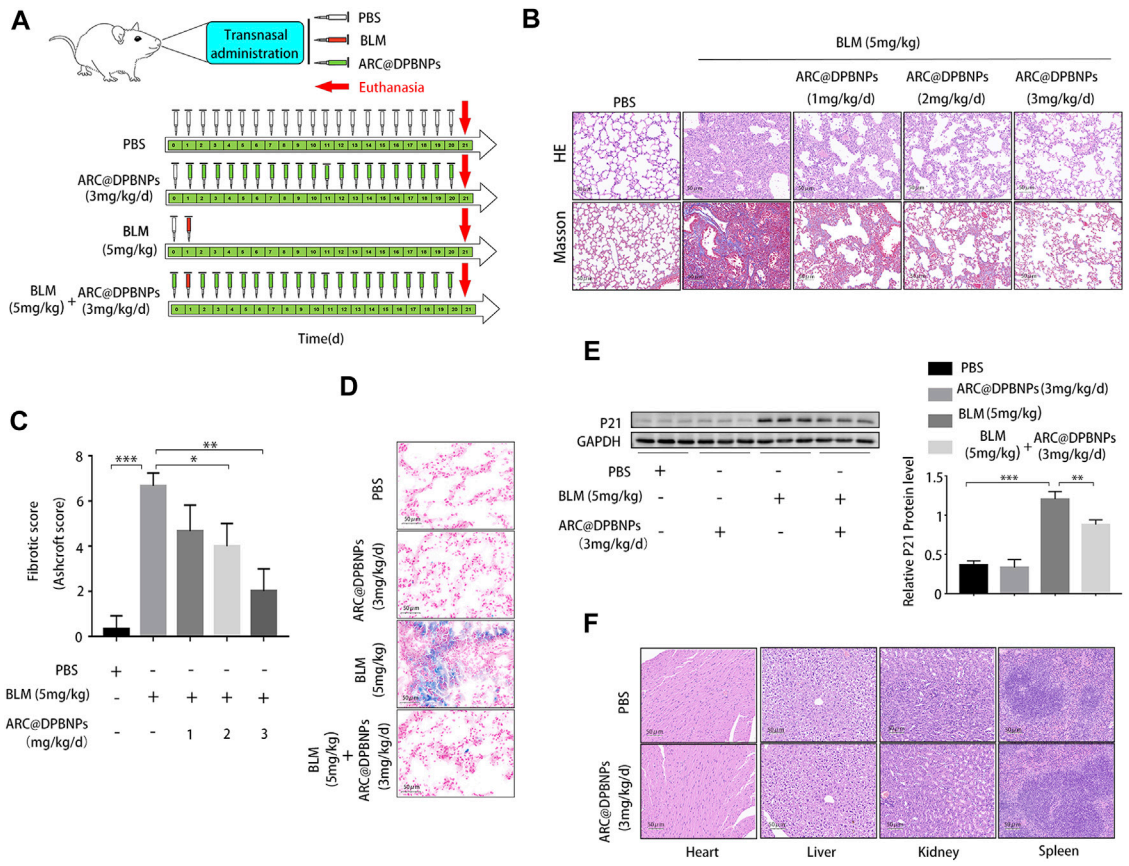

FIGURE 3
Effect and toxicity of arctiin-encapsulated DSPE-PEG bubble-like nanoparticles (ARC@DPBNPs) on pulmonary fibrosis in the mouse model **(A)** Schematic representation of the regimens of ARC@DPBNPs, phosphate-buffered saline, and bleomycin local pulmonary administration in mice **(B)** Representative photographs of lung sections of the pulmonary fibrosis in a mouse model treated with various ARC@DPBNP concentrations stained with hematoxylin–eosin (HE) and Masson's trichrome (MA). Scale bar = 50 μm. **(C)** Fibrotic scores were analyzed. **(D)** Representative results of senescence-associated ß-galactosidase staining of mice lung tissues. Scale bar = 50 μm. **(E)** Senescent marker p21 in mice lung tissues measured through Western blotting. **(F)** Hematoxylin and Eosin staining of the heart, liver, spleen, and kidney performed after intrapulmonary administration of ARC@DPBNPs (3 mg/kg/d) for 21 d *$p < 0.05$, **$p < 0.01$, ***$p < 0.001$.

protein binding, ion binding, signaling receptor binding, phosphatase binding, etc. Cellular component mainly included the plasma membrane, plasma membrane region, cell surface, etc. (Figure 1C). Kyoto Encyclopaedia of Genes and Genome enrichment was most involved in signal transduction, cell growth and death, immune system, and Cancer: specific types, etc. (Figure 1D). To further screen the core components and targets of *F. arctii* in treating IPF, the medicine-ingredients-targets-disease network was constructed. The results indicated that ARC, kaempferol, cynarine, beta-sitosterol, and arctigenin methyl ether regulate IPF progression by targeting 50 potential sites (Figure 1E).

3.2 Characterization of ARC-encapsulated DPBNPs

The molecular structures of DPBNPs and ARC and a schematic representation of the ARC@DPBNP preparation method are shown in Figure 2A. TEM analysis was performed to characterize the shape, size, and homogeneity of ARC@DPBNPs. The results showed ARC@DPBNPs had a uniform microbubble-like structure and particle size of 56.56 ± 9.78 nm (Figure 2B). The ARC@DPBNPs particles were 185.5 ± 22.3 nm according to the Nano ZS zetasizer (Figure 2C). A previous study suggested that 50–200 nm nanoparticle sizes are effective for alveolar deposition and cellular internalization after nebulization administration while avoiding clearance by alveolar macrophages (Dandekar et al., 2010). The zeta potential of ARC@DPBNPs was −31.8 ± 8.36 mV (data not shown). The prepared ARC@DPBNPs displayed the characteristic absorption peak of ARC at 324 nm. This indicated that ARC was successfully encapsulated in the DPBNPs (Figure 2D).

3.3 Local administration of ARC@DPBNPs mitigated pulmonary fibrosis in mice model

The therapeutic effects of ARC@DPBNPs were evaluated in C57BL/6 mice after BLM induction for 21 days. The mice were randomly divided into four groups: PBS-treated; ARC@DPBNP-treated; BLM-treated; and BLM + ARC@DPBNP-treated. Three

10.3389/fphar.2023.1141800

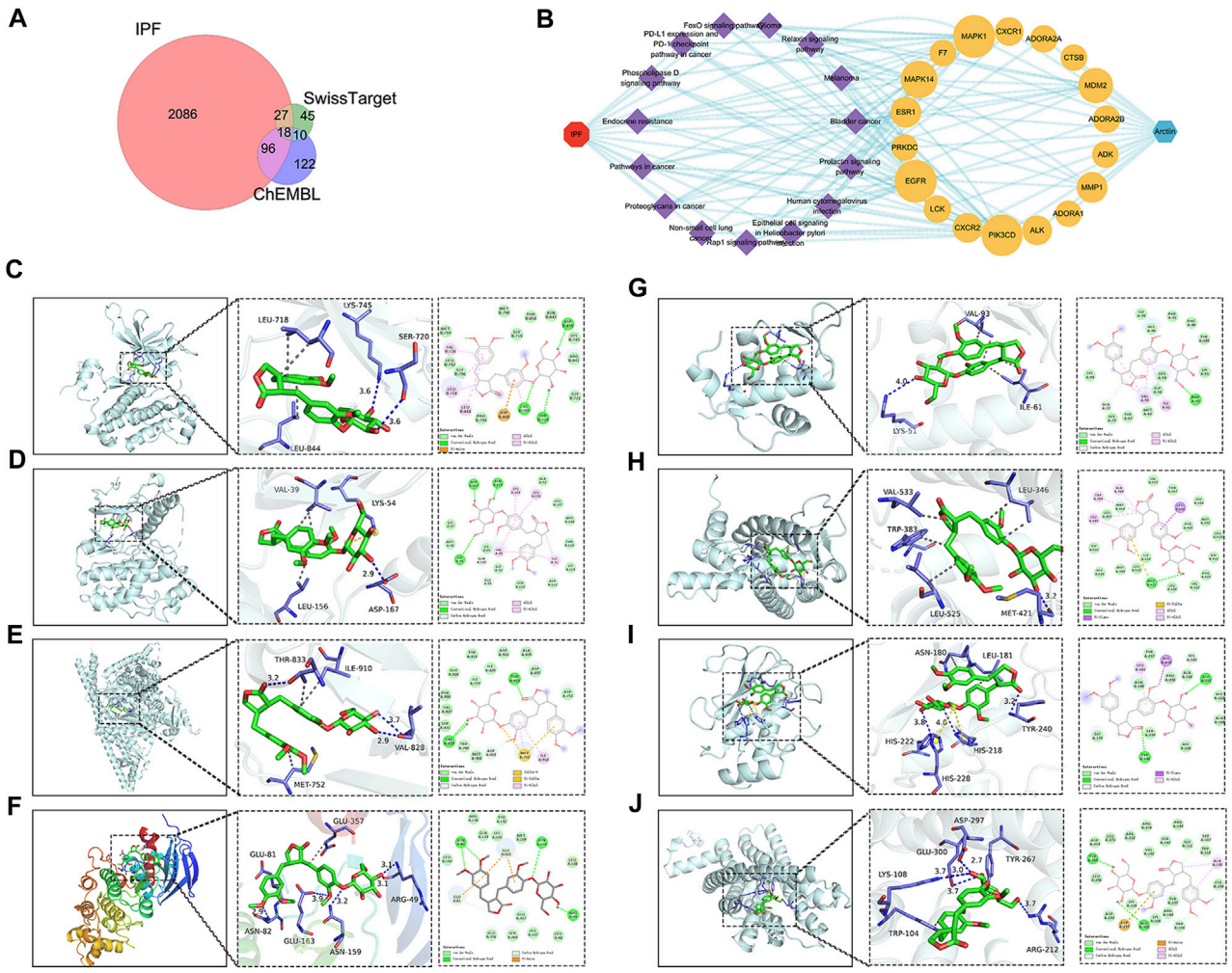

FIGURE 4
Network construction of arctiin (ARC) related to idiopathic pulmonary fibrosis (IPF) and molecular docking. **(A)** Venn diagram summarizing the intersected gene targets between ARC and the IPF. **(B)** ARC-target-pathway-IPF network. **(C–J)** ARC molecular docking and the top 8 target proteins related to IPF after visualization.

TABLE 4 Top ten targets information of PPI network.

Name	Degree	Betweenness	Closeness
EGFR	16	133.059	0.630
MAPK1	16	126.667	0.630
PIK3CD	15	109.995	0.607
MAPK14	11	64.344	0.531
MDM2	9	45.223	0.515
ESR1	5	16.6286	0.459
MMP1	5	13.724	0.447
CXCR2	4	13.315	0.447

doses (1, 2, and 3 mg/kg/day) were trialed to determine the optimal effective dose of ARC@DPBNPs for use in the experiment (Figure 3A). Pathological results showed that after ARC@DPBNP treatment, lung fibrosis was gradually reversed according to the dosage, compared with that in the BLM group manner (Figure 3B). The final Ashcroft fibrotic score was negatively correlated with the dose of ARC@DPBNPs (Figure 3C). Lung fibrosis was dramatically alleviated after treatment with 3 mg/kg/day ARC@DPBNPs for 21 days. SA-β-Gal-positive (blue) cell numbers increased significantly in the BLM group, and ARC@DPBNPs obviously decreased the number of SA-β-Gal-positive cells in the lung tissue of the mouse model (Figure 3D). Meanwhile, Western blot analysis showed that p21 increased significantly in the BLM group compared to that in the PBS and ARC@DPBNP groups ($p < 0.001$), whereas ARC@DPBNP treatment significantly inhibited its expression ($p < 0.001$, Figure 3E). These results indicated that ARC@DPBNPs inhibited BLM-induced cellular senescence *in vivo*. The mice administered nasal drops of ARC@DPBNPs (3 mg/kg/d) for 21 days exhibited no substantial organ damage, as evidenced by the histology of the heart, liver, spleen, and kidney (Figure 3F). Based on these results, 3 mg/kg/day was a suitable dose for subsequent animal experiments.

10.3389/fphar.2023.1141800

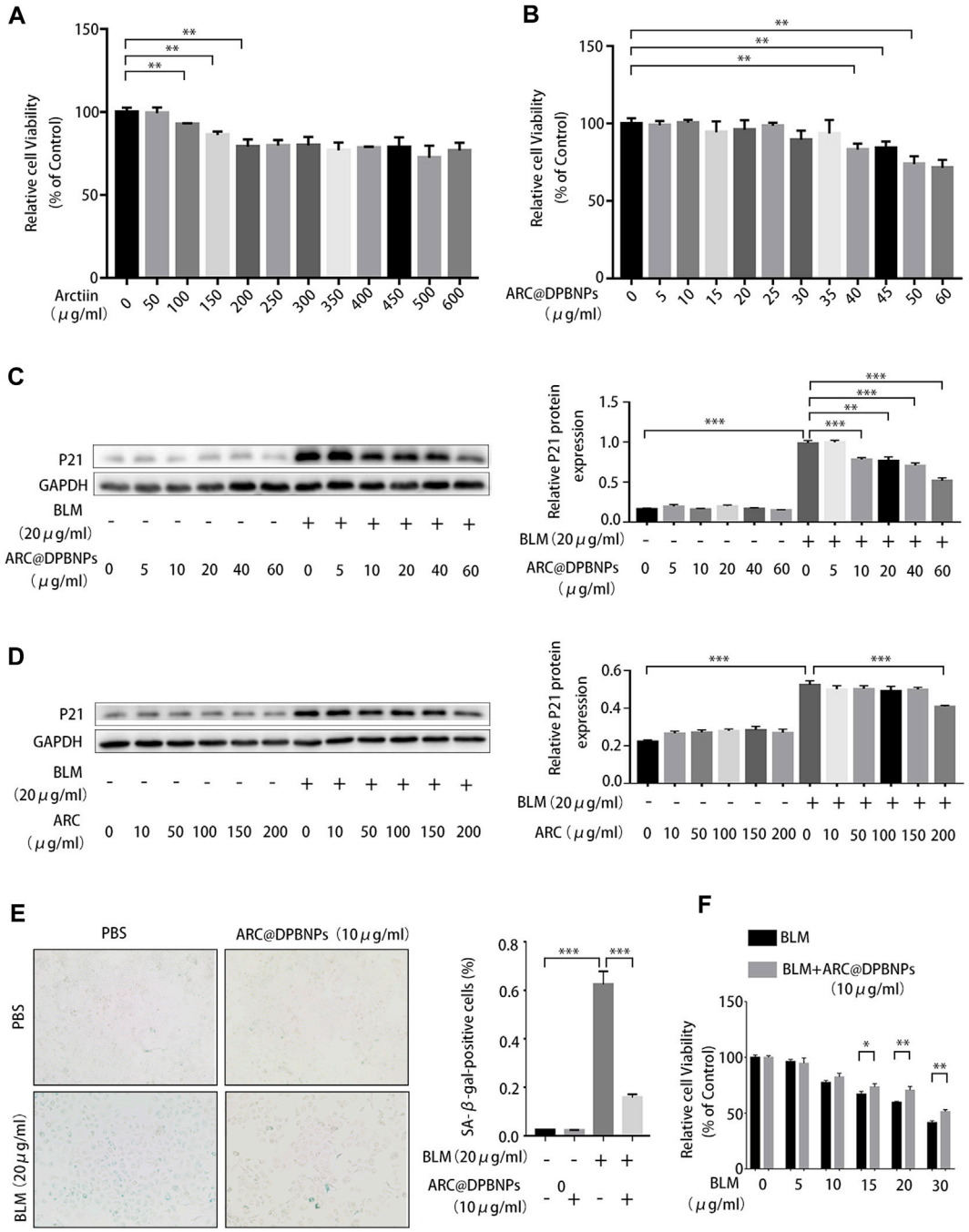

FIGURE 5
Arctiin (ARC)-encapsulated DSPE-PEG bubble-like nanoparticles (ARC@DPBNPs) inhibit A549 cell senescence induced by bleomycin (BLM) with less effect on cell vitality compared to the arctiin monomer **(A,B)** Cell counting kit-8 (CCK-8) assays were performed after A549 cells were stimulated with ARC (0–600 μg/mL) or ARC@DPBNPs (0–60 μg/mL) for 72 h **(C,D)** ARC@DPBNP (0–60 μg/mL) or ARC (0–600 μg/mL) was used to cure A549 cell senescence induced by BLM. **(E)** Senescence-associated ß-galactosidase (SA-β-gal) staining was used to identify cellular senescence (original magnification = ×200) **(F)** Decreased A549 proliferation stimulated with 20 μg/mL or 30 μg/mL bleomycin can be partially reversed by ARC@DPBNPs. *$p < 0.05$, **$p < 0.01$, ***$p < 0.001$.1.

3.4 Targets prediction of ARC for the treatment of IPF

In order to clarify the novel drug target of ARC in treating IPF, network pharmacology and molecular docking analyses were employed. There were 28 genes in the intersection of the SwissTarget and ChEMBL databases, representing the most probable target for ARC. Subsequently, taking the intersection of the ARC and IPF-related targets, a total of 18 potential active targets were obtained, as shown in Figure 4A. The components-

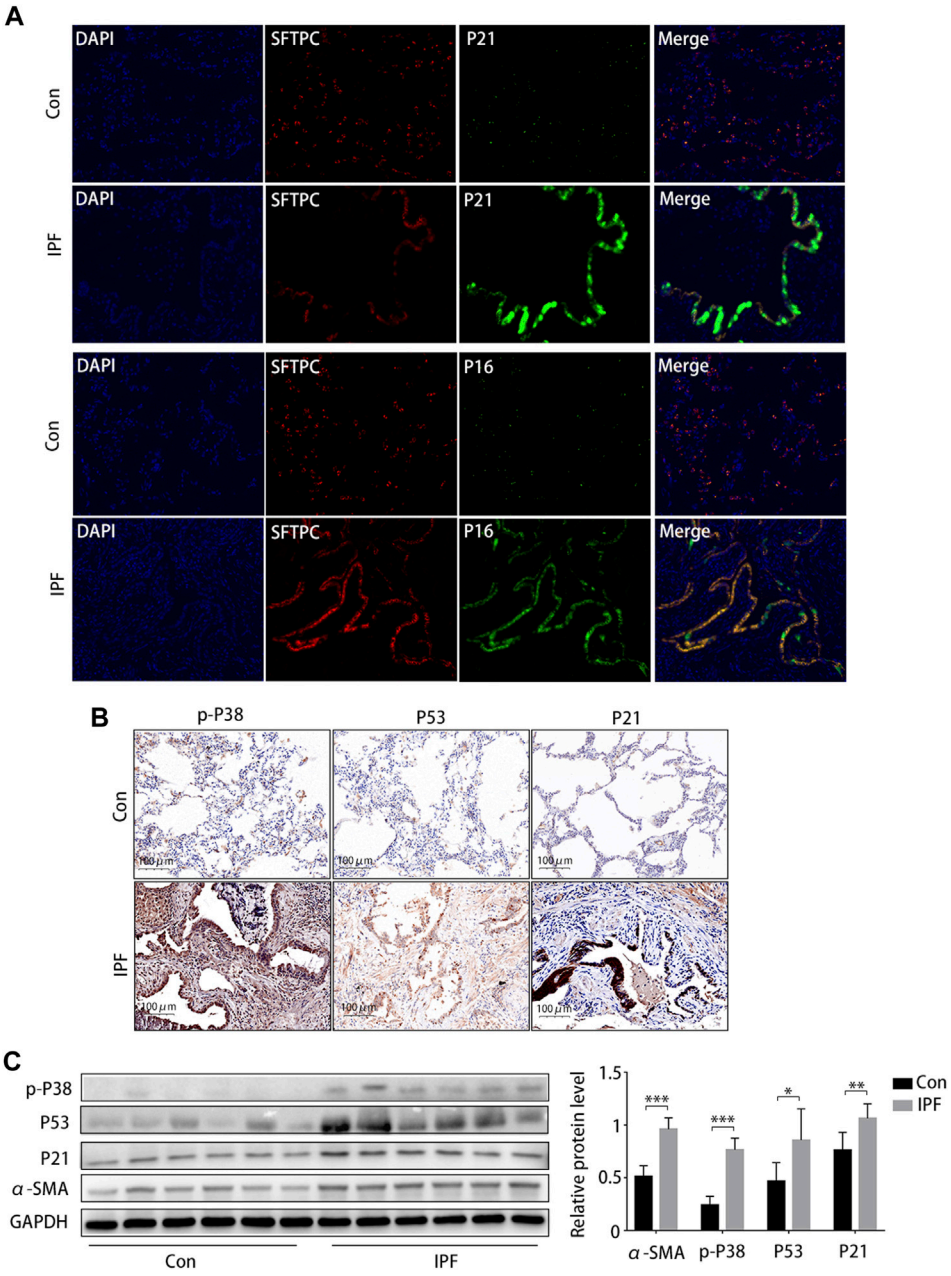

FIGURE 6
Activated p38/p53/p21 pathway in lung tissue from patients with idiopathic pulmonary fibrosis (IPF). **(A)** Immunofluorescence staining of SFTPC (an AEC2-specific marker, red), p21 (green), and p16 (green) to confirm the expression of increased senescent markers in patients with IPF (original magnification, ×400). **(B)** Representative results of immunohistochemical staining for p-p38, p53, and p21 in the lungs of patients with IPF and normal lungs (scale bar, 50 μm). **(C)** Western blot of p-p38, p53, and p21 expression. *$p < 0.05$, **$p < 0.01$, ***$p < 0.001$.

targets-pathways-disease network was then constructed to see whether ARC is combined with the top 8 core target proteins (Table 4). Figures 4C–J depicts images of the optimal docking of proteins and ARC after visualization. The docking scores for ARC with the top eight targets (EGFR, MAPK1, PIK3CD, MAPK14 (p38), MDM2, ESR1, MMP1, and CXCR2) of IPF were −7.6, −8.0, −6.5, −8.2, −6.4, −7.6, −6.6, and −6.8 kcal/mol (Supplementary Table S2), respectively. Among them, the docking of MAPK14 (p38) had the lowest binding score −8.2 kcal/mol). Given that a lower docking score represents a stronger binding affinity, and a score <−5 indicates strong binding activity (Liu X. et al., 2021), the molecular docking results indicate that ARC has a high affinity with MAPK14 (p38), which plays an essential role in cellular senescence. Figure 4G shows that the structure of ARC is linked to ARG49, ASN82, ASN159, and GLU163 in p38 through hydrogen bonds and has a hydrophobic interaction with GLU81 and GLU357.

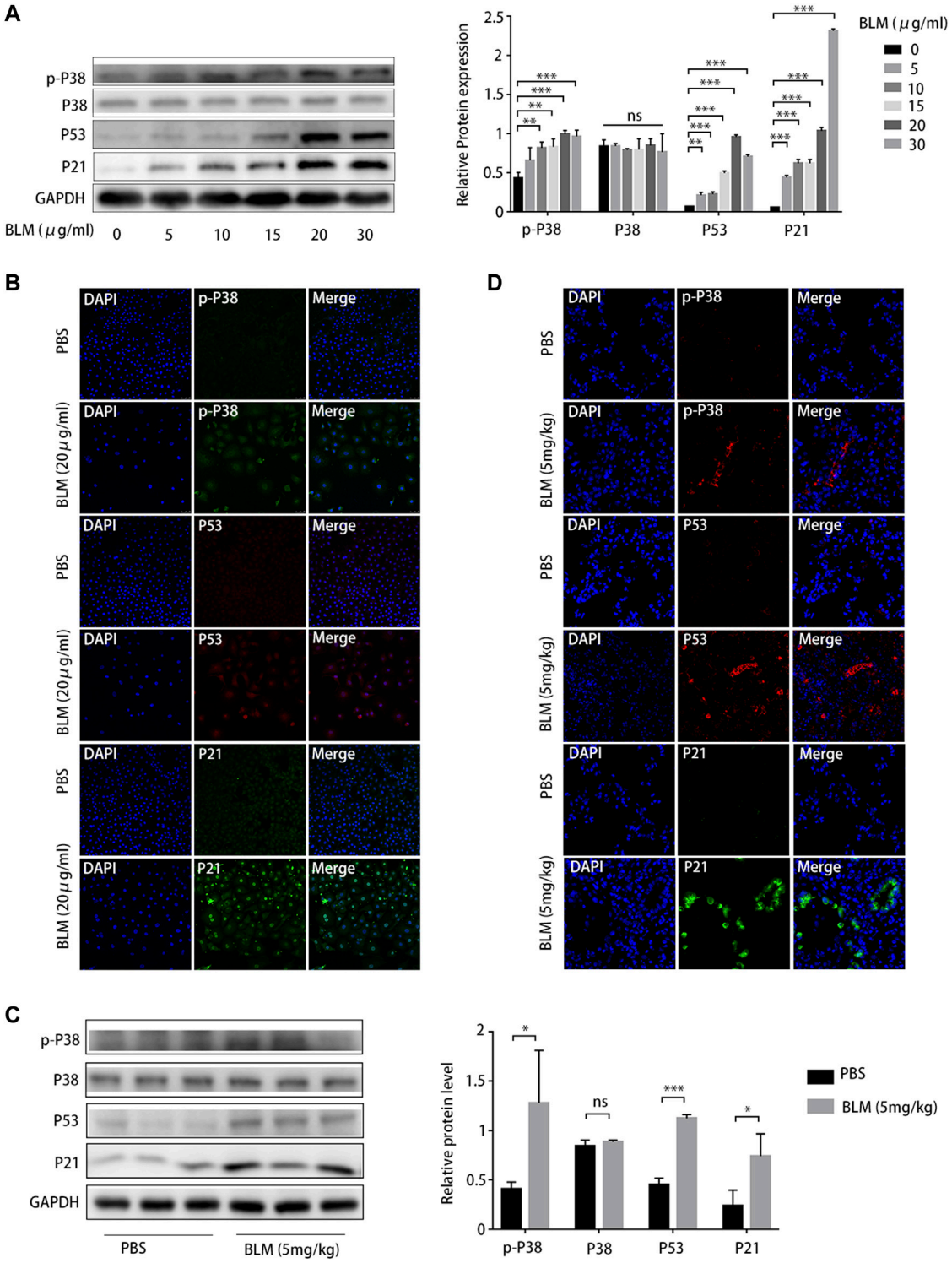

FIGURE 7
P38/P53/P21 pathway is activated in A549 senescent cells and bleomycin (BLM)-induced pulmonary fibrosis mouse model. **(A)** Western blot of p-p38, p53, and p21 levels in A549 cells treated with different BLM concentrations (0–30 μg/mL). **(B)** Immunofluorescence staining of p-p38, p53, and p21 in A549 cells treated with phosphate-buffered saline (PBS) or BLM (20 μg/mL). **(C)** Western blot of p-p38, p53, and p21 expression in lung tissue from mouse models treated with PBS or BLM (5 mg/kg) for 21 d. **(D)** Immunofluorescence staining of p-p38, p53, and p21 in lung sections of a mouse model treated with PBS or BLM (5 mg/kg) for 21 d. *$p < 0.05$, **$p < 0.01$, ***$p < 0.001$; ns: not statistically significant.

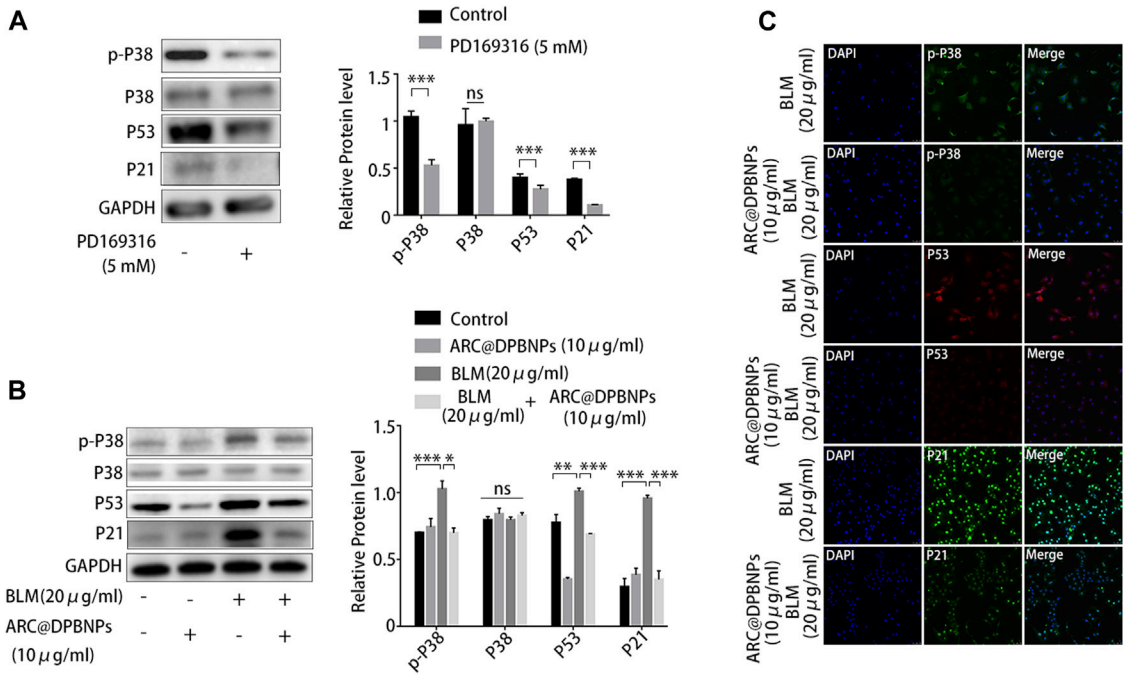

FIGURE 8
Arctiin-encapsulated DSPE-PEG bubble-like nanoparticles (ARC@DPBNPs) attenuated A549 senescence inhibiting the p38/p53/p21 pathway. **(A)** Western blot showing PD169316 selectively inhibits the kinase activity of phosphorylated p38 and p38/p53/p21 pathway activation. **(B)** Western blot showing that ARC@DPBNPs significantly attenuated A549 senescence by downregulating p-p38^{MAPK}, p53, and p21 expression. **(C)** Immunofluorescence staining of p-p38^{MAPK}, p53, and p21 in A549 cells treated with PBS, ARC@DPBNPs (10 μg/mL), bleomycin (BLM) (20 μg/mL), and BLM (20 μg/mL) + ARC@DPBNPs (10 μg/mL) respectively. *$p < 0.05$, **$p < 0.01$, ***$p < 0.001$; ns: not significant.

3.5 ARC@DPBNPs inhibited A549 cell senescence induced by BLM and had less effect on cell vitality compared to the ARC monomer

Cellular senescence caused by AEC2 plays a critical role in IPF. Targeting key regulators of cellular senescence is a potential therapeutic direction for IPF (Qiu et al., 2019; Tian et al., 2019). We assessed the effects of ARC monomer and ARC@DPBNPs on AEC2 senescence in A549 cells induced by BLM. A549 cells are commonly used as a human AEC2 model account of AEC2 as AECs are difficult to obtain and maintain in *ex vivo* culture. BLM was added at gradually increasing concentrations (0–30 μg/mL) to 5% fetal bovine serum culture medium for 72 h to stimulate A549 cells to generate the cellular senescence model. The percentage of SA-β-gal-positive cells gradually increased with higher concentrations of BLM (Supplementary Figure S1A). Furthermore, the relative mRNA and protein levels of senescence-related markers (p21 and p16) increased in a dose-dependent manner in stimulated A549 cells (Supplementary Figures S1B, S1C).

The CCK-8 assay was performed after A549 cells were stimulated with ARC (0–600 μg/mL) or ARC@DPBNPs (0–60 μg/mL) for 72 h. The proliferation of A549 cells was reduced by 7.25% ($p < 0.01$) with the addition of ARC at 100 μg/mL, and the value of OD450 was significantly reduced (16.8%, $p < 0.01$) at 40 μg/mL ARC@DPBNP compared to that in the control group (Figures 5A,B). We then treated senescent A549 cells with different concentrations of ARC and ARC@DPBNPs. P21 levels increased significantly in both groups in response to 20 μg/mL BLM. As shown in Figures 5C,D, the effective concentration of ARC for A549 senescence was above 200 μg/mL, whereas the minimal effective dose of ARC@DPBNPs was 10 μg/mL. A 10 μg/mL concentration of ARC@DPBNPs was selected for further detection. The intensity of positive SA-β-gal staining decreased significantly in the ARC@DPBNPs + BLM group compared to the BLM group ($p < 0.001$, Figure 2E). The decrease in A549 proliferation stimulated with 20 or 30 μg/mL BLM was partially reversed by ARC@DPBNPs (Figure 5F).

Overall, these results indicate that ARC@DPBNPs substantially inhibited A549 senescence without cell toxicity. Meanwhile, the effective dose required for the ARC monomer to downregulate p21 induced by BLM in A549 cells was beyond the toxic dose.

3.6 Senescent markers and the p38/p53/p21 pathway were significantly increased in IPF, BLM-induced A549 cell senescence, and pulmonary fibrosis

Staining (HE and MA) showed notable damage to pulmonary tissue and collagen deposition in patients with IPF compared to the

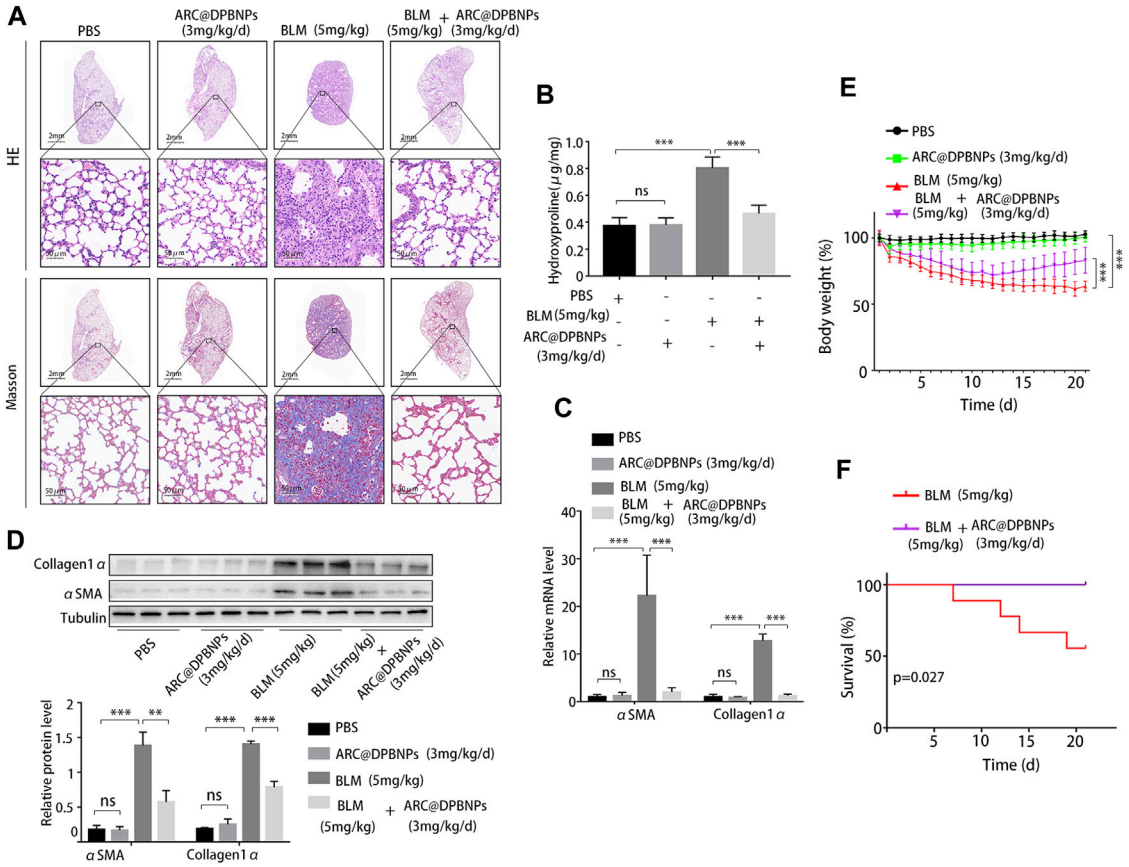

FIGURE 9
Arctiin-encapsulated DSPE-PEG bubble-like nanoparticle (ARC@DPBNP) treatment significantly alleviated pathological changes and improved the outcome of the bleomycin (BLM) mouse model. **(A)** Typical images of lung sections with hematoxylin–eosin and Masson's trichrome staining showing that ARC@DPBNPs (3 mg/kg/d) significantly alleviated the disturbed pulmonary structure of the BLM-induced pulmonary fibrosis mouse model. No excessive pulmonary damage was observed. **(B)** Hydroxyproline content in the mouse lungs was measured on day 21. **(C)** Relative mRNA expression and **(D)** relative protein levels of lung fibrosis markers (α-SMA and collagen1α) in the lungs of mouse models on day 21. **(E)** Body weight was measured daily, and the variations (in grams) from the starting point are shown. **(F)** Survival curve of the BLM and BLM + ARC@DPBNP groups (n = 9 for each group). *p < 0.05, **p < 0.01, ***p < 0.001.

control group, and immunohistochemical results suggested that p16 and p21 were overexpressed in the lung tissue of patients with IPF (Supplementary Figure S2). Subsequently, the Immunofluorescence staining results showed that p21 and p16 were significantly upregulated in AEC2 (SFTPC positive) cells in IPF lung tissues (Figure 6A). The immunohistochemical results (Figure 6B) and Western blotting results (Figure 6C) showed that the protein expression of α-SMA, p-p38^{MAPK}, p53, and p21 was significantly increased.

As cellular senescence markers were overexpressed in IPF lung tissues and the p38/p53/p21 pathway was activated, we investigated whether the p38/p53/p21 pathway participates in the senescence of A549 cells and BLM-induced pulmonary fibrosis. The p38/p53/p21 pathway was gradually activated as the BLM concentration increased (Figure 7A). The level of p-p38^{MAPK}, p53, and p21 increased markedly at 20 mg/mL BLM. Meanwhile, the total p38 did not change significantly (Figure 7A). This followed immunofluorescence analysis of the p38/p53/p21 pathway in A549 cells, showing that the fluorescence intensity of p-p38^{MAPK}, p53, and p21 increased markedly after 20 mg/mL BLM treatment (Figure 7B). Western blotting showed that p-p38^{MAPK}, p53, and p21 protein levels were significantly upregulated in the mouse model of BLM-induced pulmonary fibrosis, and no changes in total p38 protein expression were observed (Figure 7C). The fluorescence intensity of p-p38^{MAPK}, p53, and p21 increased significantly in the mouse model of BLM-induced pulmonary fibrosis compared to that in the PBS group (Figure 7D). This correlates with the results of the *in vitro* experiment. Together, these findings suggest that the p38/p53/p21 pathway is significantly activated in IPF, BLM-induced AEC2 senescence, and pulmonary fibrosis.

3.7 ARC@DPBNPs attenuated A549 senescence by inhibiting the p38/p53/p21 pathway

Because p38/p53/p21 plays an important role in AEC2 senescence and pulmonary fibrosis, the effect of ARC@DPBNPs on the p38/p53/p21 signaling pathway was further investigated *in vitro*. PD169316, a specific p38 inhibitor, selectively inhibits the kinase activity of phosphorylated p38 (Chen et al., 2020).

PD169316 added at a concentration of 5 Mm significantly inhibited p38 phosphorylation and downregulated p53 and p21 in A549 (Figure 8A). Western blotting showed that 10 μg/mL ARC@DPBNP inhibited the protein expression of p-p38^{MAPK}, p53, and p21 (which

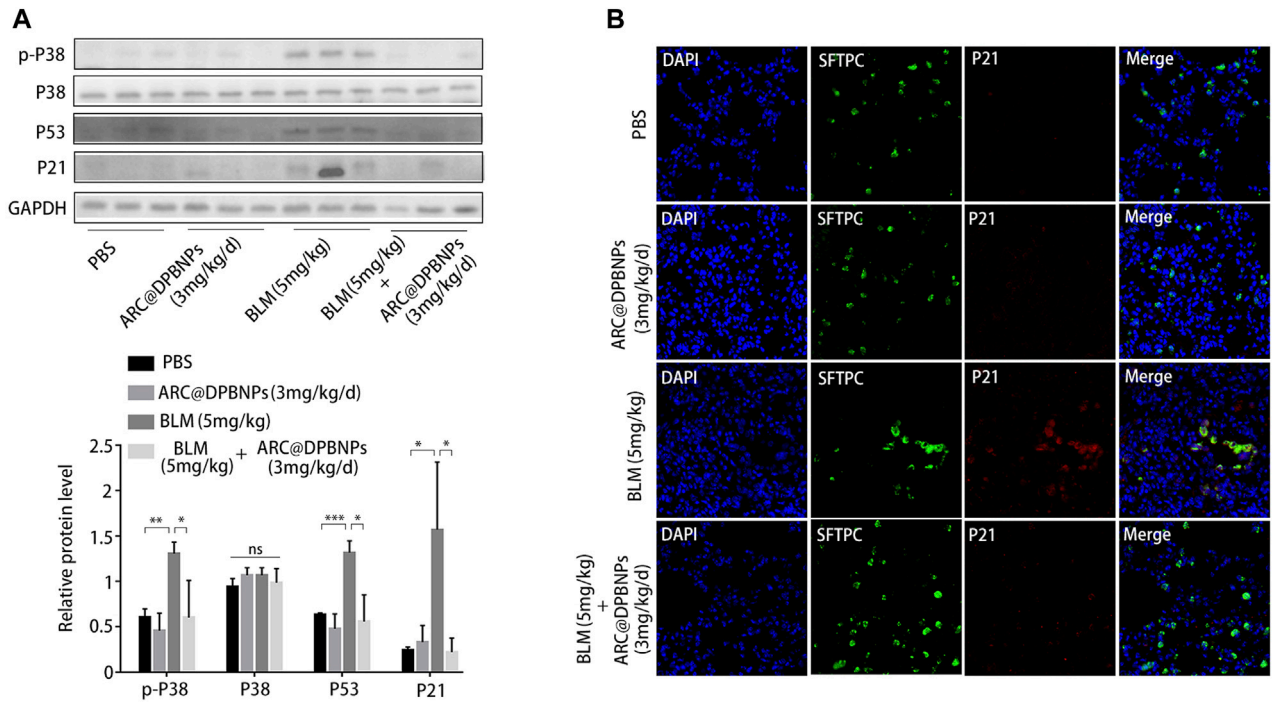

FIGURE 10
Arctiin-encapsulated DSPE-PEG bubble-like nanoparticles (ARC@DPBNPs) suppress AEC2 senescence by inhibiting the p38/p53/p21 pathway. **(A)** Western blot of p-p38MAPK, p53, and p21 expression in lung tissue of mouse models treated with phosphate-buffered saline, ARC@DPBNPs (3 mg/kg/mL), bleomycin (BLM) (5 mg/kg), and BLM (5 mg/kg) + ARC@DPBNPs (3 mg/kg/mL) respectively. **(B)** Immunofluorescence staining of SFTPC (an AEC2-specific marker, green) and p21 (red) was performed to confirm that senescent markers were expressed primarily in the AECs (original magnification = ×400). *$p < 0.05$, **$p < 0.01$, ***$p < 0.001$; ns: not significant.

was increased by 20 μg/mL BLM) in A549 cells (Figure 8B). These observations were validated through immunofluorescence staining (Figure 8C). The fluorescence intensity of p-p38^{MAPK}, p53, and p21 decreased markedly in BLM-induced A549 senescence models after ARC@DPBNP treatment. Furthermore, p-p38^{MAPK}, P53, and P21 decreased markedly in mice treated with a combination of BLM and ARC@DPBNPs compared with those in the BLM group (Figure 8C). This shows that ARC@DPBNPs exert anti-senescent and antifibrotic effects by suppressing p38/p53/p21 pathway activation *in vitro*.

3.8 ARC@DPBNPs attenuated pulmonary fibrosis and suppress AEC2 senescence by inhibiting the p38/p53/p21 pathway

Based on the above results, 3 mg/kg/day of ARC@DPBNPs was chosen for subsequent experiments. Mice aged 6–8 weeks were divided into four groups, with 9 mice in each group. The lung tissues showed interstitial inflammation, fibrotic thickening of the alveolar walls, ablation of the alveolar space, and severe interstitial fibrosis after the BLM administration. Treatment with ARC@DPBNPs led to a noticeable alleviation of pathological lung lesions (Figure 9A). HYP content in the lungs of mouse models was measured as an index of collagen accumulation. As expected, the concentration of HYP in the BLM group was significantly higher than that in the PBS and ARC@DPBNP groups (Figure 9B). Collagen1α and α-SMA are commonly used as biomarkers for pulmonary fibrosis. The mRNA and protein levels of these markers in the BLM group were significantly increased compared with those in the PBS and ARC@DPBNP groups (Figures 9C,D). Mice in the BLM group gradually lost weight during the 21-day experimental period, whereas those in the BLM + ARC@DPBNP group slowly decreased body weight, and the trend reversed more quickly than the BLM group ($p < 0.001$, Figure 9E). Four mice (44.4%) died owing to the severity of the model during the 21-day experiment period, but the survival rate increased significantly after ARC@DPBNP treatment ($p = 0.027$, Figure 9F).

Western blot results showed that p-p38MAPK ($p < 0.05$), P53 ($p < 0.05$), and P21 ($p < 0.05$) decreased markedly in mice treated with a combination of BLM and ARC@DPBNPs compared with those in the BLM group (Figure 10A). Meanwhile, the expression of p21 in AEC2 cells was significantly decreased in the BLM + ARC@DPBNP group compared with that in the BLM group (Figure 10B).

Taken together, these data confirmed that ARC@DPBNPs alleviated BLM-induced pulmonary fibrosis and suppressed cellular senescence by inhibiting the p38/p53/p21 pathway.

4 Discussion

In this study, DPBNPs was first used to encapsulate ARC as a pulmonary drug delivery system. DPBNPs dramatically improved the

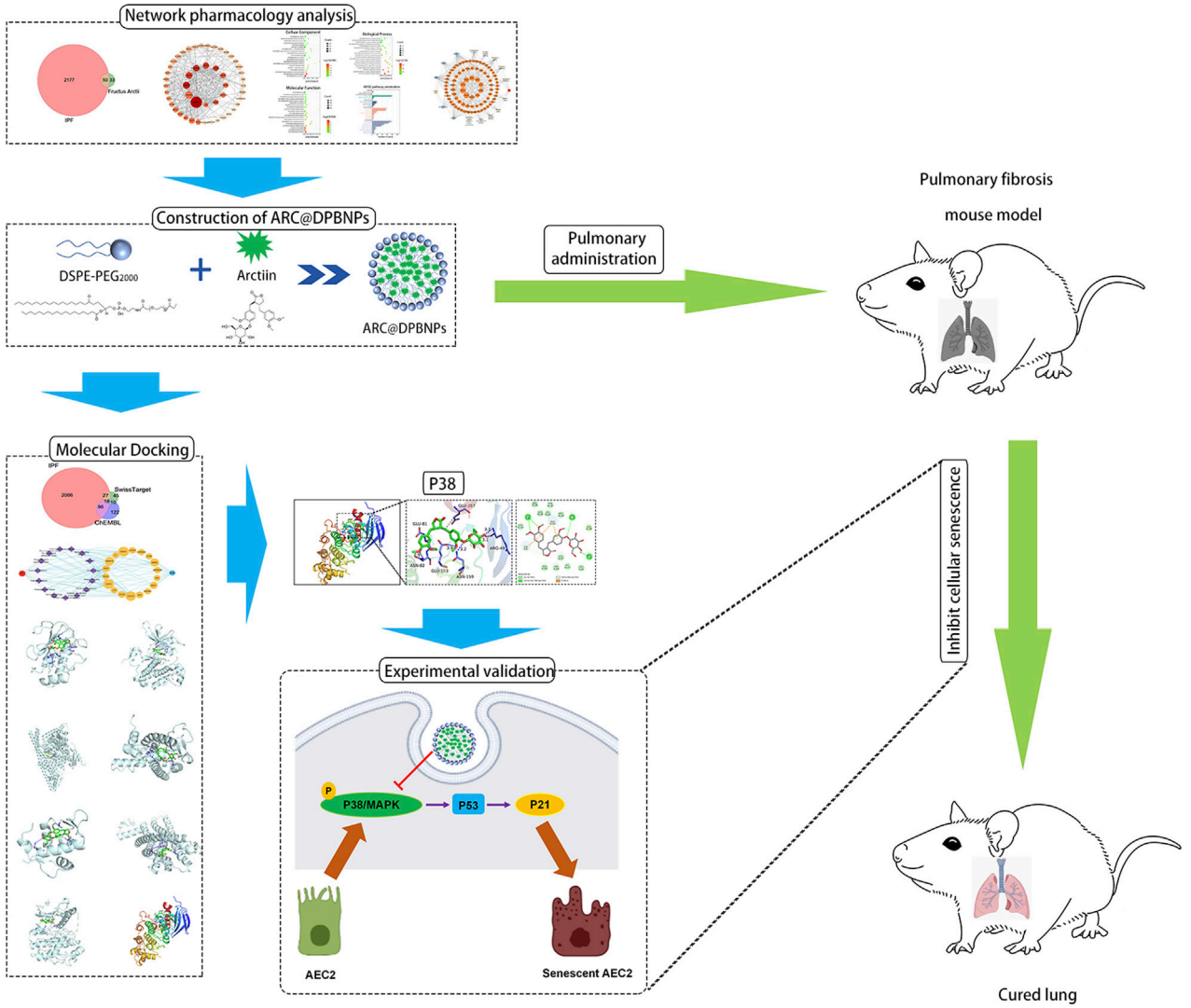

FIGURE 11
The workflow to identify the proposed mechanism showing that arctiin (ARC)-encapsulated DSPE-PEG bubble-like nanoparticles (ARC@DPBNPs) inhibit senescence of AEC2 to alleviate pulmonary fibrosis *via* the p38/p53/p21 pathway.

hydrophilicity and deliverability of ARC. The effects of ARC@DPBNPs on BLM-induced pulmonary fibrosis and senescence were assessed *in vivo* and *in vitro*. The result indicated that pulmonary administration ARC@DPBNPs significantly reduce BLM-induced lung fibrosis and inhibited AEC2 senescence. Systematic network pharmacology and molecular docking were used to predict the mechanisms of ARC in alleviating pulmonary fibrosis, which suggested that ARC has a high affinity with p38. We confirmed the p38/p53/p21 signaling axis was significantly activated in the lung tissues of patients with IPF, senescent AEC2, and BLM-induced lung fibrosis. Our results further defined that ARC@DPBNPs attenuated AEC2 senescence and pulmonary fibrosis by inhibiting the p38/p53/p21 pathway. This study offers the first concrete proof that ARC@DPBNPs reduce BLM-induced lung fibrosis and AEC2 senescence. The workflow and proposed mechanism of ARC@DPBNPs alleviate pulmonary fibrosis are shown in Figure 11.

TCM has a long history in the treatment of pulmonary fibrosis through a multi-level and multi-targeted approach (Zhang et al., 2021). ARC is the active ingredient of biennial dried ripe burdock (*Arctium lappa* L.) belonging to the Asteraceae family. *In vitro* incubation of ARC with different cells showed anti-necroptosis and anti-oxidative effects (Bae et al., 2014; Chen et al., 2020). However, the systemic administration of ARC has several limitations, including the first-pass elimination effect and internal metabolism, causing decreased efficacy and increased side effects. DSPE-PEG is an amphiphilic material that constitutes the main structural framework of the DPBNP wall; it contains a hydrophilic PEG polymer as the external shell and a hydrophobic DSPE core. PEG modifies the surface of nanocarriers to increase the permeability of the airway mucous layer and facilitates efficient pulmonary drug delivery (Rommasi and Esfandiari, 2021; D'Souza and Shegokar, 2016). The DPBNP system has been used as a nanocarrier for hydrophobic agents (Zeng et al., 2012; Zariwala et al., 2014; Wang et al., 2021). This study used

nanoparticles to load the hydrophobic ARC, thereby improving the water solubility and biocompatibility of ARC. The observed particle size of ARC@DPBNP under TEM (56.56 ± 9.78 nm) was smaller than the Nano ZS zetasizer data (185.5 ± 22.3 nm), which correlates with the results of a previous study (Zeng et al., 2012). This might be mainly attributed to the thicker PEG hydrogel layer encapsulating the surface of the nanoparticles that can be detected by the Nano ZS zetasizer. The thicker PEG hydrogel layer and smaller particle size contribute to the high-water solubility and mucus penetration ability (Han et al., 2022).

This study demonstrated that ARC inhibited BLM-induced senescence in A549 cells, and DEPG modification enhanced the biological activity of ARC@DPBNPs. ARC suppressed AEC2 senescence at 200 μg/mL *in vitro* while affecting cell viability at 100 μg/mL. However, ARC@DPBNPs had a therapeutic effect on A549 cell senescence at a lower dose and no obvious effect on cell viability. Meanwhile, intratracheal administration of ARC@DPBNPs significantly reversed BLM-induced pulmonary fibrosis without obvious side effects.

Accumulating evidence indicates that IPF is an aging-related disease, and senescent epithelial cells secrete high levels of growth factors, cytokines, chemokines, and matrix metalloproteinases that promote abnormal and persistent fibroblast activation and remodeling (Mora et al., 2017). Cellular senescence is characterized by prolonged and essentially irreversible cell-cycle arrest due to the upregulation of cell-cycle inhibitors (including p53/p21 and/or p16) and the high activity of SA-β-gal. This study confirmed AEC2 senescence in IPF lungs, BLM-induced mice, and A549 cells. ARC@DPBNP treatment significantly decreased BLM-induced p38/p53/p21 and ß-galactosidase levels.

$P38^{MAPK}$ is an evolutionarily conserved serine/threonine MAPK that links extracellular signals to intracellular machinery to regulate various cellular processes, including cell apoptosis, cell cycle, and migration (Kim et al., 2017). P38 signaling is involved in the pathogenesis of pulmonary fibrosis (Matsuda et al., 2020). P38 inhibitors (SB239063 and FR-167653) alleviate BLM-induced pulmonary fibrosis (Underwood et al., 2000; Matsuoka et al., 2002). Macrophage-specific loss of function of forkhead box M1 (a p38 signaling pathway inhibitor) exacerbates BLM-induced pulmonary fibrosis (Goda et al., 2020). Furthermore, the activity of p38 and its related molecules increases in AEC2 in BLM-induced pulmonary fibrosis in mice. P53 is considered one of the most important downstream targets of $p38^{MAPK}$. $P38^{MAPK}$ activation promotes p53 function, and inhibition of $p38^{MAPK}$ prevents the induction of p53 transcriptional activity (Sanchez-Prieto et al., 2000). This study observed increased p38/p53/p21 signaling in IPF AEC2 and BLM-induced models, which is consistent with the results of previous studies. SwissTarget and ChEMBL showed that p38 was one of the top 15 targets of ARC. Taken together, we hypothesized that ARC@DPBNPs inhibit AEC2 by blocking the p38 pathway.

This study had several limitations. First, we did not investigate the tissue biodistribution of ARC@DPBNPs. We also observed that the antifibrotic effects of ARC@DPBNPs at 3 mg/kg were significantly lower than those observed in other *in vivo* experiments (Li et al., 2017). In addition, we did not compare the biological activity and side effects of ARC@DPBNPs with those of the ARC monomer in a mouse model. The experiment was difficult to perform owing to the different routes of administration, bioavailability, and pharmacokinetics. Moreover, the safe dose range of ARC@DPBNP was not determined, but hematoxylin–eosin staining showed that there were no significant histological changes in the heart, liver, kidney, and spleen of the ARC@DPBNP group compared to those in the PBS group.

In conclusion, the DPBNP delivery system significantly increased the water solubility and biocompatibility of ARC. AEC2 senescence controlled by the p38-p53 pathway is a characteristic of lung fibrosis, and intratracheal injection of ARC@DPBNPs attenuated BLM-induced pulmonary fibrosis in male C57BL/6 mice. ARC@DPBNPs blocked BLM-induced AEC senescence *in vivo* and *in vitro*, probably through regulation of the p38/p53/p21 signaling pathway. These findings could guide the exploration of the therapeutic potential of ARC@DPBNPs in patients with IPF.

Data availability statement

The original contributions presented in the study are included in the article/Supplementary Materials, further inquiries can be directed to the corresponding authors.

Ethics statement

The studies involving human participants were reviewed and approved by the Research Ethics Committees of Nanjing Medical University Affiliated Wuxi People's Hospital. The patients/participants provided their written informed consent to participate in this study. The animal study was reviewed and approved by the Research Ethics Committees of Nanjing Medical University Affiliated Wuxi People's Hospital. Written informed consent was obtained from the individual(s) for the publication of any potentially identifiable images or data included in this article.

Author contributions

DX, FG, JC, and JL contributed to the conception and design of the study. DX, JS, YP, and SW performed the statistical analysis. DX and FG wrote the first draft of the manuscript. DW, YC, SY, RC, and BY wrote the sections of the manuscript. All authors contributed to the manuscript revision. All authors read and approved the final manuscript.

Funding

This study was supported by the National Natural Science Foundation of China (No. 82070059, China), Natural Science Foundation Youth Project of China of Jiangsu Province (No. BK20220224, China), and Youth Project of Wuxi Health and Family Planning Commission (No. Q202127, China).

Conflict of interest

The authors declare that the research was conducted in the absence of any commercial or financial relationships that could be construed as a potential conflict of interest.

Publisher's note

All claims expressed in this article are solely those of the authors and do not necessarily represent those of their affiliated organizations, or those of the publisher, the editors and the reviewers. Any product that may be evaluated in this article, or claim that may be made by its manufacturer, is not guaranteed or endorsed by the publisher.

Supplementary material

The Supplementary Material for this article can be found online at: https://www.frontiersin.org/articles/10.3389/fphar.2023.1141800/full#supplementary-material

References

Amberger, J. S., Bocchini, C. A., Schiettecatte, F., Scott, A. F., and Hamosh, A., (2015). OMIM.org: Online Mendelian Inheritance in Man (OMIM®), an online catalog of human genes and genetic disorders. *Nucleic Acids Res.* 43, D789–D798. doi:10.1093/nar/gku1205

Bae, S., Lim, K. M., Cha, H. J., An, I. S., Lee, J. P., Lee, K. S., et al. (2014). Arctiin blocks hydrogen peroxide-induced senescence and cell death though microRNA expression changes in human dermal papilla cells. *Biol. Res.* 47, 50. doi:10.1186/0717-6287-47-50

Chen, H., Tang, L. J., Tu, H., Zhou, Y. J., Li, N. S., Luo, X. J., et al. (2020). Arctiin protects rat heart against ischemia/reperfusion injury via a mechanism involving reduction of necroptosis. *Eur. J. Pharmacol.* 875, 173053. doi:10.1016/j.ejphar.2020.173053

da Silva, A. L., Cruz, F. F., Rocco, P. R. M., and Morales, M. M. (2017). New perspectives in nanotherapeutics for chronic respiratory diseases. *Biophys. Rev.* 9, 793–803. doi:10.1007/s12551-017-0319-x

Dandekar, P., Venkataraman, C., and Mehra, A. (2010). Pulmonary targeting of nanoparticle drug matrices. *J. Aerosol Med. Pulm. Drug Deliv.* 23, 343–353. doi:10.1089/jamp.2009.0784

D'Souza, A. A., and Shegokar, R. (2016). Polyethylene glycol (PEG): A versatile polymer for pharmaceutical applications. *Expert Opin. Drug Deliv.* 13, 1257–1275. doi:10.1080/17425247.2016.1182485

Gaulton, A., Hersey, A., Nowotka, M., Bento, A. P., Chambers, J., Mendez, D., et al. (2017). The ChEMBL database in 2017. *Nucleic Acids Res.* 45, D945–D954. doi:10.1093/nar/gkw1074

Gfeller, D., Michielin, O., and Zoete, V. (2013). Shaping the interaction landscape of bioactive molecules. *Bioinformatics* 29, 3073–3079. doi:10.1093/bioinformatics/btt540

Ghumman, M., Dhamecha, D., Gonsalves, A., Fortier, L., Sorkhdini, P., Zhou, Y., et al. (2021). Emerging drug delivery strategies for idiopathic pulmonary fibrosis treatment. *Eur. J. Pharm. Biopharm.* 164, 1–12. doi:10.1016/j.ejpb.2021.03.017

Goda, C., Balli, D., Black, M., Milewski, D., Le, T., Ustiyan, V., et al. (2020). Loss of FOXM1 in macrophages promotes pulmonary fibrosis by activating p38 MAPK signaling pathway. *PLOS Genet.* 16, e1008692. doi:10.1371/journal.pgen.1008692

Han, M., Song, Y., Liu, S., Lu, X., Su, L., Liu, M., et al. (2022). Engineering of stimulus-responsive pirfenidone liposomes for pulmonary delivery during treatment of idiopathic pulmonary fibrosis. *Front. Pharmacol.* 13, 882678. doi:10.3389/fphar.2022.882678

Hayashi, K., Narutaki, K., Nagaoka, Y., Hayashi, T., and Uesato, S. (2010). Therapeutic effect of arctiin and arctigenin in immunocompetent and immunocompromised mice infected with influenza A virus. *Biol. Pharm. Bull.* 33, 1199–1205. doi:10.1248/bpb.33.1199

Hirose, M., Yamaguchi, T., Lin, C., Kimoto, N., Futakuchi, M., Kono, T., et al. (2000). Effects of arctiin on PhIP-induced mammary, colon and pancreatic carcinogenesis in female Sprague-Dawley rats and MeIQx-induced hepatocarcinogenesis in male F344 rats. *Cancer Lett.* 155, 79–88. doi:10.1016/s0304-3835(00)00411-0

Kellogg, D. L., Kellogg, D. L., Jr, Musi, N., and Nambiar, A. M. (2021). Cellular senescence in idiopathic pulmonary fibrosis. *Curr. Mol. Biol. Rep.* 7, 31–40. doi:10.1007/s40610-021-00145-4

Kim, K. Y., Park, K. I., Kim, S. H., Yu, S. N., Park, S. G., Kim, Y. W., et al. (2017). Inhibition of autophagy promotes salinomycin-induced apoptosis via reactive oxygen species-mediated PI3K/AKT/mTOR and ERK/p38 MAPK-dependent signaling in human prostate cancer cells. *Int. J. Mol. Sci.* 18. doi:10.3390/ijms18051088

King, C. S., and Nathan, S. D. (2015). Practical considerations in the pharmacologic treatment of idiopathic pulmonary fibrosis. *Curr. Opin. Pulm. Med.* 21, 479–489. doi:10.1097/MCP.0000000000000190

Kropski, J. A., and Blackwell, T. S. (2019). Progress in understanding and treating idiopathic pulmonary fibrosis. *Annu. Rev. Med.* 70, 211–224. doi:10.1146/annurev-med-041317-102715

Lee, S., Shin, S., Kim, H., Han, S., Kim, K., Kwon, J., et al. (2011). Anti-inflammatory function of arctiin by inhibiting COX-2 expression via NF-κB pathways. *J. Inflamm. (Lond).* 8, 16. doi:10.1186/1476-9255-8-16

Li, J., Yuan, Y. P., Xu, S. C., Zhang, N., Xu, C. R., Wan, C. X., et al. (2017). Arctiin protects against cardiac hypertrophy through inhibiting MAPKs and AKT signaling pathways. *J. Pharmacol. Sci.* 135, 97–104. doi:10.1016/j.jphs.2017.05.012

Li, Y., Wang, Q., Wei, H. C., Liang, Y. Y., Niu, F. J., Li, K. W., et al. (2022). Fructus arctii: An overview on its traditional uses, pharmacology and phytochemistry. *J. Pharm. Pharmacol.* 74, 321–336. doi:10.1093/jpp/rgab140

Liu, J., Liu, J., Tong, X., Peng, W., Wei, S., Sun, T., et al. (2021). Network pharmacology prediction and molecular docking-based strategy to discover the potential pharmacological mechanism of Huai Hua san against ulcerative colitis. *Drug Des. Dev. Ther.* 15, 3255–3276. doi:10.2147/DDDT.S319786

Liu X., X., Wang, J., Dou, P., Zhang, X., Ran, X., Liu, L., et al. (2021). The ameliorative effects of arctiin and arctigenin on the oxidative injury of lung induced by silica via TLR-4/NLRP3/TGF-β signaling pathway. *Oxid. Med. Cell. Longev.* 2021, 5598980. doi:10.1155/2021/5598980

Matsuda, S., Kim, J. D., Sugiyama, F., Matsuo, Y., Ishida, J., Murata, K., et al. (2020). Transcriptomic evaluation of pulmonary fibrosis-related genes: Utilization of transgenic mice with modifying p38 signal in the lungs. *Int. J. Mol. Sci.* 21. doi:10.3390/ijms21186746

Matsuoka, H., Arai, T., Mori, M., Goya, S., Kida, H., Morishita, H., et al. (2002). A p38 MAPK inhibitor, FR-167653, ameliorates murine bleomycin-induced pulmonary fibrosis. *Am. J. Physiol. Lung Cell. Mol. Physiol.* 283, L103–L112. doi:10.1152/ajplung.00187.2001

Matsuzaki, Y., Koyama, M., Hitomi, T., Yokota, T., Kawanaka, M., Nishikawa, A., et al. (2008). Arctiin induces cell growth inhibition through the down-regulation of cyclin D1 expression. *Oncol. Rep.* 19, 721–727. doi:10.3892/or.19.3.721

Mora, A. L., Rojas, M., Pardo, A., and Selman, M. (2017). Emerging therapies for idiopathic pulmonary fibrosis, a progressive age-related disease. *Nat. Rev. Drug Discov.* 16, 755–772. doi:10.1038/nrd.2017.170

Oh, K. K., Adnan, M., and Cho, D. H. (2022). Uncovering a hub signaling pathway of antimicrobial-antifungal-anticancer peptides' axis on short cationic peptides via network pharmacology study. *Int. J. Mol. Sci.* 23. doi:10.3390/ijms23042055

Ono, K., and Han, J. (2000). The p38 signal transduction pathway Activation and function. *Cell. Signal.* 12, 1–13. doi:10.1016/S0898-6568(99)00071-6

Parimon, T., Hohmann, M. S., and Yao, C. (2021). Cellular senescence: Pathogenic mechanisms in lung fibrosis. *Int. J. Mol. Sci.* 22. doi:10.3390/ijms22126214

Porsio, B., Craparo, E. F., Mauro, N., Giammona, G., and Cavallaro, G. (2018). Mucus and cell-penetrating nanoparticles embedded in Nano-into-micro formulations for pulmonary delivery of ivacaftor in patients with cystic fibrosis. *ACS Appl. Mat. Interfaces.* 10, 165–181. doi:10.1021/acsami.7b14992

Qiu, T., Tian, Y., Gao, Y., Ma, M., Li, H., Liu, X., et al. (2019). PTEN loss regulates alveolar epithelial cell senescence in pulmonary fibrosis depending on Akt activation. *Aging (Albany, NY)* 11, 7492–7509. doi:10.18632/aging.102262

Rommasi, F., and Esfandiari, N. (2021). Liposomal nanomedicine: Applications for drug delivery in cancer therapy. *Nanoscale Res. Lett.* 16, 95. doi:10.1186/s11671-021-03553-8

Ru, J., Li, P., Wang, J., Zhou, W., Li, B., Huang, C., et al. (2014). Tcmsp: A database of systems pharmacology for drug discovery from herbal medicines. *J. Cheminform.* 6, 13. doi:10.1186/1758-2946-6-13

Safran, M., Dalah, I., Alexander, J., Rosen, N., Iny, S. T., Shmoish, M., et al. (2010). GeneCards. Version 3: The human gene integrator. *Database (Oxf.)* 2010, baq020.

Sanchez-Prieto, R., Rojas, J. M., Taya, Y., and Gutkind, J. S. (2000). A role for the p38 mitogen-acitvated protein kinase pathway in the transcriptional activation of p53 on genotoxic stress by chemotherapeutic agents. *Cancer Res.* 60, 2464–2472.

Szklarczyk, D., Gable, A. L., Nastou, K. C., Lyon, D., Kirsch, R., Pyysalo, S., et al. (2021). The STRING database in 2021: Customizable protein–protein networks, and

functional characterization of user-uploaded gene/measurement sets. *Nucleic Acids Res.* 49, D605–D612. doi:10.1093/nar/gkaa1074

Tian, Y., Li, H., Qiu, T., Dai, J., Zhang, Y., Chen, J., et al. (2019). Loss of PTEN induces lung fibrosis via alveolar epithelial cell senescence depending on NF-κB activation. *Aging Cell* 18, e12858. doi:10.1111/acel.12858

Underwood, D. C., Osborn, R. R., Bochnowicz, S., Webb, E. F., Rieman, D. J., Lee, J. C., et al. (2000). SB 239063, a p38 MAPK inhibitor, reduces neutrophilia, inflammatory cytokines, MMP-9, and fibrosis in lung. *Am. J. Physiol. Lung Cell. Mol. Physiol.* 279, L895–L902. doi:10.1152/ajplung.2000.279.5.L895

Wang, X., Li, Y., Deng, X., Jia, F., Cui, X., Lu, J., et al. (2021). Colloidally stabilized DSPE-PEG-glucose/calcium phosphate hybrid nanocomposites for enhanced photodynamic cancer therapy via complementary mitochondrial Ca(2+) overload and autophagy inhibition. *ACS Appl. Mat. Interfaces.* 13, 39112–39125. doi:10.1021/acsami.1c11583

Wishart, D. S., Feunang, Y. D., Guo, A. C., Lo, E. J., Marcu, A., Grant, J. R., et al. (2018). DrugBank 5.0: A major update to the DrugBank database for 2018. *Nucleic Acids Res.* 46, D1074–D1082. doi:10.1093/nar/gkx1037

Wolters, P. J., Blackwell, T. S., Eickelberg, O., Loyd, J. E., Kaminski, N., Jenkins, G., et al. (2018). Time for a change: Is idiopathic pulmonary fibrosis still idiopathic and only fibrotic? *Lancet Respir. Med.* 6, 154–160. doi:10.1016/S2213-2600(18)30007-9

Xu, Y., Mizuno, T., Sridharan, A., Du, Y., Guo, M., Tang, J., et al. (2016). Single-cell RNA sequencing identifies diverse roles of epithelial cells in idiopathic pulmonary fibrosis. *JCI Insight* 1, e90558. doi:10.1172/jci.insight.90558

Yao, C., Guan, X., Carraro, G., Parimon, T., Liu, X., Huang, G., et al. (2021). Senescence of alveolar type 2 cells drives progressive pulmonary fibrosis. *Am. J. Respir. Crit. Care Med.* 203, 707–717. doi:10.1164/rccm.202004-1274OC

Zariwala, M. G., Farnaud, S., Merchant, Z., Somavarapu, S., and Renshaw, D. (2014). Ascorbyl palmitate/DSPE-PEG nanocarriers for oral iron delivery: Preparation, characterisation and *in vitro* evaluation. *Colloids Surf. B Biointerfaces.* 115, 86–92. doi:10.1016/j.colsurfb.2013.11.028

Zeng, N., Hu, Q., Liu, Z., Gao, X., Hu, R., Song, Q., et al. (2012). Preparation and characterization of paclitaxel-loaded DSPE-PEG-liquid crystalline nanoparticles (LCNPs) for improved bioavailability. *Int. J. Pharm.* 424, 58–66. doi:10.1016/j.ijpharm.2011.12.058

Zhang, Y., Lu, P., Qin, H., Zhang, Y., Sun, X., Song, X., et al. (2021). Traditional Chinese medicine combined with pulmonary drug delivery system and idiopathic pulmonary fibrosis: Rationale and therapeutic potential. *Biomed. Pharmacother.* 133, 111072. doi:10.1016/j.biopha.2020.111072

Zhou, Y., Zhang, Y., Lian, X., Li, F., Wang, C., Zhu, F., et al. (2022). Therapeutic target database update 2022: Facilitating drug discovery with enriched comparative data of targeted agents. *Nucleic Acids Res.* 50, D1398–D1407. doi:10.1093/nar/gkab953

Frontiers in Pharmacology

Explores the interactions between chemicals and living beings

The most cited journal in its field, which advances access to pharmacological discoveries to prevent and treat human disease.

Discover the latest Research Topics

See more →

Frontiers

Avenue du Tribunal-Fédéral 34
1005 Lausanne, Switzerland
frontiersin.org

Contact us

+41 (0)21 510 17 00
frontiersin.org/about/contact